NASA CONTRACTOR
REPORT

AN INVESTIGATION OF RELATIONSHIPS BETWEEN MESO- AND SYNOPTIC-SCALE PHENOMENA

*by James R. Scoggins, James E. Wood,
Henry E. Fuelberg, and William L. Read*

Prepared by
TEXAS A&M UNIVERSITY
College Station, Texas 77843
for George C. Marshall Space Flight Center

NATIONAL AERONAUTICS AND SPACE ADMINISTRATION • WASHINGTON, D. C. • JUNE 1972

1. REPORT NO. NASA CR-2030	2. GOVERNMENT ACCESSION NO.	3. RECIPIENT'S CATALOG NO.
4. TITLE AND SUBTITLE AN INVESTIGATION OF RELATIONSHIPS BETWEEN MESO- AND SYNOPTIC-SCALE PHENOMENA		5. REPORT DATE June 1972
		6. PERFORMING ORGANIZATION CODE
7. AUTHOR(S) James R. Scoggins, James E. Wood, Henry E. Fuelberg and William L. Read		8. PERFORMING ORGANIZATION REPORT #
9. PERFORMING ORGANIZATION NAME AND ADDRESS The Department of Meteorology Texas A&M University College Station, Texas 77843		10. WORK UNIT NO.
		11. CONTRACT OR GRANT NO. NAS8-25400
		13. TYPE OF REPORT & PERIOD COVERED
12. SPONSORING AGENCY NAME AND ADDRESS NASA Washington, D. C. 20546		CONTRACTOR REPORT Final
		14. SPONSORING AGENCY CODE
15. SUPPLEMENTARY NOTES		

16. ABSTRACT

Relationships between meso- and synoptic-scale systems are investigated for four cases, using both statistical and semi-quantitative (synoptic) approaches in the analysis. Methods based on the vorticity equation, the adiabatic method, the curvature of the vertical wind profile, and the structure of synoptic waves are used to determine areas of positive vertical motion in the mid-troposphere for each case. Parameters indicative of low-level moisture and conditional instability are areas in which mesoscale systems (radar echoes) may be present. The best association between mesoscale and synoptic-scale phenomena was found for a period during December when synoptic-scale systems were well developed. A good association between meso- and synoptic-scale events also was found for a period during March, while the poorest association was found for a June period. Daytime surface heating apparently is an important factor in the formation of mesoscale systems during the summer. The association between meso- and synoptic-scale events was better for a September period than for a June period, but not so good as the March period. In general, it is concluded that the formation of mesoscale phenomena may be determined essentially from synoptic-scale conditions during winter, late fall, and early spring. In these cases, regarding the mesoscale systems which are associated with and which may be inferred from large-scale (synoptic) systems as an "article of faith" appears to have at least some validity. The analyses show that the "article of faith" has little or no validity over the southeastern United States during the summer, as well as for selected times and locations during other seasons.

17. KEY WORDS		18. DISTRIBUTION STATEMENT
19. SECURITY CLASSIF. (of this report) Unclassified	20. SECURITY CLASSIF. (of this page) Unclassified	21. NO. OF PAGES 235 · 22. PRICE $3.00

MSF

FOREWORD

This report is composed of seven sections and four appendices. The first three sections contain information relating to the sections which follow. Section 4 contains the methods of analysis used in Section 6. Section 5 contains a statistical analysis of relationships between synoptic- and meso-scale systems, while Section 6 follows an analytical approach. The report is written such that Sections 1, 2, 5, and 7 may be treated as a unit, or Section 5 may be omitted and the remainder of the report treated as a unit. In addition, Appendix A is complete within itself and may be treated independently. Although this appendix is not related directly to the main body of the report, it may be considered as background material.

ACKNOWLEDGMENTS

TABLE OF CONTENTS

LIST OF FIGURES

LIST OF FIGURES (continued)

LIST OF FIGURES (continued)

LIST OF TABLES

1. INTRODUCTION AND BACKGROUND

Atmospheric systems may be divided into various scales which are suitable for study. Analysis of upper-air data from the regularly reporting network of stations reveals wave-shaped patterns with dimensions generally 1800-9000 km or more; these dimensions may be called the synoptic scale (Byers, 1959). Not revealed in the synoptic-scale analysis but imbedded in it are mesoscale systems. These systems generally have dimensions from about 1 km to several hundred kilometers (Fujita, 1963), and are responsible for much of the observed clouds and precipitation. The interaction between meso- and synoptic-scale systems is not yet fully understood; this problem is the principal subject of this report.

It is generally believed that the limit of predictability of large-scale (synoptic and larger) motion systems in about two weeks (Smagorinsky, 1969), with the "ultimate limit of predictability" being about three weeks (Smagorinsky, et al., 1970). Based on dimensional reasoning, Robinson (1967) estimates five days for a scale (synoptic) of 5000-km, one day for a scale of 500 km, and two hours for a scale of 5 km. A review of present forecasting capability (Appendix A) tends to support Robinson's time scales. The prediction of large-scale systems for periods of several days is influenced by small-scale systems* (mesoscale and smaller), and since these latter systems cannot be forecast they must be functionally related to the former. It has been stated that, "A hypothesis that is fundamental to all numerical models of the general circulation is that the effects of features of the atmosphere which have a scale smaller than 500 km (i.e., mesoscale) must be essentially determinable from larger-scale motions. This can be considered a kind of "article of faith" in dynamic meteorology."** It has been shown that synoptic data would have to be analyzed every 2 hours and preferably every hour in order to detect mesoscale systems (House, 1964). This, of course, is not practical and illustrates the need to better understand the "article of faith."

---

*GARP Topics, Bull. Amer. Meteor. Soc., 50 (3), p. 136-141.

**TROMEX: A Research Plan for a Tropical Meteorology Experiment, National Center for Atmospheric Research, March, 1968.

The objective of this research was to investigate relationships between synoptic- and meso-scale systems. Two basic approaches were taken. The first was statistical in nature and followed somewhat the procedures used by Teweles and Forst (1953) except that actual rather than predicted synoptic charts were used. The second approach, which was treated much more extensively than the statistical approach, was synoptic in nature and based on principles of dynamics, kinematics, and thermodynamics. The synoptic approach led to a more voluminous text than desired because of its descriptive character, but the results seem to have justified the approach. The sign of vertical motion in the mid-troposphere was estimated from synoptic charts by a method based on the vorticity equation combined with Dines' Compensation Principle, properties of troughs, the adiabatic method, and the curvature of the vertical wind profile. Positive vertical motion was combined with parameters of stability and moisture to delineate areas in which mesoscale systems, the existence of which was inferred from radar echoes, should have been present.

Theory gives the relationships between many meteorological variables. The equations of motion relate wind speed to pressure gradient, the hydrostatic equation relates pressure and height, the thermal wind equation relates horizontal temperature gradient to vertical wind shear, and there are many other similar relationships. There are no theories, as such, which relate cloud formation or precipitation to meteorological variables such as pressure, temperature, gradients of these quantities, etc., although it is known from experience that such relationships exist. When the relationships cannot be specified in analytical form, statistical methods are often used to infer the relationships. Statistical methods have been used for many years, particularly in local forecast studies, to relate the occurrence of fog, precipitation, clouds, and other variables to parameters such as wind speed, the gradient of height on constant pressure surfaces, the height of constant pressure surfaces, thickness between pressure surfaces, the gradient of temperature, and numerous other synoptic variables. As pointed out by Panofsky and Brier (1958) the selection of variables to use as predictors should be based on physical reasoning as much as possible. If theory predicts a relationship between two variables, or between two

2

variables jointly with a third, it is more likely that a statistical relationship will be found than if the variables are not related theoretically. Thus, the choice of variables often determines the degree of success obtained from statistical studies. A number of studies have been made on the relationship between large- and small-scale systems. A select few of these studies are reviewed below.

It has been found (Jorgensen, 1953) that pressure and pressure height is more effective in determining rainfall at a given station than temperature and stability. This result is probably related to the fact that pressure and its gradient is better related to vertical motion than is temperature or stability. This is not to say that temperature and stability are not important factors in rainfall; however, clouds will not form, in general, unless vertical motion is present. Thus, it is logical to expect a relationship between vertical motion, and precipitation and clouds.

Jorgensen (1953) investigated the relationships between precipitation and sea-level pressure at several stations, the temperature-dew point difference between levels, the height difference at the 500-mb level between various stations, and the height of the 500-mb level and sea-level pressure at different points. These parameters were chosen on the basis of observed synoptic conditions when precipitation occurred along the west coast of the United States. Scatter diagrams prepared from the data showed a reasonable separation of rain and no-rain cases, but with considerable overlap in some instances.

More recent studies on the problem of associating precipitation, and therefore clouds, to synoptic parameters and conditions have concentrated on synoptic patterns. For example, Younkin (1968) related snowfall to maximum relative vorticity and the direction of movement of the center of maximum vorticity. In addition, he found that warm advection in the troposphere corresponded with areas of heavy snowfall. Both of these factors, the advection of relative vorticity and of temperature, are related to vertical motion. In another study Endlich and Mancuso (1968) performed an objective analysis of environmental conditions associated with severe thunderstorms and tornadoes. These authors related various kinematic and thermodynamic variables to the formation of thunderstorms and tornadoes over the United States. It was found that vertical motion, divergence

3

of temperature and moisture fluxes, destabilizing advection, and fronto-
genetical effects were important in the formation of thunderstorms and
tornadoes. The approach is that of considering an area rather than a
point. Many studies such as the two briefly discussed here have been made
during recent years.

Snowstorms near the Great Lakes are often a result of the lake effect.
The formation of lake-effect snowstorms is caused by heating of the air
by the warm lake (mesoscale) but movement is controlled by winds aloft
(synoptic-scale) (Pierce and Sykes, 1966). In the western United States,
orography is an important factor in winter precipitation, while circulation
near the surface rather than at upper levels is more closely associated
with snowfall (Klein et al., 1968).

Severe local storms (SLS) are mesoscale phenomena which are related
to synoptic systems. For example, in the midwestern United States SLS
usually occur in advance of a synoptic-scale trough in the spring and
early summer (Carlson and Ludlam, 1966). It is known also that the forma-
tion of hail in severe storms over northeastern Colorado is associated with
low-level moisture, synoptic-scale baroclinity, an increase in winds aloft,
and surface convergence (Renne and Sinclair, 1969). Miller (1967) has
studied synoptic- and meso-scale features associated with severe storms.
He showed that the conditions necessary for the development of severe storms
are: conditional instability, low level moisture, a lifting mechanism,
a favorable distribution of strong winds and wind shear, and a favorable
height of the Wet-Bulb-Zero.

Kreitzberg and Brown (1970) studied mesoscale systems associated with
an occlusion in New England. They stated that, "The mechanism directly
governing the mesoscale thermal features and weather systems is the release
of potential instability by the larger-scale vertical motions within the
cyclone." This mechanism is important in severe storms, tropical dis-
turbances, and in yielding a significant amount of precipitation in
extratropical cyclones. Other investigators have shown that small-scale
convective systems exist where large-scale conditions are favorable, that
is, regions where both upward parcel displacement and convective insta-
bility occur simultaneously (Reap and Alaka, 1969).

Convective precipitation in the tropics may be a mesoscale phenomenon. It is known that "hot towers" transport mass and energy to upper levels as required for a general circulation model, and that downdrafts are important for initiating new convection to continue the vertical transport of mass and energy (Zipser, 1970). It is difficult to relate convection in the tropics to synoptic parameters (vorticity, temperature, heights of constant-pressure surfaces, etc.) frequently used in the mid-latitudes. However, showers are more likely to occur when a moist layer extends above the 850-mb level (Frank and Smith, 1968) than when one does not.

Stability indexes often are associated with convection. However, in a study of stability indexes and convective clouds over Texas, Booth (1970) showed that stability indexes alone did not correlate well with convective clouds. He showed also that when stability indexes were combined with an indicator of vertical motion a good correlation was present.

Space-mean charts of height ($\bar{Z}$) showing smoothed synoptic-scale waves were apparently first constructed graphically by Fjörtoft (1952). By subtracting the original contours from the space-mean contours, he obtained perturbations (Z') which he showed were proportional to vorticity. Kuhn (1953) used graphical procedures to determine vertical velocity at four levels (950, 850, 700, and 500 mb) and combined this with a moisture parameter to calculate a rainfall rate. He found that the greatest contribution to precipitation was in the layers between 950 and 700 mb even though vertical velocities were greater at higher levels. Thus, he concluded that the moisture content is as important as vertical velocity in quantitative forecasts of precipitation. Collins and Kuhn (1954) constructed space-mean ($\bar{Z}$) and perturbation (Z') charts and used advection of Z' to infer vertical velocity. Their method yielded poor forecasts for ill-defined systems, but the study gave an indication of the extent to which the vertical motion associated with large-scale circulations could explain precipitation systems of smaller scale. Penner's (1963) method for determining large-scale vertical velocities at 600 mb by the advection of Z' at 500 mb was combined by Harley (1965) with the moisture in a layer to give precipitation rates. Harley also attempted to incorporate the effects of latent heat and topography. The success of the work by Penner and Harley

5

was limited since each considered vorticity advection at only one level to determine vertical velocity.

The approach taken in the present research is similar to that of Collins and Kuhn (1954) in that space-mean and perturbation charts are used to infer areas of positive vertical motion on a synoptic scale in the mid-troposphere. However, the present research goes farther than Collins and Kuhn since it considers upper levels (300 and 200 mb), thermal advection and the curvature of the vertical wind profile as indicators of vertical motion, and a means of estimating the magnitude of vorticity (Z') at troughs and ridges from the structure of the synoptic waves. The relationships investigated in this research make it possible to determine, from the broad-scale patterns over the eastern United States, the general areas, but not the specific location, where mesoscale systems (i.e., clouds and radar echoes) should be present.

The results of an investigation by Frank and Smith (1968) indicate that the vorticity methods used in the present research may be a poor indicator of mesoscale systems in some regions of the southeastern United States, especially the Florida peninsula, during the summer. Also, topographic influences and disturbances which exist beneath the 850-mb level may enhance precipitation that the methods of the present research do not indicate.

Numerous other authors have had various degrees of success in dealing with the problem of relating synoptic- to meso-scale systems. However, many of the techniques used were applicable to specific cities or areas and synoptic situations.

2. PERIODS CHOSEN FOR STUDY

Four cases were chosen for study in each of which a synoptic-scale trough was present over the continental United States. These periods were chosen to represent the four seasons, and also because a significant amount of weather activity indicative of mesoscale systems was present during each time period. Each case consists of six consecutive time periods spaced 12 hours apart. The four cases are: 12Z, 5 December 1969 to 00Z, 8 December 1969; 00Z, 23 March 1969 to 12Z, 25 March 1969; 12Z, 11 June 1969 to 00Z, 14 June 1969; and, 12Z, 20 September 1969 to 00Z, 23 September 1969. All of the data were obtained from the Meteorological Archives of Texas A&M University.

3. PARAMETERS IMPORTANT IN THE FORMATION OF CONVECTIVE CLOUDS (MESOSCALE SYSTEMS)

For the formation of convective clouds and precipitation, the following three conditions must be present:

1) Low-level moisture,

2) Conditional instability, and

3) Vertical motion.

Convection will not necessarily occur if these three conditions are present, but it will not occur if any one condition is absent. These three conditions must be considered collectively to determine if convection will occur.

The amount of moisture and its distribution with height are important factors in the formation of convective clouds. In the atmosphere condensation usually occurs when moist unsaturated air rises and cools by expansion to temperatures below its dew-point temperature. The amount of condensation depends on the amount of water vapor present and the rate of ascent. Thus, if much water vapor and strong positive vertical motion are present, a large amount of liquid water will condense and convective clouds may occur even in a stable atmosphere. Of course the amount of condensation and convection is greatly enhanced if the air becomes unstable when lifted. The distribution of moisture in the lower atmosphere is important in the initiation of convection since it is closely related to convective instability (Miller, 1967). A moist layer below 850 mb with drier air above may be convectively unstable.

A layer is said to be conditionally unstable if its temperature lapse rate is greater than the saturation adiabatic lapse rate but less than the dry adiabatic lapse rate. A parcel of air that is initially saturated will be unstable if lifted in a conditionally unstable atmosphere. A moist unsaturated parcel may become unstable when lifted past its condensation level. Convective instability may be a more significant criterion than conditional instability for the formation of convective clouds since it depends upon the distribution of moisture in a layer. The degree of conditional instability is relatively more important during the summer months when showers and thunderstorms are the principal causes of precipitation. During the winter months, synoptic systems are well organized and, if only

8

a relatively small amount of moisture is present, positive vertical motion
may create clouds and precipitation even though the parcel may remain
stable.

4. METHODS OF ANALYSIS

Four methods of estimating the sign of vertical motion in the mid-troposphere were employed using charts of space-mean contours, vorticity fields, isotherms, and curvature of the vertical wind profile. The first method is based on the simplified vorticity equation from which the sign of divergence is determined at each level; the sign of vertical motion is inferred using Dines' Compensation Principle (Petterssen, 1956). A second method, called the adiabatic method, uses thermal advection to infer the sign of vertical motion. The third method estimates the magnitude of vorticity at the trough using the amplitude and wavelength of the trough as well as the mean westerly wind speed to infer vertical motion in the mid-troposphere by the procedures of the first method. In the fourth method, the sign of divergence is determined from the curvature of the vertical wind profile and the sign of vertical motion in the mid-troposphere inferred from the fields of divergence.

Areas where positive vertical motion and low-level (850-mb) moisture coincide are delineated for each period. These are areas where mesoscale systems should be present and are compared with observed radar echoes which are assumed (with some risk of error) to be indicative of mesoscale systems. Additionally, a measure of stability is included for the June case since convective clouds in the summer are closely related to stability.

a. Estimation of the Sign of Vertical Motion

1) Vorticity Method

The sign and magnitude of vertical motion cannot be measured directly and must be inferred from synoptic data. One method used to determine the sign (magnitude per se is not considered in this research) of vertical motion in the mid-troposphere is based on the vorticity equation combined with Dines' Compensation Principle.

The simplified vorticity equation may be written (Haltiner and Martin, 1957):

$$\frac{d(\zeta+f)}{dt} = - (\zeta+f) \ \vec{\nabla}_2 \cdot \vec{V}.$$

This can be expanded to become:

$$\frac{\partial \zeta}{\partial t} + \vec{V} \cdot \vec{\nabla}_2 \zeta + \beta v = - (\zeta + f) \vec{\nabla}_2 \cdot \vec{V} \qquad (1)$$

where $\partial \zeta / \partial t$ is the local time rate-of-change of relative vorticity, $\vec{V} \cdot \vec{\nabla}_2 \zeta$ is the horizontal advection of relative vorticity, β is the coriolis term, $(\zeta + f)$ is absolute vorticity, and $\vec{\nabla}_2 \cdot \vec{V}$ is horizontal velocity divergence.

Haltiner and Martin (1957) have shown that geostrophic relative vorticity may be expressed by

$$\zeta_g = \frac{4g}{fd^2} (\bar{Z} - Z) \qquad (2)$$

or

$$\zeta_g = \frac{4g}{fd^2} Z' \qquad (2a)$$

where g is the gravitational acceleration, f the coriolis parameter, d the spacing between grid points, $\bar{Z}$ the space-mean height, and $Z' = (\bar{Z} - Z)$. A grid similar to Fig. 1 is used to evaluate $\bar{Z}$ and Z' graphically. It is assumed that $\zeta = \zeta_g \propto Z'$ and, therefore, substitution of ζ_g for ζ in (1) yields

$$\vec{\nabla}_2 \cdot \vec{V} \propto - \frac{\partial Z'}{\partial t} - \vec{V} \cdot \vec{\nabla} Z' - K\beta v \qquad (3)$$

where K is a constant. The sign of divergence at each level can be estimated from (3). The latitudinal term usually is large in the lower levels (850 and 700 mb) east of a trough and contributes to convergence at these levels. At the higher altitudes, the wind is more westerly and positive vorticity advection contributes to divergence at these levels.

11

The sign of vertical motion at any particular level may be inferred from the net (integrated) vertical divergence below or above the level. This may be shown mathematically by assuming an inviscid and incompressible fluid so that

$$\vec{\nabla} \cdot \vec{V} \;\; = \;\; \frac{\partial u}{\partial x} + \frac{\partial v}{\partial y} + \frac{\partial w}{\partial z} \;\; = \;\; 0$$

or,

$$\frac{\partial w}{\partial z} \;\; = \;\; - \; \vec{\nabla}_2 \cdot \vec{V}. \tag{3a}$$
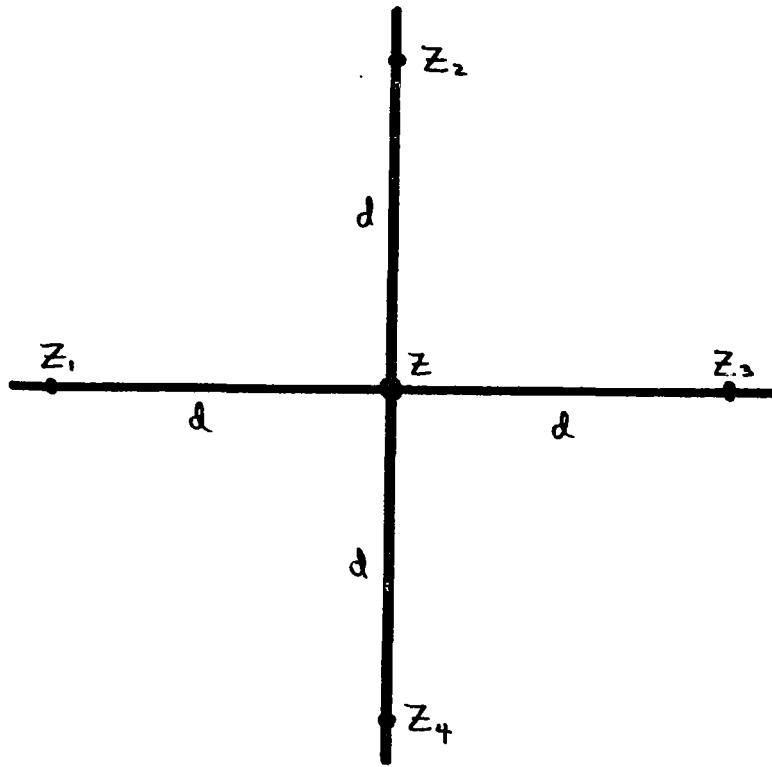
Fig. 1. Example of grid used to evaluate $\bar{Z}$ and Z'. (A value of d = 300 NM (550 km) was used in the graphical procedure.)

Integration from the surface (S) to some level (L) in the atmosphere yields

$$w_L = w_S - \int_S^L \vec{\nabla}_2 \cdot \vec{V} \, dZ \qquad (4)$$

and neglecting w_S gives

$$w_L = - \int_S^L \vec{\nabla}_2 \cdot \vec{V} \, dZ. \qquad (5)$$

Equation (5) states that vertical motion at a particular level (L) is determined by the net two-dimensional velocity divergence in the layer from the surface to the level L. Negative divergence (convergence) in the layer from the surface to the level contributes to positive vertical motion at that level. If (3a) is integrated from level L to the top of the atmosphere it becomes

$$w_L = \int_L^\infty \vec{\nabla}_2 \cdot \vec{V} \, dZ. \qquad (6)$$

Equation (6) states that net positive divergence in the layer from the level L to the top of the atmosphere contributes to positive vertical motion at the level L.

Dines' Compensation Principle (Petterssen, 1956), which may be thought of as the sum of the contributions to positive vertical motion at the level L from (5) and (6), says that, if there is convergence in the lower levels and divergence aloft, then there will be positive vertical motion in the intervening layer, and vice versa. This principle will be referred to repeatedly in succeeding sections. Thus by determining the sign of divergence at each level, we may infer the sign of vertical motion in the mid-troposphere.

13

2) Adiabatic Method

A second method of estimating the sign of vertical motion involves thermal advection. This method is called the adiabatic method and is derived by manipulation of the first law of thermodynamics and the individual rate-of-change of pressure and temperature. The equation for vertical motion in this case is (Haltiner and Martin, 1957):

$$w = \frac{-1}{\gamma_d - \gamma} \left\{ \vec{V} \cdot \vec{\nabla}_2 T + \frac{\partial T}{\partial t} \right\} \tag{7}$$

where $\vec{V} \cdot \vec{\nabla}_2 T$ is the horizontal advection of temperature, $\partial T/\partial t$ is the local rate-of-change of temperature, and γ_d and γ are the dry adiabatic and existing lapse rates of temperature, respectively. Since $\partial T/\partial t$ is usually the same sign as, but smaller than, $\vec{V} \cdot \vec{\nabla}_2 T$, temperature advection is the dominant term. This equation must be examined with care. Warm advection should contribute to positive vertical motion, but strong warm advection aloft over weak warm advection will decrease γ, increase $\gamma_d - \gamma$, and reduce vertical motion. Optimum conditions for positive vertical motion are strong warm advection in the low levels with weaker warm advection aloft. The advection of temperature by the space-mean wind at each level will be used in conjunction with the vorticity method to explain radar echoes.

3) Structure of Troughs and Ridges

The equation of a sinusoidal wave moving in the x-direction with speed c is

$$y = A \sin \frac{2\pi}{L} (x - ct) \tag{8}$$

where A is the amplitude and L the wavelength of the wave. Sinusoidal streamlines may be represented by this equation.

The equation of a streamline also is given by (Haltiner and Martin, 1957):

14

$$v\, dx = u\, dy \tag{9}$$

so that from (8) and (9)

$$v = u\, 2\pi\, \frac{A_s}{L}\, \cos\frac{2\pi}{L}\, (x-ct) \tag{10}$$

where the subscript s refers to streamlines. Relative vorticity (vertical component) may be expressed by (Byers, 1959):

$$\zeta = \frac{\partial v}{\partial x} - \frac{\partial u}{\partial y} \,, \tag{11}$$

and if evaluated at the axis of a trough or ridge where $\partial u/\partial y = 0$, substitution of (10) into (11) gives

$$\zeta = \frac{\partial v}{\partial x} = -u\, 4\pi^2\, \frac{A_s}{L^2}\, \sin\frac{2\pi}{L}\, (x-ct). \tag{12}$$

If the following assumptions are made: 1) stationary system, i.e., $c = 0$, and 2) upstream inflection point is the origin so that $x = L/4$, then

$$\frac{\partial v}{\partial x} = -u\, 4\pi^2\, \frac{A_s}{L^2}\, \sin\frac{2\pi}{L}\left(\frac{L}{4}\right)$$

$$\tag{13}$$

$$= -u\, 4\pi^2\, \frac{A_s}{L^2} = \zeta$$

at a trough or ridge axis. A_s is negative for troughs and positive for ridges.

The expression for geostrophic relative vorticity is given by (2a),

$$\zeta_g = \frac{4g}{fd^2} Z'$$

and equating this expression for ζ_g with the expression for ζ at a trough gives

$$-\pi^2 u \frac{A_s}{L^2} = \frac{g}{fd^2} Z'$$

or

$$Z' = -65.485 \, u \frac{A_s}{L^2} \tag{14}$$

where u is the mean westerly wind speed in meters per second, A_s and L in degrees latitude, and Z' in meters.

Equation (14) yields an approximate value for the magnitude of Z' and is appropriate for sinusoidal waves along the axis of a trough or ridge. Fields of Z' may be present at places other than the trough or ridge and this method may give no indication of them. However, in many cases Z' fields are defined best at trough and ridge axes, and this method will give a measure of their magnitude. The equation shows that large values of Z' are favored by a large wind speed (i.e., large height gradient) and a wave of large amplitude but small wavelength. Figure 2 is a diagram with which the magnitude of Z' at a trough or ridge may be determined if the mean westerly wind speed is 30 m sec^{-1}. The figure shows that the magnitude of Z' increases with increasing amplitude and/or decreasing wavelength. Similar diagrams may be constructed for any particular wind speed and may be applied to any reasonably sinusoidal waves. By estimation of the magnitude of relative vorticity at the trough at each level, the relative magnitude of the advective and latitudinal terms (assuming that the local time rate-of-change is small or zero) in (3) may be estimated to determine

16
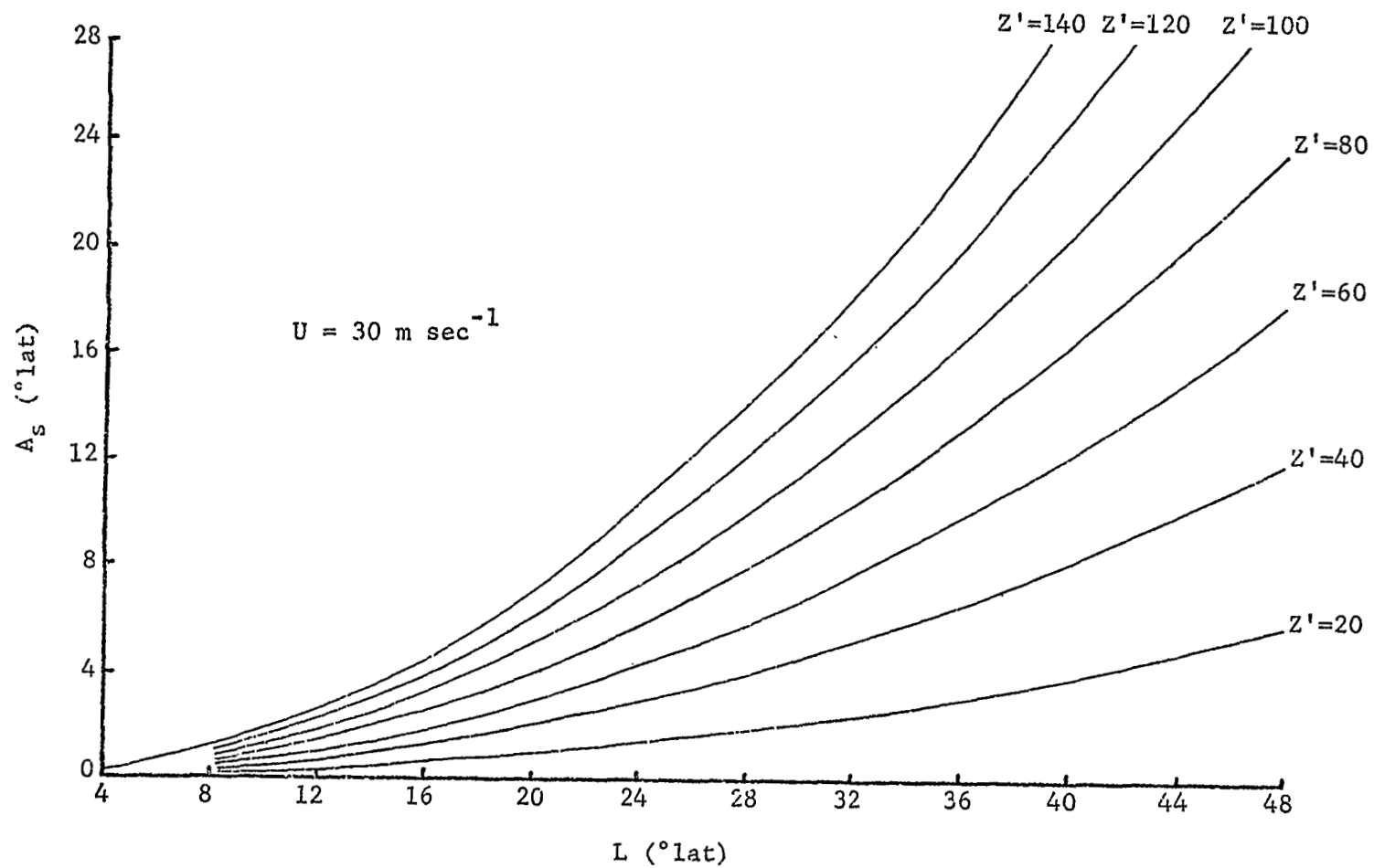
Fig. 2. Example of diagrams used to determine the magnitude of Z' at a trough or ridge axis.

the sign of divergence at each level. Equations (5) and/or (6), and Dines' Compensation Principle may be used to estimate the sign of vertical motion in the mid-troposphere.

The vertical as well as horizontal structure of the atmosphere must be considered to determine areas of positive vertical motion in the mid-troposphere. Three vertical cross sections showing theoretical optimum conditions for positive vertical motion in the mid-troposphere are dipicted schematically in Fig. 3. Figure 3a shows a schematic vertical cross section of a synoptic wave which is well developed at all levels (850, 700, 500, 300, and 200 mb), and positive vertical motion in the mid-troposphere is enhanced by events at each level. The axis of the trough tilts to the left (westward) with height. Under the assumption that Z' is a maximum at the trough, along the line AB negative vorticity advection creates convergence at 850 and 700 mb, positive vorticity advection creates divergence at 500, 300, and 200 mb, and by Dines' Compensation Principle there will be positive vertical motion in the mid-troposphere. Positive vertical motion in the mid-troposphere also is probable in Fig. 3a to the right of the 850-mb trough since that is the area where the south wind at 850 and 700 mb creates convergence. Figure 3b shows a schematic cross section of a wave which is well developed at low levels (850 and 700 mb) and poorly developed at upper levels (500, 300, and 200 mb) with the chief inducement to positive vertical motion from the low levels. If Z' is a maximum at the trough, positive vorticity advection just to the right (east) of the trough leads to divergence. However, farther east of the trough along the line AB the wind is more southerly, advection of Z' may be small, and convergence may be present at the low levels (850 and 700 mb). If there is convergence at 850 and 700 mb then by (5) there will be positive vertical motion at least to a height of 700 mb. Negative vorticity advection to the left (west) of the trough at 850 and 700 mb also creates convergence, but observation has shown that often cold air advection west of a low-level trough negates the effect of convergence. Figure 3c shows a schematic cross section of a wave which is best developed at upper levels (300 and 200 mb), and positive vertical motion depends primarily on events at the upper levels. If Z' is a maximum at the trough, then positive vorticity advection east of the trough creates divergence along the line AB. If there is divergence aloft

18
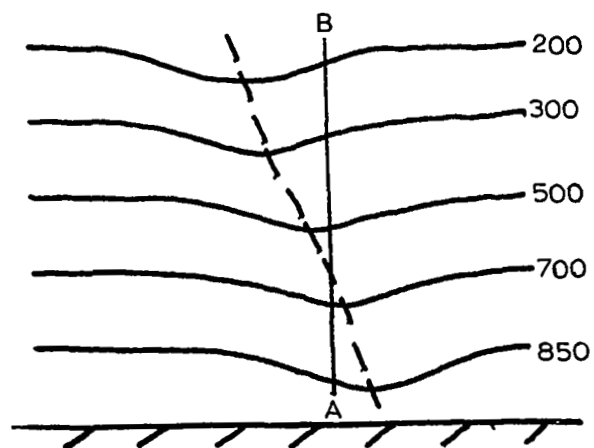
(a)
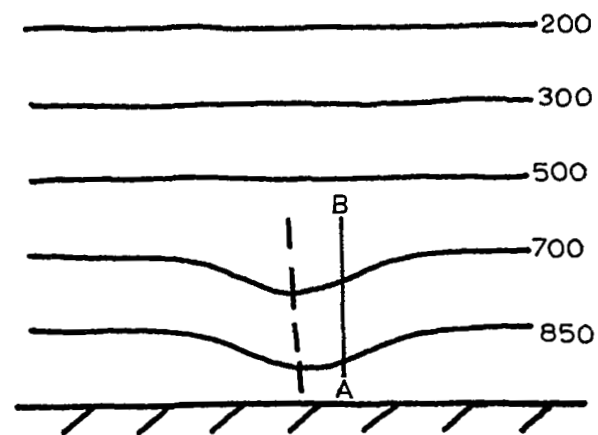
(b)
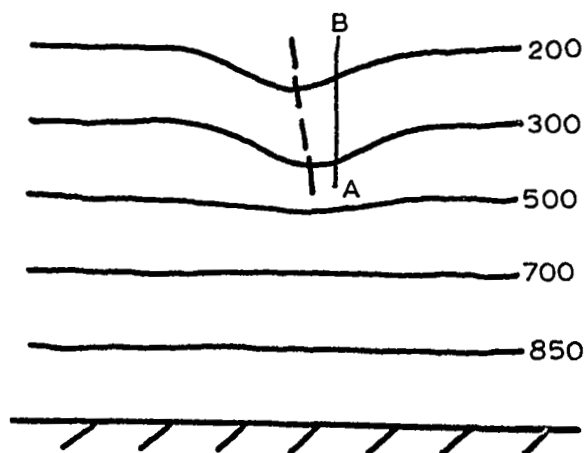
(c)

Fig. 3. Schematic vertical cross-sections.
(Constant pressure surfaces are in
solid lines; dashed lines indicate
troughs. Positive vertical motion
may occur in the vicinity of line AB.)

then there is likely to be positive vertical motion in the mid-troposphere. From observation and (6), when there is divergence aloft (500, 300, or 200 mb), positive vertical motion in the mid-troposphere is likely.

The models presented in Fig. 3 represent typical examples in which positive vertical motion in the mid-troposphere is probable. An almost infinite variety of configurations is possible that would create positive vertical motion in the mid-troposphere. Any configuration that creates low-level (850 and 700 mb) convergence and/or upper-level (500, 300, and 200 mb) divergence may lead to positive vertical motion in the mid-troposphere.

4) Curvature of the Vertical Wind Profile

The sign of vertical motion may be estimated from the equation of motion and velocity divergence, and Dines' Compensation Principle as follows. The first and second equations of motion with friction included may be written:

$$\frac{d\bar{u}}{dt} = f\bar{v} - \frac{1}{\bar{\rho}}\frac{\partial \bar{P}}{\partial x} + \frac{\mu}{\bar{\rho}}\frac{\partial^2 \bar{u}}{\partial z^2} \tag{15}$$

and

$$\frac{d\bar{v}}{dt} = -f\bar{u} - \frac{1}{\bar{\rho}}\frac{\partial \bar{P}}{\partial y} + \frac{\mu}{\bar{\rho}}\frac{\partial^2 \bar{v}}{\partial z^2}. \tag{16}$$

With the assumptions that

$$\frac{d\bar{u}}{dt} = \frac{d\bar{v}}{dt} = 0 ,$$

(15) and (16) become

$$\bar{v} = \frac{1}{f\bar{\rho}}\frac{\partial \bar{P}}{\partial y} - \frac{\mu}{f\bar{\rho}}\frac{\partial^2 \bar{u}}{\partial z^2} \tag{17}$$

20

and

$$\bar{u} = -\frac{1}{f\bar{\rho}} \frac{\partial \bar{P}}{\partial y} + \frac{\cdot\mu}{f\bar{\rho}} \frac{\partial^2 \bar{v}}{\partial z^2} . \tag{18}$$

The equation for the divergence of the average wind is

$$\text{div}_2 \vec{V} = \frac{\partial \bar{u}}{\partial x} + \frac{\partial \bar{v}}{\partial y} . \tag{19}$$

Upon substitution of $\bar{u}$ and $\bar{v}$ from (17) and (18) into equation (19) gives

$$\text{div}_2 \vec{V} = \frac{\mu}{\bar{\rho}f} \left[\frac{\partial}{\partial x} \left(\frac{\partial^2 \bar{v}}{\partial z^2} \right) - \frac{\partial}{\partial y} \left(\frac{\partial^2 \bar{u}}{\partial z^2} \right) \right] \tag{20}$$

where $\partial^2 \bar{v}/\partial z^2$ and $\partial^2 \bar{u}/\partial z^8$ represent the curvatures of the $\bar{u}$ and $\bar{v}$ profiles, respectively, and will be denoted by K_v and K_u. If the parameters outside the brackets in (20) are considered constant, we may write

$$\text{div}_2 \vec{V} \propto \frac{\partial K_v}{\partial x} - \frac{\partial K_u}{\partial y} . \tag{21}$$

Thus, when $\partial K_v/\partial x < 0$ and $\partial K_u/\partial y > 0$, negative divergence (convergence) results, and when $\partial K_v/\partial x > 0$ and $\partial K_u/\partial y < 0$, positive divergence results.

When lower layers of the atmosphere undergoing convergence are underneath upper layers undergoing divergence, Dines' Compensation Principle may be applied which implies upward motion through the intermediate layers. If there is sufficient moisture in the regions of upward motion, clouds and precipitation may result.

Wind data at the 850-, 700-, 500-, 400-, 300-, and 200-mb levels were put in table form and the $\bar{u}$ and $\bar{v}$ components of the wind were computed for each level at each station. From these components the curvatures at all the levels except 850 and 200 mb were computed. In calculating the curvatures a somewhat inaccurate assumption was made. Using finite differences,

$$\frac{\partial^2 \bar{u}}{\partial z^2} = \frac{\partial}{\partial z}\left(\frac{\partial \bar{u}}{\partial z}\right) = \frac{1}{\Delta z_1}\left(\frac{\bar{u}_H - \bar{u}_M}{\Delta z_2} - \frac{\bar{u}_M - \bar{u}_L}{\Delta z_3}\right)$$

$$= \frac{\bar{u}_H - \bar{u}_M - \bar{u}_M - \bar{u}_L}{(\Delta z)^2} = \frac{\bar{u}_H + \bar{u}_L - 2\bar{u}_M}{(\Delta z)^2}$$

or

$$\frac{\partial^2 \bar{u}}{\partial z^2} \propto \bar{u}_H + \bar{u}_L - 2\bar{u}_M \tag{22}$$

where subscripts L and H refer to the next lower and higher level, respectively, than the level where the curvature is being computed (M). In the above derivation it was assumed that $\Delta z_1 = \Delta z_2 = \Delta z_3 = \Delta z$. ($\bar{u}_H + \bar{u}_L - 2\bar{u}_M$) was the value used for the curvature. The inaccuracies come from assuming the ΔZ's to be the same between the layers, but since the layers are rather deep, and the ΔZ's don't differ much on a percentage basis, the results are not affected significantly.

The curvature calculated from the 850-, 700-, and 500-mb levels is labeled the 700-mb curvature; from the 700-, 500-, and 400-mb levels the 500-mb curvature; from the 500-, 400-, and 300-mb the 400-mb curvature, and; from the 400-, 300-, and 200-mb levels, the 300-mb curvature.

Two maps for each curvature level were plotted, one for K_u and one for K_v. These were then analyzed for increments of 10, labeling the centers with either + or -, as shown in Fig. 4.

The curvature levels of 700 and 500 mb were analyzed for regions of low-level convergence. From (21), $\partial K_v/\partial x$ must be negative and/or $\partial K_u/\partial y$ positive in order to have convergence. $\partial K_v/\partial x < 0$ means that the value of K_v would be decreasing to the east, and $\partial K_u/\partial y > 0$ would mean that the value K_u would be increasing to the north. By overlaying a transparent map and shading in the regions of maximum gradient for contributions to convergence for both K_u and K_v, the regions of maximum convergence were found for each level. Then regions of convergence occurring on both the 500- and

22
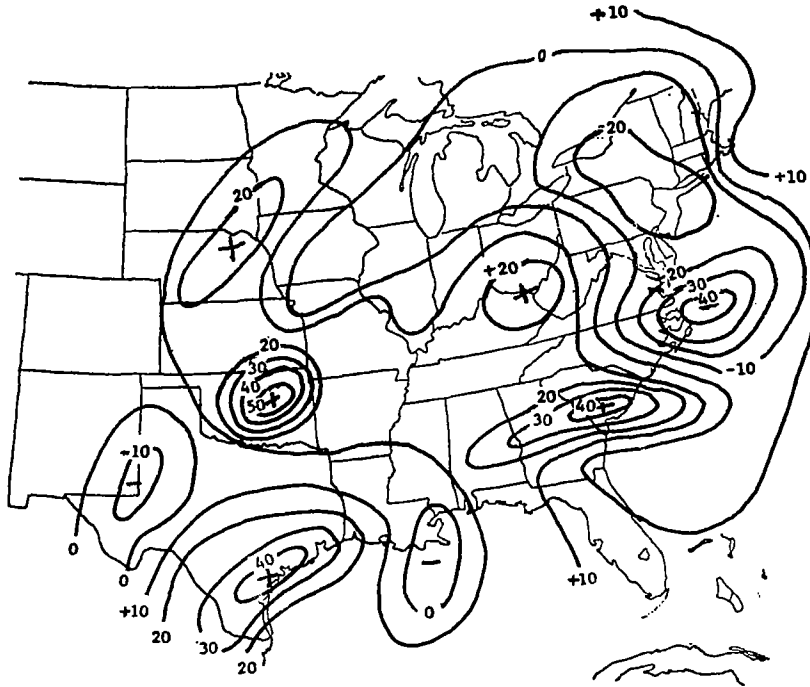
Fig. 4. Analyzed field of K_V at 700 mb for 12Z,
5 December 1969.

700-mb maps were superimposed on one map and these regions shaded. Any
shaded area was considered to be a region of convergence in the lower
levels. This seems reasonable since only the regions of maximum gradients
were shaded. For illustration purposes, the regions of maximum gradient
for the 700-mb K_V for 12Z, 5 December 1969 are shown in Fig. 5.

The same method of analysis was used to obtain the regions of upper-
level divergence using the curvature charts computed for the 400- and
300-mb levels. From (21), for maximum divergence the value of $\partial K_v / \partial x$
should be positive and the value of $\partial K_u / \partial y$ should be negative. On the maps
for K_V, regions of maximum increase going east were shaded, as well as K_V
going north as contributions to upper-level divergence. Any shaded region
shown at either level was superimposed on one map to give a composite chart
of regions of upper-level divergence. The method of determining contribu-
tions to divergence is shown in Fig. 6 for the 300 mb K_V, 12Z, 5 December
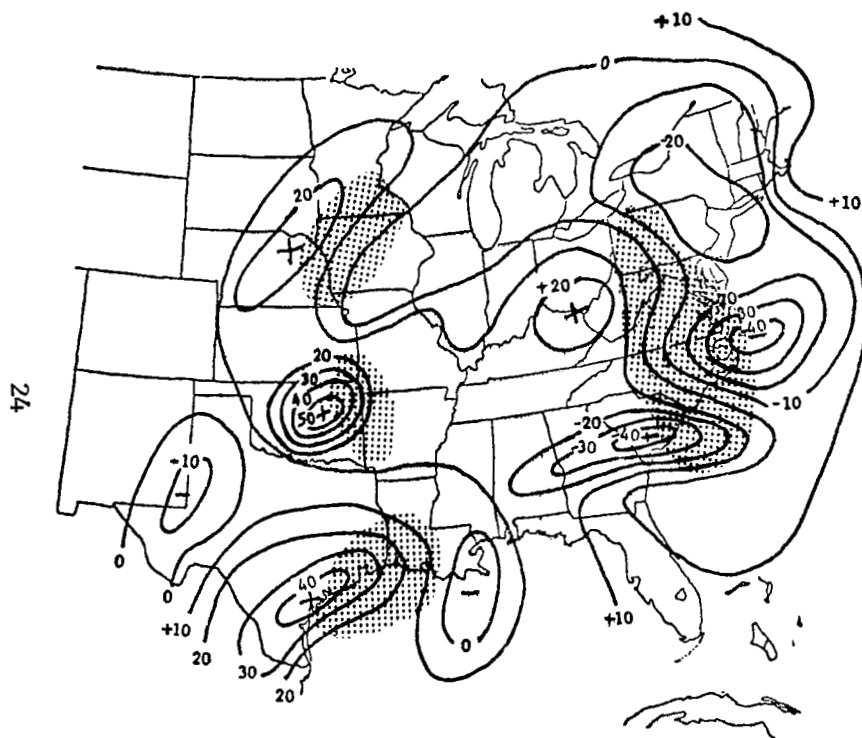
Fig. 5. Analyzed field of K_V at 700 mb for 12Z, 5 December 1969 with regions shaded where $\partial K_v/\partial x$ is large and negative.

Fig. 6. Analyzed field of K_V at 300 mb for 12Z, 5 December 1969.

1969. Figure 7 shows the analyzed field of K_V at 300 mb for 12Z, 5 December 1969 with regions shaded where $\partial K_v/\partial x$ is positive.
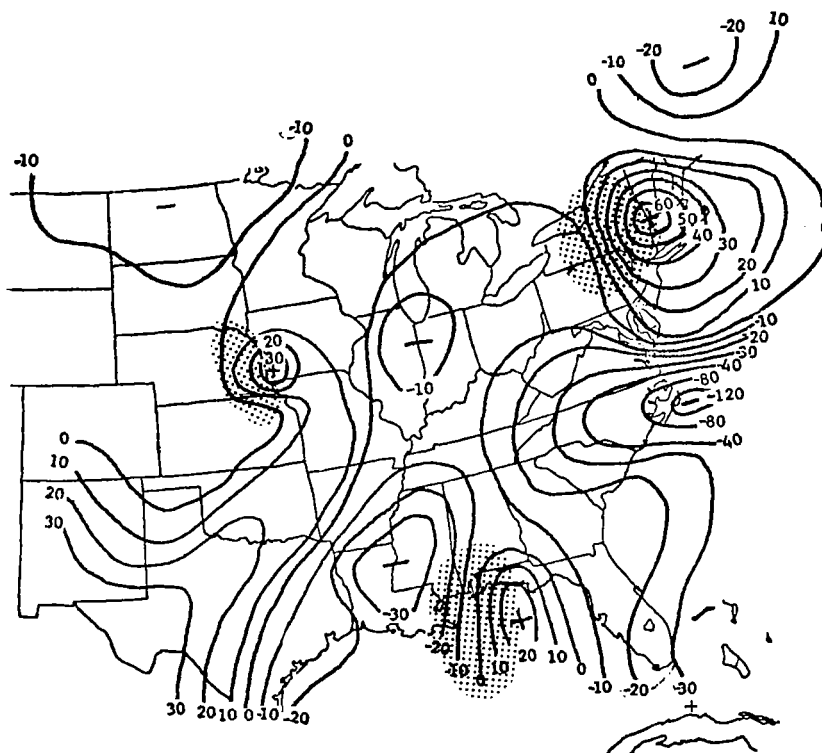
Fig. 7. Analyzed field of K_V at 300 mb for 12Z, 5 December 1969 with regions shaded where $\partial K_v/\partial x$ is large and positive.

The regions of upper-level divergence were then superimposed onto the regions of low-level convergence. Areas where upper-level divergence over-lapped low-level convergence were considered as regions of upward vertical motion through the intermediate layers (Dines' Compensation Principle). From the 850-mb charts, areas in which $T - T_D \leq 5°C$ were obtained and superimposed onto the maps containing convergence and divergence. Areas where upper-level divergence, low-level convergence, and $T - T_D \leq 5°C$ over-lapped were shaded as areas of expected radar echoes.

b. Moisture

The spread of the ambient and dew-point temperatures at 850 mb is used
as an indicator of the amount of moisture in the layer from the surface to
850 mb. The amount of moisture and its distribution with height are close-
ly associated with convective instability. In general, during winter a
larger amount of moisture is required for instability because the tempera-
ture laps rate is smaller than in summer.

c. Stability

During the summer months the number and intensity of mesoscale systems
are closely related to stability. The difference in temperature between
850 and 500 mb is used as a measure of stability in the June case. However,
during the winter months when systems are well developed, strong positive
vertical motion may lead to clouds and precipitation even though the atmo-
sphere may not be convectively unstable.

5. STATISTICAL RELATIONSHIPS BETWEEN MESO- AND SYNOPTIC-SCALE PHENOMENA

This phase of the present research is aimed at establishing relationships on a statistical basis between the gradients of temperature and height taken from analyzed 850-, 500-, and 300-mb charts, and clouds and radar echoes. Specific features of synoptic systems and conditions existing within synoptic systems are not considered.

a. Analysis of Charts and Locations Selected

Synoptic charts from the surface to 200 mb were available from the Texas A&M University Weather Station. Some of these were taken from the Facsimile Network while others were plotted from teletype data and analyzed. Care was taken to assure the best possible analysis for each chart. Radar summary charts were available and a nephanalysis was performed for each time (12-hr intervals) during each period.

Data were extracted from the analyzed maps at 11 locations east of the Rocky Mountains. These stations were chosen because of their location, and without regard to terrain or synoptic conditions. The stations are shown in Fig. 8. Distance between the stations was kept large enough so that a given mesoscale system would not likely affect two or more stations at the same time.

b. Methods of Establishing Relationships

Data were extracted from the 850-, 500-, and 300-mb charts as well as the neph and radar summary charts for each time period at each station. An example of the data extracted from the charts is shown in Table 1 for 00Z, 23 March 1969. A "yes" or "no" was entered in the first three columns when a ceiling (0.6 or greater cloud coverage) or radar echoes were observed within 100 nautical miles of the station. The magnitude of the temperature gradient at the 850-, 500-, and 300-mb levels in units of °C/5°lat (550 km) appears in the next three columns, and the magnitude of the gradient of height in m/5°lat appears in the last three columns. If the gradient of either temperature or height was too small to be determined with reasonable reliability a value was not entered in the table. Three such cases appear in the column of temperature gradient at 300 mb.

Fig. 8. Stations where data were extracted from analyzed charts.

TABLE 1

AN EXAMPLE OF DATA EXTRACTED FROM SYNOPTIC CHARTS

DATE: 23 March 1969   TIME: 00Z

Station	Ceiling ≤10 K ft	Ceiling ≤ 5 K ft	Echoes	$\overrightarrow{\nabla T}_{850}$	$\overrightarrow{\nabla T}_{500}$	$\overrightarrow{\nabla T}_{300}$	$\overrightarrow{\nabla z}_{850}$	$\overrightarrow{\nabla z}_{500}$	$\overrightarrow{\nabla z}_{300}$
317	No	No	No	5	6	8	40	120	210
340	No	No	No	3	5	6	60	80	180
445	No	No	No	6	4	9	85	90	150
429	No	No	No	7	3	6	40	100	140
327	Yes	No	No	6	4	8	20	80	160
311	No	No	No	6	6	7	30	120	240
768	No	No	Yes	6	6	3	45	80	220
213	No	No	No	7	4	4	25	100	200
520	No	No	No	4	4		35	120	150
518	No	No	No	5	3		70	100	120
645	No	No	No	3	4		75	110	180

Scatter diagrams were prepared for various combinations of the gradients of temperature and height when a ceiling was or was not observed as indicated in Table 1, and when radar echoes were or were not observed within 100 nautical miles of each station. Relative frequency distributions were then computed for each variable on each scatter diagram, the linear correlation coefficient was computed between the two variables in each scatter diagram, and a first degree regression line was computed by the method of least squares for each diagram. This information appears adequate to determine whether or not a relationship is likely to exist between various combinations of the gradients of temperature and height, and the presence or absence of ceilings and radar echoes.

c. <u>March Period</u>

1) Radar Echoes/No Echoes versus Gradients of Temperature and Height

Selected scatter diagrams prepared from the data taken from the analyzed charts are shown in Figs. 9-11 when radar echoes were and were not observed within 100 nautical miles of each station for each time period.

For the March period (Fig. 9) a good relationship between the gradients of height at 850 and 500 mb is found when no echoes were present, but the relationship essentially vanishes when echoes were present. The correlation coefficient was 0.55 when echoes were not present as compared with -0.02 when echoes were present. (The statistical significance of the correlation coefficients is considered in Paragraph h.) Similar relationships were found between the gradients at 850 and 300 mb. The relative frequency distributions do not show any preferred peaks in any of these four scatter diagrams (Figs. 9a-9d); however, when echoes were present there were more cases with larger gradients at the 850-mb level than when echoes were not present. Since the gradient of height is proportional to geostrophic wind speed, an increase in wind speed at the 850-mb level is accompanied by an increase in speed at both the 500- and 300-mb levels when no echoes are present, but this is not necessarily the case when echoes are present.

Scatter diagrams showing relationships between the gradient of temperature at 850, 500, and 300 mb are shown in Figs. 9e-9h. The gradient of temperature at 850 mb is correlated with that of 500 mb to the same extent when echoes were or were not present. The correlation between the gradient of temperature at 850 and 300 mb was -0.39 when echoes were not present, and was 0.13 when echoes were present. The relative frequency distributions at 850 and 500 mb were essentially the same when echoes were or were not present, however, the modal value at 300 mb shifted from 6 when no echoes were present to $3°C/5°$lat when echoes were present. Thus, there are two significant features of the gradient of temperature which distinguishes between echoes and no echoes. One is the shift in the modal value of the frequency distributions and the other is the change in the correlations from 0.13 between the gradient of temperature at 850 and that of 300 mb when echoes were observed to -0.39 when no echoes were observed.

2) Ceiling/No Ceiling $\leq$ 5K ft versus Gradients of Temperature and Height

Scatter diagrams for this period are shown in Fig. 10. The correlation coefficients between the gradients of height at 850 and 500 mb shown in Fig. 10a and 10b is 0.47 when no ceilings were present and -0.03 when ceilings were present. The large positive correlation in the first case appears
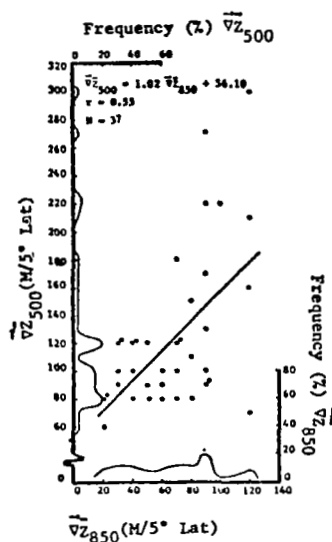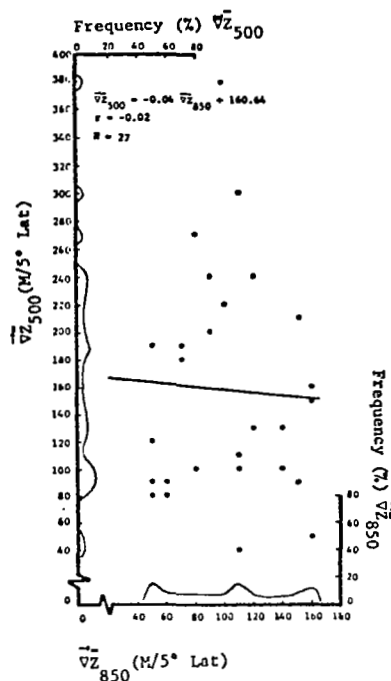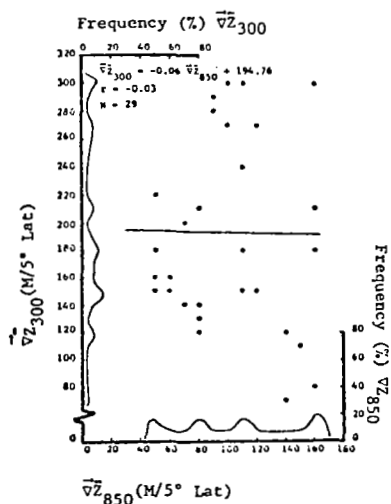
Fig. 9. Radar echoes/no echoes within 100 n mi of selected stations versus gradients of temperature and height at 850, 500, and 300 mb for the March 1969 period.
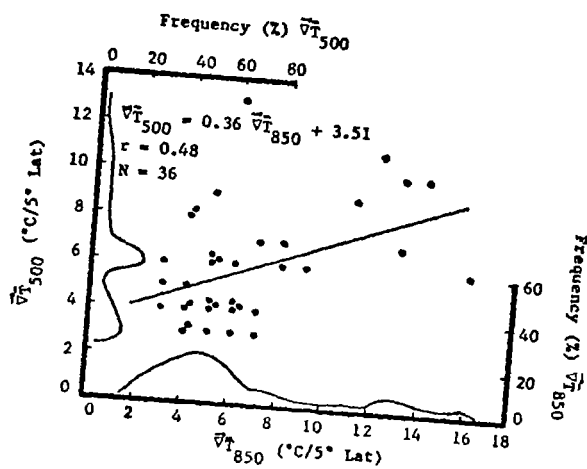
(e)   No Echoes
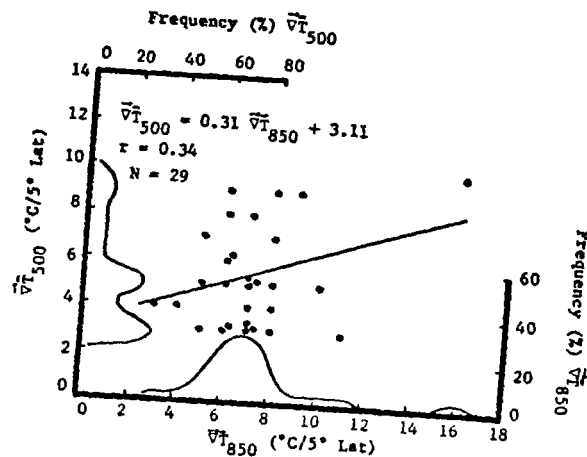
(f)   Echoes

(g)   No Echoes

(h)   Echoes

Fig. 9 continued.

(a) No Ceilings

(b) Ceilings
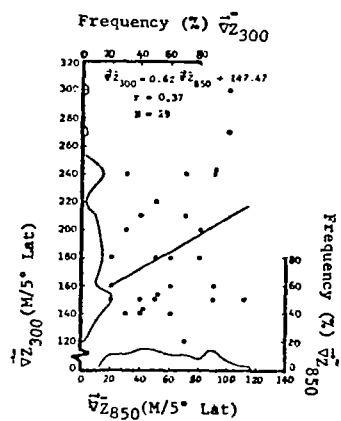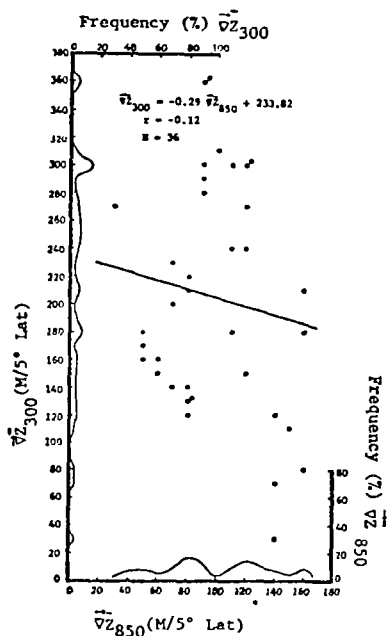
(c) No Ceilings

(d) Ceilings

Fig. 10. Ceiling/no ceiling $\leq$ 5K ft within 100 n mi of selected stations versus gradients of temperature and height at 850, 500, and 300 mb for the March 1969 period.

(e) No Ceilings

(f) Ceilings

(g) No Ceilings

(h) Ceilings

Fig. 10 continued.

to be due primarily to three points which are shown in Fig. 10a. Without
these three points the correlation would be much smaller. An interesting
difference in the frequency distributions of the gradient of height at
500 mb is shown in these two scatter diagrams. When no ceilings were
present a prominent peak appears in the frequency distribution near values
of 80 to 100 m/5°lat with a very small percentage of the points having
values greater than 140. When ceilings were present (Fig. 10b) the fre-
quency distribution does not show any predominant peak and points were
spread nearly equally between values of 40 and 300 m/5°lat. In addition,
the magnitude of the gradient at 850 mb was greater in more cases when
ceilings were present than when they were not present, although the fre-
quency distributions for the 850-mb level in the two cases did not show
any dominant peaks. The greater values of the gradients at both 850 and
500 mb associated with ceiling conditions is to be expected. The greater
gradients imply greater wind speeds which are usually associated with condi-
tions favorable for clouds. The relationship between the gradient of
height at 850 and 300 mb is similar to that between 850 and 500 mb. When
no ceilings were present the correlation coefficient was 0.37 decreasing
to -0.12 when ceilings were present. In these cases, the range in the
magnitude of the gradient at both levels was large although it was somewhat
greater at both the 850- and 300-mb levels when ceilings were present than
when they were not present. The frequency distribution at the 300-mb level
when no ceilings were present shows a grouping of points in the range
between 120 and 250 m/5°lat (Fig. 10c), while there are no significant
peaks in the corresponding frequency distribution when ceilings were
present. The positive correlations between the gradient of height at 850
and that at 500 and 300 mb when no ceilings were present indicates an
increase in wind speed at each of the higher levels corresponding to that
of 850 mb. The near zero or negative correlations between these parameters
when ceilings were present indicates near independence or perhaps a slight
decrease in the gradients at high levels with a corresponding increase at
the 850-mb level. No attempt will be given here to explain the causes of
these relationships, but they are probably related to factors which produce
vertical motion.

Scatter diagrams showing the relationships between the gradient of temperature at 850 mb and that at 500 and 300 mb are shown in Figs. 10e-10h. A positive correlation was found between the gradient of temperature at 850 and 500 mb whether or not ceilings were present, while a negative correlation was found between the gradient of temperature at 850 and 300 mb whether or not ceilings were present. Correlations between the gradient of temperature at 850 and 500 mb were 0.17 and 0.42 for no ceilings and ceilings, respectively. The corresponding values between the gradient of temperature at 850 and 300 mb were -0.20 and -0.24. The frequency distribution of the gradient of temperature at 850 mb did not show any significant difference between the cases, however at 500 mb the peak on the distribution occurred at smaller values when ceilings were present than when they were not present. The same features were observed at 300 mb.

3) Ceiling/No Ceiling $\leq$ 10K ft versus Gradients of Temperature and Height

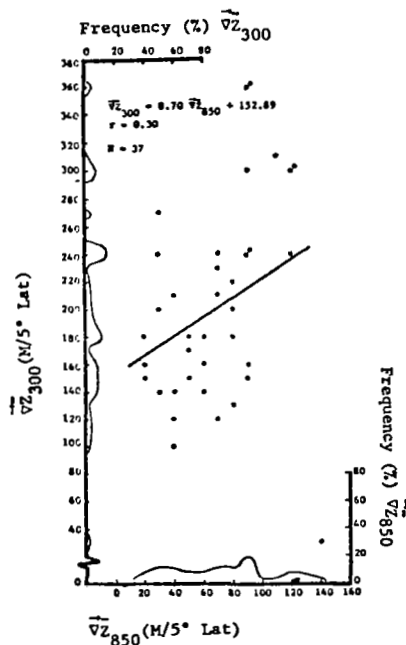The figures in this section are very similar to those presented above except for the limits on height of the ceiling. Scatter diagrams for the March period are shown in Fig. 11. The correlation coefficients between the gradient of height at 850 and 500 mb are 0.25 and 0.39 corresponding to no ceilings and ceilings, respectively. The frequency distributions at either level are not significantly different between the two cases, and hence it is not possible to distinguish between ceilings and no ceilings. The relationships between the gradient of height at 850 and 300 mb do show some significant differences. The correlation coefficients are -0.06 and 0.40 corresponding to no ceilings and ceilings, respectively. The frequency distributions at the 850- and 300-mb levels do not show any significant differences between the two cases and the range of the variables involved appear to be essentially the same in both cases.

Scatter diagrams relating the gradients of temperature at the three levels to ceilings and no ceilings are shown in Figs. 11e-11h. The correlation coefficients between the gradient of temperature at 850 and 500 mb are 0.43 and 0.42 corresponding with no ceilings and ceilings, respectively.

36
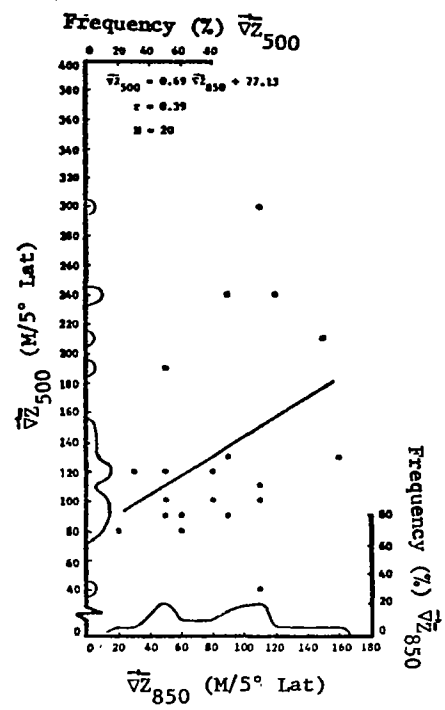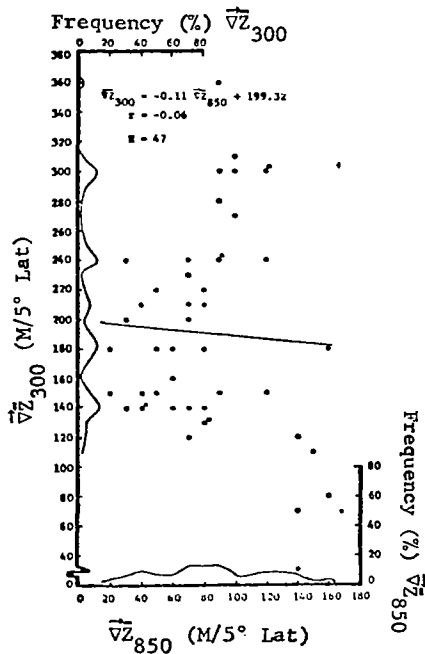
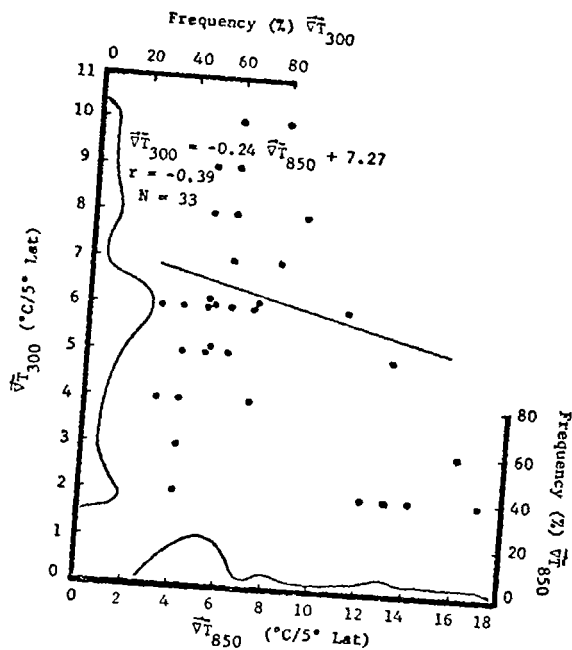Fig. 11. Ceiling/no ceiling ≤ 10K ft within 100 n mi of selected stations versus gradients of temperature and height at 850, 500, and 300 mb for the March 1969 period.
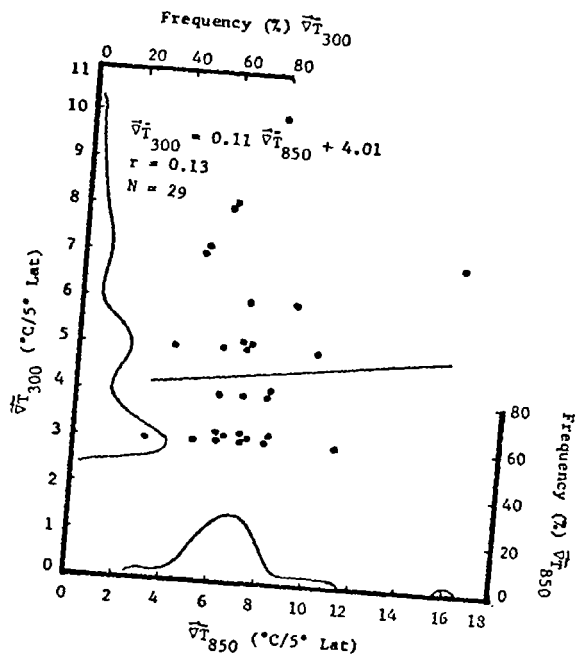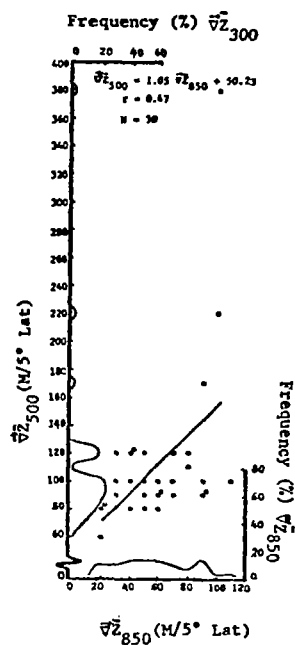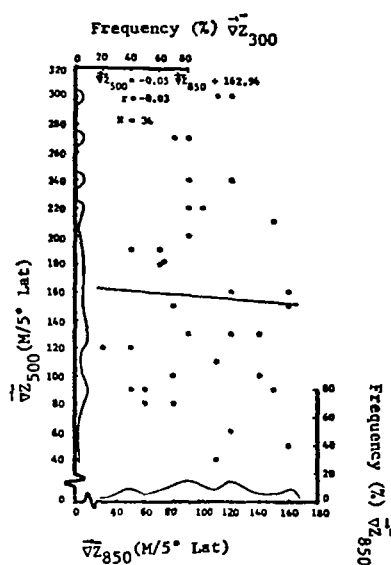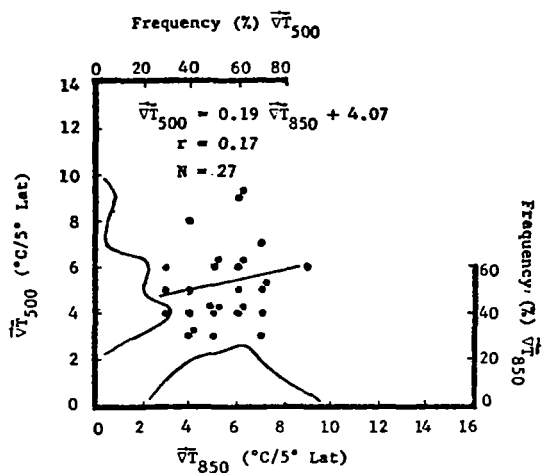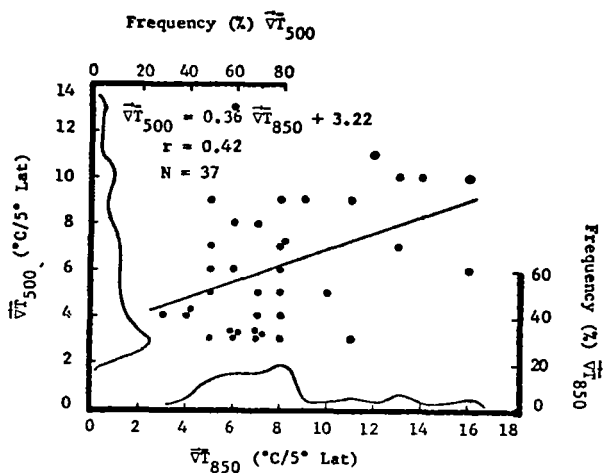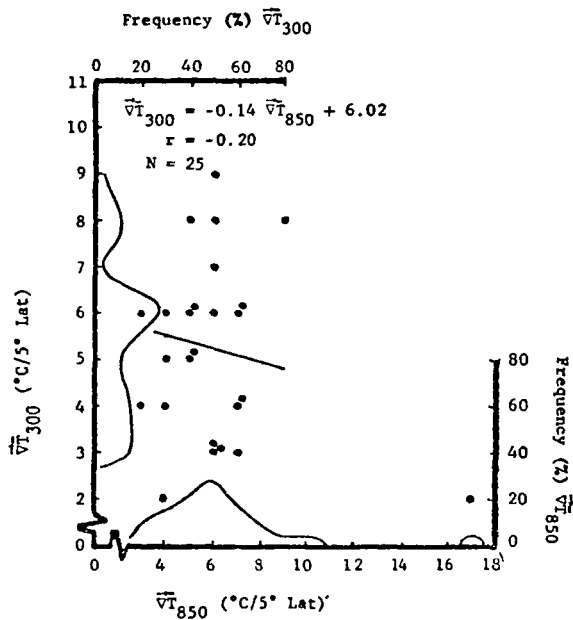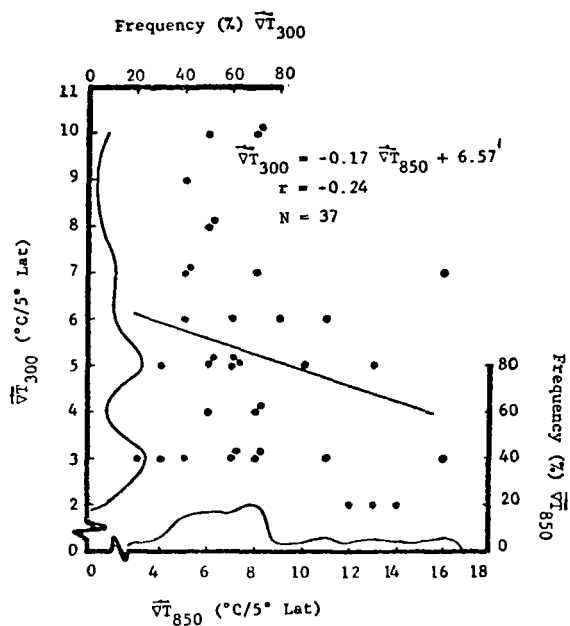
(e)   No Ceilings

(f)   Ceilings

(g)   No Ceilings
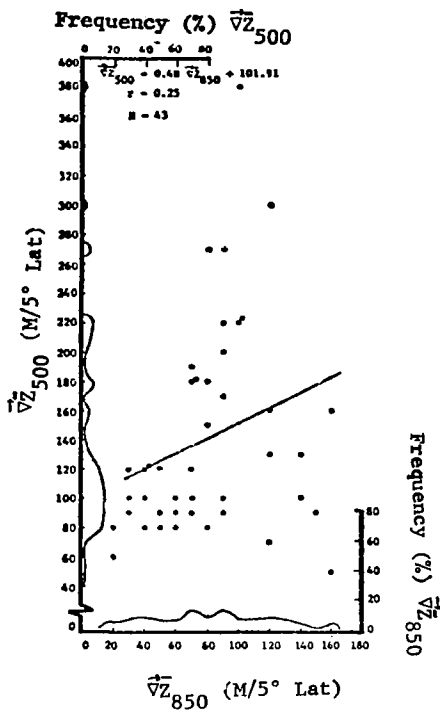

(h)   Ceilings

Fig. 11 continued.

In addition, the frequency distributions do not show any apparent differences. The correlation coefficients between the gradient of temperature at 850 and 300 mb are -0.19 and -0.24 for no ceilings and ceilings, respectively. The differences between the frequency distributions in these two cases do not appear to be significantly different. Thus, the gradients of temperature for this period at 850, 500, and 300 mb do not appear to distinguish between ceiling and no ceiling cases.

d. June Period

1) Radar Echoes/No Echoes versus Gradients of Temperature and Height

During this period the correlation between the gradient of height at 850 and 500 mb was 0.18 when no echoes were observed but increased to 0.64 when echoes were observed within 100 nautical miles of the station (see Fig. 12). The correlations between the gradient of height at 850 and 300 mb follow a similar trend with the correlation coefficients being 0.05 and 0.56 for no echoes and echoes, respectively. The frequency distributions were irregular as shown in Figs. 12a-12d, but there was a tendency for the peaks to shift toward lower values when echoes were present. Thus, there are two features indicated in Figs. 12a-12d which distinguish between echoes and no echoes. One is that the correlation between the gradient of height at 850 mb and that at 500 and 300 mb was positively correlated when echoes were present and the correlation essentially vanished when no echoes were present within 100 nautical miles of the station, and the other feature is that the peaks on the frequency distributions shifted toward lower values when echoes were present as compared to when they were not present. Scatter diagrams showing relationships between the gradient of temperature at 850 mb and that at 500 and 300 mb are shown in Fig. 12e-12h. The correlation coefficient is positive and of approximately the same magnitude in all four figures, hence the gradient of temperature at the various levels does not distinguish between echoes and no echoes. The relative frequency distributions do not show any significant differences between echoes and no echoes.
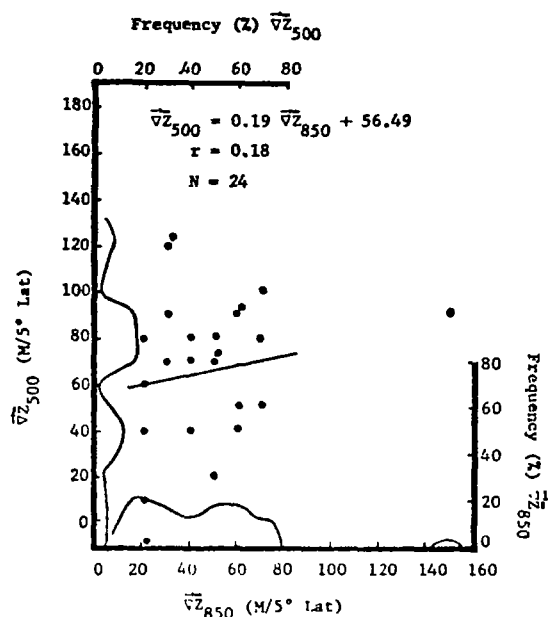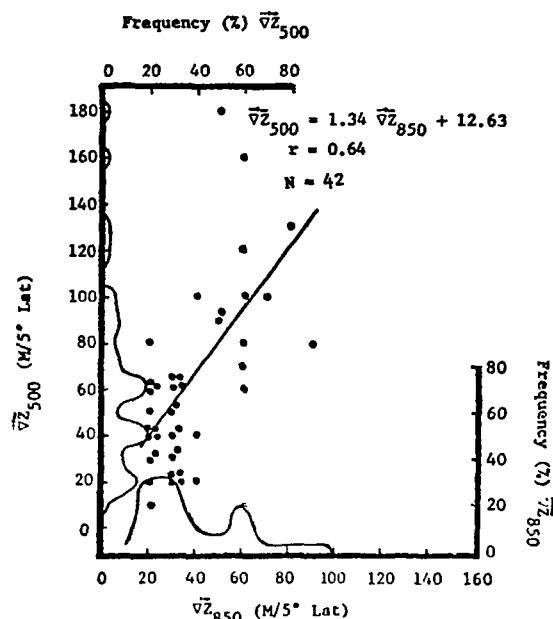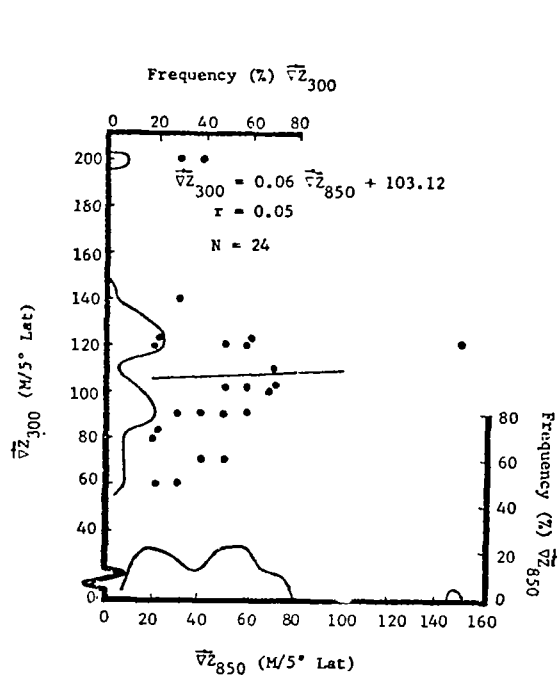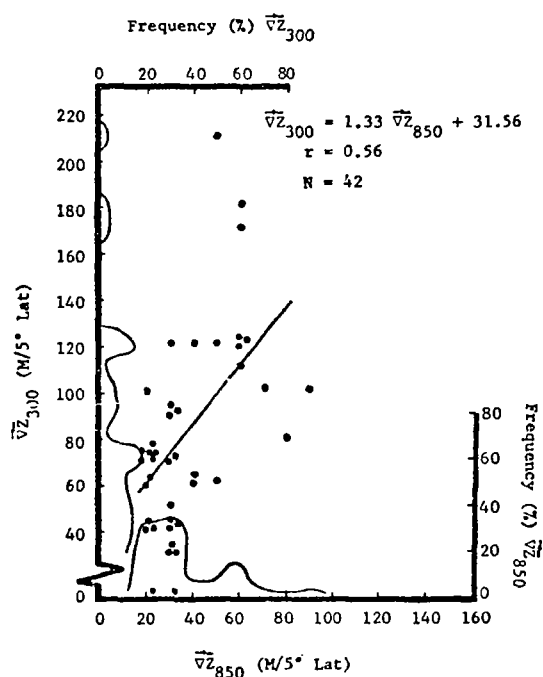
Fig. 12. Radar echoes/no echoes within 100 n mi of selected stations versus gradients of temperature and height at 850, 500, and 300 mb for the June 1969 period.

40

Frequency (%) $\overrightarrow{\nabla T}_{500}$

$\overrightarrow{\nabla T}_{500} = 0.25 \ \overrightarrow{\nabla T}_{850} + 1.80$
$r = 0.54$
$N = 24$

(e)   No Echoes

Frequency (%) $\overrightarrow{\nabla T}_{500}$

$\overrightarrow{\nabla T}_{500} = 0.09 \ \overrightarrow{\nabla T}_{850} + 2.00$
$r = 0.28$
$N = 42$

(f)   Echoes

Frequency (%) $\overrightarrow{\nabla T}_{300}$

$\overrightarrow{\nabla T}_{300} = 0.16 \ \overrightarrow{\nabla T}_{850} + 1.75$
$r = 0.39$
$N = 24$

(g)   No Echoes

Frequency (%) $\overrightarrow{\nabla T}_{300}$

$\overrightarrow{\nabla T}_{300} = 0.11 \ \overrightarrow{\nabla T}_{850} + 2.36$
$r = 0.24$
$N = 42$

(h)   Echoes

Fig. 12 continued.

41

2) Ceiling/No Ceiling ≤ 5K ft versus Gradients of Temperature and Height

Scatter diagrams for this period are shown in Fig. 13. The information presented in this figure is interesting in that all correlation coefficients are positive and most of them quite large. In addition, the frequency distributions of the gradient of height at all three levels (850, 500, and 300 mb) are all irregular and spread out over a wide range of values with no prominent peaks. In all four of the scatter diagrams relating the gradient of temperature at 850 mb and that of 500 and 300 mb with ceilings and no ceilings, all show an increase in the frequency of occurrence of small values at 850 mb, and a peak at 500 and 300 mb in the vicinity of 2-3°C/5°lat. Hence, for the June period there does not appear to be any distinguishing features in the scatter diagrams which differentiate between ceilings and no ceilings.

3) Ceiling/No Ceiling ≤ 10K ft versus Gradients of Temperature and Height

Scatter diagrams for this period are shown in Fig. 14. All correlation coefficients for this period are positive and none of the frequency distributions show any features which distinguish between ceiling and no ceiling cases. The correlation coefficients in Fig. 14 do not show any large differences between no ceiling and ceiling cases. Hence, it is not possible to distinguish between these cases on the basis of the gradient of height or temperature.

e. September Period

1) Radar Echoes/No Echoes versus Gradients of Temperature and Height

Scatter diagrams for this period are shown in Fig. 15. Correlations between the gradient of height at 850 and 500 mb are 0.49 and 0.43 corresponding with no echoes and echoes, respectively. The scatter diagrams are essentially the same for both cases, and there is little distinction between no echoes and echoes in Figs. 15a and 15b. The correlation coefficients between the gradient of height at 850 and 300 mb are 0.21 and 0.36 corresponding to no echoes and echoes, respectively. This difference in

42

(a) Plot (a):

$\overline{\nabla Z}_{500} = 0.70\ \overline{\nabla Z}_{850} + 16.84$

$r = 0.62$

$N = 23$

Axes: $\overline{\nabla Z}_{500}$ (M/5° Lat); $\overline{\nabla Z}_{850}$ (M/5° Lat); Frequency (%) $\overline{\nabla Z}_{850}$

(b) Plot (b):

$\overline{\nabla Z}_{500} = 1.01\ \overline{\nabla Z}_{850} + 30.51$

$r = 0.52$

$N = 31$

Axes: $\overline{\nabla Z}_{500}$ (M/5° Lat); $\overline{\nabla Z}_{850}$ (M/5° Lat); Frequency (%) $\overline{\nabla Z}_{850}$
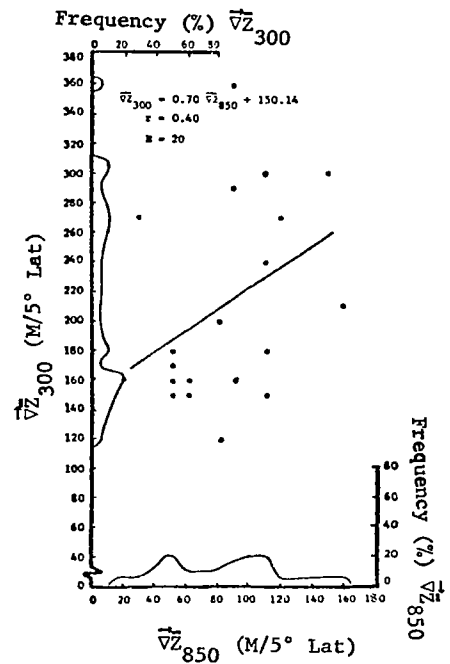
(a) No Ceilings   (b) Ceilings

(c) Plot (c):

$\overline{\nabla Z}_{300} = 0.75\ \overline{\nabla Z}_{850} + 47.64$

$r = 0.47$

$N = 24$

Axes: $\overline{\nabla Z}_{300}$ (M/5° Lat); $\overline{\nabla Z}_{850}$ (M/5° Lat); Frequency (%) $\overline{\nabla Z}_{850}$

(d) Plot (d):

$\overline{\nabla Z}_{300} = 0.86\ \overline{\nabla Z}_{850} + 59.63$

$r = 0.42$

$N = 31$

Axes: $\overline{\nabla Z}_{300}$ (M/5° Lat); $\overline{\nabla Z}_{850}$ (M/5° Lat); Frequency (%) $\overline{\nabla Z}_{850}$
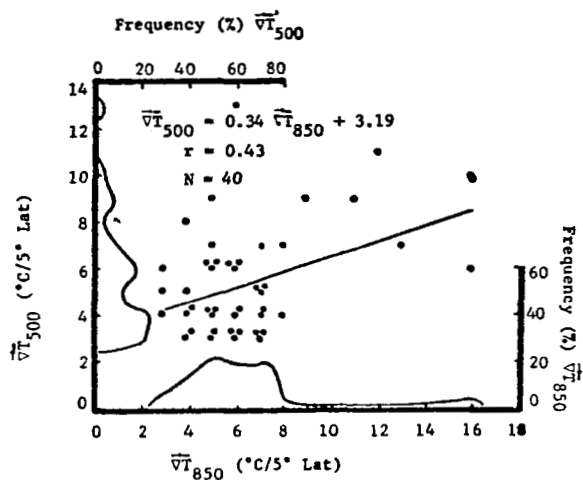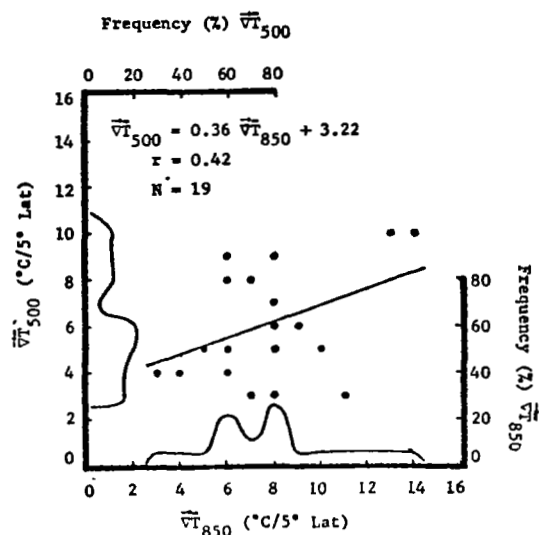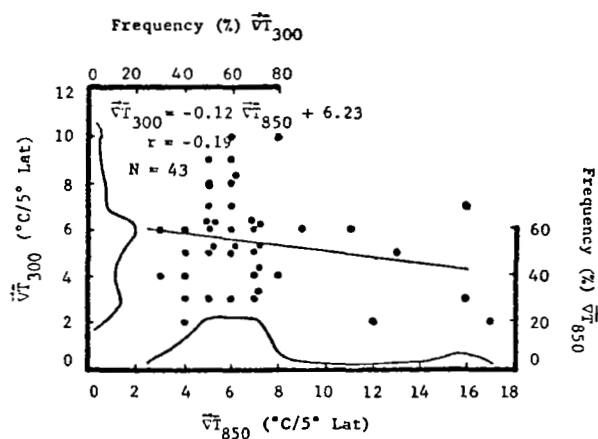
(c) No ceilings   (d) Ceilings

Fig. 13. Ceiling/no ceiling $\leq$ 5K ft within 100 n mi of selected stations versus gradients of temperature and height at 850, 500, and 300 mb for the June 1969 period.
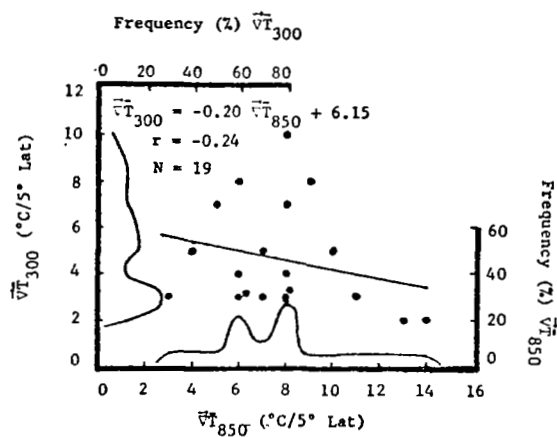
Frequency (%) $\vec{\nabla T}_{500}$

$\vec{\nabla T}_{500} = 0.14\ \vec{\nabla T}_{850} + 2.07$
r = 0.24
N = 24

$\vec{\nabla T}_{500}$ (°C/5° Lat)

$\vec{\nabla T}_{850}$ (°C/5° Lat)

Frequency (%) $\vec{\nabla T}_{850}$

(e) No Ceilings

Frequency (%) $\vec{\nabla T}_{500}$

$\vec{\nabla T}_{500} = 0.15\ \vec{\nabla T}_{850} + 1.97$
r = 0.45
N = 31

$\vec{\nabla T}_{500}$ (°C/5° Lat)

$\vec{\nabla T}_{850}$ (°C/5° Lat)

Frequency (%) $\vec{\nabla T}_{850}$

(f) Ceilings

Frequency (%) $\vec{\nabla T}_{300}$

$\vec{\nabla T}_{300} = 0.24\ \vec{\nabla T}_{850} + 1.67$
r = 0.36
N = 24

$\vec{\nabla T}_{300}$ (°C/5° Lat)

$\vec{\nabla T}_{850}$ (°C/5° Lat)

Frequency (%) $\vec{\nabla T}_{850}$

(g) No ceilings

Frequency (%) $\vec{\nabla T}_{300}$

$\vec{\nabla T}_{300} = 0.06\ \vec{\nabla T}_{850} + 2.35$
r = 0.19
N = 31

$\vec{\nabla T}_{300}$ (°C/5° Lat)

$\vec{\nabla T}_{850}$ (°C/5° Lat)

Frequency (%) $\vec{\nabla T}_{850}$

(h) Ceilings

Fig. 13 continued.

44

Fig. 14. Ceiling/no ceiling ≤ 10K ft within 100 n mi of selected stations versus gradients of temperature and height at 850, 500, and 300 mb for the June 1969 period.

Frequency (%) $\overrightarrow{\nabla T}_{500}$

0 20 40 60 80

$\overrightarrow{\nabla T}_{500} = 0.19\ \overrightarrow{\nabla T}_{850} + 2.00$
r = 0.43
N = 35

$\overrightarrow{\nabla T}_{500}$ (°C/5° Lat)

Frequency (%) $\overrightarrow{\nabla T}_{850}$

$\overrightarrow{\nabla T}_{850}$ (°C/5° Lat)

(e) No Ceilings

Frequency (%) $\overrightarrow{\nabla T}_{500}$

0 20 40 60 80

$\overrightarrow{\nabla T}_{500} = 0.14\ \overrightarrow{\nabla T}_{850} + 1.89$
r = 0.37
N = 20

$\overrightarrow{\nabla T}_{500}$ (°C/5° Lat)

Frequency (%) $\overrightarrow{\nabla T}_{850}$

$\overrightarrow{\nabla T}_{850}$ (°C/5° Lat)

(f) Ceilings

Frequency (%) $\overrightarrow{\nabla T}_{300}$

0 20 40 60

$\overrightarrow{\nabla T}_{300} = 0.18\ \overrightarrow{\nabla T}_{850} + 1.97$
r = 0.29
N = 34

$\overrightarrow{\nabla T}_{300}$ (°C/5° Lat)

Frequency (%) $\overrightarrow{\nabla T}_{850}$

$\overrightarrow{\nabla T}_{850}$ (°C/5° Lat)

(g) No Ceilings

Frequency (%) $\overrightarrow{\nabla T}_{300}$

0 20 40 60

$\overrightarrow{\nabla T}_{300} = 0.03\ \nabla T_{850} + 2.26$
r = 0.09
N = 20

$\overrightarrow{\nabla T}_{300}$ (°C/5° Lat)

Frequency (%) $\overrightarrow{\nabla T}_{850}$

$\overrightarrow{\nabla T}_{850}$ (°C/5° Lat)

(h) Ceilings

Fig. 14 continued.
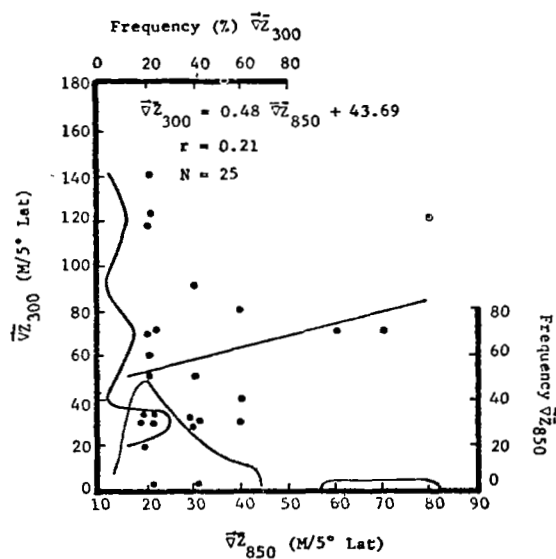
46

Fig. 15. Radar echoes/no echoes within 100 n mi of selected stations versus gradients of temperature and height at 850, 500, and 300 mb for the September 1969 period.

47

Frequency (%) $\vec{\nabla}\bar{T}_{500}$

0   20   40   60

$$\vec{\nabla}\bar{T}_{500} = 0.19\ \vec{\nabla}\bar{T}_{850} + 1.73$$
$$r = 0.19$$
$$N = 27$$

$\vec{\nabla}\bar{T}_{500}$ (°C/5° Lat)

Frequency (%) $\vec{\nabla}\bar{T}_{850}$

$\vec{\nabla}\bar{T}_{850}$ (°C/5° Lat)

(e)   No Echoes

Frequency (%) $\vec{\nabla}\bar{T}_{500}$

0   20   40   60   80

$$\vec{\nabla}\bar{T}_{500} = 0.73\ \vec{\nabla}\bar{T}_{850} + 0.27$$
$$r = 0.81$$
$$N = 27$$

$\vec{\nabla}\bar{T}_{500}$ (°C/5° Lat)

Frequency (%) $\vec{\nabla}\bar{T}_{850}$

$\vec{\nabla}\bar{T}_{850}$ (°C/5° Lat)

(f)   Echoes

Frequency (%) $\vec{\nabla}\bar{T}_{300}$

0   20   40   60

$$\vec{\nabla}\bar{T}_{300} = 0.01\ \vec{\nabla}\bar{T}_{850} + 2.47$$
$$r = 0.01$$
$$N = 28$$

$\vec{\nabla}\bar{T}_{300}$ (°C/5° Lat)

Frequency (%) $\vec{\nabla}\bar{T}_{850}$

$\vec{\nabla}\bar{T}_{850}$ (°C/5° Lat)

(g)   No Echoes

Frequency (%) $\vec{\nabla}\bar{T}_{300}$

0   20   40   60   80

$$\vec{\nabla}\bar{T}_{300} = 0.53\ \vec{\nabla}\bar{T}_{850} + 1.24$$
$$r = 0.64$$
$$N = 25$$

$\vec{\nabla}\bar{T}_{300}$ (°C/5° Lat)

Frequency (%) $\vec{\nabla}\bar{T}_{850}$

$\vec{\nabla}\bar{T}_{850}$ (°C/5° Lat)

(h)   Echoes

Fig. 15 continued.

48

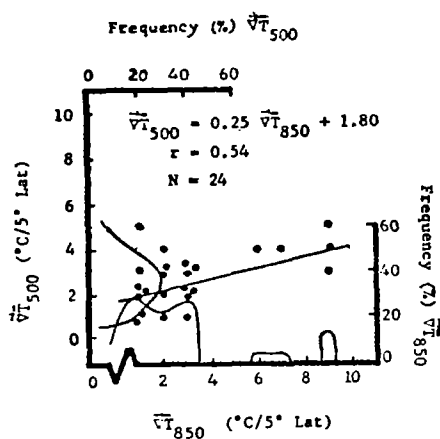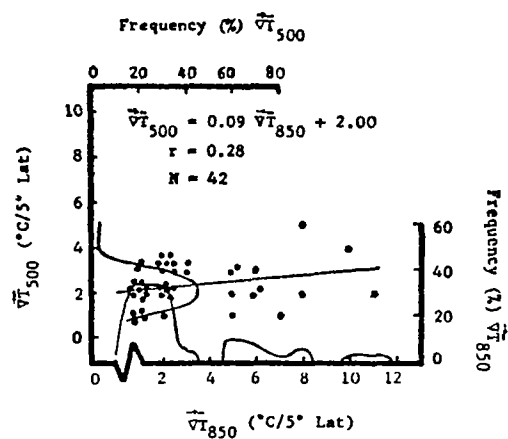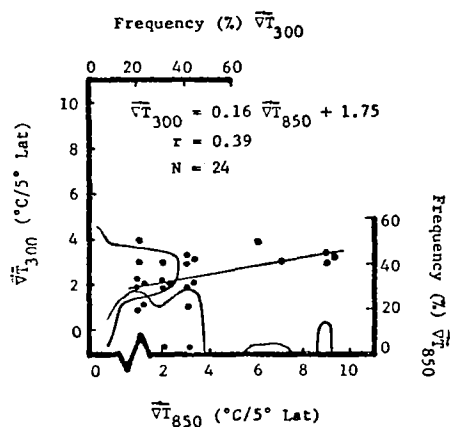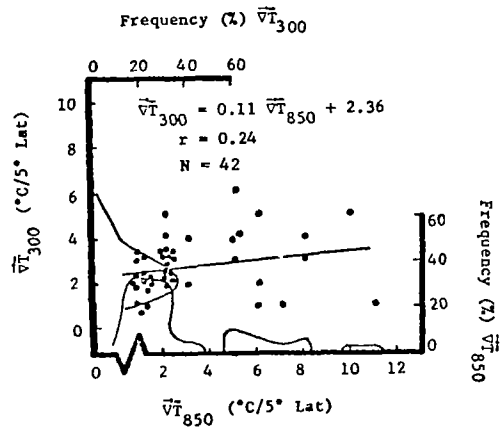the correlation coefficient is not sufficient to distinguish between echoes and no echoes, and neither are the frequency distributions shown in Figs. 15c and 15d. Thus, during this period, the gradient of height at the different levels do not distinguish between echoes and no echoes.

Scatter diagrams relating the gradient of temperature at the different pressure surfaces to echoes and no echoes are shown in Figs. 15e-15h. The correlations between the gradient of temperature at 850 and 500 mb for no echoes and echoes are 0.19 and 0.81, respectively. While the frequency distributions are similar in both cases, the differences in the correlations provide a basis for distinguishing between echoes and no echoes. The correlations between the gradient of temperature at 850 and 300 mb are 0.01 and 0.64 for no echoes and echoes, respectively. The frequency distribution of the gradient of temperature at 300 mb shows a peak at higher values of the gradient when echoes occurred than when they did not occur, but otherwise the frequency distributions of the gradient of temperature at the various levels do not distinguish between echoes and no echoes.
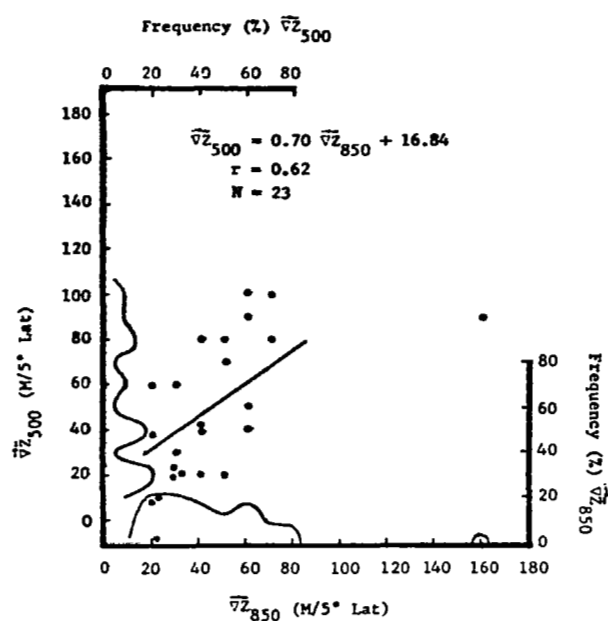
2) Ceiling/No Ceiling ≤ 5K ft versus Gradients of Temperature and Height

Scatter diagrams for the September period are shown in Fig. 16. The correlation between the gradient of height at 850 and 500 mb when no ceilings were observed is essentially zero and increases to 0.25 when ceilings were present. The frequency distributions do not show any significant difference in these two cases except that a greater number of cases were observed with higher values of the gradient at 500 mb when ceilings were present than when they were not present. The correlation coefficients between the gradient of height at 850 and 300 mb were 0.50 with no ceilings and 0.21 with ceilings. There are no significant differences in the frequency distributions in these two cases and, hence, there does not appear to be any feature which distinguishes between ceilings and no ceilings in these cases.

The correlation coefficients between the gradient of temperature at 850 mb and that at 500 and 300 mb appears to distinguish well between ceilings and no ceilings. The correlation coefficients between the
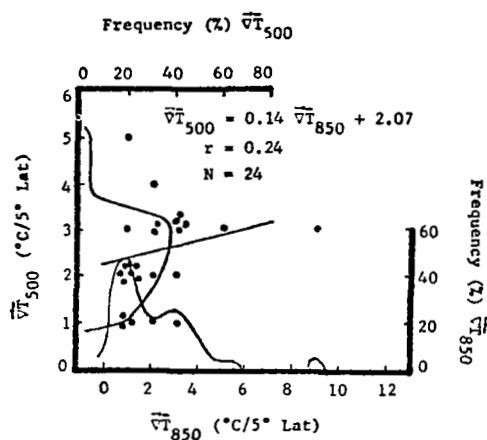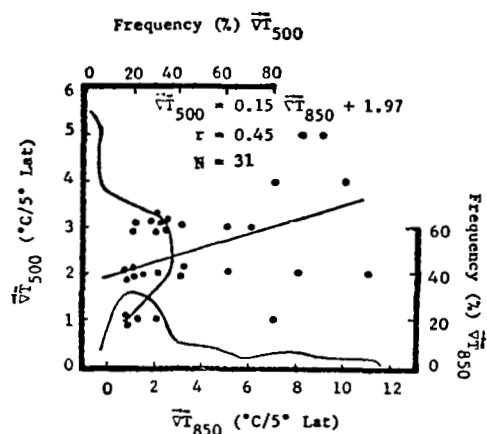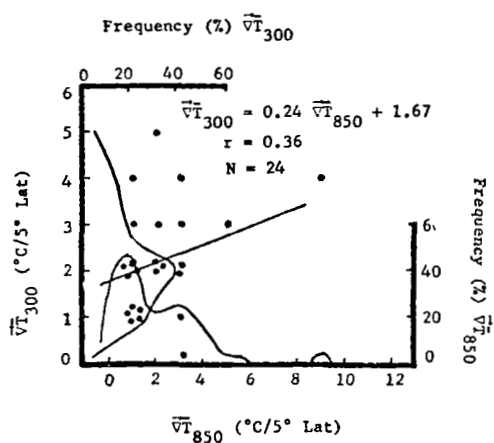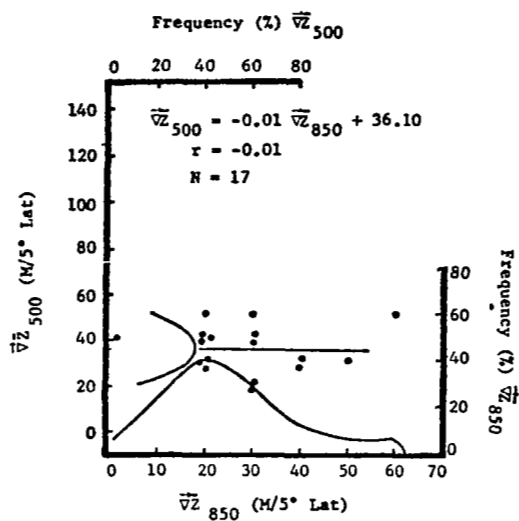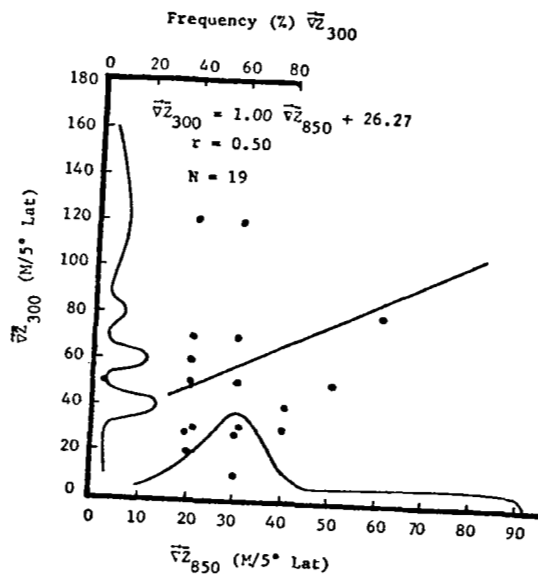
Fig. 16.   Ceiling/no ceiling ≤ 5K fṭ within 100 n mi of selected stations versus gradients of temperature and height at 850, 500, and 300 mb for the September 1969 period.
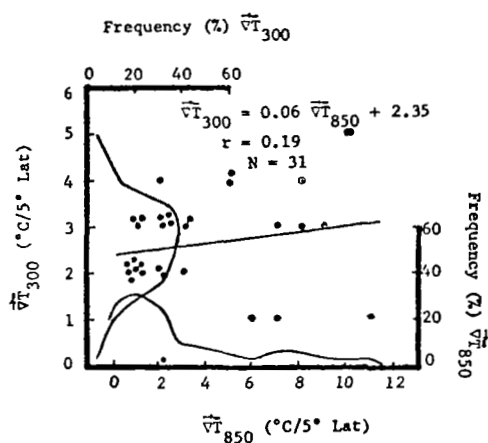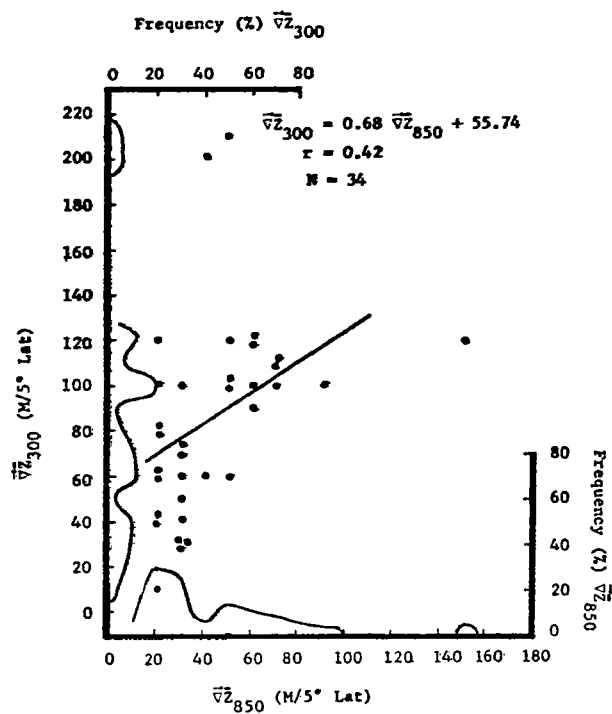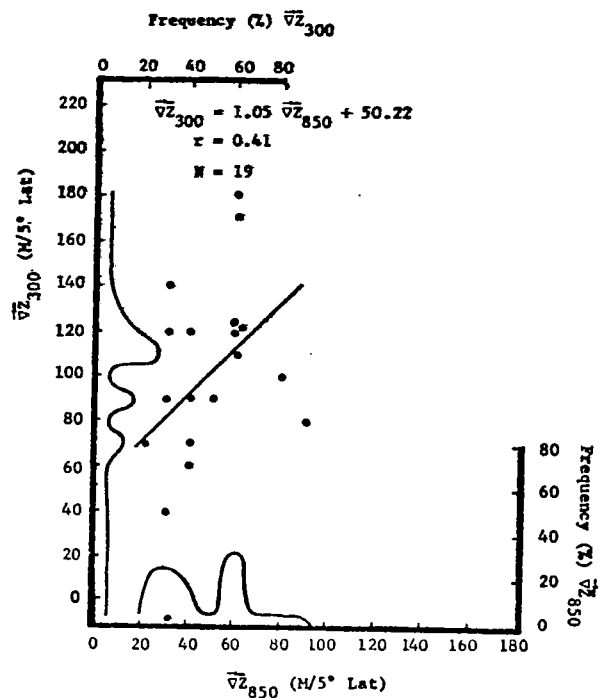
(e) No Ceilings

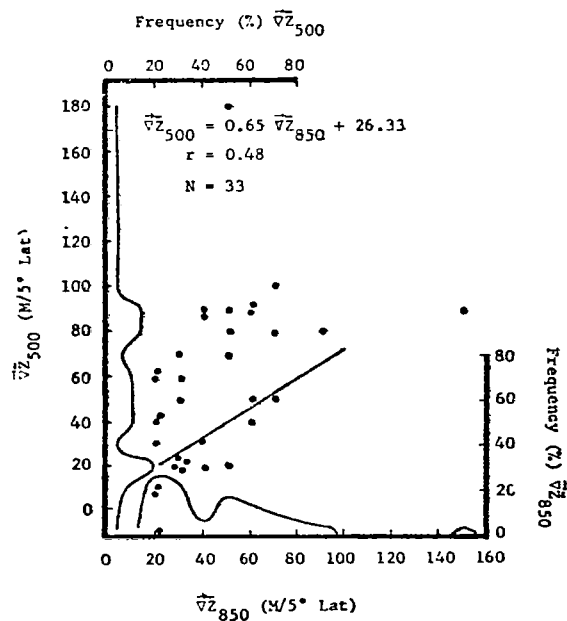(f) Ceilings

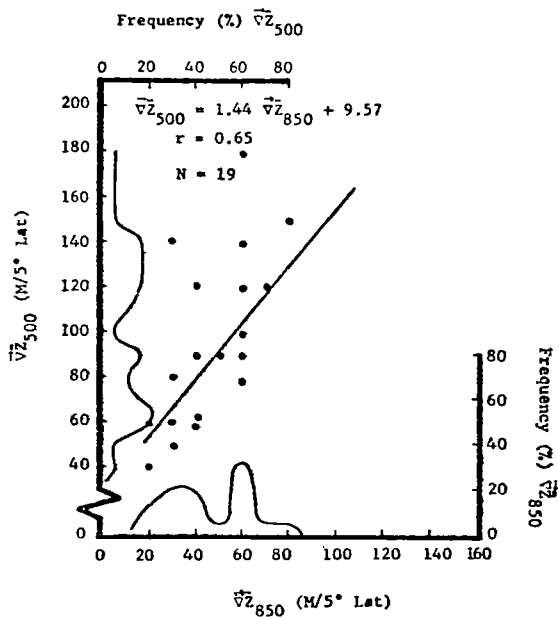(g) No Ceilings

(h) Ceilings

Fig. 16 continued.

51

gradient of temperature at 850 and 500 mb were 0.12 and 0.76 corresponding to no ceilings and ceilings, respectively, while between the 850 and 300 mb levels, they were -0.15 and 0.69 with no ceilings and ceilings, respectively. The frequency distributions did not show any significant differences between no ceiling and ceiling cases.

   3) Ceiling/No Ceiling $\leq$ 10K ft versus Gradients of Temperature and Height

Scatter diagrams for this period are shown in Fig. 17. The correlation coefficients between the gradient of height at 850 and 500 mb are 0.35 and -0.21 corresponding to no ceilings and ceilings, respectively. While the frequency distributions do not show any apparently significant differences between these two categories, the correlation coefficients are considerably different. This difference in the correlation coefficients is not observed between the gradient of height at 850 and 300 mb, where the correlation coefficients are 0.23 and 0.41 for no ceilings and ceilings, respectively. Again, the frequency distributions do not show any significant differences between the two categories.

The correlation coefficients between the gradient of temperature at 850 and that at 500 and 300 mb are all positive and about the same magnitude. The frequency distributions do not show any distinguishing features, and hence the gradient of temperature does not distinguish between ceiling and no ceiling conditions.

f.   December Period

   1) Radar Echoes/No Echoes versus Gradients of Temperature and Height

Scatter diagrams for this period are shown in Fig. 18. Correlations between the gradient of height at 850 mb and that at 500 and 300 mb is near 0.4 to 0.5 in Figs. 18a-18d, and the frequency distributions do not show any preferred peaks. Thus, the gradient of height at the levels examined do not distinguish between echoes and no echoes.

The correlations between the gradient of temperature at the 850- and 500-mb levels are -0.48 and 0.23 corresponding to no echoes and echoes, respectively. This change in the correlation coefficient distinguishes between no echoes and echoes, however the frequency distributions are
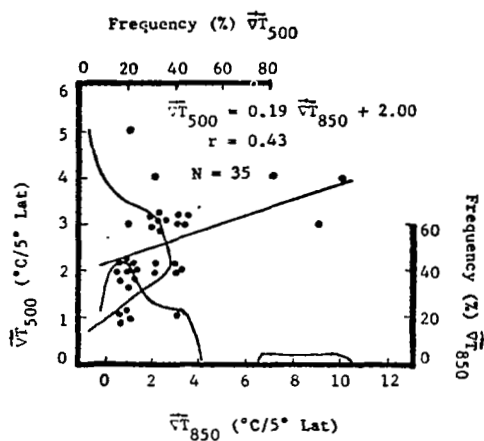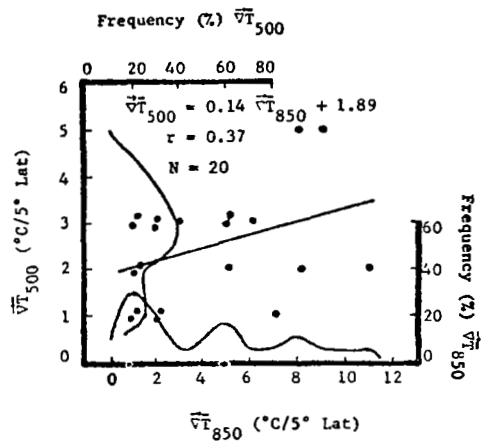
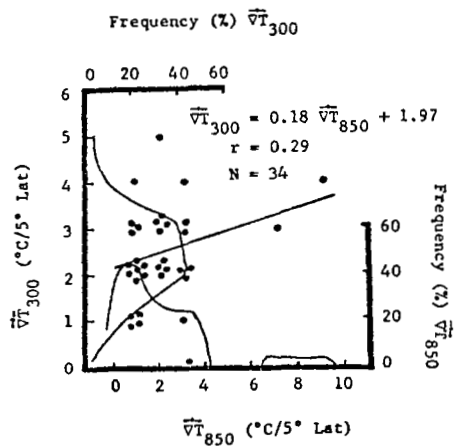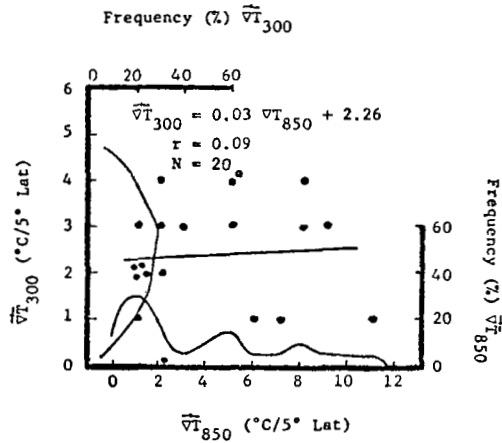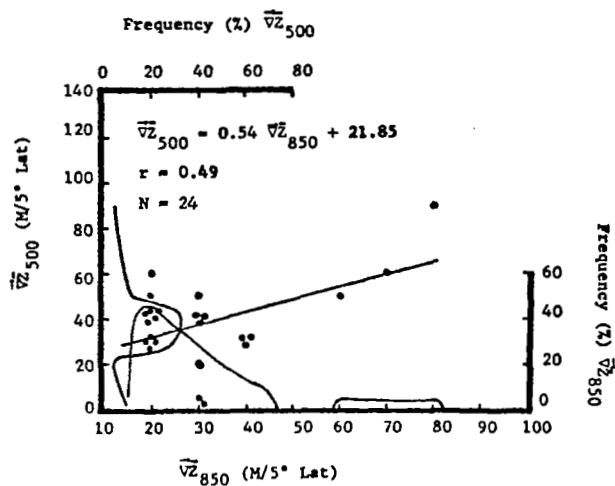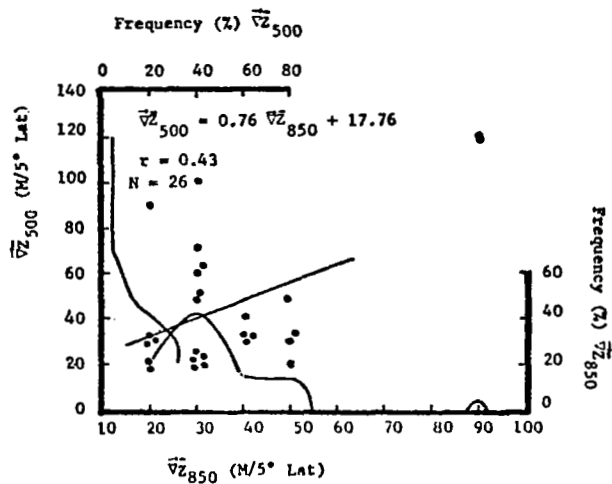(a) No Ceilings

(b) Ceilings

(c) No Ceilings

(d) Ceilings

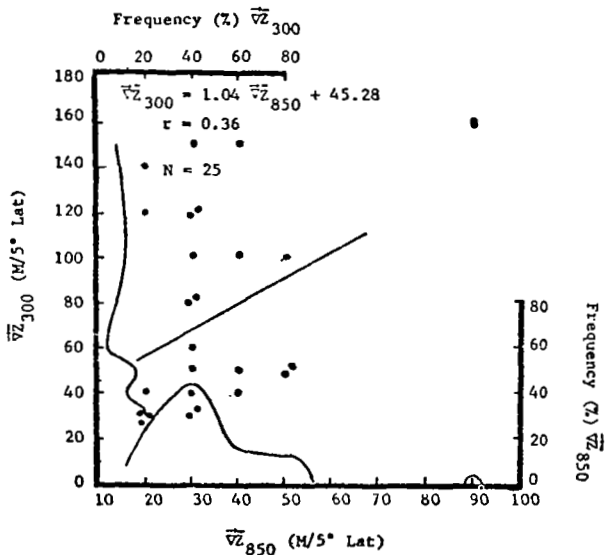Fig. 17.   Ceiling/no ceiling ≤ 10K ft within 100 n mi of selected stations versus gradients of temperature and height at 850, 500, and 300 mb for the September 1969 period.

Frequency (%) $\vec{\nabla T}_{500}$

$\overline{\vec{\nabla T}}_{500} = 0.53\ \overline{\vec{\nabla T}}_{850} + 0.74$
r = 0.46
N = 32

$\overline{\vec{\nabla T}}_{500}$ (°C/5° Lat)

Frequency (%) $\overline{\vec{\nabla T}}_{850}$

$\overline{\vec{\nabla T}}_{850}$ (°C/5° Lat)

(e)   No Ceilings

Frequency (%) $\vec{\nabla T}_{500}$

$\overline{\vec{\nabla T}}_{500} = 0.61\ \overline{\vec{\nabla T}}_{850} + 0.68$
r = 0.71
N = 22

$\overline{\vec{\nabla T}}_{500}$ (°C/5° Lat)

Frequency (%) $\overline{\vec{\nabla T}}_{850}$

$\overline{\vec{\nabla T}}_{850}$ (°C/5° Lat)

(f)   Ceilings

Frequency (%) $\vec{\nabla T}_{300}$

$\overline{\vec{\nabla T}}_{300} = 0.65\ \overline{\vec{\nabla T}}_{850} + 0.94$
r = 0.54
N = 31

$\overline{\vec{\nabla T}}_{300}$ (°C/5° Lat)

Frequency (%) $\overline{\vec{\nabla T}}_{850}$

$\overline{\vec{\nabla T}}_{850}$ (°C/5° Lat)

(g)   No Ceilings

Frequency (%) $\vec{\nabla T}_{300}$

$\overline{\vec{\nabla T}}_{300} = 0.53\ \overline{\vec{\nabla T}}_{850} + 0.34$
r = 0.62
N = 22

$\overline{\vec{\nabla T}}_{300}$ (°C/5° Lat)

Frequency (%) $\overline{\vec{\nabla T}}_{850}$

$\overline{\vec{\nabla T}}_{850}$ (°C/5° Lat)

(h)   Ceilings

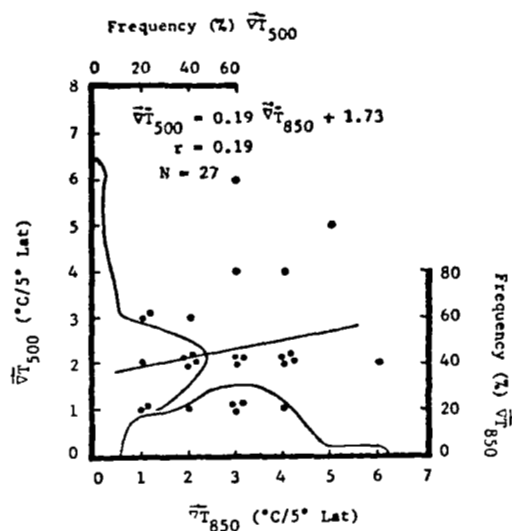Fig. 17 continued.

54

(a) No echoes
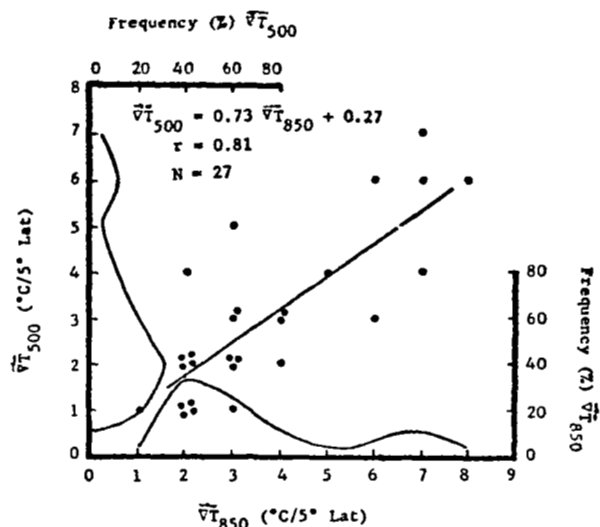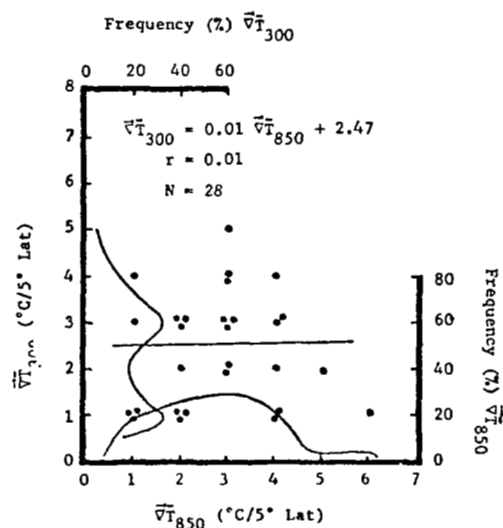
(b) Echoes

(c) No Echoes

(d) Echoes

Fig. 18. Radar echoes/no echoes within 100 n mi of selected stations versus gradients of temperature and height at 850, 500, and 300 mb for the December 1969 period.
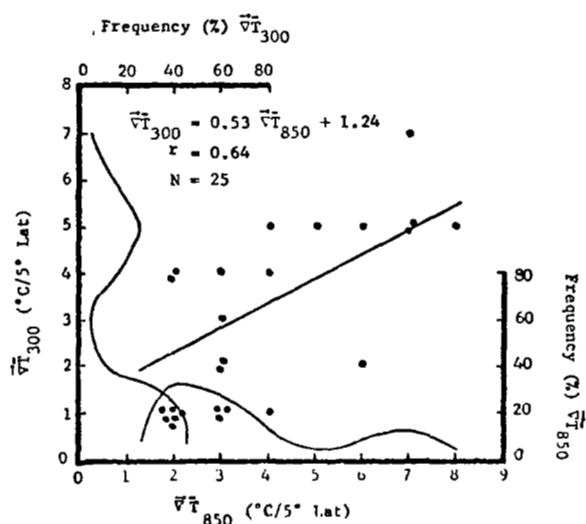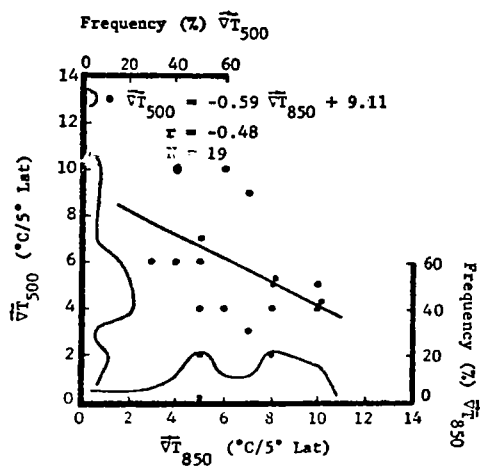
(e) No echoes
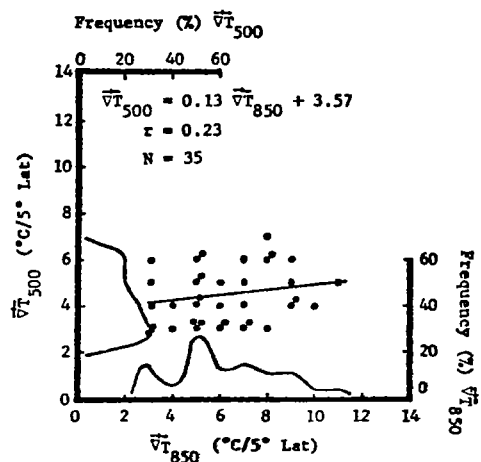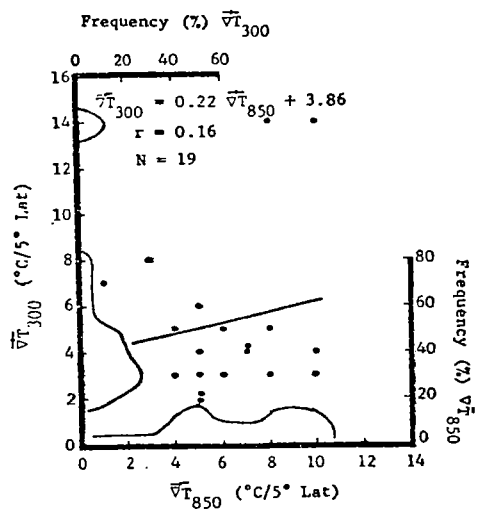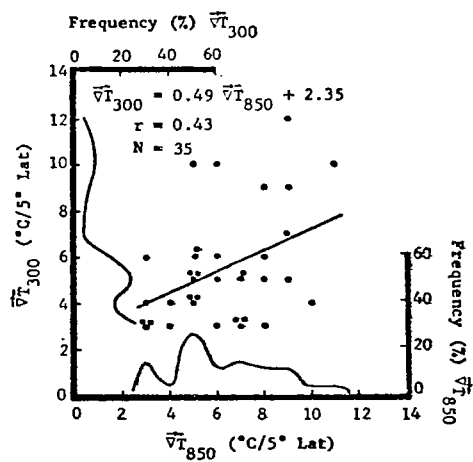
(f) Echoes

(g) No Echoes

(h) Echoes

Fig. 18 continued.

56

irregular and with peaks in the same relative positions in the two cases. The correlation coefficients between the gradient of temperature at 850 and 300 mb are 0.16 and 0.43 for no echoes and echoes, respectively. The frequency distributions for the 850-mb level show an increase in the percentage of occurrence at higher values of the gradient in the case of no echoes as compared with echoes. It appears that the major factor distinguishing echoes from no echoes in Figs. 18e-18h is the correlation between the gradient of temperature at 850 and that of 500 mb.
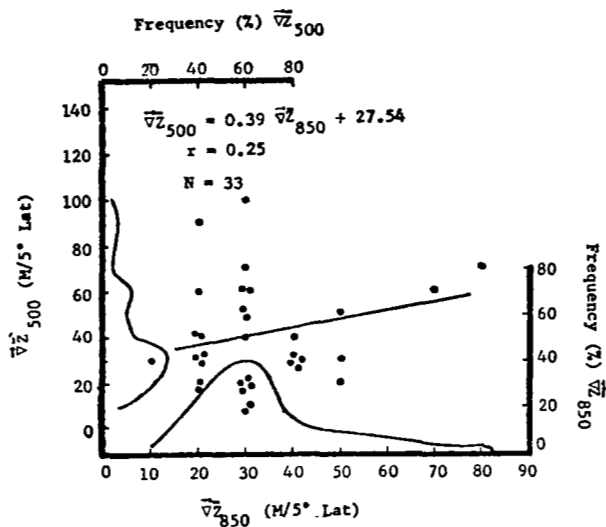
2) Ceiling/No Ceiling ≤ 5K ft versus Gradients of Temperature and Height

Scatter diagrams for this period are shown in Fig. 19. The correlations between the gradient of height at 850 and that at 500 and 300 mb is positive in all four cases with ceilings and no ceilings, and range in values between about 0.2 and 0.3. There are two apparently significant differences in the frequency distributions between no ceiling and ceiling cases. The frequency distribution of the gradient of height at 850 mb for the no ceiling cases shows a peak at values between 20 and 40 m/5°lat, whereas in the ceiling cases the distributions do not show a preferred peak. In addition, the range of the magnitude of the gradient of height at all three levels was greater when ceilings were present than when they were not present.

The scatter diagrams relating the gradient of temperature at 850 to that at 500 and 300 mb are shown in Figs. 19e-19h. The correlation coefficients between the gradient of temperature at 850 and 500 mb are 0.01 and 0.24 with no ceilings and ceilings, respectively, while the corresponding values between 850 and 300 mb are 0.49 and 0.21. The frequency distributions show peaks at both 500 and 300 mb between 2 and 7°C/5°lat with ceilings, however the distributions are more spread out in the no ceiling cases.

3) Ceiling/No Ceiling ≤ 10K ft versus Gradients of Temperature and Height

Scatter diagrams for this period are shown in Fig. 20. The correlation coefficients between the gradient of temperature at 850 and 500 mb are 0.20 and 0.44 for no ceilings and ceilings, respectively. The frequency
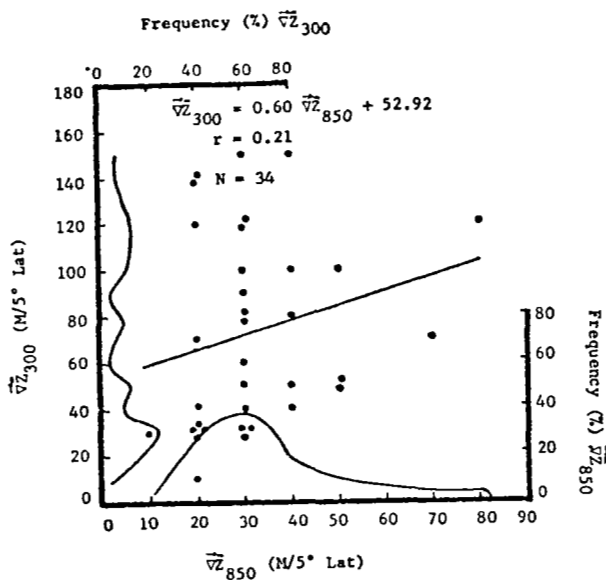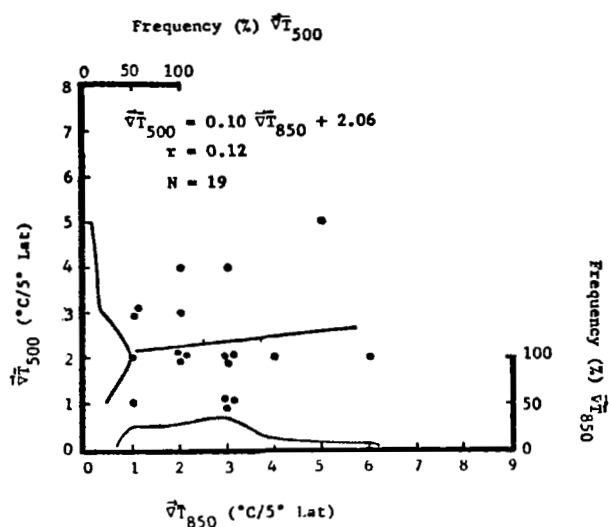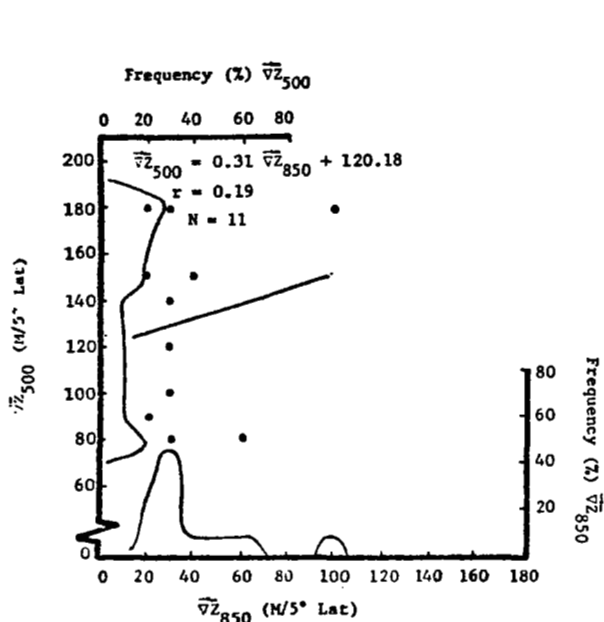
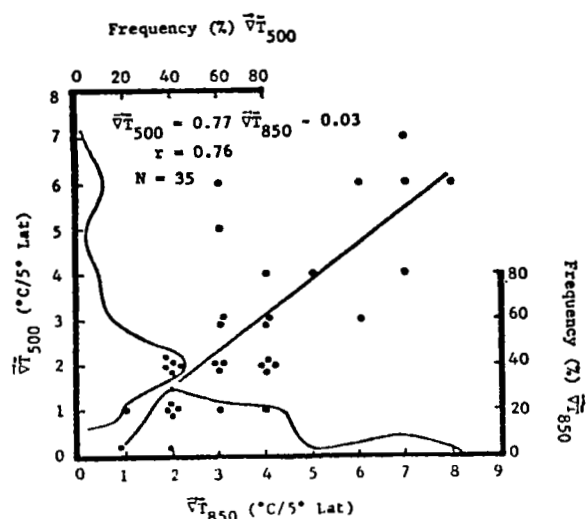(a) No Ceilings
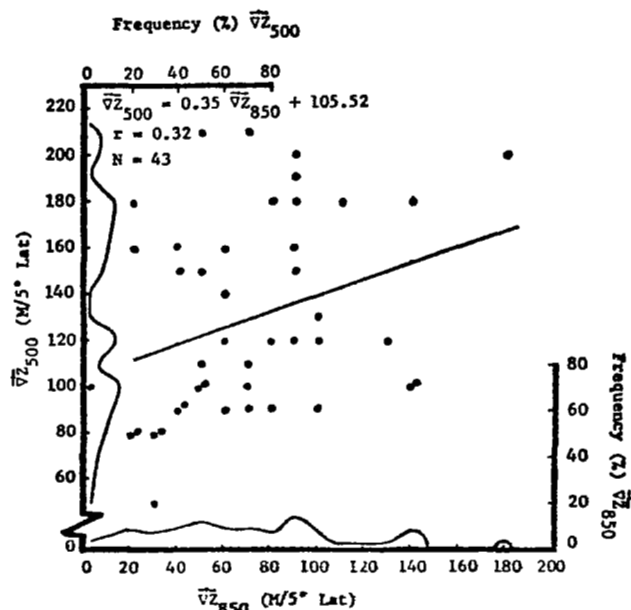
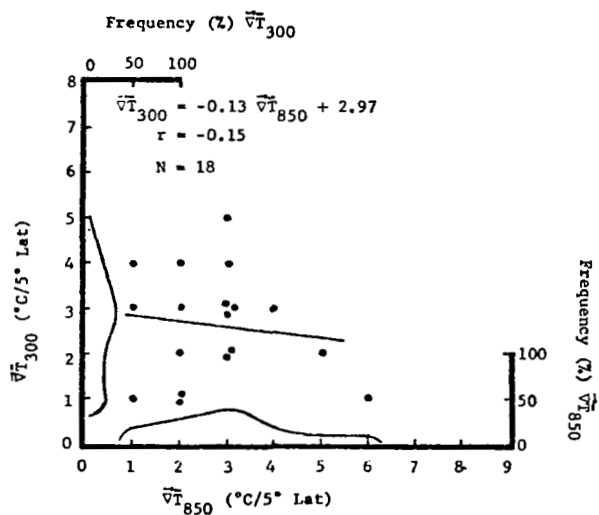(b) Ceilings
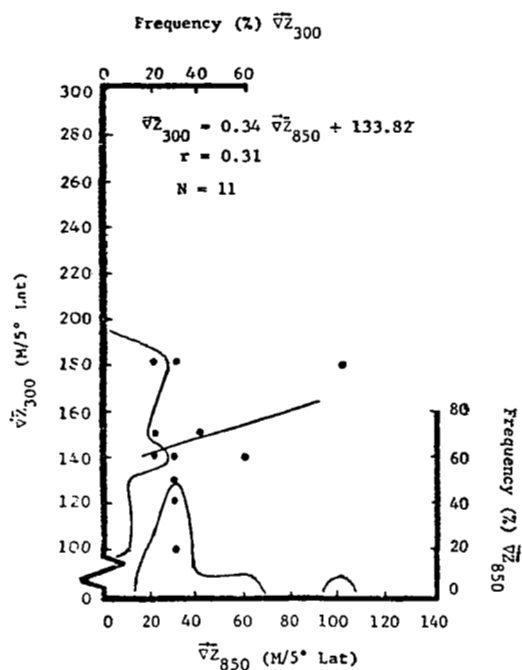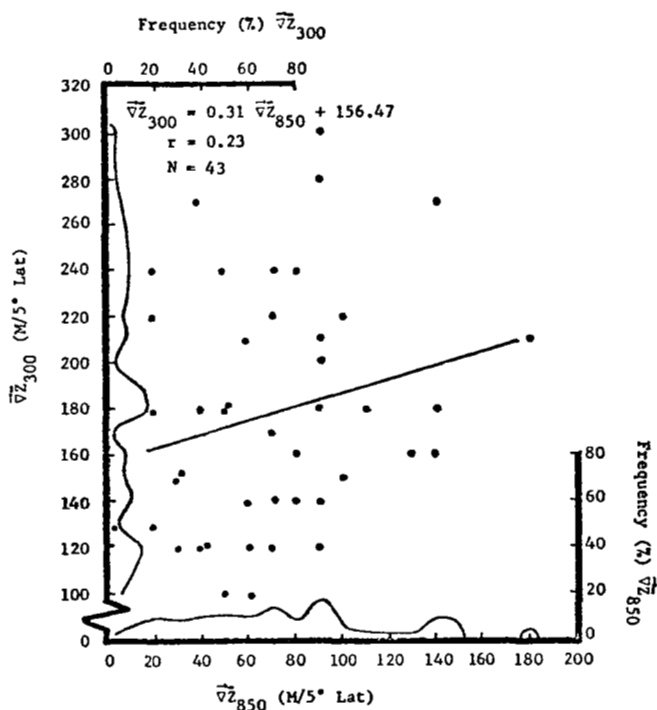
(c) No Ceilings

(d) Ceilings

Fig. 19. Ceiling/no ceiling $\leq$ 5K ft within 100 n mi of selected stations versus gradients of temperature and height at 850, 500, and 300 mb for the December 1969 period.
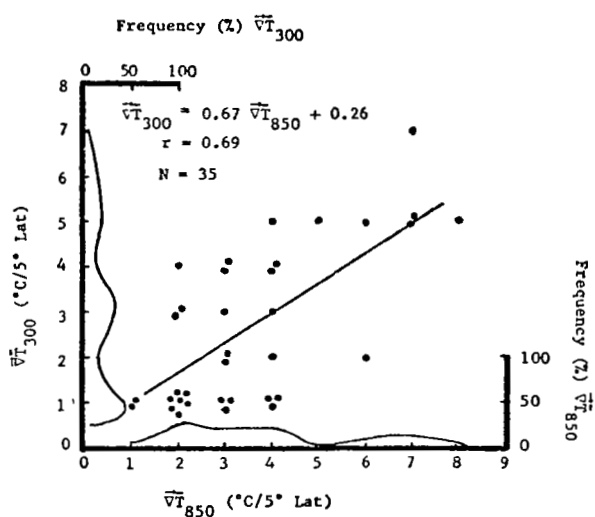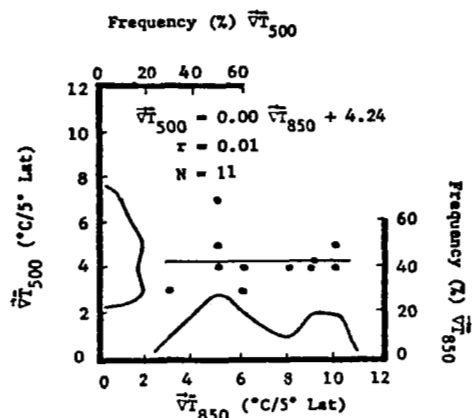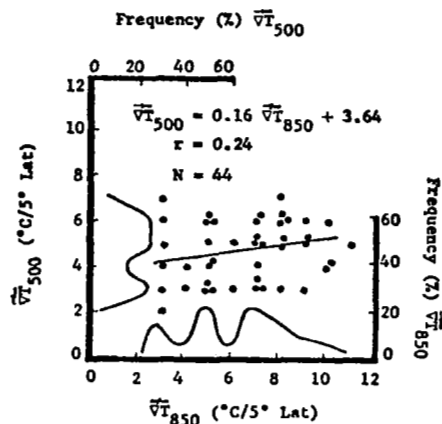
(e) No Ceilings
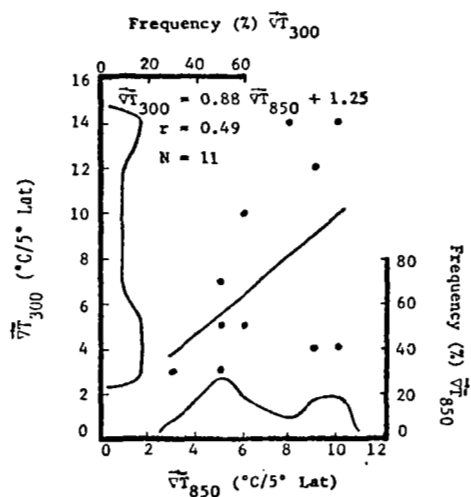
(f) Ceilings
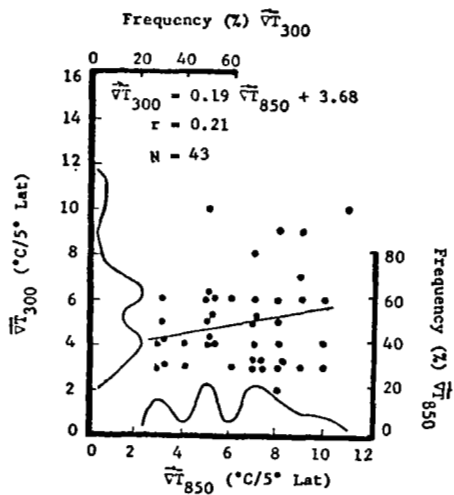
(g) No Ceilings

(h) Ceilings

Fig. 19 continued.

59

Frequency (%) $\vec{\nabla}z_{500}$

0 20 40 60 80

$\vec{\nabla}z_{500} = 0.20\ \vec{\nabla}z_{850} + 120.60$

r = 0.20

N = 32

$\vec{\nabla}z_{500}$ (M/5° Lat)

$\vec{\nabla}z_{850}$ (M/5° Lat)

Frequency (%) $\vec{\nabla}z_{850}$

(a) No ceilings

Frequency (%) $\vec{\nabla}z_{500}$

0 20 40 60 80

$\vec{\nabla}z_{500} = 0.41\ \vec{\nabla}z_{850} + 76.74$

r = 0.44

N = 22

$\vec{\nabla}z_{500}$ (M/5° Lat)

$\vec{\nabla}z_{850}$ (M/5° Lat)

Frequency (%) $\vec{\nabla}z_{850}$

(b) Ceilings

Frequency (%) $\vec{\nabla}z_{300}$

0 20 40 60 80

$\vec{\nabla}z_{300} = 0.18\ \vec{\nabla}z_{850} + 178.38$

r = 0.16

N = 33

$\vec{\nabla}z_{300}$ (M/5° Lat)

$\vec{\nabla}z_{850}$ (M/5° Lat)

Frequency (%) $\vec{\nabla}z_{850}$

(c) No ceilings

Frequency (%) $\vec{\nabla}z_{300}$

0 20 40 60 80

$\vec{\nabla}z_{300} = 0.13\ \vec{\nabla}z_{850} + 132.47$

r = 0.15

N = 22

$\vec{\nabla}z_{300}$ (M/5° Lat)

$\vec{\nabla}z_{850}$ (M/5° Lat)
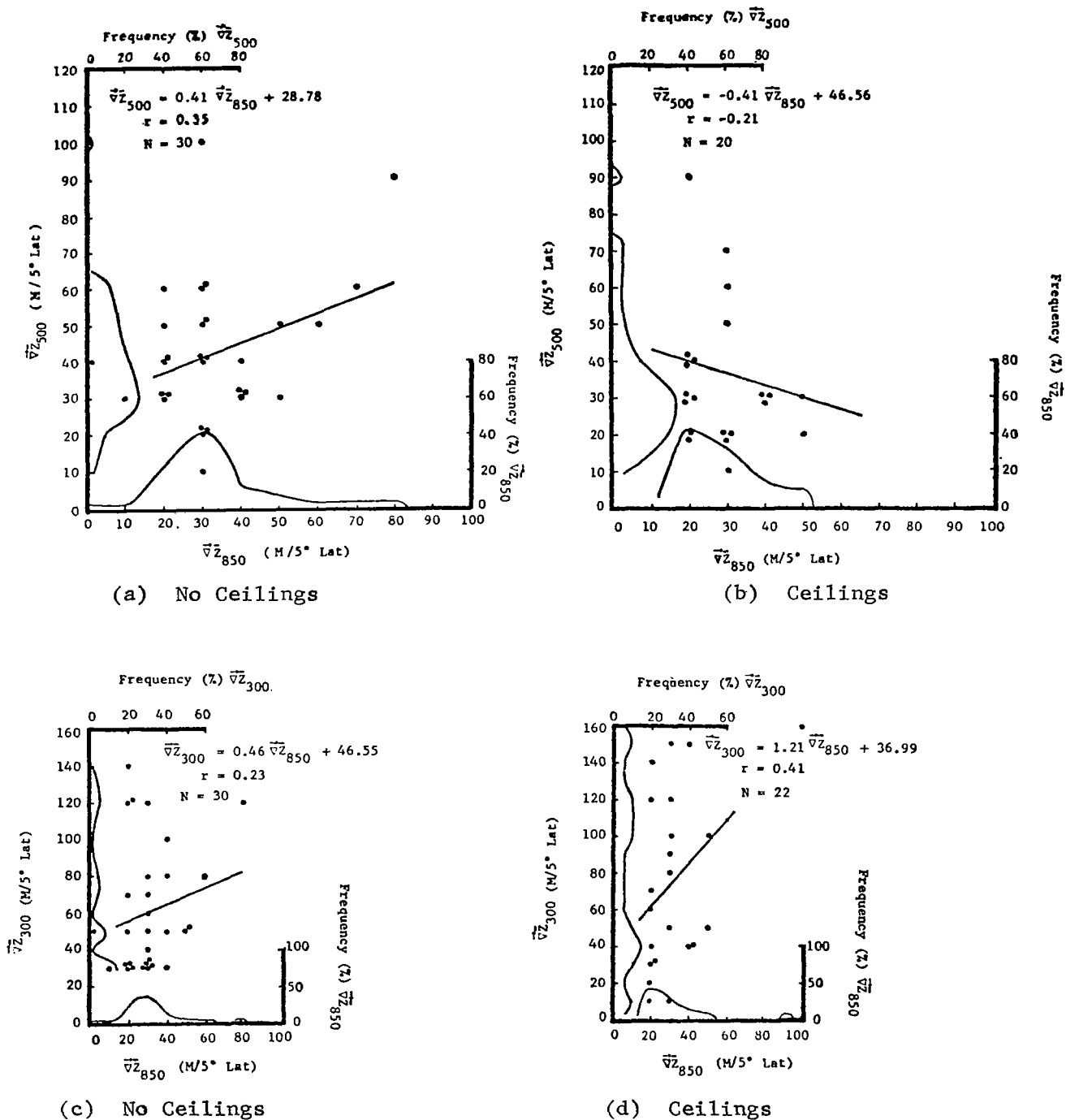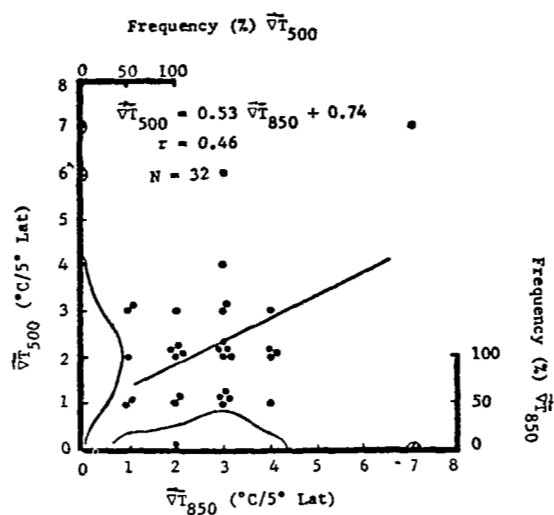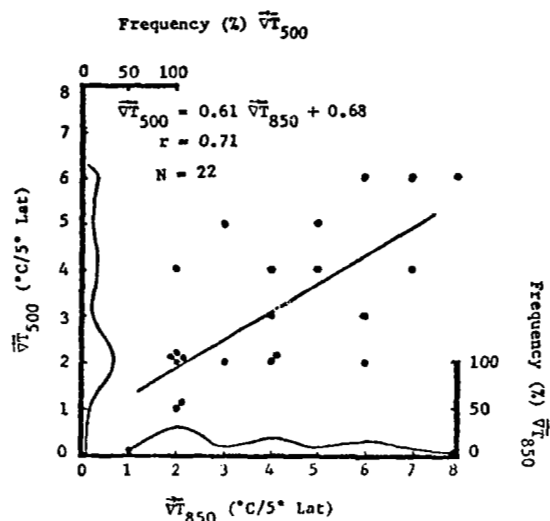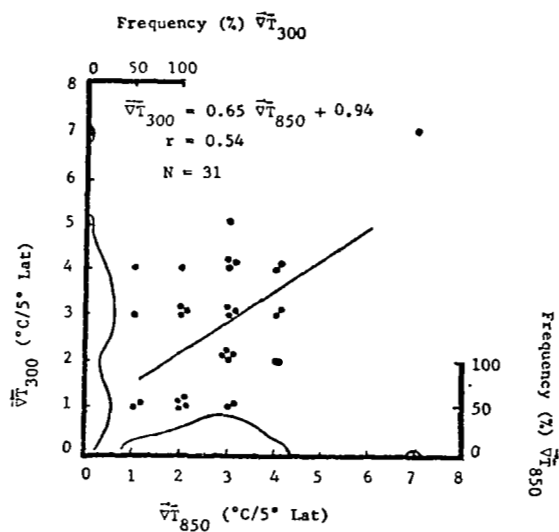
Frequency (%) $\vec{\nabla}z_{850}$
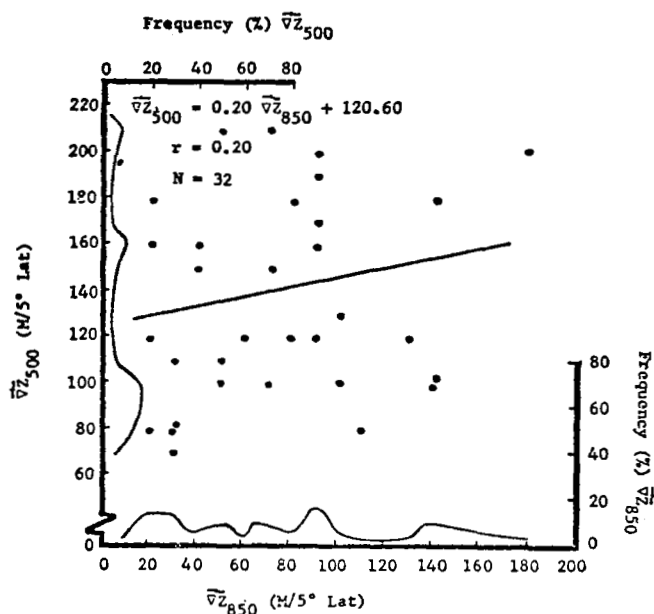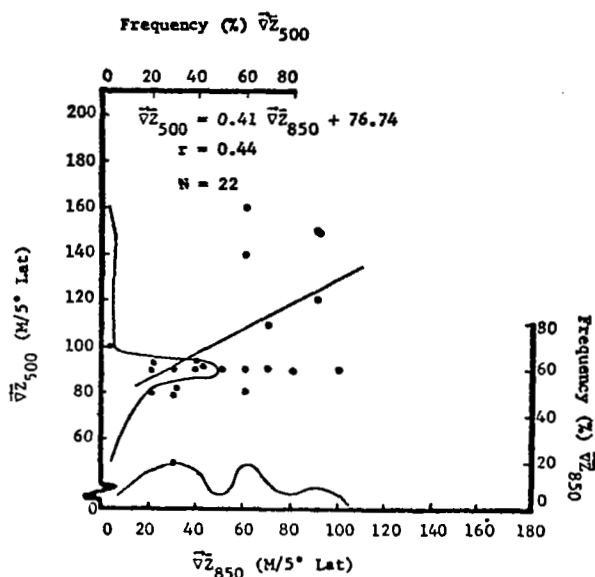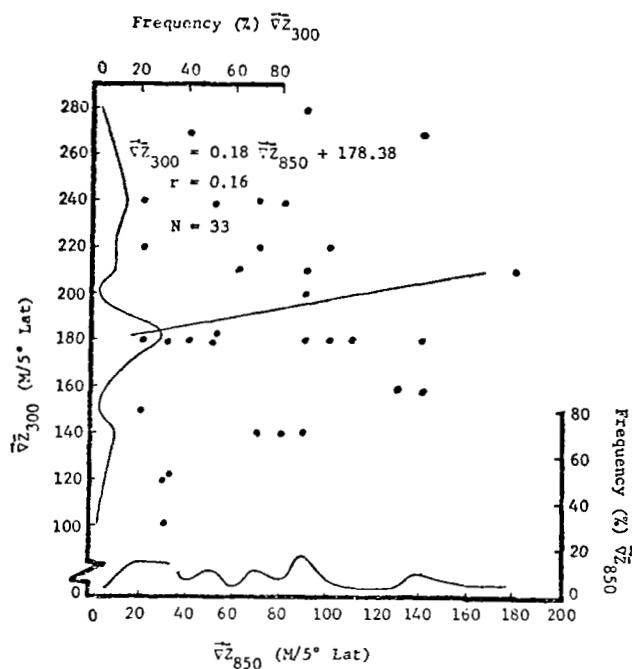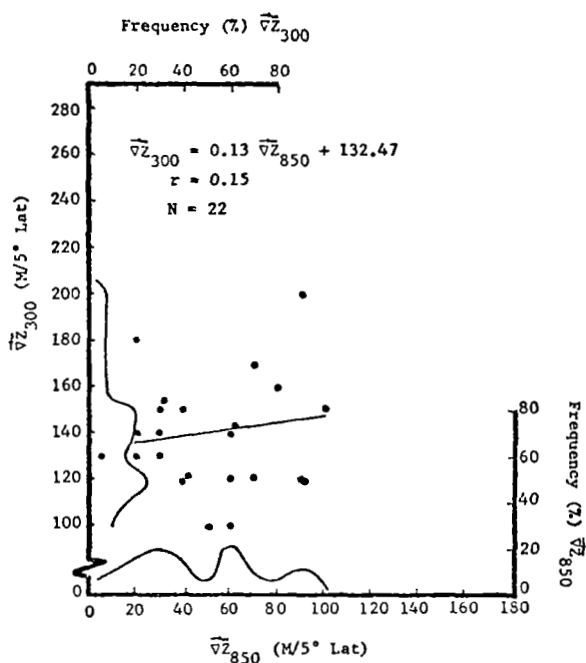
(d) Ceilings

Fig. 20. Ceiling/no ceiling ≤ 10K ft within 100 n mi of selected stations versus gradients of temperature and height at 850, 500, and 300 mb for the December 1969 period.
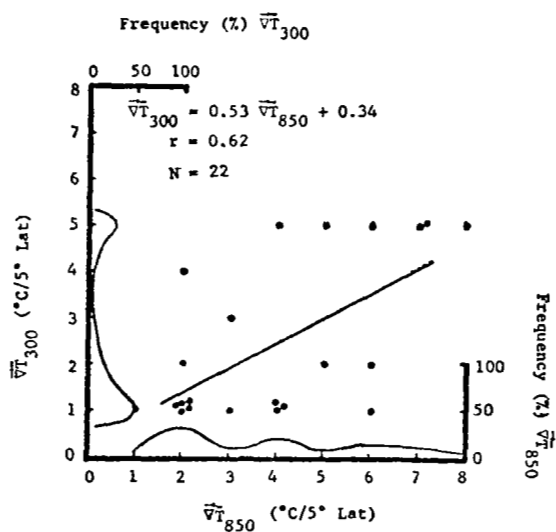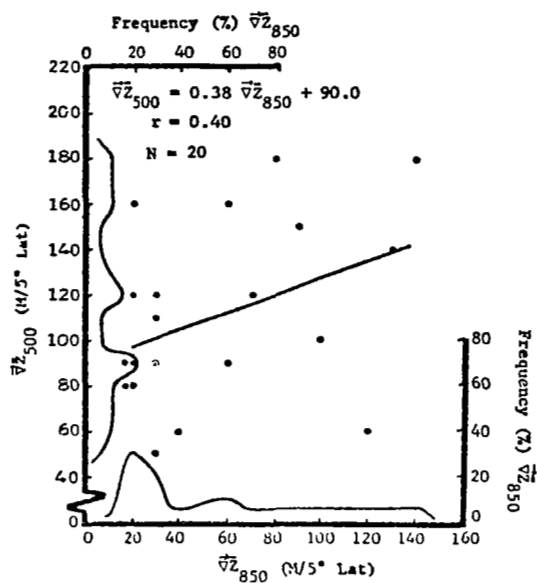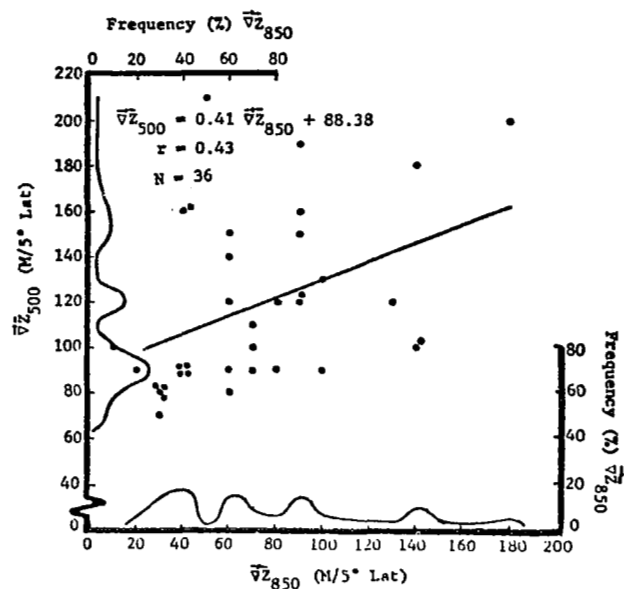
60
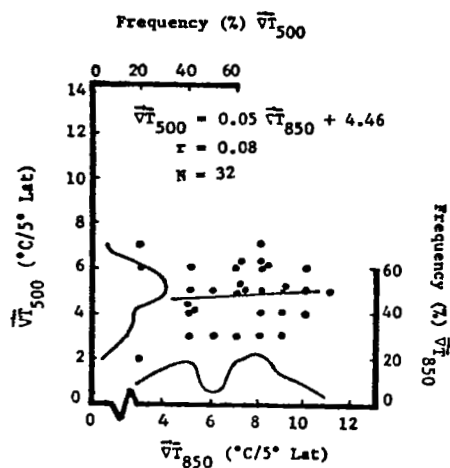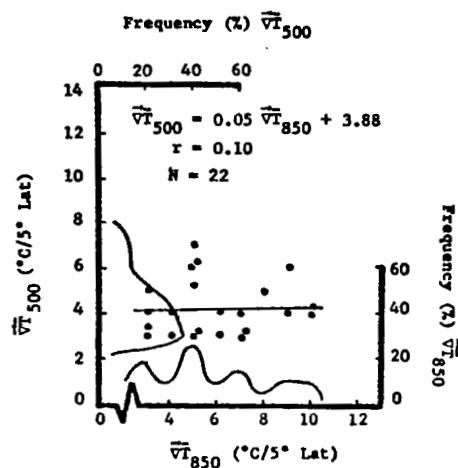
(e) No ceilings
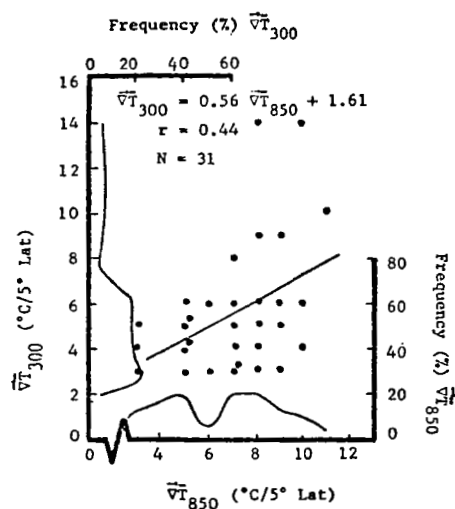
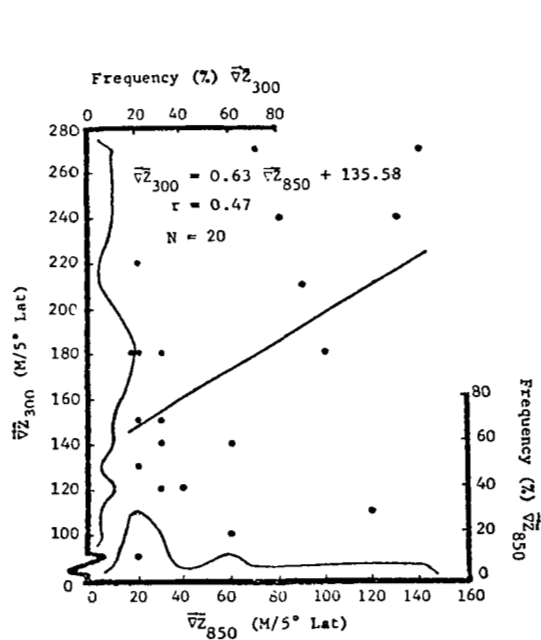(f) Ceilings

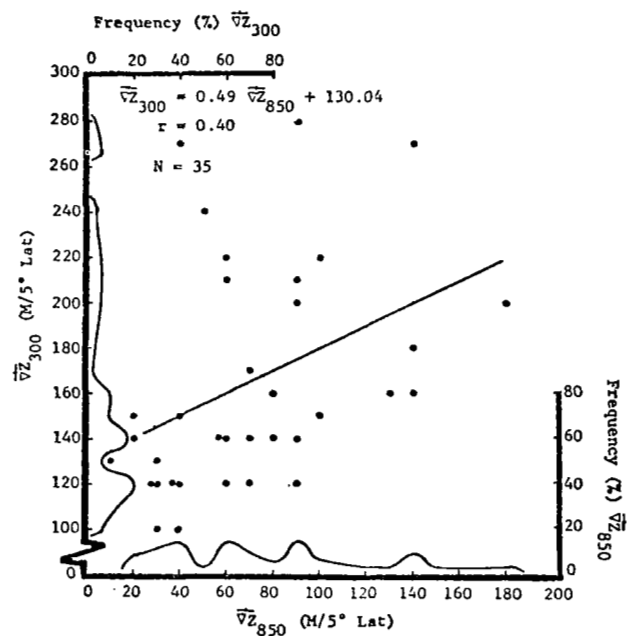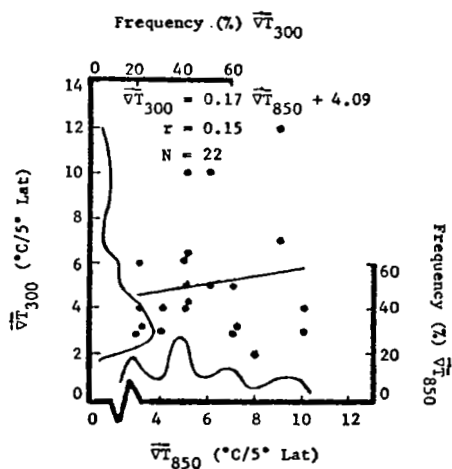(g) No ceilings

(h) Ceilings

Fig. 20 continued.

61

distribution at 500 mb shows a prominent peak between 80 and 100 m/5°lat in the ceiling case which is not pronounced in the no ceiling case. The correlation coefficients between the gradient of height at 850 and 300 mb are essentially the same with a value near 0.15. The only distinguishing feature between the no ceiling and ceiling cases is that a peak appears in the frequency distribution near 180 m/5°lat in the no ceiling case, while a rather broad peak appears between 100 and 150 m/5°lat in the ceiling case. The distributions at 850 mb are not significantly different.

The correlation coefficients between the gradient of temperature at 850 and 500 mb is small and positive for the no ceiling and ceiling cases. The correlation coefficients between the gradient of temperature at 850 and 300 mb are 0.44 and 0.15 for no ceilings and ceilings, respectively. This appears to be the only distinguishing factor relating the gradient of temperature at the three levels to ceilings and no ceilings.

g. Other Relationships Between Radar Echoes and No Echoes, and Gradients of Height and Temperature

Another approach to the problem of investigating relationships between various parameters is that of preparing graphical relationships between three or more variables. In the above analysis only two variables were associated with echoes or ceilings. It is possible for a variable to be correlated with several other variables and, hence, it is instructive to investigate more than two variables associated with, for example, radar echoes or ceilings.

Radar echoes/no echoes are plotted as functions of three variables in Figs. 21-24 for the June and December periods. Figure 21 is a graphical representation showing the relationships between the gradients of height at 850 and 500 mb, and the gradient of temperature at 850 mb. Echoes are associated with small gradients of height at the 850- and 500-mb levels, and with small gradients of temperature at the 850-mb level. The absence of echoes tend to cluster within the region where the gradient of height at the 500-mb level is between 60 and 90, at 850 mb between 30 and 70, and in an area where the gradient of temperature at 850 is relatively small. With the exception of these two limited areas there does not appear to be any grouping of the points which indicates a relationship between the echoes

62
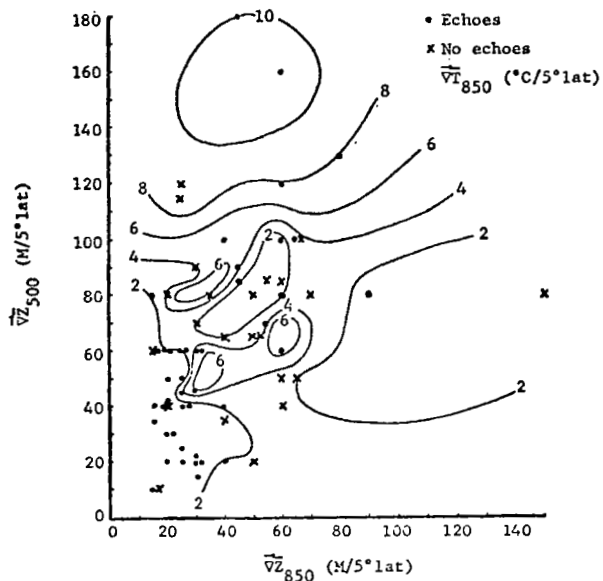
Fig. 21. Gradients of height at 850 and 500 mb and temperature at 850 mb versus echoes and no echoes for the June 1969 period.
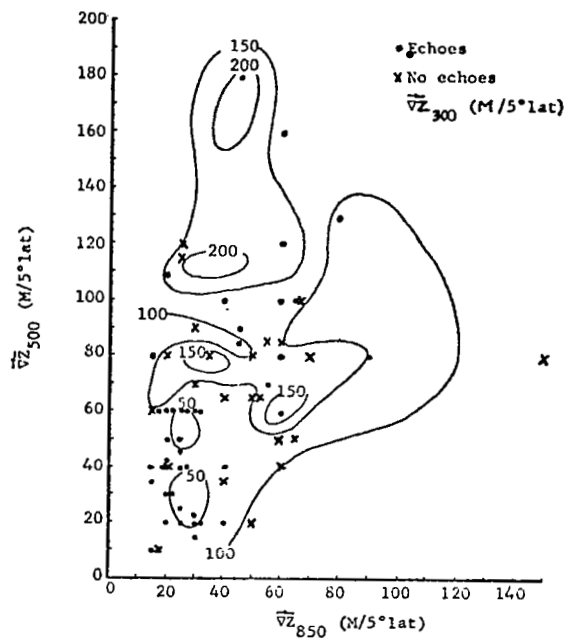
Fig. 22. Gradients of height at 850, 500, and 300 mb versus echoes and no echoes for the June 1969 period.
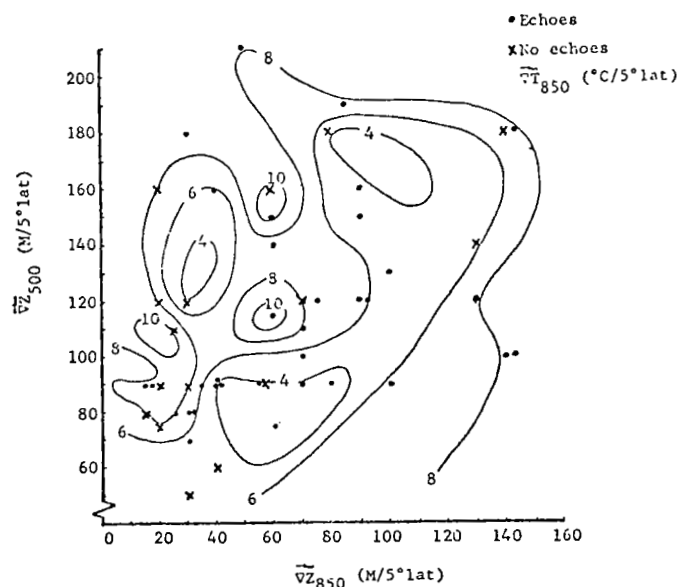
Fig. 23. Gradients of height at 850 and 500 mb and temperature at 850 mb versus echoes and no echoes for the December 1969 period.
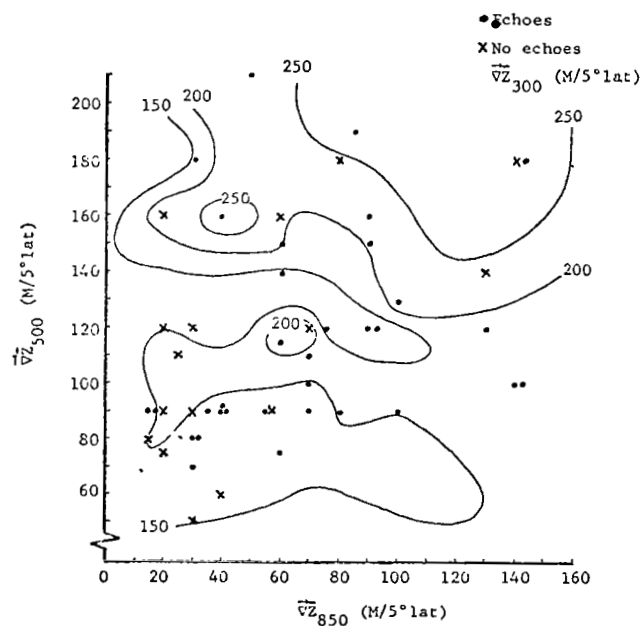
Fig. 24. Gradients of height at 850, 500, and 300 mb versus echoes and no echoes for the December 1969 period.

63

and the three parameters considered. The addition of the gradient of temperature did not appear to improve the relationship exhibited between the gradients of height at 850 and 500 mb, and echoes/no echoes.

Figure 22 is similar to Fig. 21 with the gradient of height at 300 mb replacing the gradient of temperature at 850 mb. The echoes are associated with small values of the gradient of height at all three levels, but when the gradients exceed approximately 60 for any of the variables, there is no apparent grouping of the points. The fact that radar echoes of a convective nature are associated with small gradients of height at all levels would be expected especially when surface heating is the principal triggering mechanism.

Similar figures for the December period are shown in Figs. 23 and 24. In Fig. 23 there is some tendency for the echoes to be associated with small gradients of height at the 850- and 500-mb levels when the gradient of temperature at 850 mb is small. However, there is no clear separation of points anywhere in the figure. Again, the addition of the gradient of temperature at 850 mb does not seem to improve the relationship found between echoes/no echoes and the gradients of height at 850 and 500 mb.

As in the June period, the echoes in Fig. 24 cluster in an area where all the gradients of height are small. Since most radar echoes are probably convective in origin, it would be expected that they would appear primarily in regions where the gradient of height was small, i.e., the average wind speed is low. When the gradients become large at any height there is no apparent grouping of the points in Fig. 24.

h. Comparison of Results for the Four Periods

It is apparent from the above discussion of the relationships between echoes and ceilings, and gradients of height and temperature, that no generally valid relationship appears in the data for the four cases considered. A summary of the correlation coefficients which are statistically significant at the 5% level* are shown in Table 2 for each period as well as a composite for all periods. The significance is based on a table

---

*The significance level of 5% was chosen arbitrarily. If the 10 or 15% level had been chosen, more of the correlations would have been significant.

TABLE 2

SUMMARY OF STATISTICALLY SIGNIFICANT CORRELATION COEFFICIENTS

Parameters	Radar Echoes		Ceiling 5k ft		Ceiling 10k ft	
	No	Yes	No	Yes	No	Yes
March Period						
$\overline{\nabla Z}$, 850-500 mb	.55		.47			
$\overline{\nabla Z}$, 850-300 mb			.37			
$\overline{\nabla T}$, 850-500 mb	.48			.42	.43	
$\overline{\nabla T}$, 850-300 mb	-.39					
June Period						
$\overline{\nabla Z}$, 850-500 mb		.64	.62	.52	.48	.65
$\overline{\nabla Z}$, 850-300 mb		.56	.47	.42	.42	
$\overline{\nabla T}$, 850-500 mb	.54			.45	.43	
$\overline{\nabla T}$, 850-300 mb						
September Period						
$\overline{\nabla Z}$, 850-500 mb	.49	.43	.50			
$\overline{\nabla Z}$, 850-300 mb						
$\overline{\nabla T}$, 850-500 mb		.81		.76	.46	.71
$\overline{\nabla T}$, 850-300 mb		.64		.69	.54	.62
December Period						
$\overline{\nabla Z}$, 850-500 mb		.43		.32		.44
$\overline{\nabla Z}$, 850-300 mb	.47	.40				
$\overline{\nabla T}$, 850-500 mb	-.48					
$\overline{\nabla T}$, 850-300 mb		.43			.44	
Composite of All Periods						
$\overline{\nabla Z}$, 850-500 mb	.55M* .49S	.64J .43D .43S	.47M .62J	.52J .32D	.48J	.65J .44D
$\overline{\nabla Z}$, 850-300 mb	.47D	.56J .40D	.37M .50S .47J	.42J	.42J	
$\overline{\nabla T}$, 850-500 mb	.54J .48D .48M	.81S		.42M .76S .45J	.43M .46S .43J	.71S
$\overline{\nabla T}$, 850-300 mb	-.39M	.64S .43D		.69S	.54S .44D	.62S

* M - March; J - June; S - September; D - December

given on p. 221 by Brooks and Carruthers (1953). As shown in the table, there is very little consistency between the periods and there was not a single category in which the correlation coefficient was statistically significant at the 5% level for all four periods. The composite of all periods shows five categories in which the correlation coefficients for at least three periods were significant. In addition, there are three categories in which none of the correlation coefficients was significant. There does not appear to be any consistency between the two winter periods, March and December, or between the two summer periods, June and September. The lack of consistency between any of the periods seems to imply that other factors are important which are not considered in this analysis.

6. ANALYTICAL RELATIONSHIPS BETWEEN MESO- AND SYNOPTIC-SCALE PHENOMENA

a. March Period

1) Synoptic Conditions

Initially a synoptic-scale trough is present at 850 mb from New Mexico northward through North Dakota and slopes to the west with height (see Figs. 27-32 which are discussed later). A large area of radar echoes indicative of mesoscale systems is present east of the 850-mb trough. Rapid deepening of the trough takes place during the first 24 hours. The trough moves eastward and becomes very broad so that the exact location of the trough line is difficult to determine. Mesoscale systems become dispersed coincident with the broadening of the trough.

2) Moisture

The spread of the ambient and dew-point temperatures at 850 mb, shown for the entire period in Fig. 25 in solid lines supermiposed on the composite radar summary, is used as a measure of the moisture present. The figure shows that most radar echoes are present where the spread between the ambient and dew-point temperatures is less than 10C.

3) Vertical Motion
a) Kinematic and Adiabatic Methods

The sign of each of the terms on the right-hand side of (3) is evaluated for the case of March 23-25, 1969. Areas of convergence are outlined in Fig. 26 at the lower levels (850 and 700 mb) and divergence at the upper levels (500, 300, and 200 mb). Areas where convergence is present at the lower levels and divergence at the upper levels are hatched and represent probable areas of positive vertical motion in the mid-troposphere. All charts of space-mean contours, Z' fields, and isotherms are included for the discussion of this case. Only selected charts are shown for the other periods.

Space-mean contours (solid lines) and Z' fields (dashed lines) are shown in Fig. 27 for 00Z, 23 March 1969. In Fig. 27a, the strong south wind east of the 850-mb trough makes the βv-term dominant in (3) in the principal area of radar echoes. Both advection and the local change of Z' are small or zero at 850 mb over most of the radar echoes. In Fig. 27b,

(a) 00Z, 23 March 1969

(b) 12Z, 23 March 1969

(c) 00Z, 24 March 1969

67
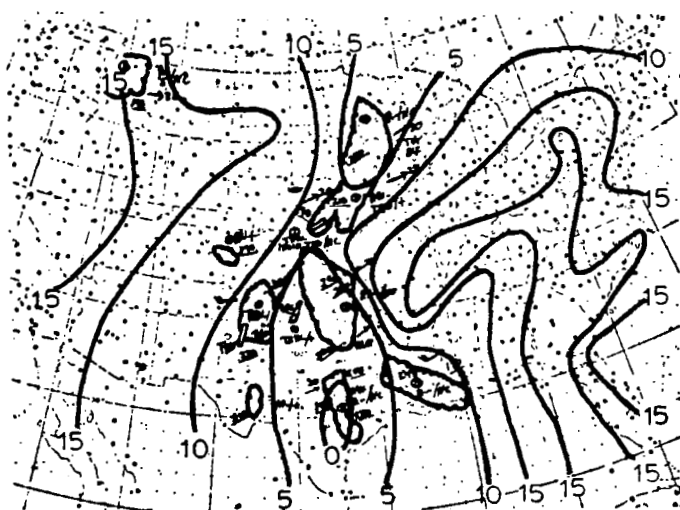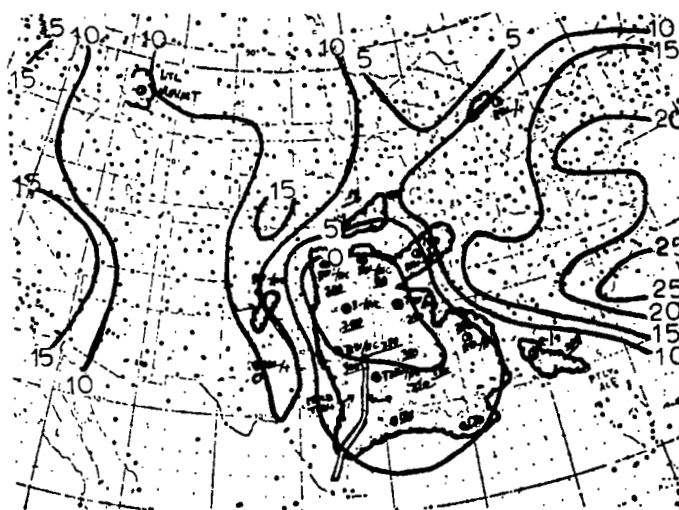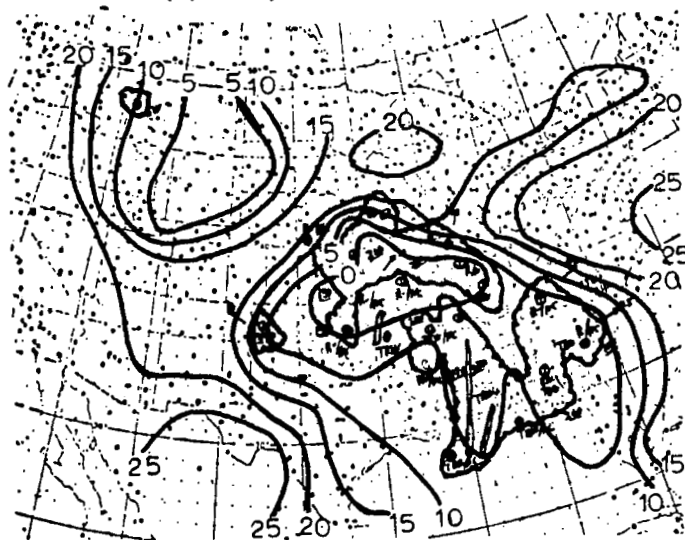
Fig. 25. The spread of the ambient
and dew-point temperatures
at 850 mb (solid lines)
superimposed on radar
summaries for 00Z, 23 March
1969 to 12Z, 25 March 1969.
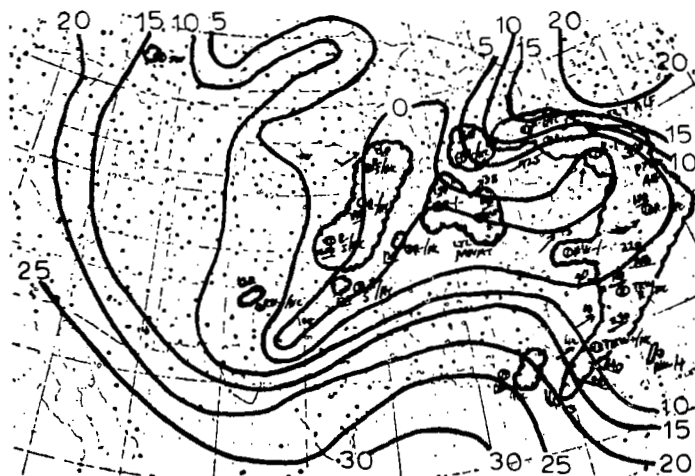
(d) 12Z, 24 March 1969
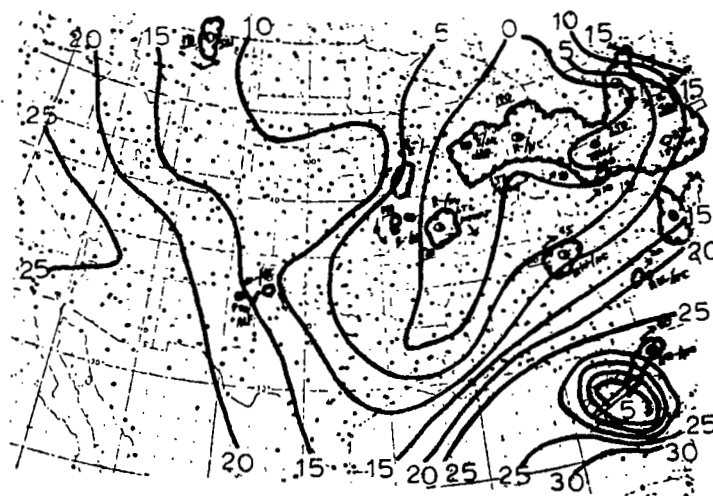
(e) 00Z, 25 March 1969

(f) 12Z, 25 March 1969

Fig. 25. (Cont'd from previous page)
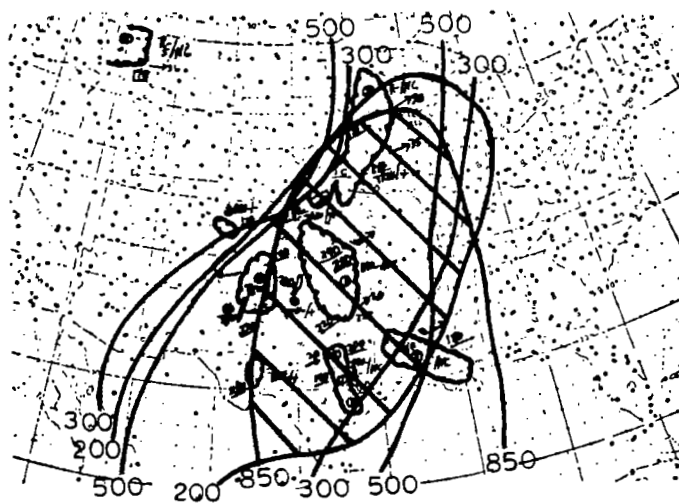
(a) 00Z, 23 March 1969
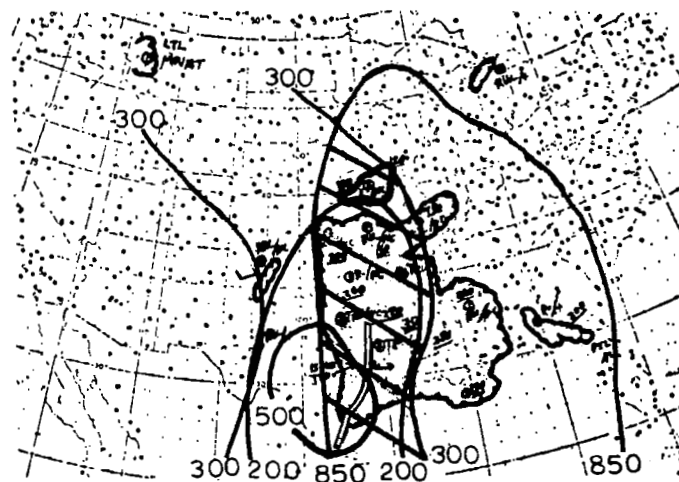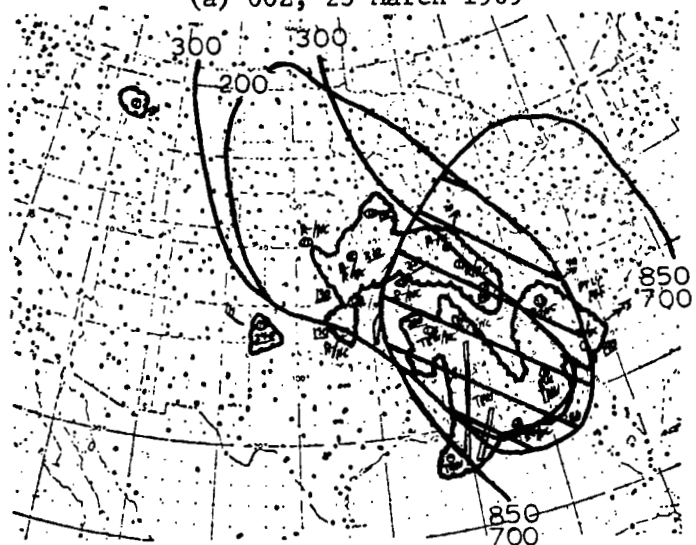
(b) 12Z, 23 March 1969

(c) 00Z, 24 March 1969

Fig. 26. Charts of divergence and conver-
gence superimposed on radar
summaries for 00Z, 23 March 1969
to 12Z, 25 March 1969. (Areas
of convergence are outlined (or
enclosed between lines) at the
lower levels (850 and 700 mb)
and divergence at the upper
levels (500, 300, and 200 mb).
Areas where convergence occurred
at the lower levels and divergence
at the upper levels are hatched
and represent probable areas of
positive vertical motion in the
mid-troposphere.)
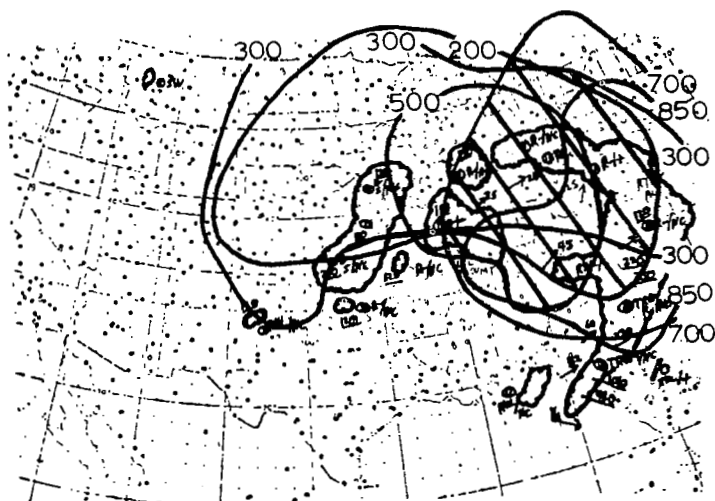
(d) 12Z, 24 March 1969
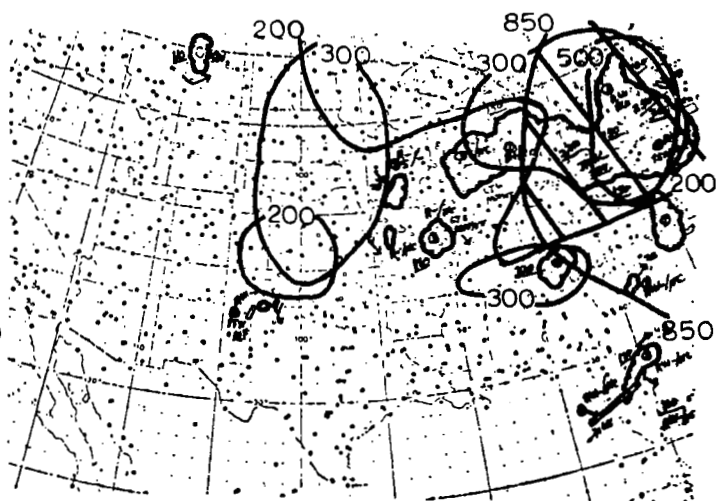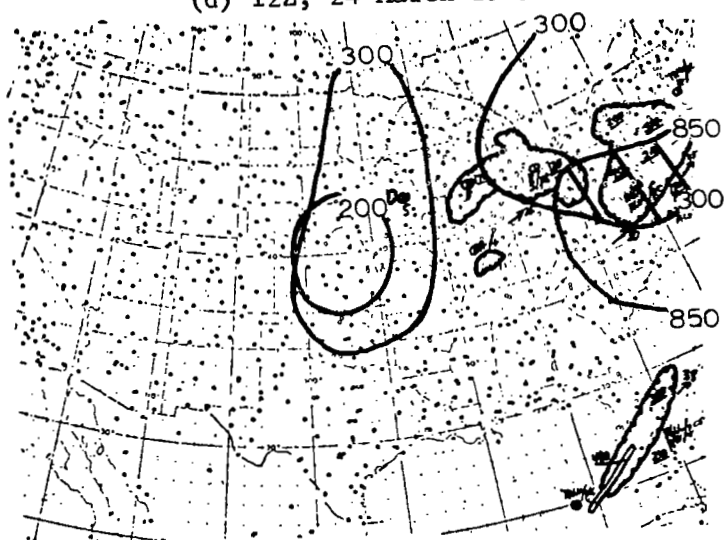
(e) 00Z, 25 March 1969

(f) 12Z, 25 March 1969

Fig. 26.   (cont'd from previous page)
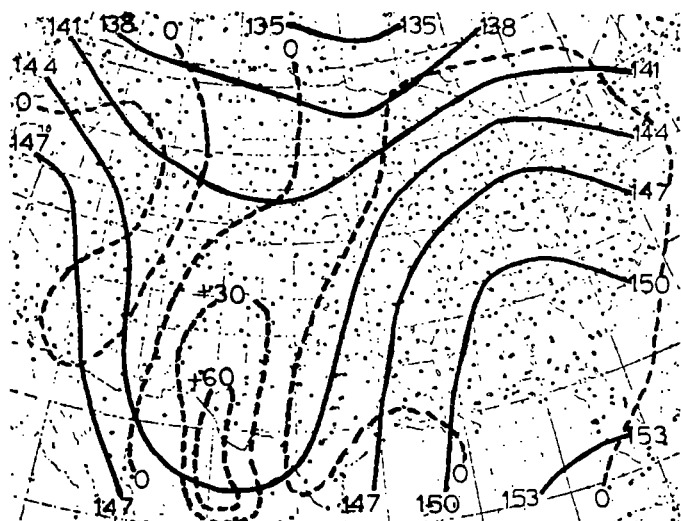
(a) 850 mb
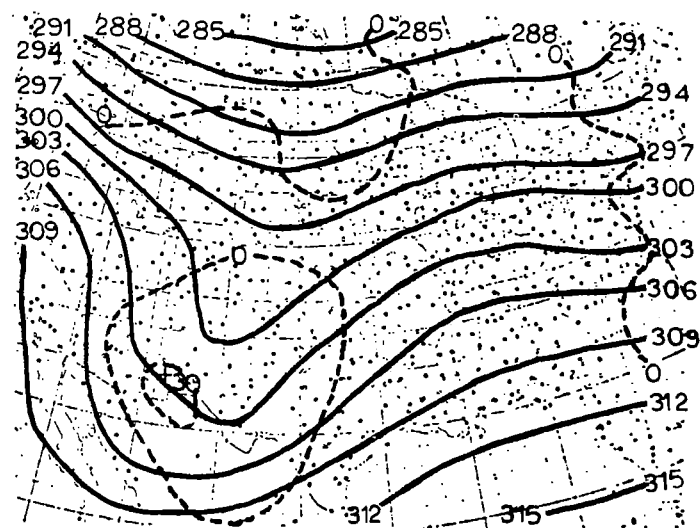
(b) 700 mb
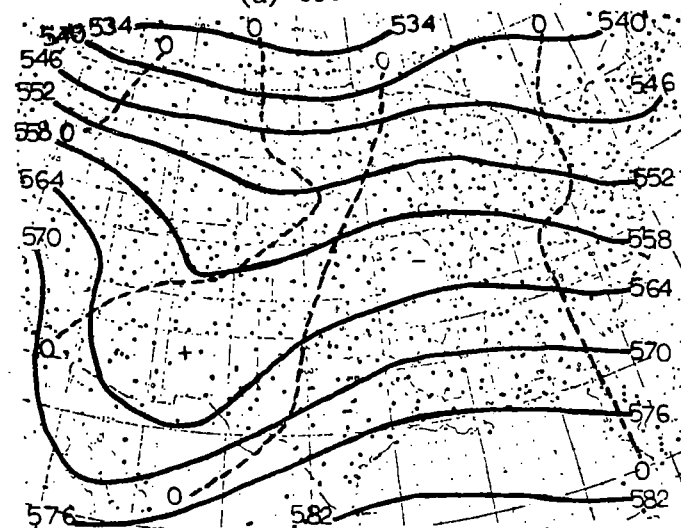
(c) 500 mb

Fig. 27. Charts of $\bar{Z}$, Z' fields, and the radar summary for 00Z, 23 March 1969. (Space-mean contours are shown in solid lines and Z' fields in dashed lines.)
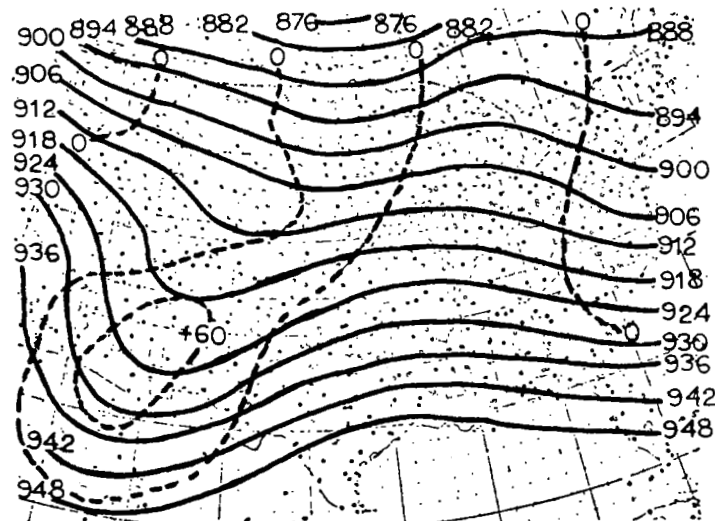
(d) 300 mb
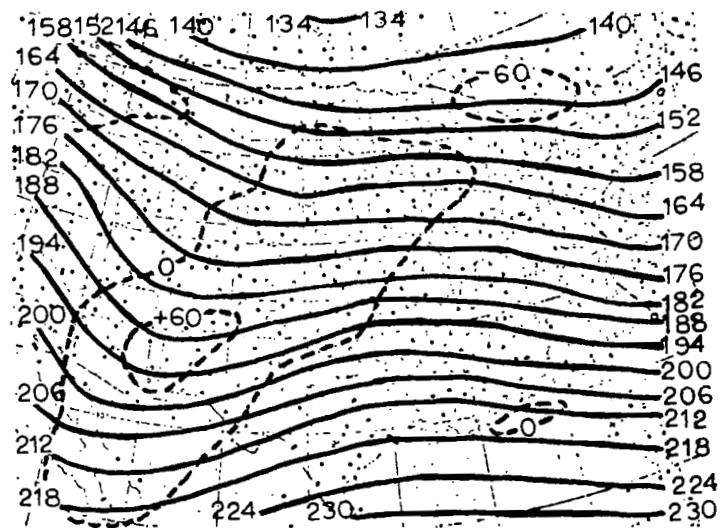
(e) 200 mb
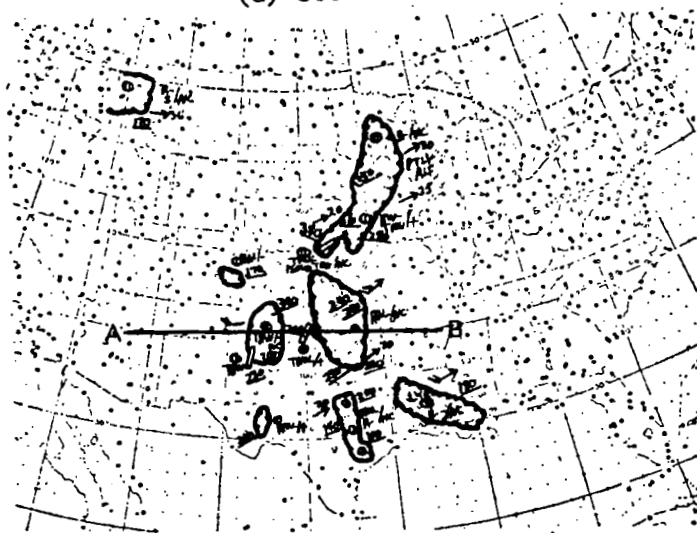
Fig. 27. (cont'd from previous page)

(f) Radar summary

positive vorticity advection (PVA) contributes to divergence east of the trough in the area of radar echoes, βv makes a contribution to convergence, and the sign of divergence at 700 mb cannot be determined. In Figs. 27c, 27d, and 27e the flow is essentially zonal and the sign of divergence is determined by PVA which leads to divergence east of the trough at each of these levels throughout the principal area of radar echoes. Examination of the entire column from 850 to 200 mb shows that there is convergence at the lowest level (850 mb), divergence aloft (500, 300, and 200 mb), and by Dines' Compensation Principle there will be positive vertical motion in the mid-troposphere in the area of radar echoes in Fig. 27f. Figure 28 is a vertical cross-section along the line AB indicated in Fig. 27f. The figure shows the trough sloping westward from 850 to 500 mb then nearly vertically above 500 mb. Radar echoes (scalloped lines) indicative of mesoscale systems are present east of the 850-mb trough in the area where convergence at 850 mb and divergence aloft (500, 300, and 200 mb) create positive vertical motion in the mid-troposphere. The hatched area in Fig. 26a, indicating the strong possibility of positive vertical motion in the mid-troposphere, coincides well with observed radar echoes. In Fig. 25a the spread between the ambient and dew-point temperatures at 850 mb is shown in solid lines superimposed on the composite radar summary. The figure shows that most radar echoes are present where the spread between the ambient and dew-point temperatures is less than 10C.

Space-mean contours are shown in solid lines and isotherms in dashed lines in Fig. 29. Warm advection at 850 mb is inferred from Fig. 29a in the principal area of radar echoes. Cold advection at 700 mb over Texas is inferred from Fig. 29b, with warm advection at 700 mb throughout most of the rest of the principal area of radar echoes. From Figs. 29c, 29d, and 29e, weak warm advection at 500, 300, and 200 mb may be inferred throughout the main area of radar echoes. By the adiabatic method, from Fig. 29 positive vertical motion in the mid-troposphere is indicated over at least the northern half of the area of radar echoes.

In Fig. 30a, negative vorticity advection (NVA) as well as the βv-term contributes to convergence east of the 850-mb trough throughout much of the main area of radar echoes. In Fig. 30b, it is impossible to determine by inspection which term, vorticity advection or the latitude effect, is dominant in the principal area of radar echoes, and the sign of divergence
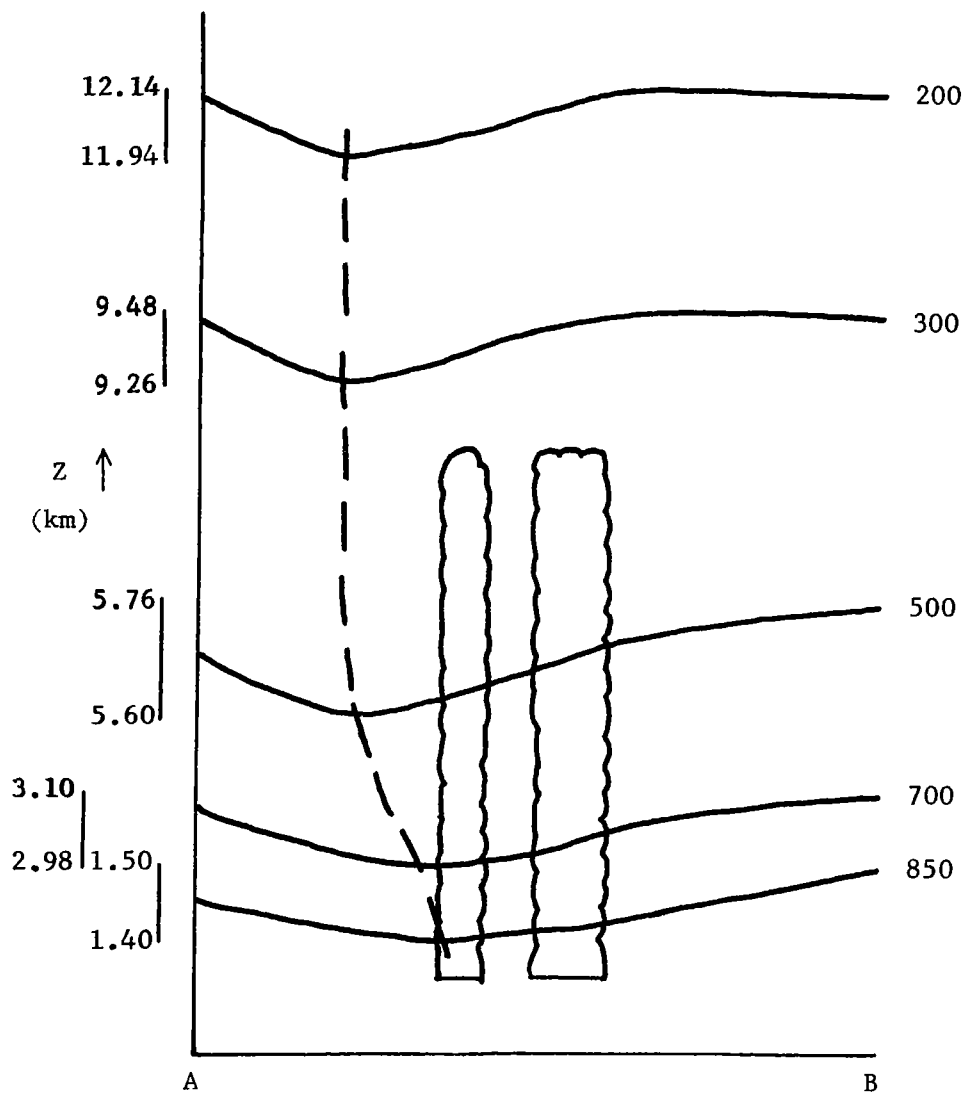
Fig. 28. Vertical cross-section along line AB in Fig. 27f.
(Constant pressure surfaces are solid lines;
the trough is indicated by a dashed line; radar
echoes are in scalloped lines.)

74
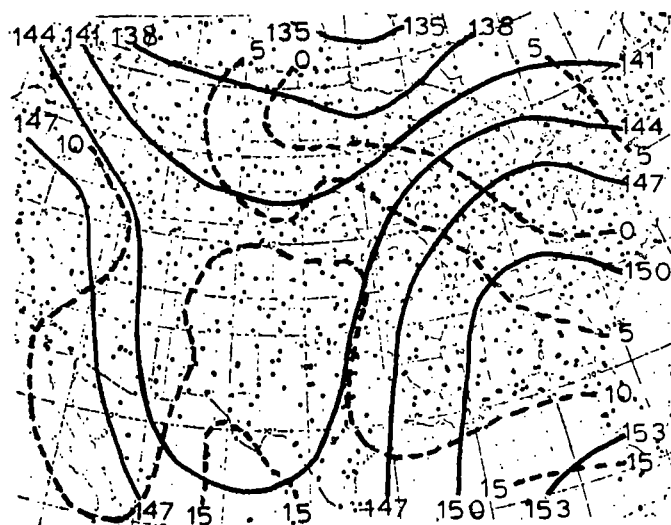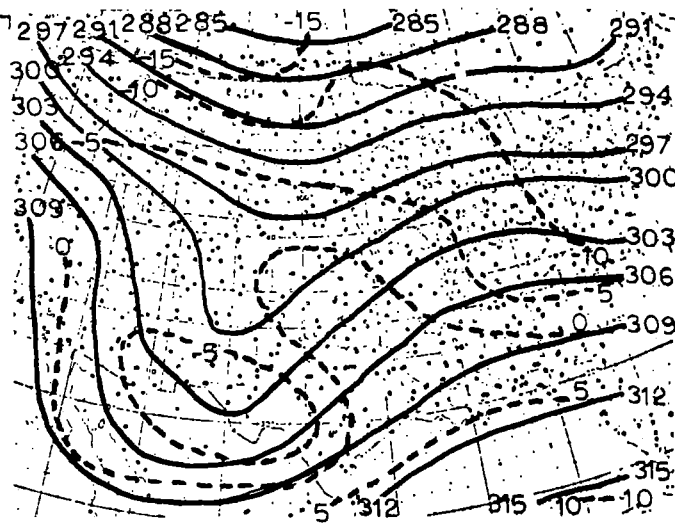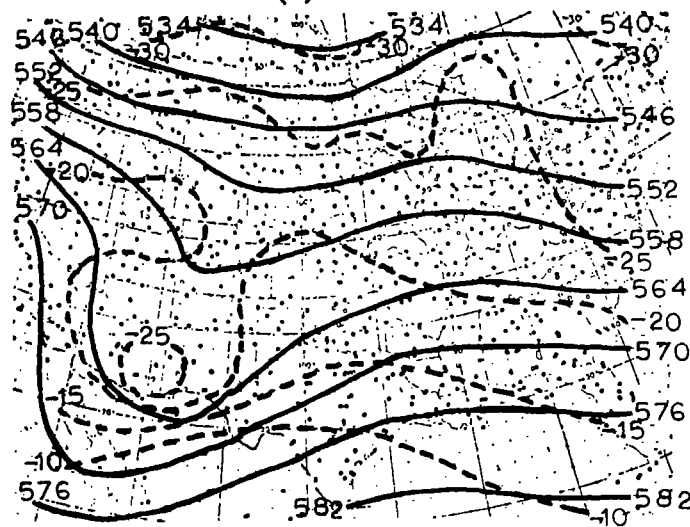
(a) 850 mb

(b) 700 mb

(c) 500 mb

Fig. 29. Charts of $\bar{Z}$, T (isotherms), and the radar summary for 00Z, 23 March 1969. (Space-mean contours are in solid lines and isotherms in dashed lines.)

(d) 300 mb

(e) 200 mb

(f) Radar summary

Fig. 29.   (cont'd from previous page)

(a) 850 mb

(b) 700 mb

(c) 500 mb

Fig. 30. Charts of $\bar{Z}$, Z' fields, and the radar summary for 12Z, 23 March 1969. (Space-mean contours are shown in solid lines and Z' fields in dashed lines.)

(d) 300 mb

(e) 200 mb

(f) Radar summary

Fig. 30. (cont'd from previous page)

at 700 mb cannot be determined. In Fig. 30c, PVA contributes to divergence in a small area over Texas east of the 500-mb trough, but the opposing effect of the βv-term makes the sign of divergence impossible to determine by inspection over much of the area of radar echoes. In Figs. 30d and 30e, PVA is present east of the trough over the main area of radar echoes and the sign of divergence is positive. Within the entire layer (850-200 mb), there is convergence at 850 mb, divergence at 500, 300, and 200 mb, and by Dines' Compensation Principle there should be positive vertical motion in the mid-troposphere in the area of radar echoes. The hatched area in Fig. 26b encloses the radar echoes of greatest vertical development. Radar echoes east of the hatched area in Fig. 26b are in the area of convergence at 850 mb that is associated with positive vertical motion in the lower- to mid-troposphere.

Figure 31 is a vertical cross-section along the line AB indicated in Fig. 30f. The figure shows that the trough slopes westward with height from 850 to 200 mb. As in Fig. 28, radar echoes are present east of the 850-mb trough position. This is because convergence is present east of the trough at 850 mb, divergence at 500, 300, and 200 mb, and by Dines' Compensation Principle there will be positive vertical motion in the mid-troposphere.

Strong positive temperature advection may be inferred from Fig. 32a at 850 mb in the principal area of radar echoes. From Figs. 32b, 32c, 32d, and 32e it is seen that the magnitude of positive temperature advection decreases with height above the area of radar echoes centered in the south-central United States. By the adiabatic method positive vertical motion in the mid-troposphere is indicated in the main area of radar echoes. Areas where (3) and (7) predict positive vertical motion coincident with a spread between the ambient and dew-point temperatures less than 10C outline very well the observed echoes.

A comparison of Figs. 30 and 33 shows that the trough has deepened rapidly in the last 12 hours and has formed a broad closed low at 850 and 700 mb. In Fig. 33, NVA and the latitude term create convergence in a large area east of the trough through much of the principal area of radar echoes. A comparison of Figs. 30b and 33b shows that the local derivative in (3) is positive which, combined with the latitude term and NVA, creates convergence at 700 mb east of the trough in the area of radar echoes. In Fig. 33c, the sign of divergence east of the trough is indeterminate due to
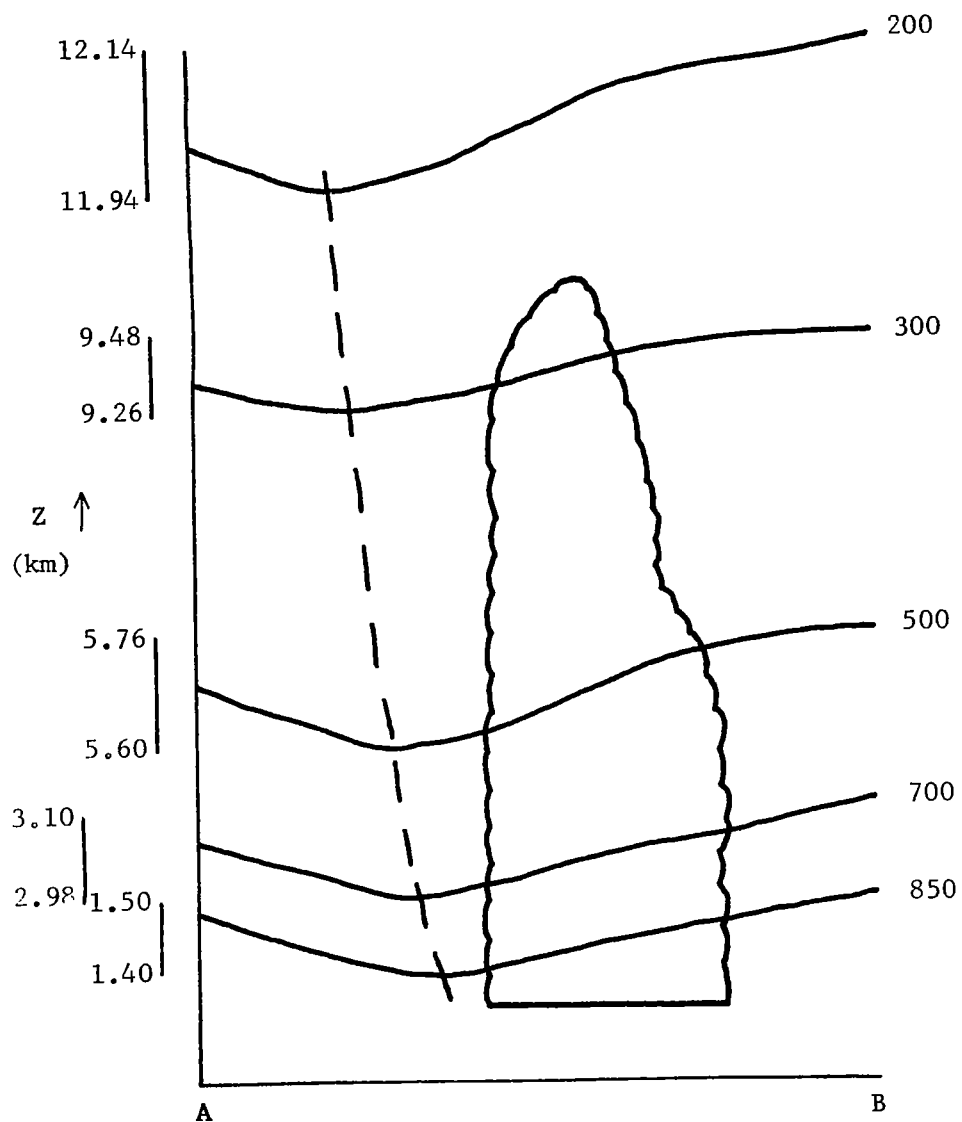
Fig. 31.   Vertical cross-section along line AB in Fig. 30f.
(Constant pressure surfaces are in solid lines;
the trough is indicated by a dashed line; radar
echoes are in scalloped lines.)

(a) 850 mb

(b) 700 mb

(c) 500 mb

Fig. 32. Charts of $\bar{Z}$, T (isotherms), and the radar summary for 12Z, 23 March 1969. (Space-mean contours are in solid lines and isotherms in dashed lines.)
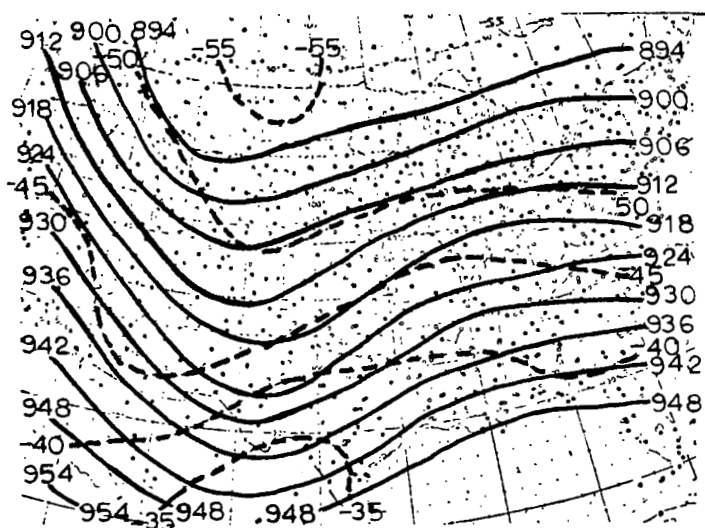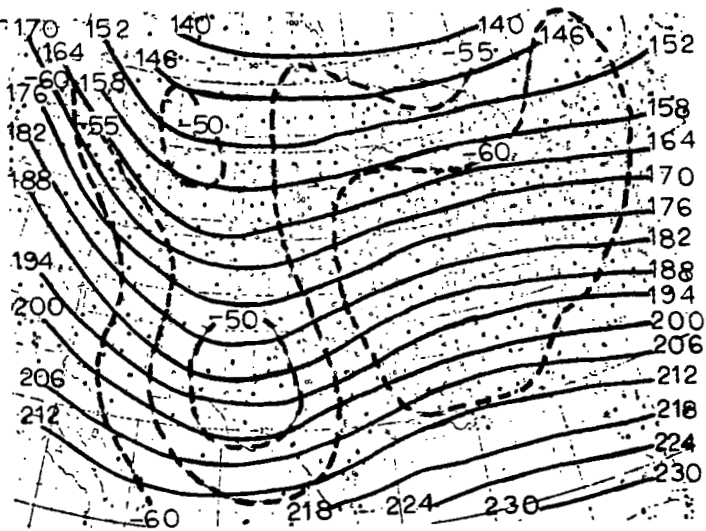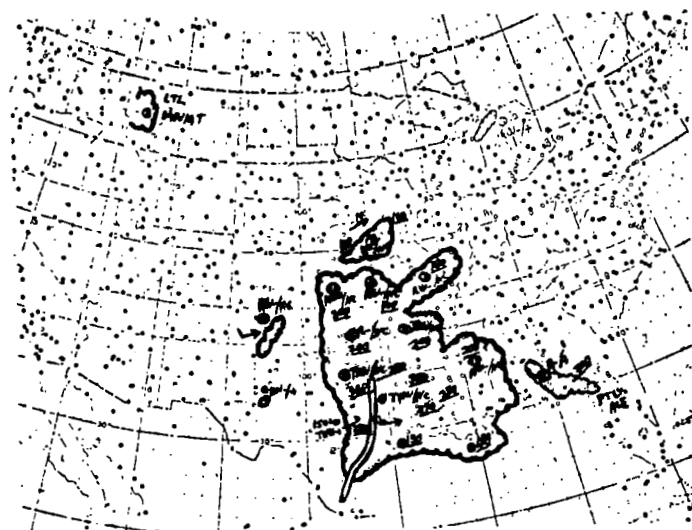
(d) 300 mb

(e) 200 mb

(f) Radar summary

Fig. 32. (cont'd from previous page)

(a) 850 mb

(b) 700 mb

(c) 500 mb

Fig. 33. Charts of $\bar{Z}$, Z' fields, and the radar summary for 00Z, 24 March 1969. (Space-mean contours are shown in solid lines and Z' fields in dashed lines.)

(d) 300 mb

(e) 200 mb

(f) Radar summary

Fig. 33. (cont'd from previous page)

the opposing contribution of the advection and latitude terms. In Figs. 33d and 33e, PVA leads to divergence at the 300- and 200-mb levels over the area of radar echoes. For the entire layer, there is convergence at 850 and 700 mb, divergence at 300 and 200 mb, and by Dines' Compensation Principle there will be positive vertical motion in the mid-troposphere. Figure 26c shows that most radar echoes are in the expected area (indicated by hatching).

Figure 34 is a vertical cross-section along the line AB shown in Fig. 33f. The figure shows that the trough slopes westward from 850 to 300 mb, then is vertical from 300 to 200 mb. Radar echoes in this case are present east and west of the trough at 850, 700, and 500 mb. This is because of positive vertical motion resulting from divergence aloft created by PVA at 300 and 200 mb.

Most of the echoes outside the hatched area of Fig. 26c are explained by thermal advection. In Fig. 35a, strong positive thermal advection is indicated at 850 mb throughout the principal area of radar echoes. By the adiabatic method positive vertical motion in the mid-troposphere is indicated in this area. It should be noted also that the thunderstorms with the greatest vertical development are present over Mississippi in the area of strong warm advection at 850 mb, convergence at low levels (850 and 700 mb), divergence aloft (300 and 200 mb), and a spread between the ambient and dew-point temperatures less than 5C (Fig. 25c).

A comparison of Figs. 33a and 36a shows that the local derivative $\partial Z'/\partial t$ in (3) is negative in the vicinity of the low at 850 mb and contributes to divergence. Negative vorticity advection over Kentucky and the south wind east of the trough create convergence over Kentucky. Also shown in Fig. 36a, the βv-term contributes to convergence in the area of radar echoes along the Atlantic Coast. In most of Fig. 36b isopleths of Z' are in phase with space-mean contours in areas of radar echoes so that the advective term in (3) is small, but the strong south wind east of the low center creates convergence in the area of radar echoes along the Atlantic Coast. Positive vorticity advection in Fig. 36c over the Ohio River Valley leads to divergence while the latitudinal term leads to convergence, and therefore the sign of divergence at 500 mb cannot be determined. In Figs. 36d and 36e there is also a difference in sign between the latitudinal and advective terms over much of the eastern United States. However, because of the well defined Z-fields at 300 and 200 mb, the advective term in (3) is probably dominant and leads
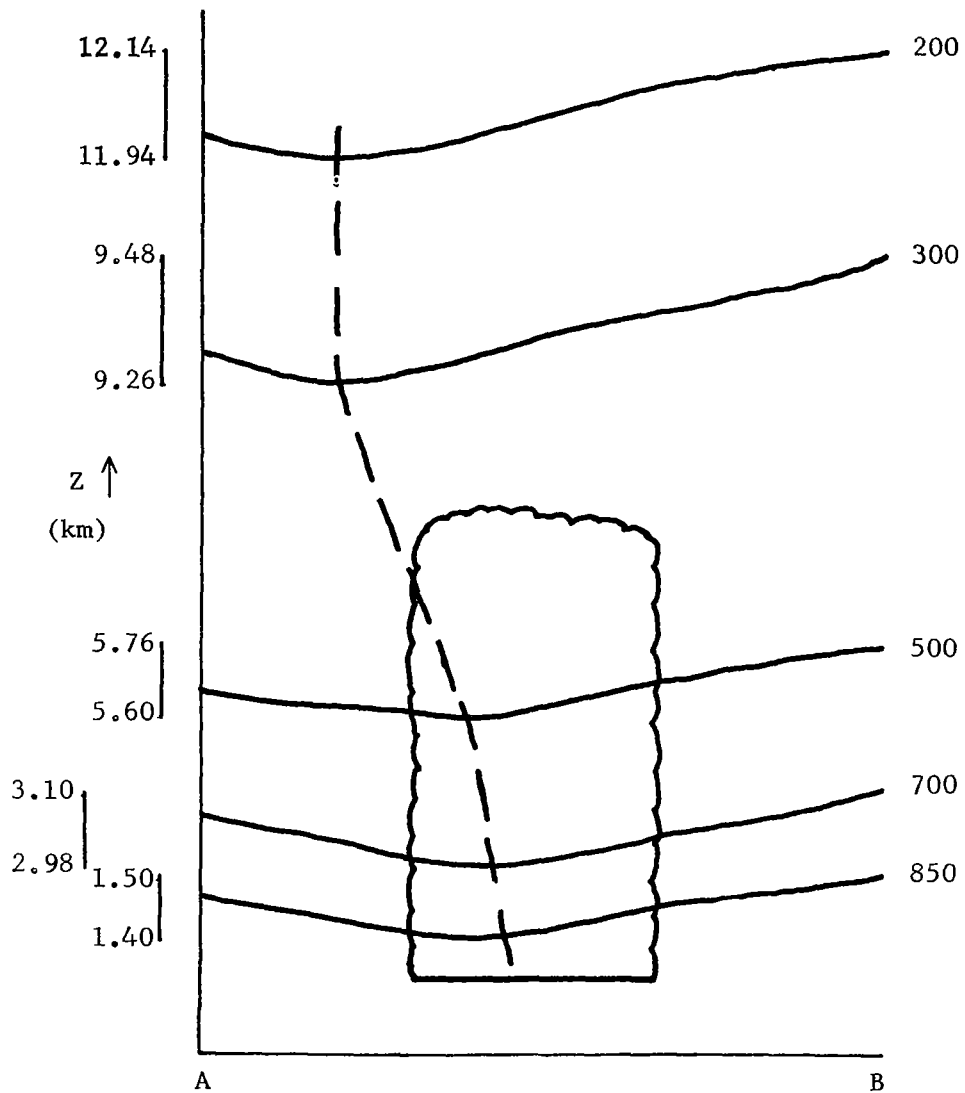
Fig. 34.   Vertical cross-section along line AB in Fig. 33f.
(Constant pressure surfaces are in solid lines;
the trough is indicated by a dashed line; radar
echoes are in scalloped lines.)

(a) 850 mb

(b) 700 mb

(c) 500 mb
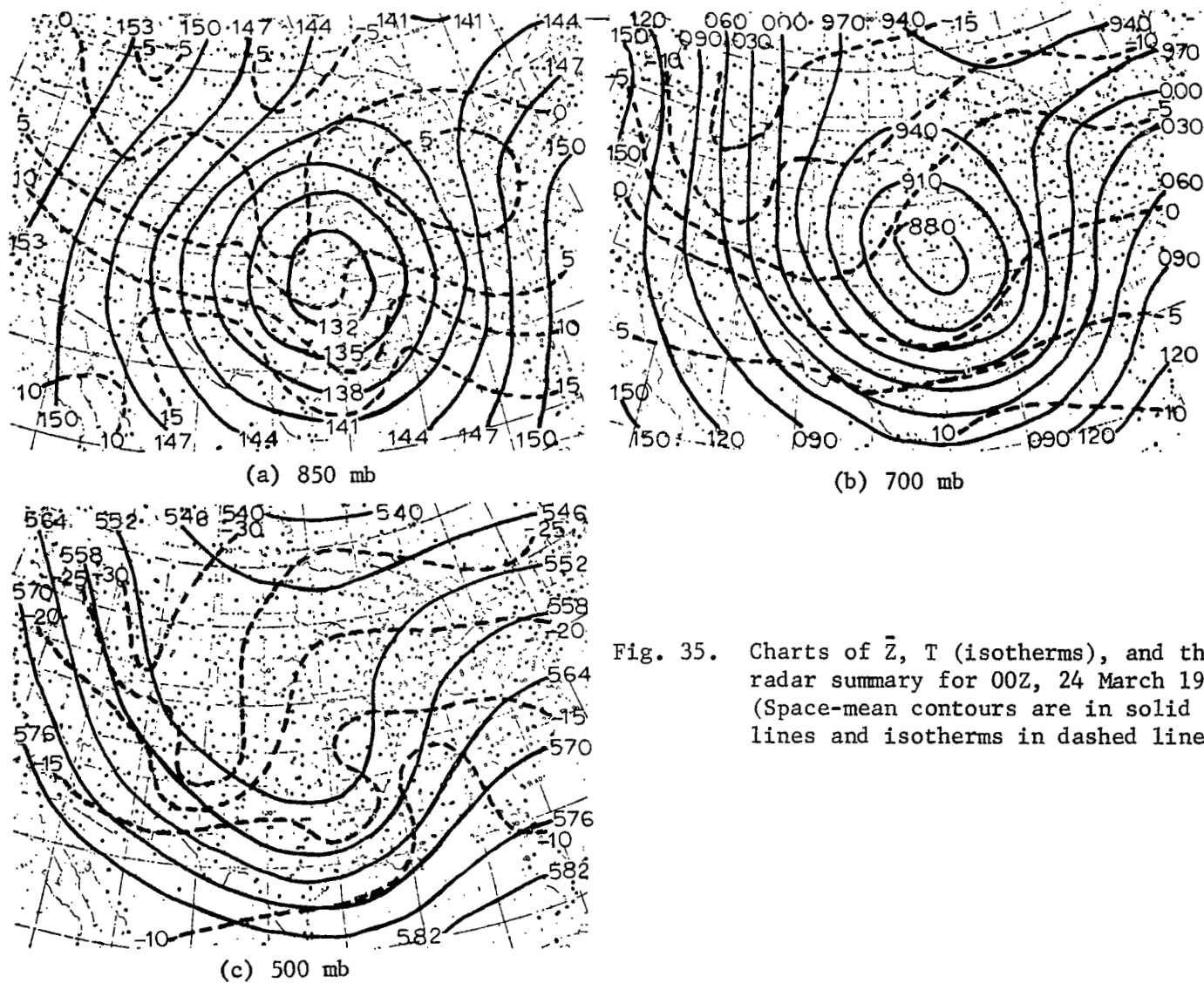
Fig. 35. Charts of $\bar{Z}$, T (isotherms), and the radar summary for 00Z, 24 March 1969. (Space-mean contours are in solid lines and isotherms in dashed lines.)
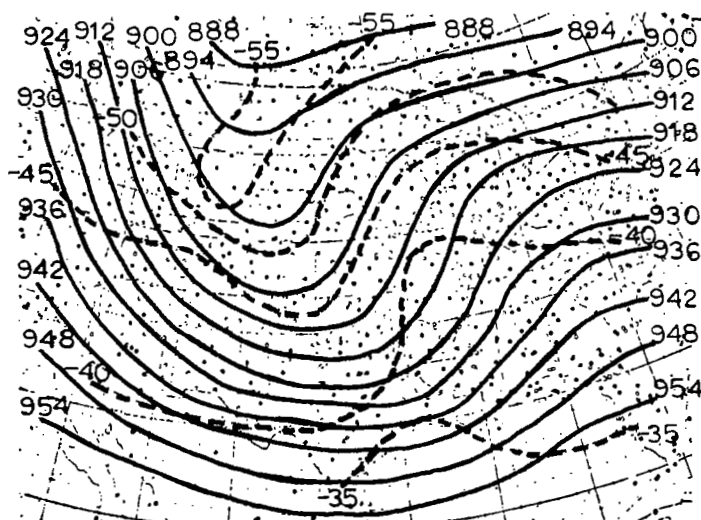
(d) 300 mb
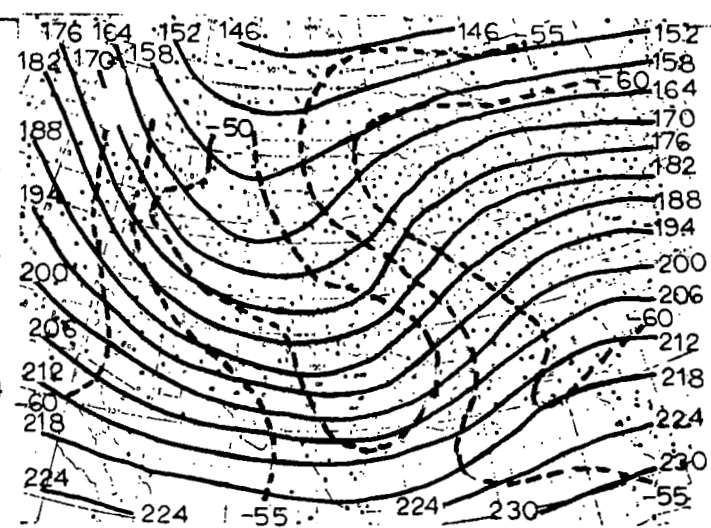
(e) 200 mb
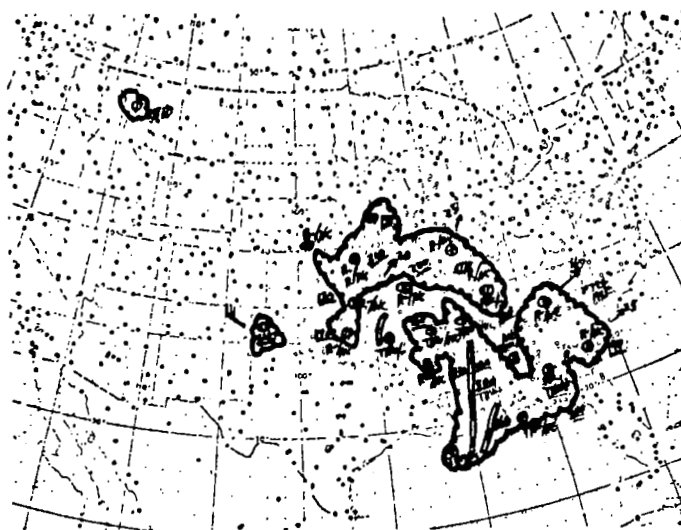
(f) Radar summary

Fig. 35. (cont'd from previous page)
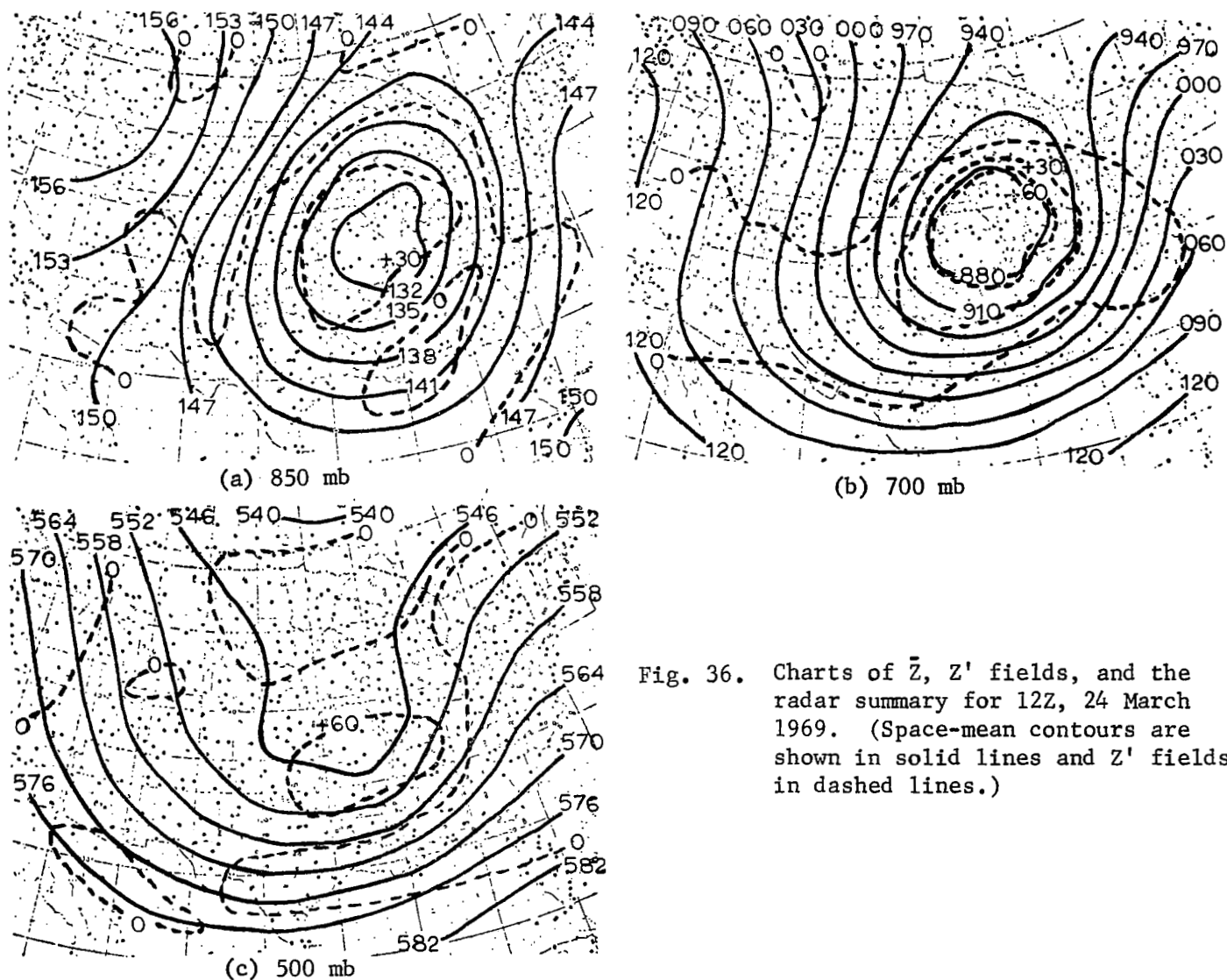
(a) 850 mb

(b) 700 mb

(c) 500 mb

Fig. 36. Charts of $\bar{Z}$, Z' fields, and the radar summary for 12Z, 24 March 1969. (Space-mean contours are shown in solid lines and Z' fields in dashed lines.)

(d) 300 mb

(e) 200 mb

(f) Radar summary
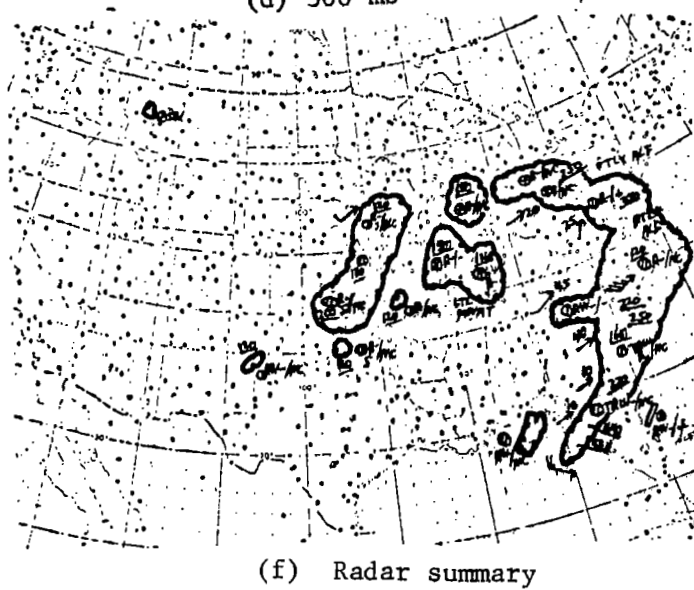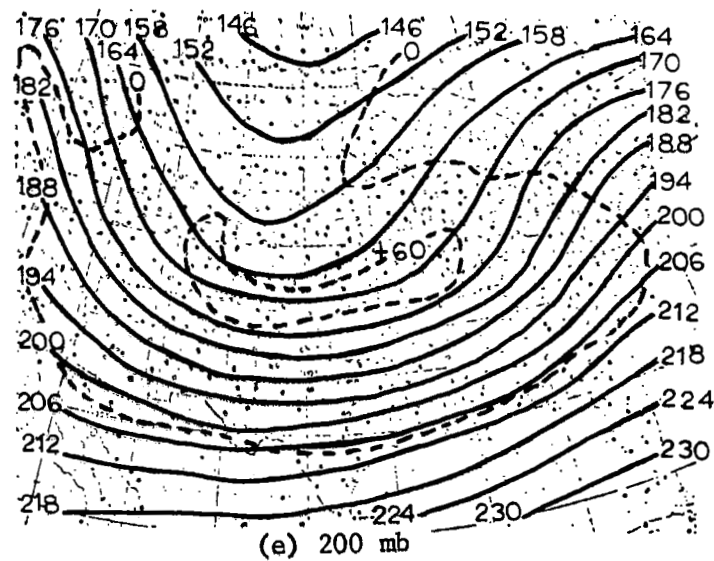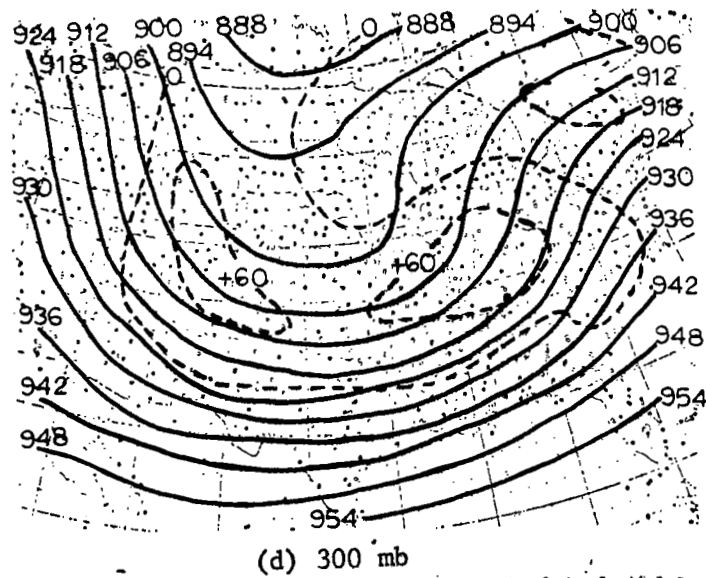
Fig. 36. (cont'd from previous page)

to divergence over much of the Ohio River Valley at these levels. The hatched area in Fig. 26d coincides well with many of the observed radar echoes.

Thermal advection, inferred from Fig. 37, also contributes to positive vertical motion in the mid-troposphere in the areas of radar echoes east of the 850 mb trough axis. Strong positive thermal advection is indicated in Figs. 37a and 37b at 850 and 700 mb over much of the eastern United States. In Figs. 37c, 37d, and 37e, weaker thermal advection is shown at 500, 300, and 200 mb over much of the eastern United States. Strong positive temperature advection at low levels (850 and 700 mb) with weaker positive advection aloft (500, 300, and 200 mb) will increase γ, decrease $\gamma_d - \gamma$ in (7), and increase positive vertical motion.

The βv-term makes the dominant contribution to convergence east of the 850-mb low center in Fig. 38a. A comparison of Figs. 36b and 37b shows that both $\partial Z'/\partial t$ and PVA contribute to divergence east of the trough, but the βv-term makes a contribution to convergence, so the sign of divergence in the principal area of radar echoes at the 700-mb level cannot be determined. The sign of divergence east of the trough over the main area of radar echoes also is indeterminate in Fig. 38c since PVA and the latitudinal terms oppose each other. Figures 38d and 38e show PVA at 300 and 200 mb which probably leads to divergence in the vicinity of the radar echoes despite a slight contribution to convergence from the βv-term. Examination of the entire column shows that there is convergence at 850 mb, divergence at 300 and 200 mb, and by Dines' Compensation Principle there should be positive vertical motion through the region of coincidence over the northeastern United States. The hatched area in Fig. 26e shows a good correlation with radar echoes over the northeastern United States.

Figures 39a and 39b indicate strong positive thermal advection at 850 and 700 mb throughout most of the areas of radar echoes in the northeastern quadrant of the United States. Figures 39c, 39d, and 39e indicate weaker warm advection at 500, 300, and 200 mb over the echo areas. By the adiabatic method, positive vertical motion in the mid-troposphere is indicated in most of the areas of radar echoes in the northeastern quadrant of the United States. Scattered radar echoes in Florida, the panhandle of Texas, and Montana are not explained by the methods presented here.
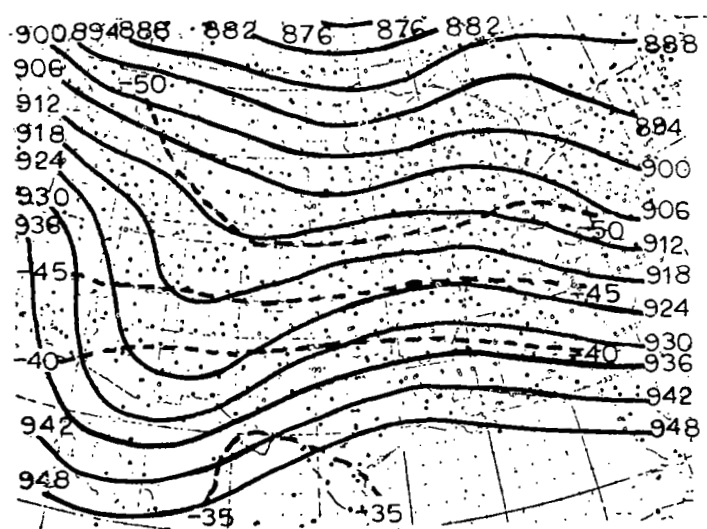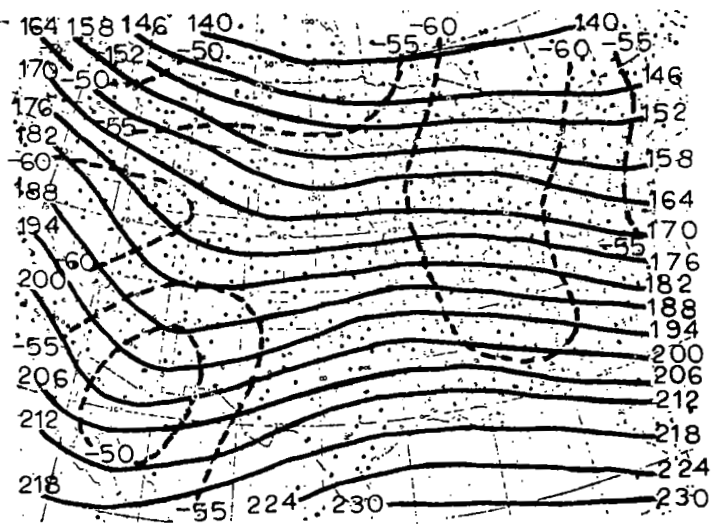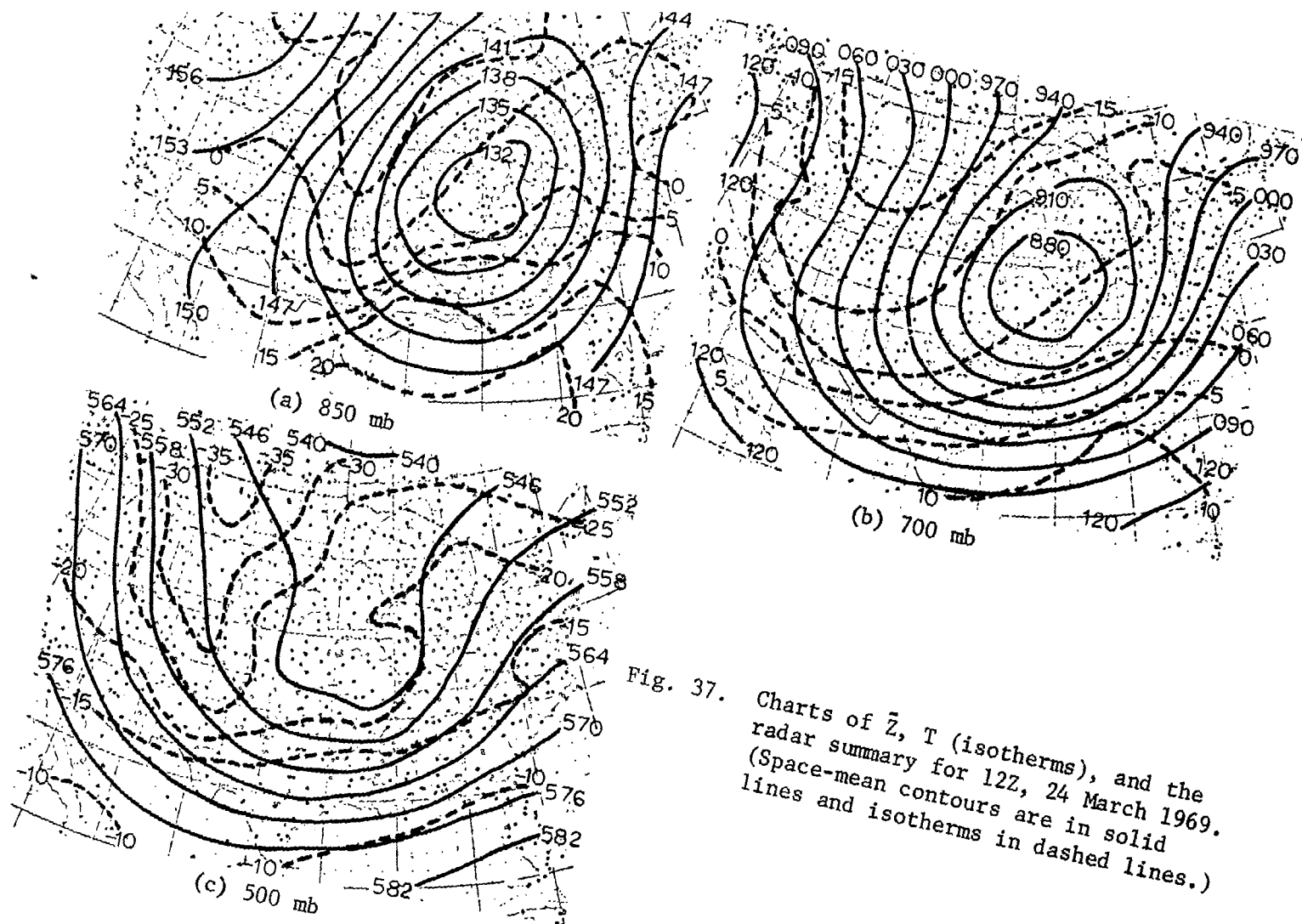
(a) 850 mb

(b) 700 mb

(c) 500 mb

Fig. 37. Charts of $\bar{Z}$, T (isotherms), and the
radar summary for 12Z, 24 March 1969.
(Space-mean contours are in solid
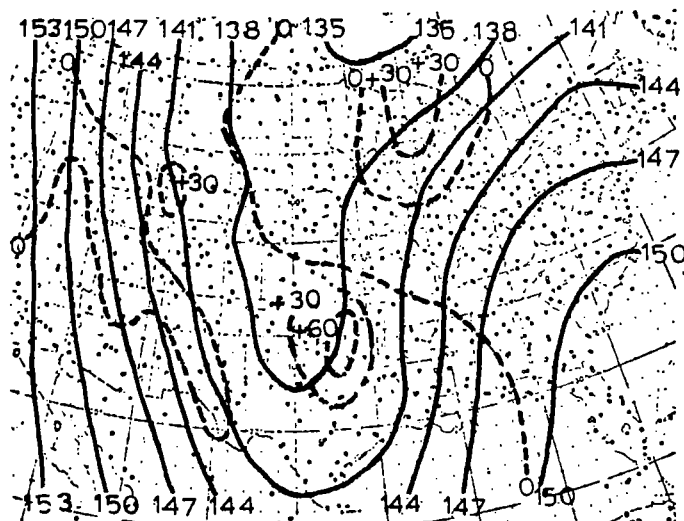lines and isotherms in dashed lines.)
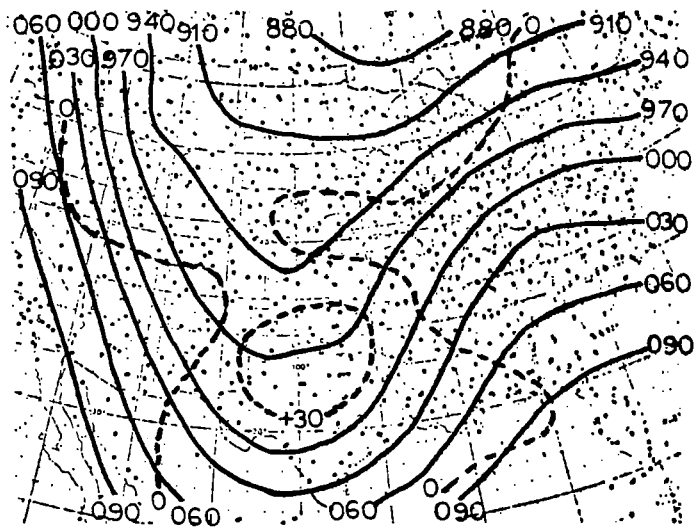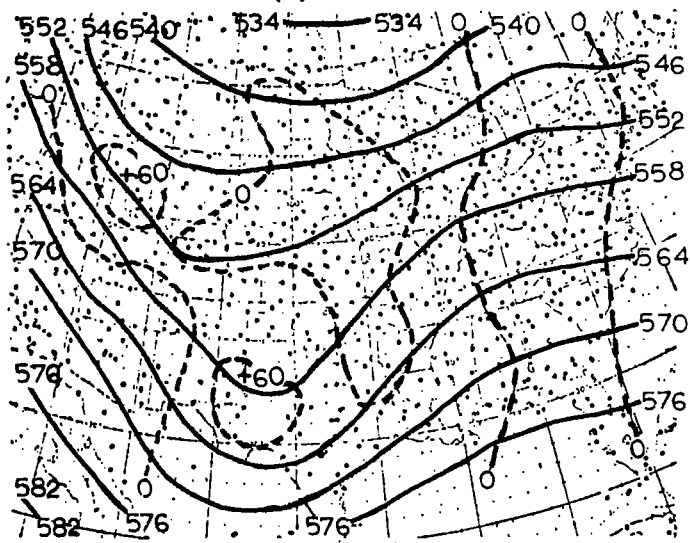
(d) 300 mb

(e) 200 mb
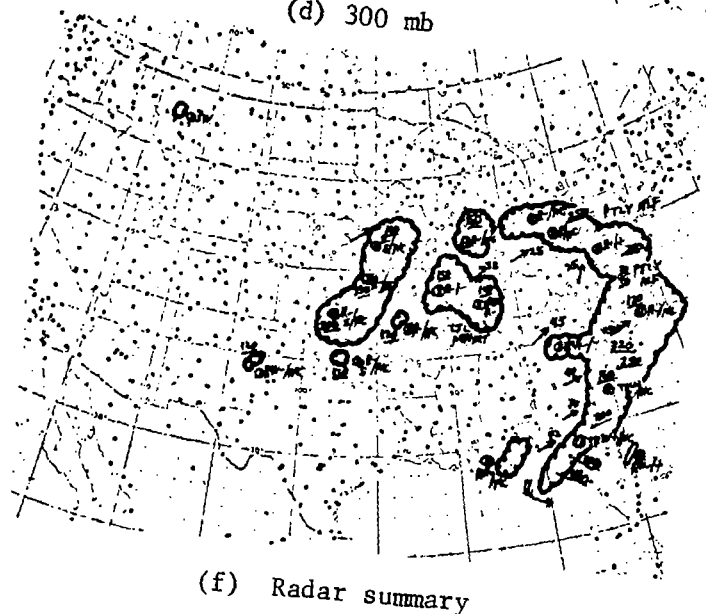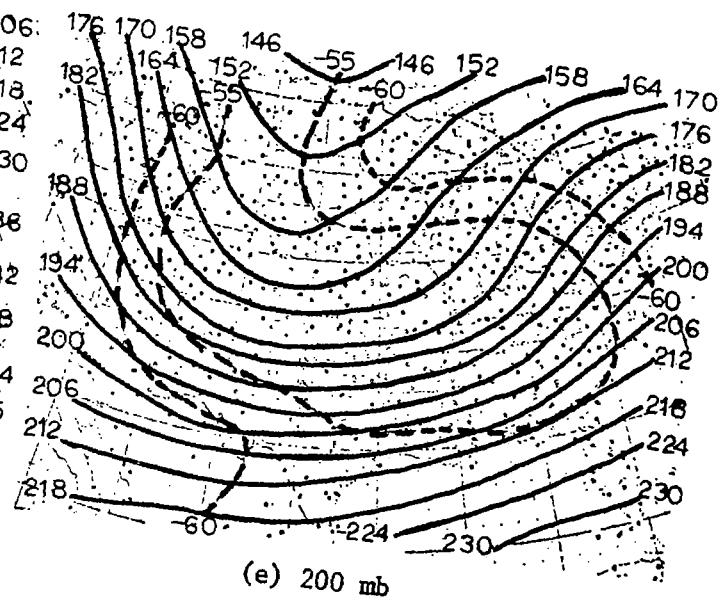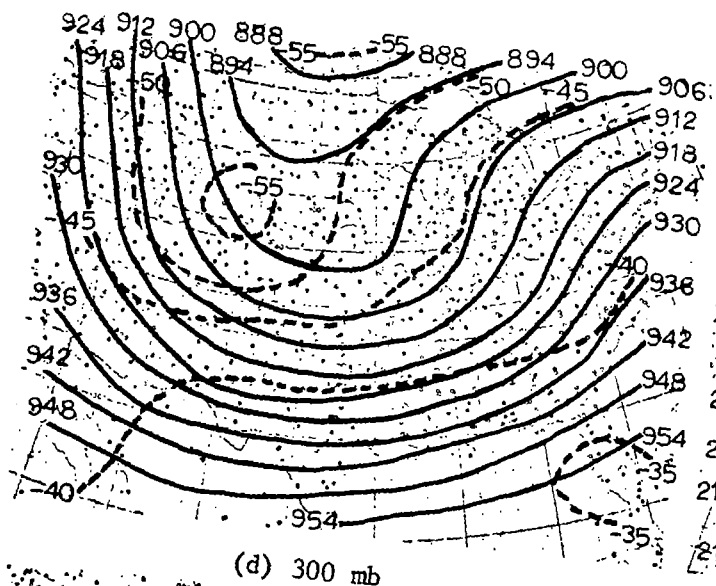
(f) Radar summary

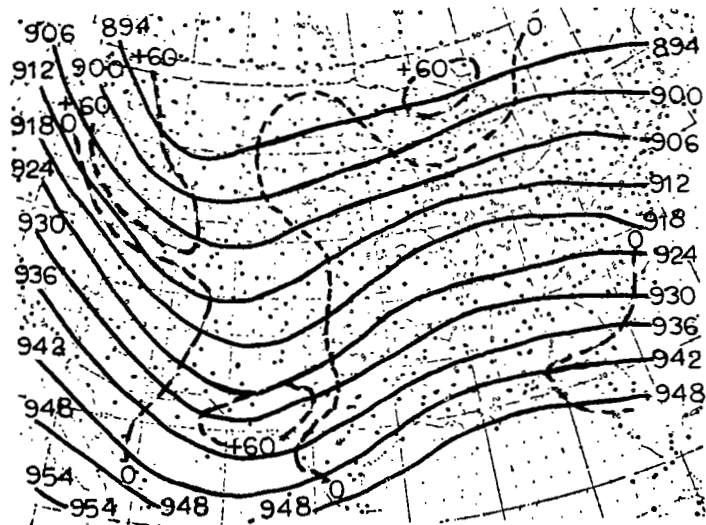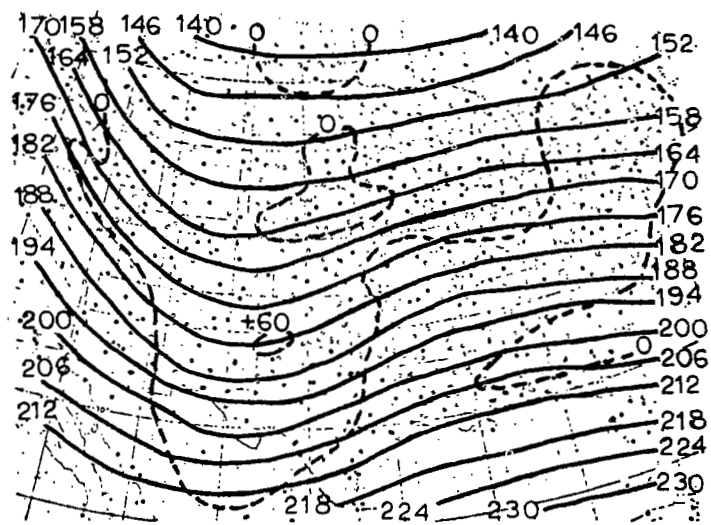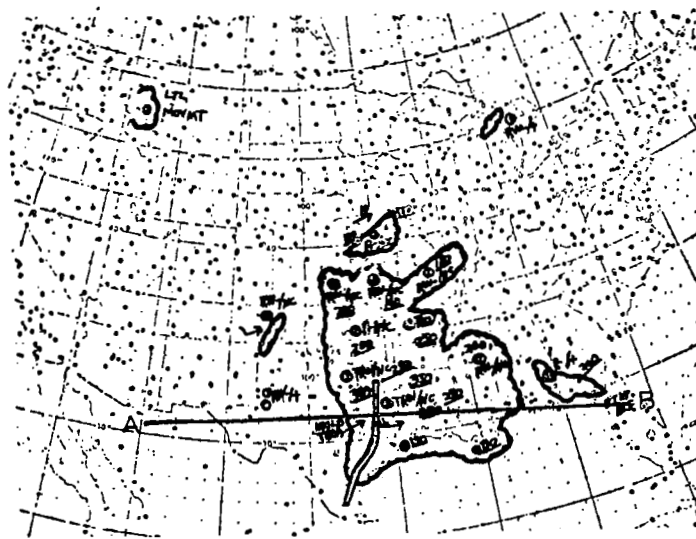Fig. 37. (cont'd from previous page)
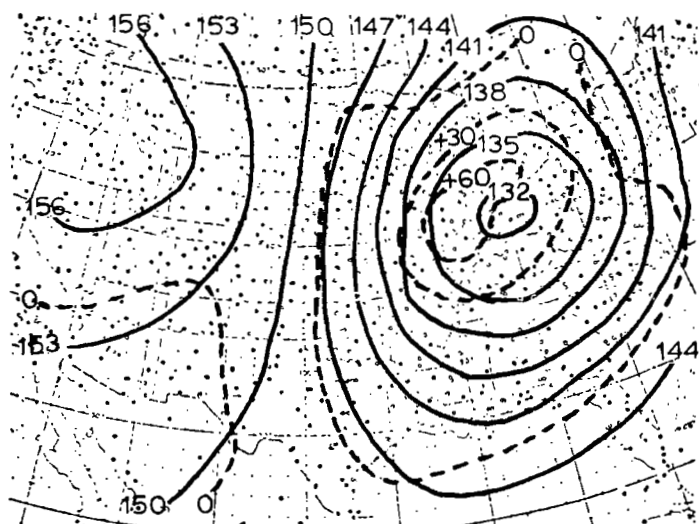
(a) 850 mb
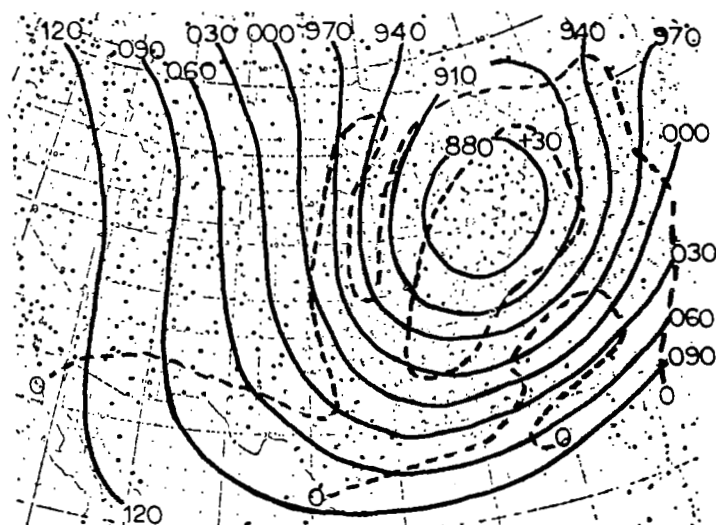
(b) 700 mb
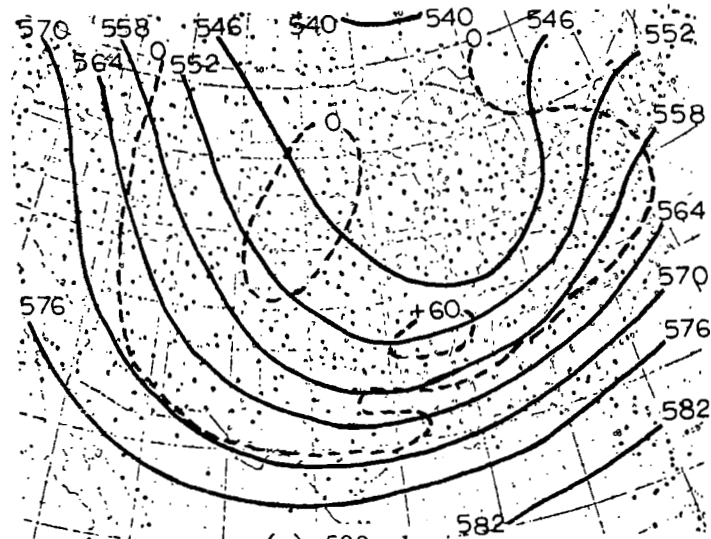
(c) 500 mb

Fig. 38. Charts of $\bar{Z}$, Z' fields, and the radar
summary for 00Z, 25 March 1969.
(Space-mean contours are shown in
solid lines and Z' fields in dashed
lines.)

(d) 300 mb

(e) 200 mb
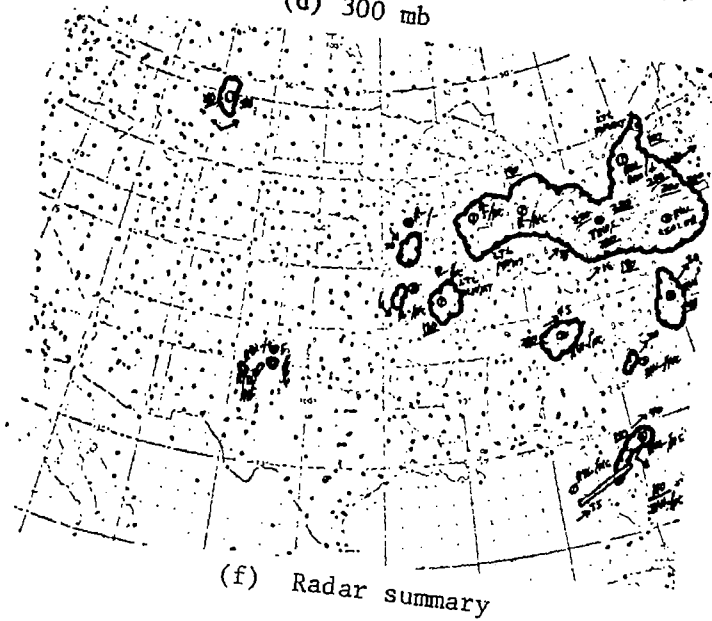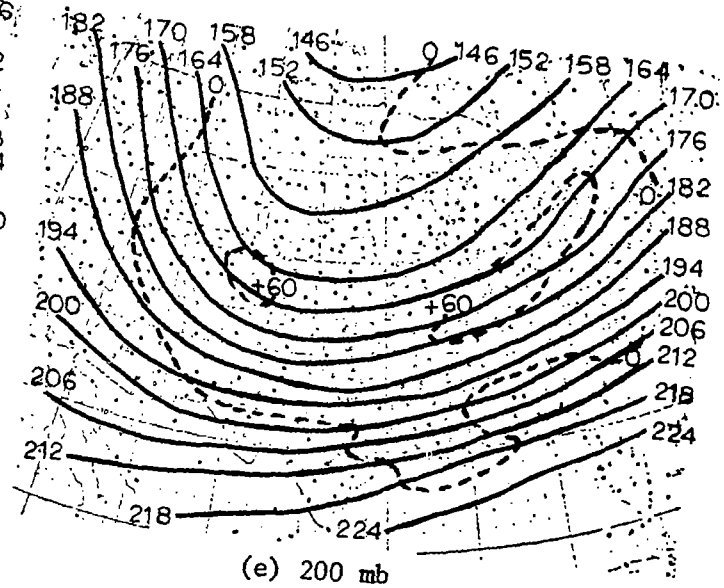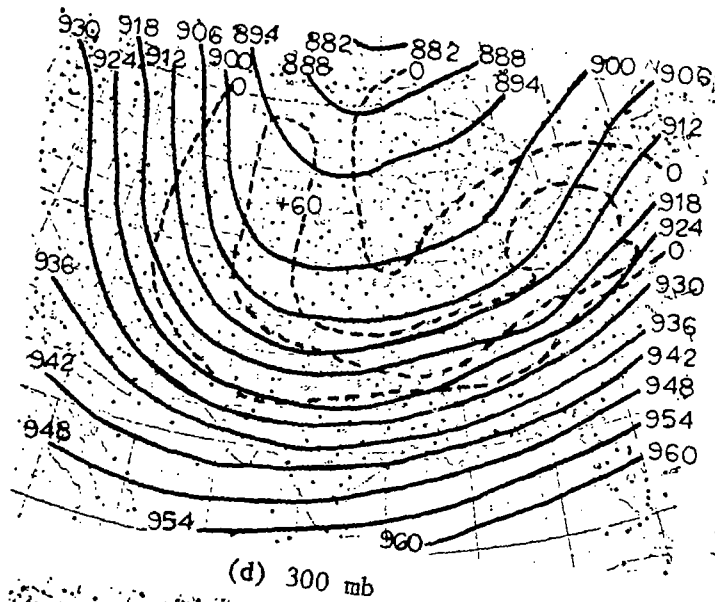
(f) Radar summary

Fig. 38. (cont'd from previous page)

(a) 850 mb

(b) 700 mb

(c) 500 mb

Fig. 39. Charts of $\bar{Z}$, T (isotherms), and
the radar summary for 00Z, 25 March
1969. (Space-mean contours are
in solid lines and isotherms in
dashed lines.)

(d) 300 mb

(e) 200 mb
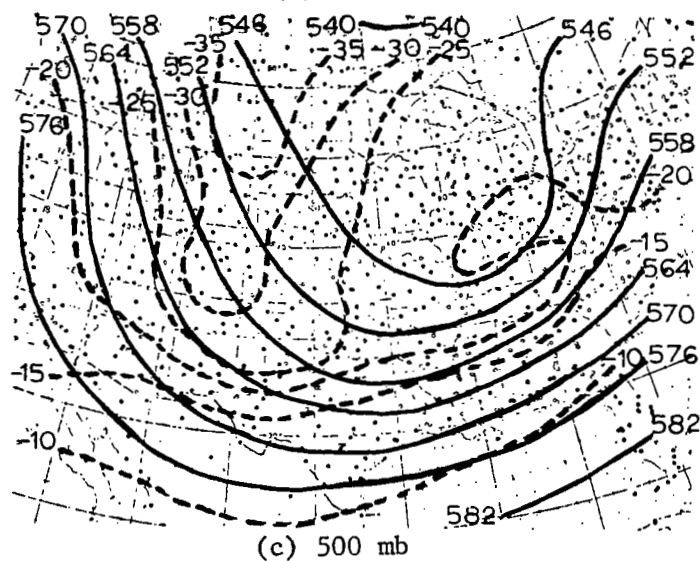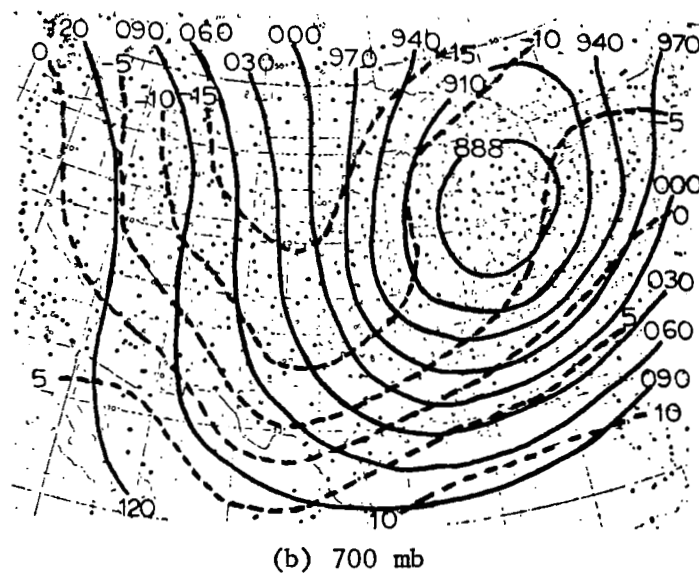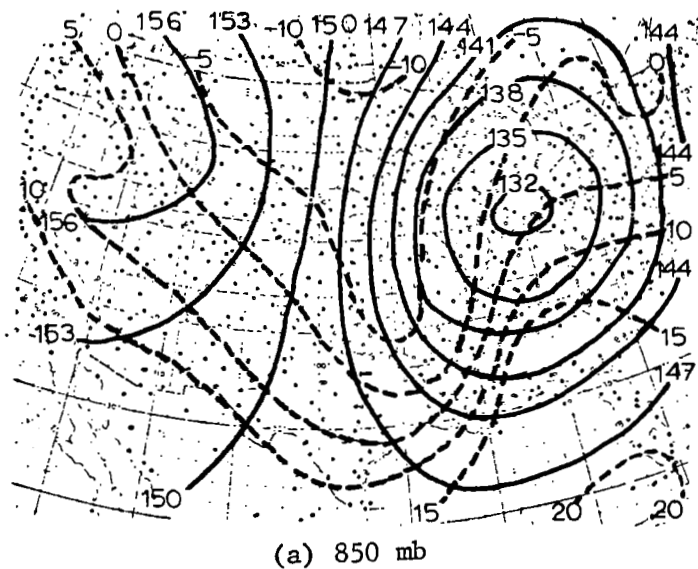
(f) Radar summary
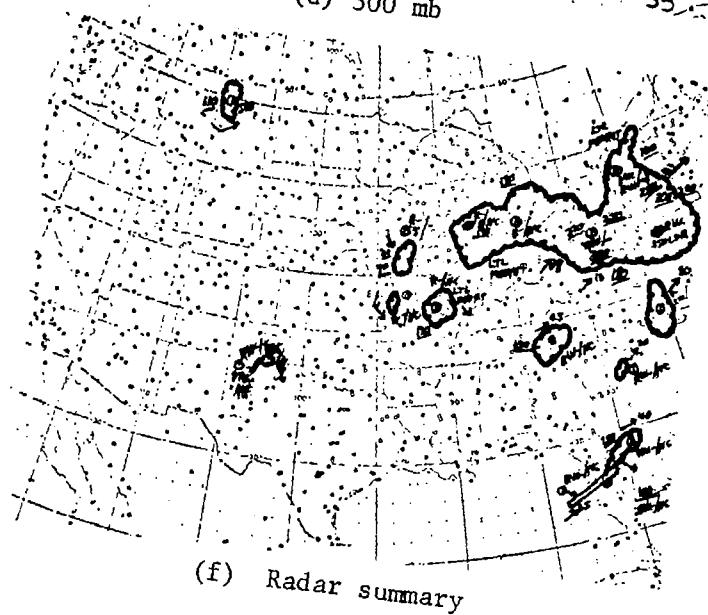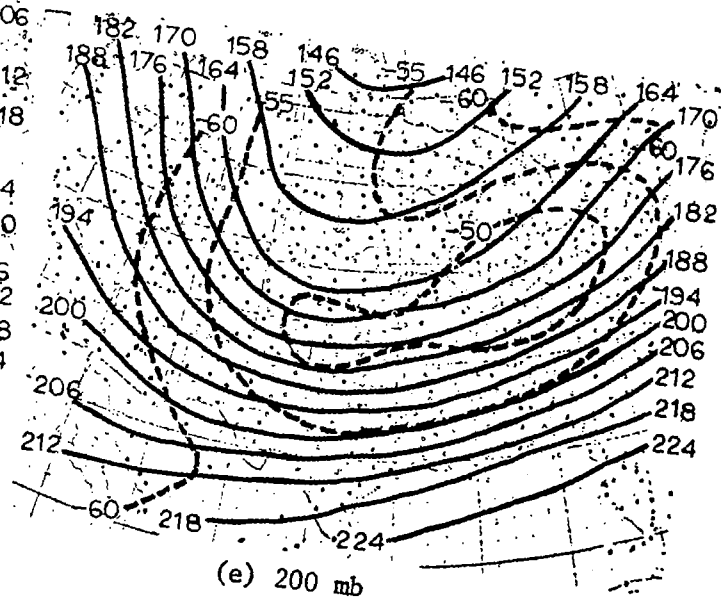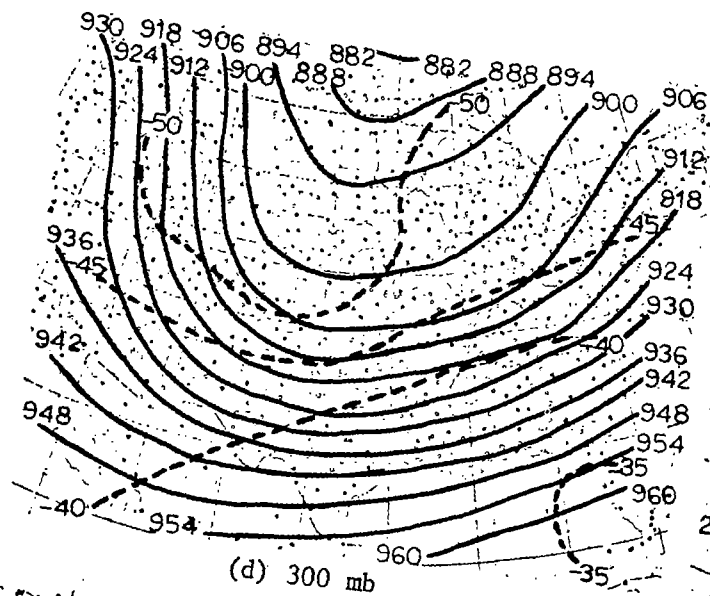
Fig. 39. (cont'd from previous page)

Figures 40a and 40b show that NVA combined with the strong south wind contritutes to convergence at 850 and 700 mb south and east of the low center. In Figs. 40c and 40d the advective and latitudinal terms are of opposite sign at 500 and 300 mb over much of the northeastern United States. However, because of well developed vorticity centers at 500 and 300 mb over the area of West Virginia, PVA probably leads to divergence at these levels over the northeastern United States. Convergence at 850 and/or divergence at 500 and 300 mb, shown in Fig. 26f, coincides with many of the radar echoes in the northeastern United States. Equations (3) and (7) evaluated over this map series delineates areas which coincide well with many of the observed mesoscale systems (radar echoes). Echoes outside the area of indicated large-scale positive vertical motion are explained partially by thermal advection.

Warm advection at 850 and 700 mb in much of the principal area of radar echoes in the northeastern United States may be inferred from Figs. 41a and 41b. Weaker warm advection over the same area at 500, 300, and 200 mb may also be inferred from Figs. 41c, 41d, and 41e, and by the adiabatic method positive vertical motion in the mid-troposphere is indicated in much of the principal area of radar echoes in the northeastern United States. Radar echoes over central Florida are not explained by the methods presented here and may be a result of surface fronts.

b) Structure of Trough

The first three time periods for the case of March have been subjected to analysis based on the structure of the wave. From the amplitude and wavelength of the trough as shown by the space-mean contours, as well as the mean westerly wind, the magnitude of Z' at the trough has been computed (using (14)) and compared in Table 3 with space-mean values. Since the magnitude of Z' varies along the axis of the trough, the wave-model value of Z' is obtained at the trough axis west of the radar echoes and compared with the space-mean magnitude of Z' at the same location. The last three time periods have not been analyzed using the wave-model because the trough is moving off the East Coast and it is·not possible to judge accurately the wavelength of the trough.

(a) 850 mb

(b) 700 mb

(c) 500 mb

Fig. 40. Charts of $\bar{Z}$, Z' fields, and the radar summary for 12Z, 25 March 1969. (Space-mean contours are shown in solid lines and Z' fields in dashed lines.)

(d) 300 mb

(e) 200 mb
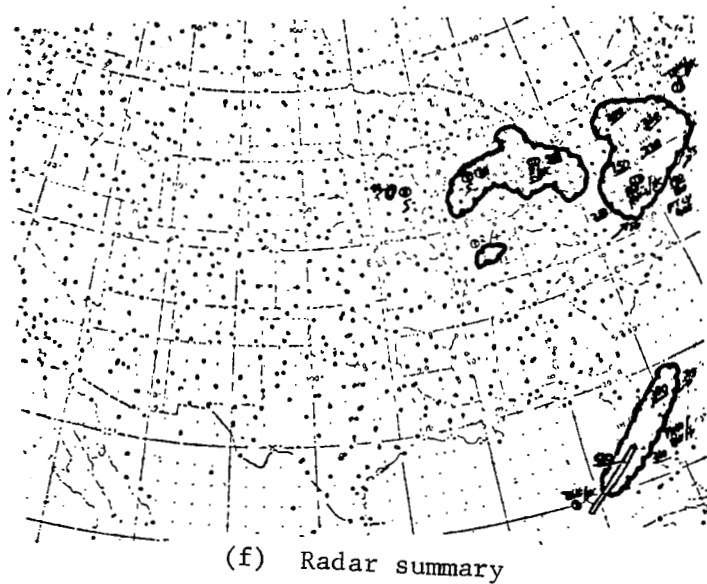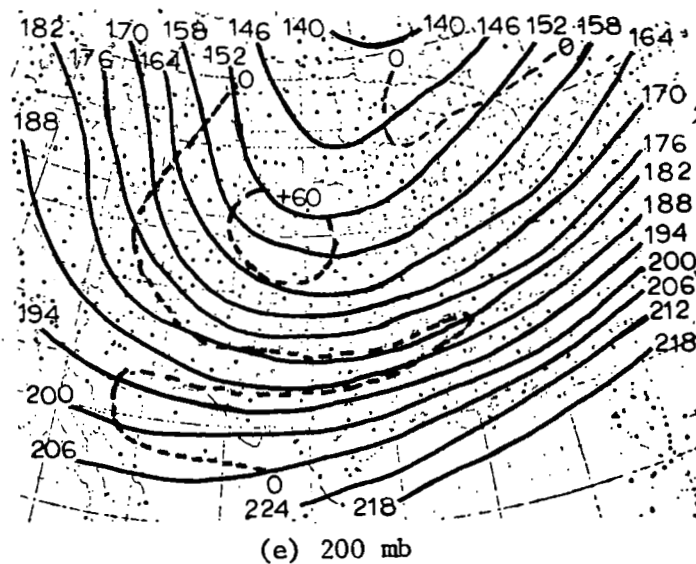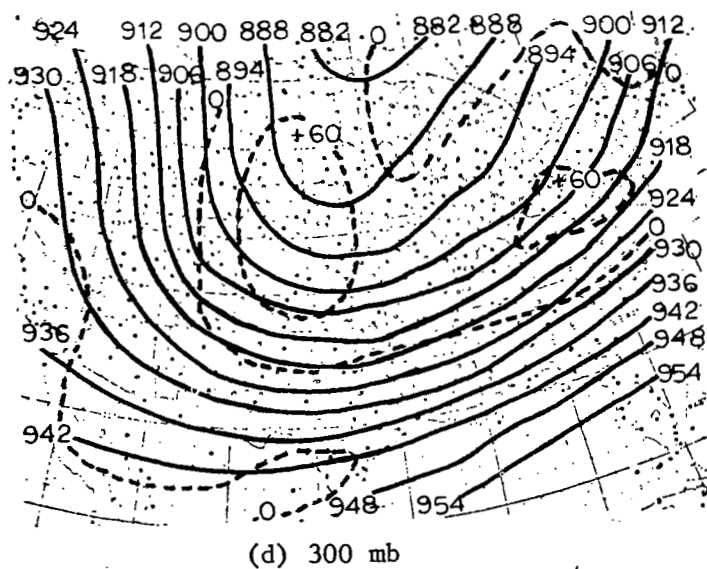
(f) Radar summary

Fig. 40. (cont'd from previous page)

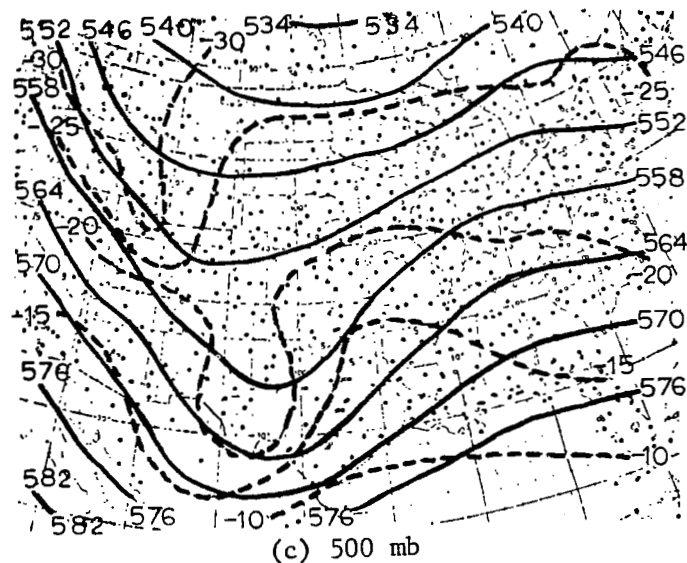(a) 850 mb

(b) 700 mb

(c) 500 mb

Fig. 41. Charts of $\bar{Z}$, T (isotherms), and the radar summary for 12Z, 25 March 1969. (Space-mean contours are in solid lines and isotherms in dashed lines.)

(d) 300 mb

(e) 200 mb
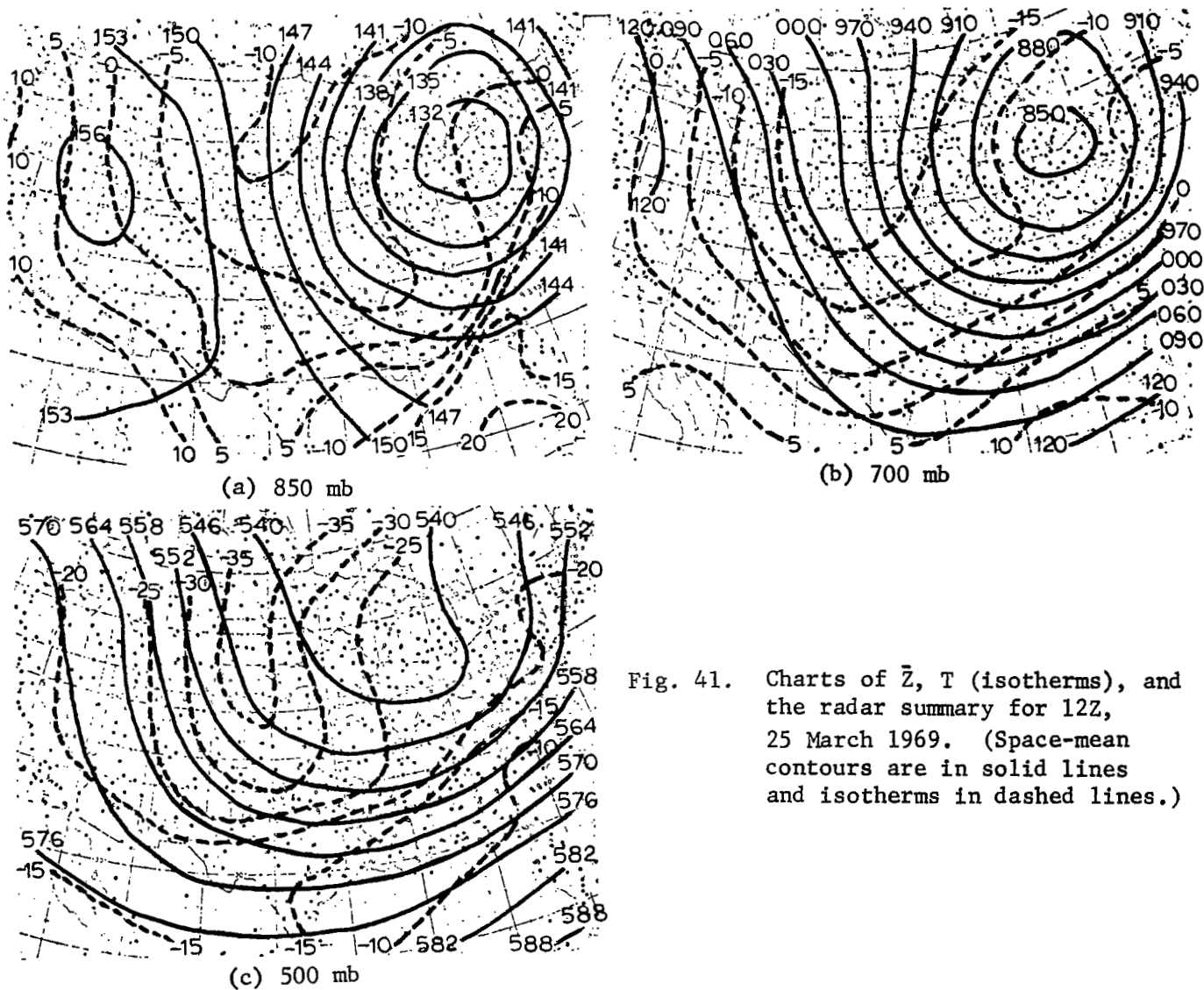
(f) Radar summary

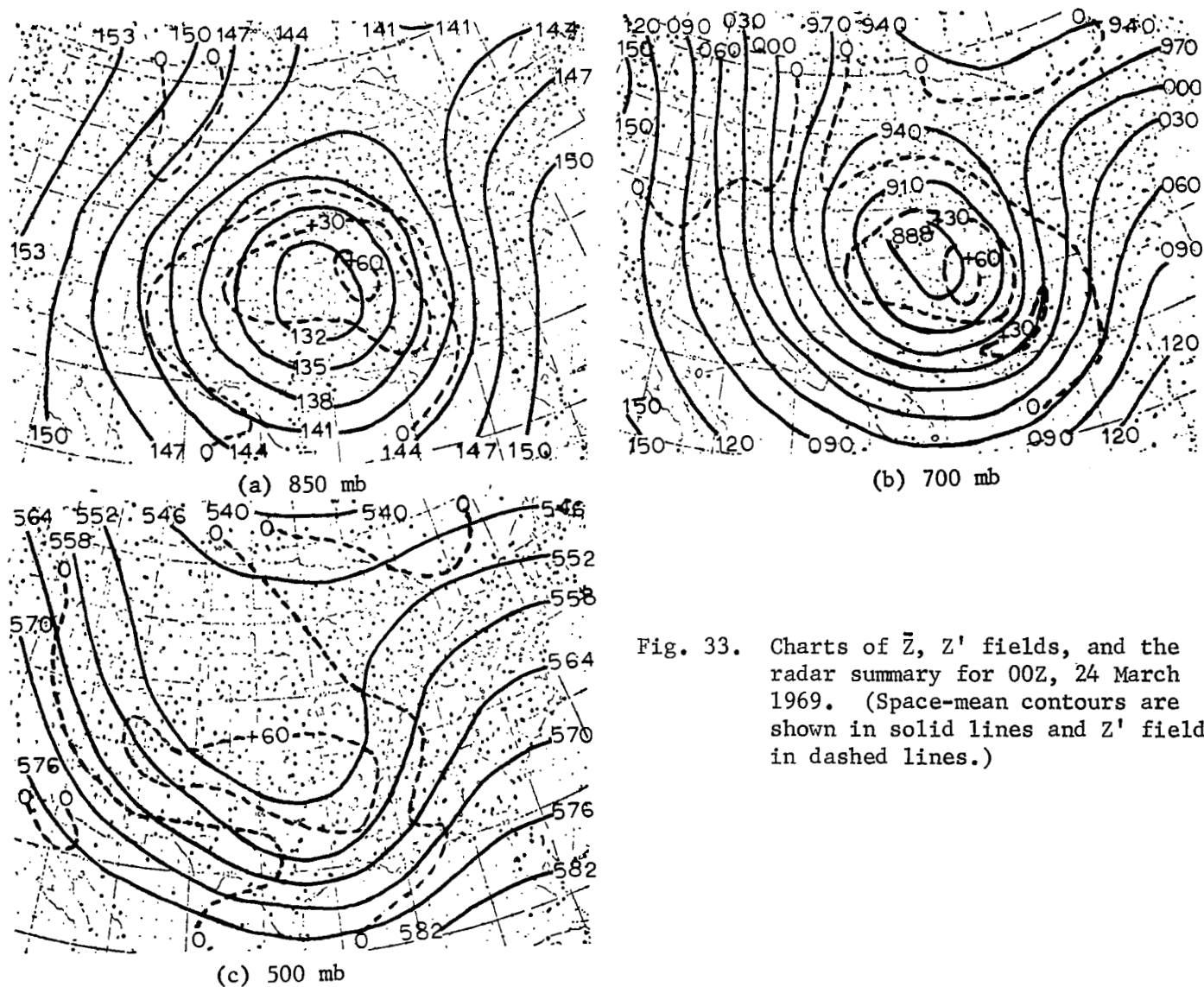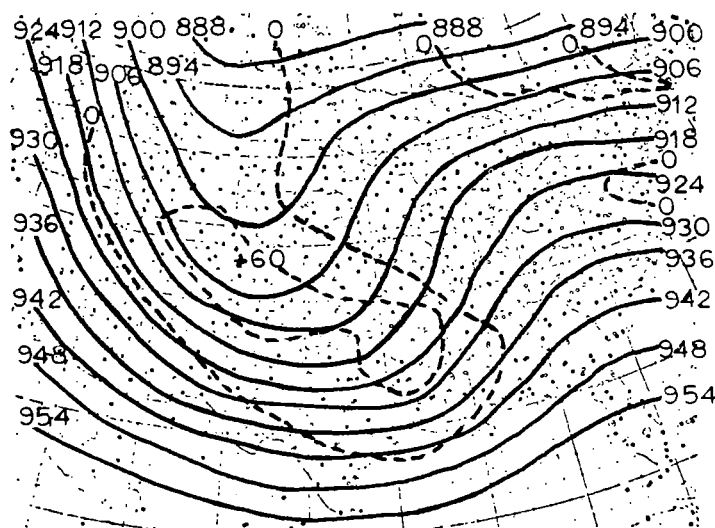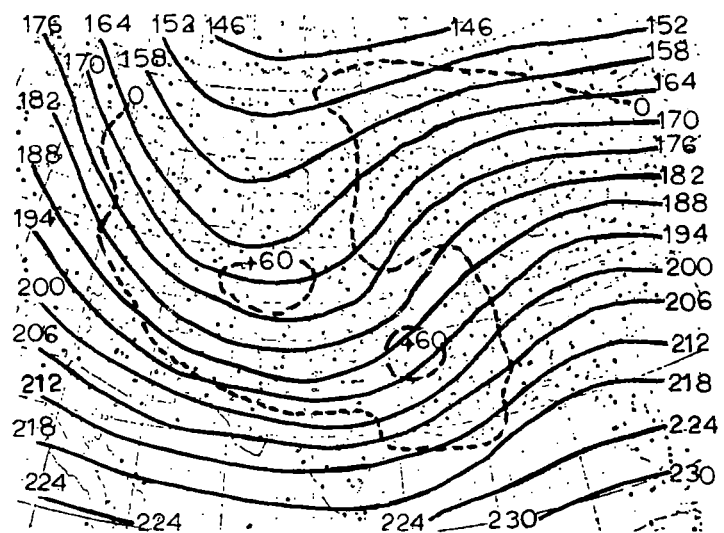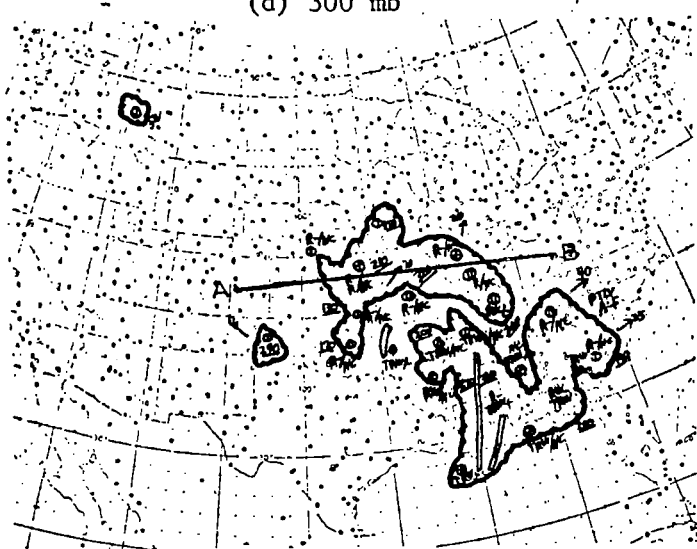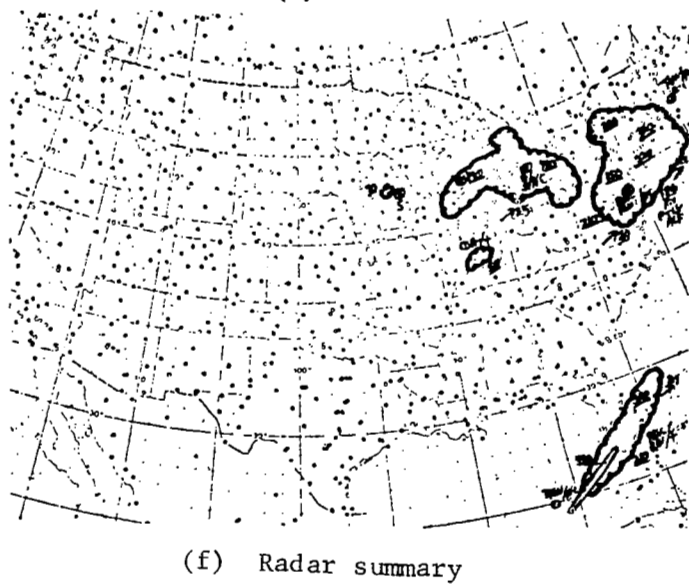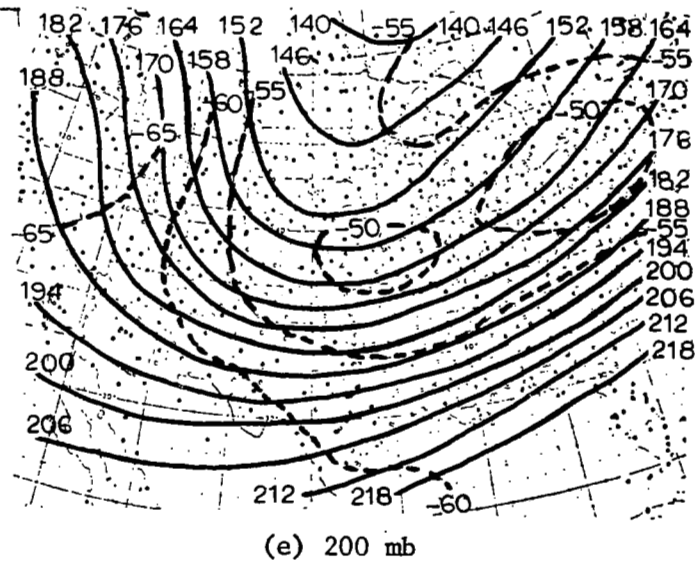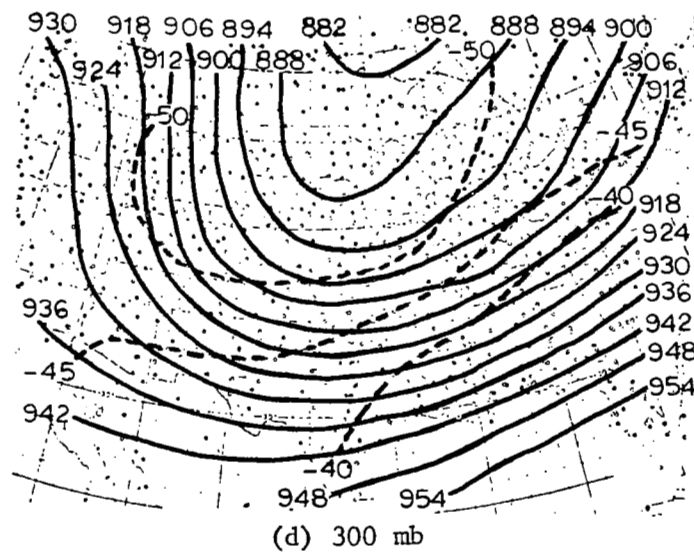Fig. 41.   (cont'd from previous page)

TABLE 3

COMPARISON OF Z' OBTAINED BY SPACE-MEAN AND WAVE-MODEL TECHNIQUES

Pressure Level (mb)	850	700	500	300	200
a. 00Z, 23 March 1969					
Space-Mean Z' (m)	60	25	20	65	65
Wave-Model Z' (m)	35	25	20	30	30
b. 12Z, 23 March 1969					
Space-Mean Z' (m)	25	30	60	60	30
Wave-Model Z' (m)	35	20	25	30	35
c. 00Z, 24 March 1969					
Space-Mean Z' (m)	15	20	60	65	30
Wave-Model Z' (m)	35	65	45	35	15

In Table 3, Part a, the space-mean magnitude of Z' at the trough for
each level is shown versus the computed magnitude of Z' at the trough for
the case of 00Z, 23 March 1969. The wave-model magnitude of Z' is less
than the space-mean magnitude of Z' at 850, 300, and 200 mb, but is in
agreement at 700 and 500 mb. Positive vertical motion in the mid-troposphere
would be indicated in the area of meso-scale systems (radar echoes) using
the vorticity method and Dines' Compensation Principle.

Shown in Table 3, Part b, for 12Z, 23 March 1969 the wave-model magni-
tudes of Z' agree closely with space-mean values of Z' at 850, 700, and
200 mb; but, wave-model values are less than space-mean values at 500 and
300 mb. Application of (3) to the entire column shows that there is con-
vergence east of the trough at 850 mb, divergence east of the trough at
300 and 200 mb, and by Dines' Compensation Principle there will be positive
vertical motion in an area coincident with observed radar echoes.

It may be seen in Table 3, Part c, that for 00Z, 24 March 1969 the
wave-model magnitude of Z' is greater than the space-mean magnitude of Z'
at 850 and 700 mb and is less than the space-mean magnitude at 500, 300,
and 200 mb. Examination of the entire column by means of (3) shows that

there is convergence at 850 and 700 mb throughout much of the area of radar echoes. Divergence at 300 and 200 mb affects the eastern parts of the echo area and positive vertical motion in the mid-troposphere would be indicated over much of the area of radar echoes.

The method of computing the magnitude of Z' at the trough or ridge axis based on the structure of the wave yields results which correlate in arith-methic sign and in approximate magnitude to space-mean values of Z'. Results shown in Parts a and b of Table 3 generally are better than those in Part c. This may be because by the time associated with values shown in Part c, the trough had become very deep and broad with closed contours at 850 and 700 mb.

A limitation to the wave-model method of computing the magnitude of Z' is that the method may give no indication of vorticity centers located away from the trough axis. However, the wave-model method gives results which, when used with the space-mean contours and (3), may be used to delineate areas of positive vertical motion in the mid-troposphere. Hence, the method may be used to delineate areas in which mesoscale systems should be present.

The structure of the wave is not used to evaluate the magnitude of Z' at the trough axis in the June, December, and September cases. The June and September cases do not lend themselves well to this method since troughs and ridges are poorly defined, difficult to locate exactly, and amplitudes and wavelengths are difficult to evaluate. A random sampling was taken from the December case and it was found that computed values of Z' at the trough compare favorably with space-mean values with a degree of accuracy similar to the March case. To include a discussion based on the structure of the wave for the December case would be both lengthy and repetitious without contributing significantly to an improved understanding of the usefulness of the method for computing the magnitude of Z'.

c) Curvature of the Vertical Wind Profile

Figure 42 shows the results of the analysis of curvature for 00Z, 23 March 1969. The corresponding composite radar chart is shown in Fig. 29f. The expected area of echoes in Minnesota and Iowa coincides closely with the observed echoes. Small expected regions in the Texas panhandle and west central Texas coincided somewhat with the observed echoes in that area.

Fig. 43. Results of curvature analysis
for 12Z, 23 March 1969.

Fig. 42. Results of curvature analysis
for 00Z, 23 March 1969.

NOTE: In each figure the area of low-level convergence is enclosed by a solid line and the area
of upper-level divergence by a dashed line. The shaded areas represent $T - T_D \leq 5°C$ at
850 mb, while the hatched areas represent those of expected echoes.

105

Observed areas of echoes in Louisiana, South Central Texas and the Oklahoma-Kansas area were not covered by expected areas. There was sufficient upward motion indicated for these areas, but the reported dew-point depressions failed to indicate sufficient moisture for these areas to have echoes.

Figure 43 shows the results of the analysis of curvature for 12Z, 23 March 1969. The corresponding composite radar chart is shown in Fig. 30f. The expected area over the Great Lakes coincided well with the observed echoes there, as did the small area in the Florida panhandle. The expected areas along the Texas Gulf Coast and in the Arkansas-Missouri-Oklahoma region fit into the large area of widespread echoes which were observed, but they were considerably smaller than what actually occurred. There was sufficient moisture and upper-level divergence indicated for most of this region. The low-level convergence was probably available in this area, but was generally weak.

Figure 44 shows the results of the analysis of curvature for 00Z, 24 March 1969. The corresponding composite radar chart is shown in Fig. 33. The small expected areas of echoes in Wisconsin and in the Northeast failed to be verified by observed echoes. Some of the expected area of echoes from northern Alabama to central Oklahoma coincided with observed areas, but most of the observed area was surrounding the expected area. In this case strong low-level convergence was indicated, but the needed region of upper-level divergence was not found in the analysis. There was also a lack of observed moisture in the southeast part of the country.

4) Summary of Results for the March Period

This case is an example of a well-developed trough with associated mesoscale systems. Initially, the trough is best developed at 850 mb. Scattered radar echoes are present between the trough and downstream ridge from Texas to Minnesota. The trough deepens rapidly during the first three time periods and associated mesoscale systems become more consolidated. The trough gradually drifts eastward and becomes very broad so that the axis of the trough is difficult to locate. The "article of faith" was investigated using moisture and synoptic parameters to infer the sign of vertical motion. Large areas coincide well with observed radar echoes which are assumed to be indicative of the presence of mesoscale systems.
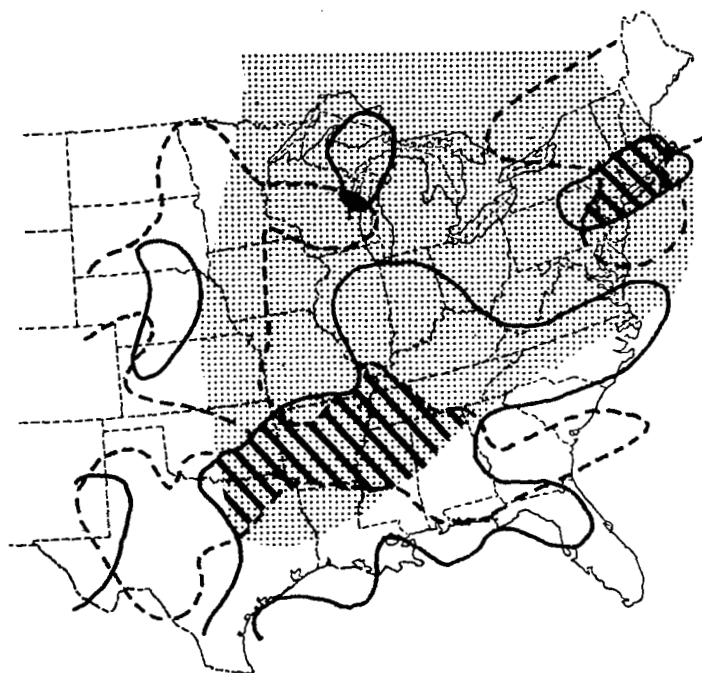
Fig. 44. Results of curvature analysis for
00Z, 24 March 1969. (The area of
low-level convergence is enclosed
by a solid line and the areas of
upper-level divergence by a dashed
line. The shaded areas represent
$T - T_D \leq 5°C$ at 850 mb, while the
hatched areas represent those of
expected echoes.)

107

b. June Period

   1) Synoptic Conditions

      Initially the synoptic-scale wave (figures not shown) is located at
850 mb along a line from New Mexico northeastward through Minnesota, and
slopes to the west with height. Wind and thermal gradients are small and
vorticity centers are poorly defined. Scattered radar echoes are present
east of the trough from Texas through Minnesota. Other radar echoes are
present along the Gulf and Atlantic coasts. The trough remains stationary
throughout the period and shows little development. Associated radar echoes,
indicative of mesoscale systems, remain scattered during the entire period
but maintain a degree of continuity in some areas.

   2) Moisture

      Figures showing the spread between the ambient and dew-point tempera-
tures at 850 mb superimposed on the composite radar summary are shown with
figures (discussed later) for each time period for this case. Most radar
echoes are present where the spread between the ambient and dew-point tem-
peratures is less than 10C.

   3) Stability

      To determine if a parcel, initially at 850 mb, will become unstable
when lifted, the 850-mb temperature and dew-point temperature profiles must
be known. Such detailed information is not available from the figures
presented here. However, a measure of the temperature profile is given by
the difference between the 500- and 850-mb temperatures. For the purposes
of this investigation, it is necessary to establish limits for the dew-
point depression at 850 mb and the temperature lapse between 850 and 500 mb
within which the air will become unstable if lifted. In the northern United
States (Canadian Border States), a typical 850-mb temperature is 15C during
June. If the temperature lapse between 850 and 500 mb is 25C and the 850-
mb dew-point depression is less than 3C, then the air will become unstable
when lifted. The limits within which the air will become unstable should
be made less restrictive since the difference in temperature between 850
and 500 mb is an approximation to the true lapse rate, and the dew-point

depression is an approximation of the supply of moisture. In this investigation, a decrease in temperature from 850 mb to 500 mb of at least 20C and a dew-point depression less than 5C at 850 mb will, in most cases, satisfy the requirements for conditional instability at least in part of the layer, and for sufficient low-level moisture in the northern United States at least in part of the layer. (Note: If the temperature difference between 850 and 500 mb is greater than 25C, then the dew-point depression can increase while still satisfying the stability condition.)

In the southern United States (Gulf Coast States) with a typical 850-mb temperature of 20C, a lapse between 850 and 500 mb of 25C, and dew-point depression less than 5C, the air will become unstable when lifted. Expanding these limits to account for the previously mentioned approximations, a lapse between 850 and 500 mb greater than 20C and a dew-point depression less than 10C at 850 mb will be used to satisfy the requirements for conditional instability (at least in part of the layer), and low-level moisture (at least in part of the layer) in the southern United States.

4) Vertical Motion

a) Kinemetic and Adiabatic Methods

Because of relatively weak winds, small thermal gradients, and poorly-defined vorticity centers, it is not possible to specify definite areas where positive vertical motion exists in the mid-troposphere. It is possible, however, to outline broad areas where weak convergence or divergence may be present. Areas of warm advection, particularly at low levels, weak convergence at low levels (850 and 700 mb), and/or divergence at upper levels (500, 300, and 200 mb) may be thought of as areas where the probability of positive vertical motion, hence mesoscale systems (given conditional instability and sufficient low-level moisture) are enhanced. Charts of space-mean contours, vorticity fields, and isotherms are not included in this and subsequent analyses due to their excessive bulk. However, figures in which areas of low-level (850-700 mb) convergence and upper-level (500, 300, and 200 mb) divergence are outlined will be shown, as well as areas of positive temperature advection.

In Fig. 45a, the difference between the 500- and 850-mb temperatures is shown in solid lines superimposed on the composite radar summary. Within
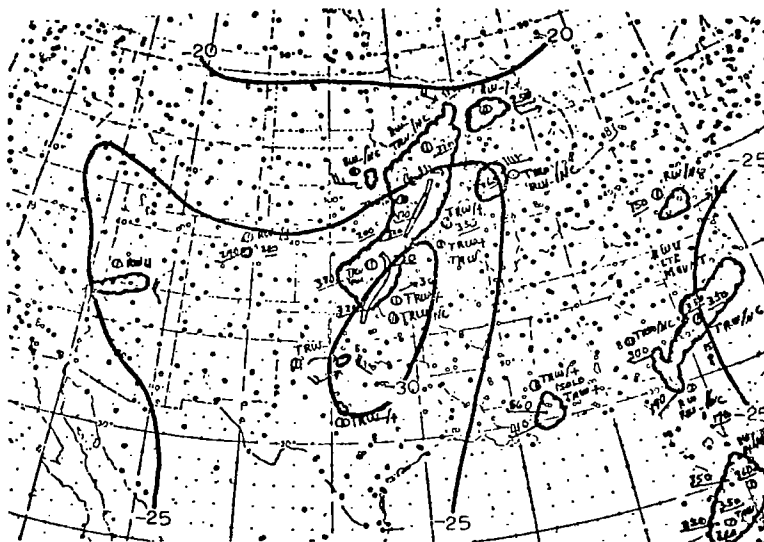
109

(a) The difference between the 500- and 850-mb tem-
peratures is shown in solid lines superimposed
on the composite radar summary.
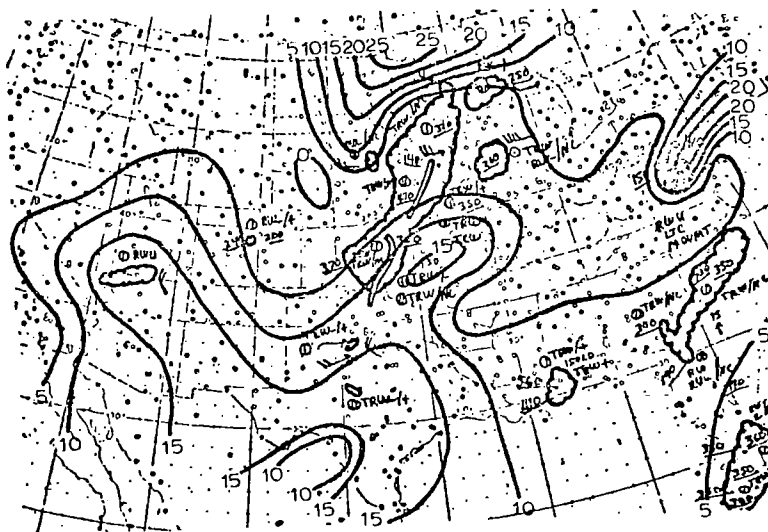
(b) The spread of the ambient and dew-point tem-
peratures at 850 mb is shown in solid lines
superimposed on the composite radar summary.

Fig. 45. Charts of the difference between the 500-
and 850-mb temperatures, the spread of
the ambient and dew-point temperatures at
850 mb, and areas of thermal advection
and divergence at each level for 12Z,
11 June 1969.
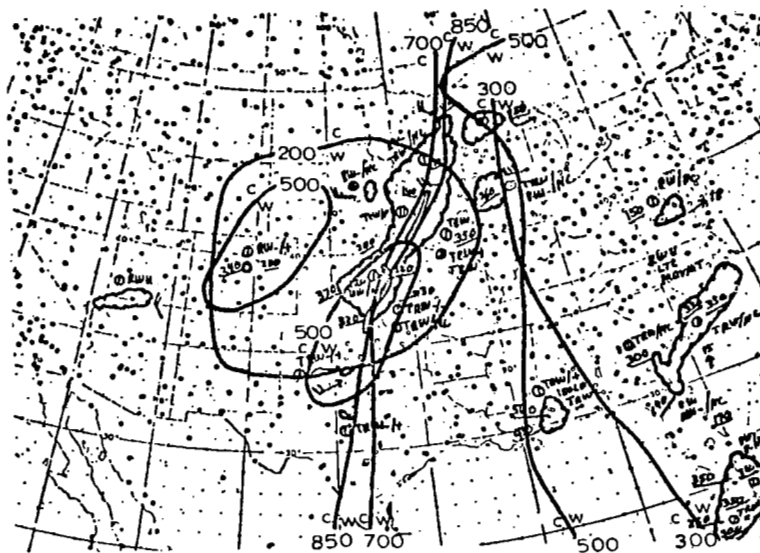
(c) Areas of temperature advection are outlined for
    each level in solid lines superimposed on the
    composite radar summary. W indicates the side
    of the line where warm advection occurs. C
    indicates the side of the line where cold or
    neutral advection occurs.
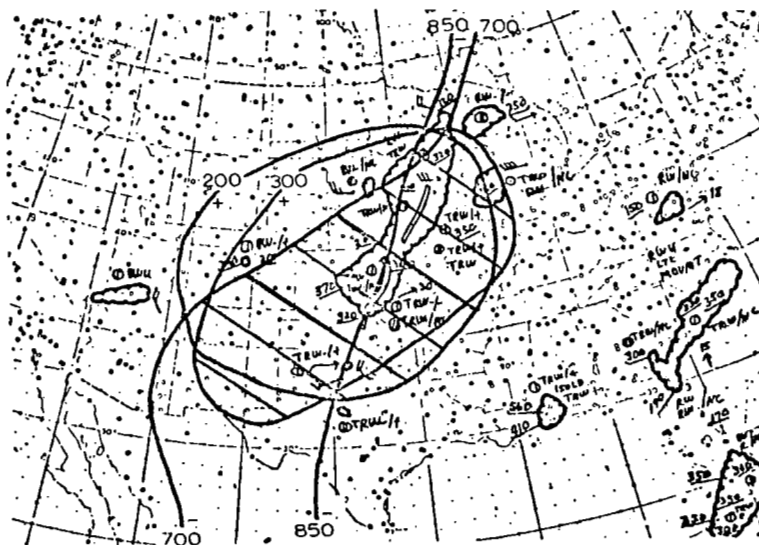
(d) Areas of divergence at each level are outlined
    in solid lines superimposed on the composite
    radar summary. The sign of divergence (+) is
    indicated on that side of the line where diver-
    gence occurs. Hatched areas are areas where
    divergence occurs over convergence.

Fig. 45. (cont'd from previous page)

111

the limits previously set forth, Fig. 45a shows that a conditionally unstable temperature lapse is present in all areas where radar echoes are reported. Figure 45b shows the spread between the ambient and dew-point temperatures at 850 mb in solid lines superimposed on the composite radar summary. The figures show, with the exception of small areas in northwestern Arizona and northern Virginia, that sufficient low-level moisture exists in the areas of radar echoes. Areas of positive temperature advection at each level are shown in Fig. 45c in solid lines superimposed on the composite radar summary. In the central United States, warm advection is present at 850 and 700 mb in the eastern half of the area of radar echoes. Areas of warm advection are present at higher levels over at least a part of the echo area, as shown in Fig. 45c. In the southeastern United States, Fig. 45c shows warm advection at 850, 700, 500, and 300 mb in the areas of radar echoes. (Exception: Cold or neutral advection is indicated at 300 mb over southern Alabama.) By the adiabatic method, warm advection indicates a contribution to positive vertical motion in the areas of radar echoes in the central and southeastern United States. Areas of divergence (or convergence) at each level are outlined in solid lines in Fig. 45d superimposed on the composite radar summary. Hatched areas indicate divergence over convergence and, by Dines' Compensation Principle, positive vertical motion in the mid-troposphere. In the area of radar echoes in the central United States, Fig. 45d shows convergence at 850 and/or 700 mb, divergence at 300 and 200 mb, and there should be positive vertical motion in the mid-troposphere. In the southeastern United States, radar echoes are present in areas where warm advection at 850, 700, 500, and 300 mb, and convergence at 850 and 700 mb, combine to provide weak broad-scale lift. Mesoscale convection may be triggered in this area by daytime surface heating or may not be directly related to events of a synoptic scale.

Figure 46a shows that the requirement of conditional instability is present in all areas where radar echoes are reported. Sufficient moisture is present at 850 mb, shown in Fig. 46b in most of the areas of radar echoes. Radar echoes in Mississippi and Alabama, as well as scattered areas of echoes in the western United States, are outside the previously-defined limits for sufficient low-level moisture. However, the two
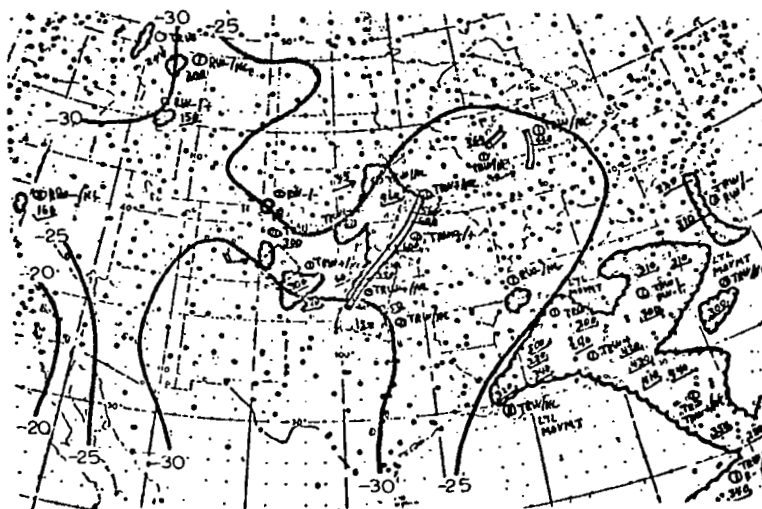
(a) The difference between the 500- and 850-mb temperatures is shown in solid lines superimposed on the composite radar summary.
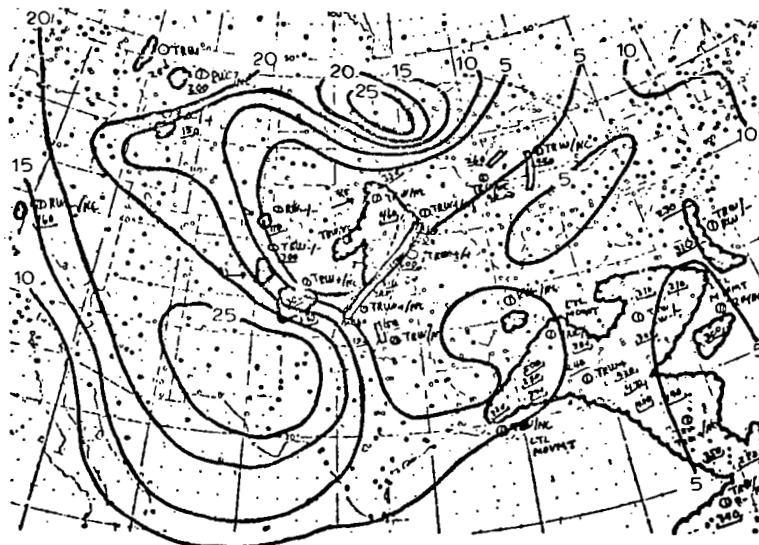
(b) The spread of the ambient and dew-point temperatures at 850 mb is shown in solid lines superimposed on the composite radar summary.

Fig. 46.   Charts of the difference between the 500- and 850-mb temperatures, the spread of the ambient and dew-point temperatures at 850 mb, and areas of thermal advection and divergence at each level for 00Z, 12 June 1969.
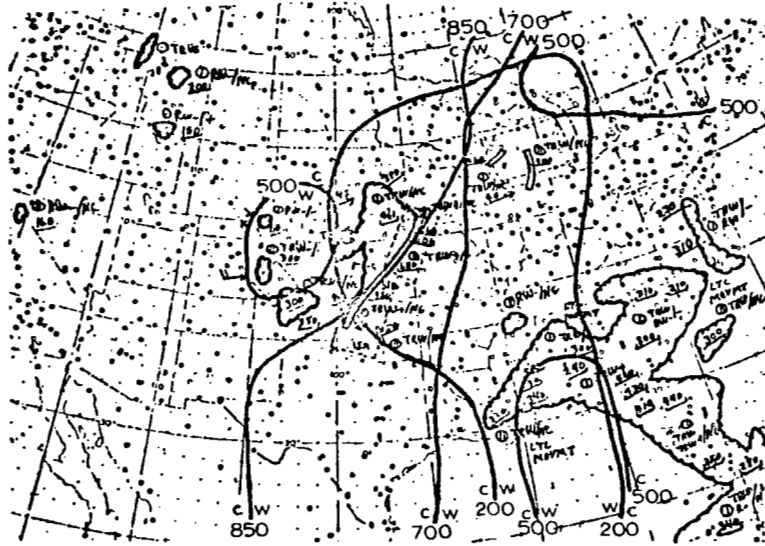
113

(c) Areas of temperature advection are outlined for
each level in solid lines superimposed on the
composite radar summary. W indicates the side
of the line where warm advection occurs. C
indicates the side of the line where cold or
neutral advection occurs.
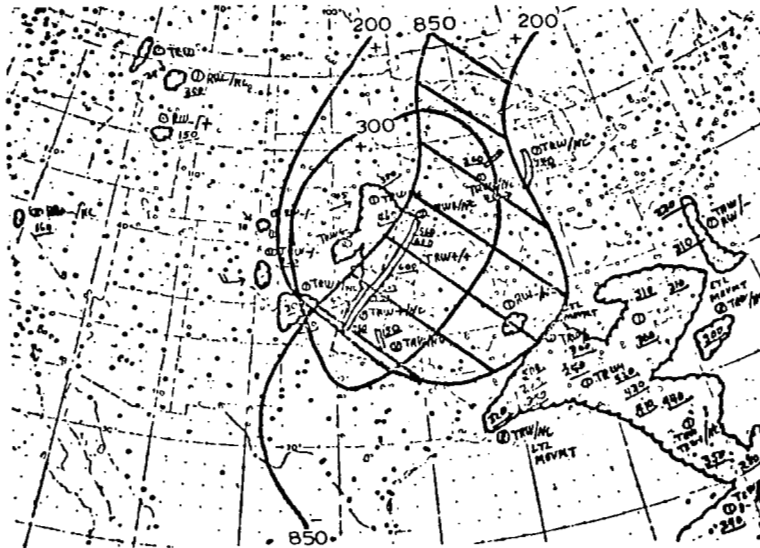
(d) Areas of divergence at each level are outlined
in solid lines superimposed on the composite
radar summary. The sign of divergence (+) is
indicated on that side of the line where diver-
gence occurs. Hatched areas are areas where
divergence occurs over convergence.

Fig. 46. (cont'd from previous page)

114

largest areas of radar echoes in the central and southeastern United States, occurred within the limits for sufficient low-level moisture.

A comparison of Figs. 45c and 46c for the central United States shows that warm advection at 850, 700, and 500 mb has decreased in the area of radar echoes. There has been a corresponding decrease in the areal extent of radar echoes. In the area of radar echoes in the southeastern United States, Fig. 46c shows warm advection at 850 and 700 mb. Warm advection over a part of the echo area is present at 500 and 200 mb. A comparison of Figs. 45c and 46c in the southeastern United States shows that there has been no significant change in the extent of warm advection. However, radar echoes have increased in horizontal and vertical extent. In the central United States, the hatched area in Fig. 46d, indicating an area of divergence over convergence (and therefore positive vertical motion in the mid-troposphere by Dines' Compensation Principle), coincides well with the observed radar echoes. Radar echoes in the central United States with maximum vertical development are contained within the hatched area. In the southeastern United States, Fig. 46d shows convergence at 850 mb. A comparison of Figs. 45d and 46d in the southeastern United States shows that convergence indicated in Fig. 45d at 700 mb is not present in Fig. 46d. In the southeastern United States, two indicators of vertical motion, thermal advection and divergence at each level based on the vorticity equation, have not changed significantly from 12Z, 11 June to 00Z, 12 June 1969. However, radar echoes have increased during the same 12-hour period. Since it has been established that the air is conditionally unstable and sufficient low-level moisture is present, daytime surface heating may be the triggering mechanism for convective precipitation in this area. Scattered areas of radar echoes in the western United States may results from terrain effects and/or may not be related to synoptic-scale systems.

Within the limits of the lapse rates of temperature and moisture established previously, Fig. 47a shows a conditionally unstable lapse of temperature between 850 and 500 mb in almost all areas where radar echoes are reported. Exceptions are in northern Minnesota and northern Idaho. Figure 47b shows that most radar echoes exist in areas where the difference between ambient and dew-point temperatures is less than 5C. With the
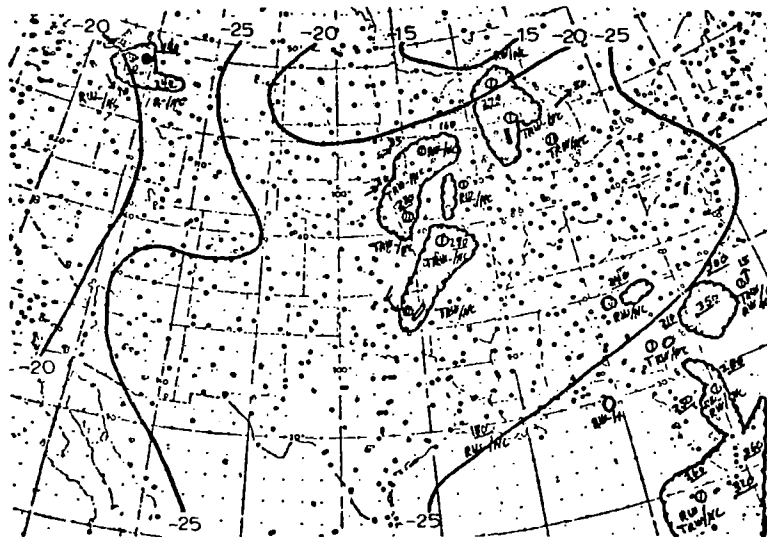
(a) The difference between the 500- and 850-mb tem-
peratures is shown in solid lines superimposed
on the composite radar summary.
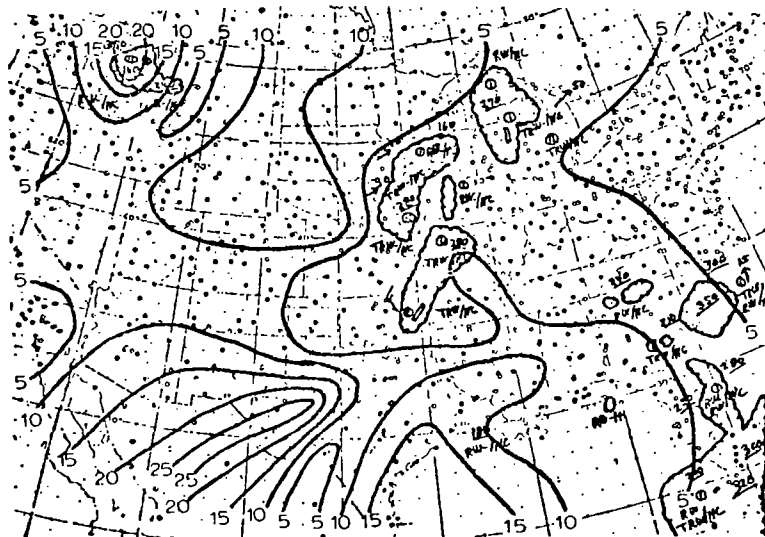
(b) The spread of the ambient and dew-point tem-
peratures at 850 mb is shown in solid lines
superimposed on the composite radar summary.

Fig. 47.   Charts of the difference between the 500-
and 850-mb temperatures, the spread of
the ambient and dew-point temperatures at
850 mb, and areas of thermal advection
and divergence at each level for 12Z,
12 June 1969.
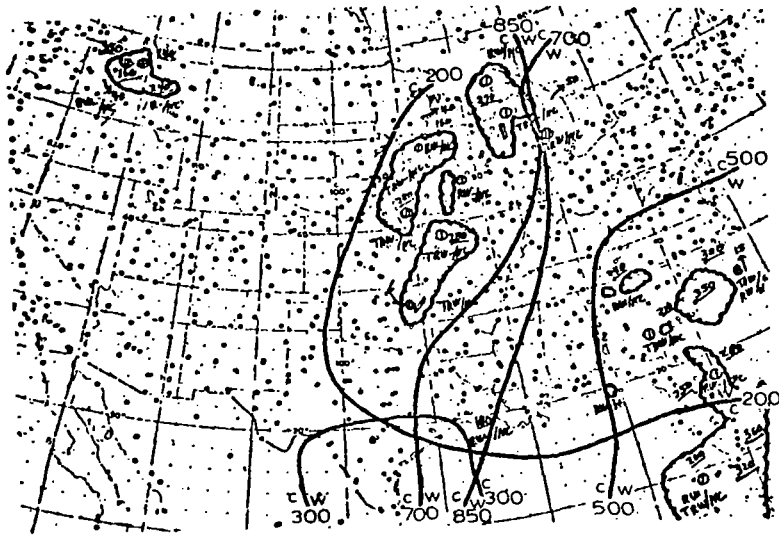
116

(c) Areas of temperature advection are outlined for
    each level in solid lines superimposed on the
    composite radar summary. W indicates the side
    of the line where warm advection occurs. C
    indicates the side of the line where cold or
    neutral advection occurs.

(d) Areas of divergence at each level are outlined
    in solid lines superimposed on the composite
    radar summary. The sign of divergence ($\pm$) is
    indicated on that side of the line where diver-
    gence occurs. Hatched areas are areas where
    divergence occurs over convergence.

Fig. 47. (cont'd from previous page)

117

exception of an area in northern Idaho, Fig. 47b shows that no radar echoes exist where the spread between the ambient and dew-point temperatures at 850 mb is greater than 10C. In the area of radar echoes in the central United States, Fig. 47c shows cold or neutral advection at 850, 700, 500, and 300 mb and warm advection at 200 mb. In the area of radar echoes in the southeastern United States, Fig. 47c shows warm advection 850, 700, and 500 mb; at 200 mb warm advection is present over some of the echoes. In the area of radar echoes in the central United States, Fig. 47d shows convergence at 850 mb affecting the eastern two-thirds, while divergence at 300 and 200 mb is present over all but the southern tip of the area.

The hatched area of Fig. 47d encloses approximately two-thirds of the radar echoes in the central United States. In the areas of radar echoes in the southeastern United States, Fig. 47d shows convergence at 850 mb and divergence at 300 and 200 mb affecting the radar echoes in northern Georgia and South Carolina. A comparison of radar echoes in Figs. 46d and 47d shows that echoes in the southeastern United States have decreased in both horizontal and vertical extent while echoes in the central United States, though decreased somewhat in vertical development, cover about the same amount of horizontal area. Note that Fig. 47 contains charts for 12Z, 12 June 1969, and Fig. 46 those for 00Z, 12 June 1969; convective clouds in the southeastern United States are probably initiated by daytime surface heating, and the echoes in the southeast in Fig. 47 may represent the remnants of convective clouds from the previous day.

Radar echoes in the central United States are initiated by vertical motion in the mid-troposphere caused by low-level (850 and 700 mb convergence and upper-level (500, 300, and 200 mb) divergence; hence they are maintained through the night. The fact that cloud tops in the central United States are lower in Fig. 46 than Fig. 47 may indicate that the effect of surface heating is additive to vertical motion in the mid-troposphere caused by low-level (850 and 700 mb) convergence and upper-level (500, 300, and 200 mb) divergence. Radar echoes in northern Idaho are not explained by the methods considered here.

Figure 48a shows that all areas of radar echoes exist within the limits for conditional instability that were established previously. For the area of radar echoes centered in the Ohio River Valley, Fig. 48b
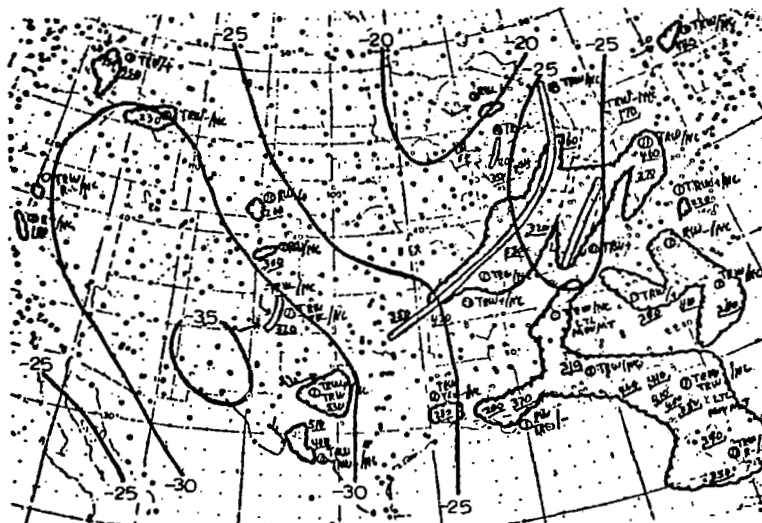
118

(a) The difference between the 500- and 850-mb temperatures is shown in solid lines superimposed on the composite radar summary.
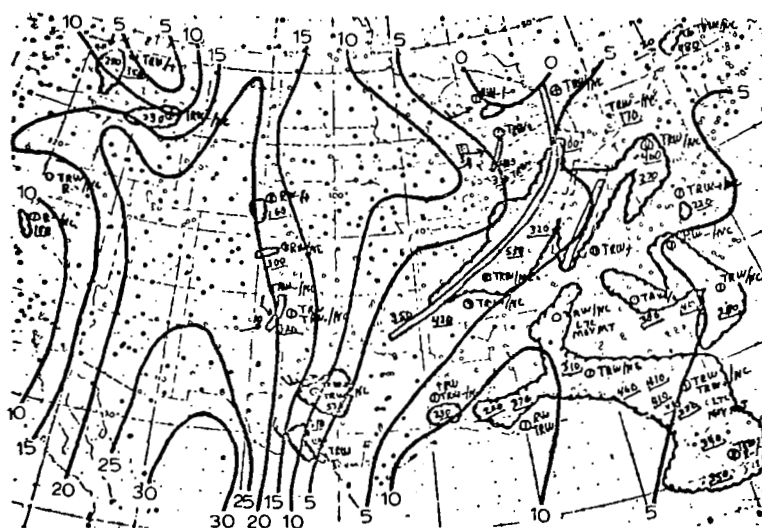
(b) The spread of the ambient and dew-point temperatures at 850 mb is shown in solid lines superimposed on the composite radar summary.

Fig. 48.   Charts of the difference between the 500- and 850-mb temperatures, the spread of the ambient and dew-point temperatures at 850 mb, and areas of thermal advection and divergence at each level for 00Z, 13 June 1969.
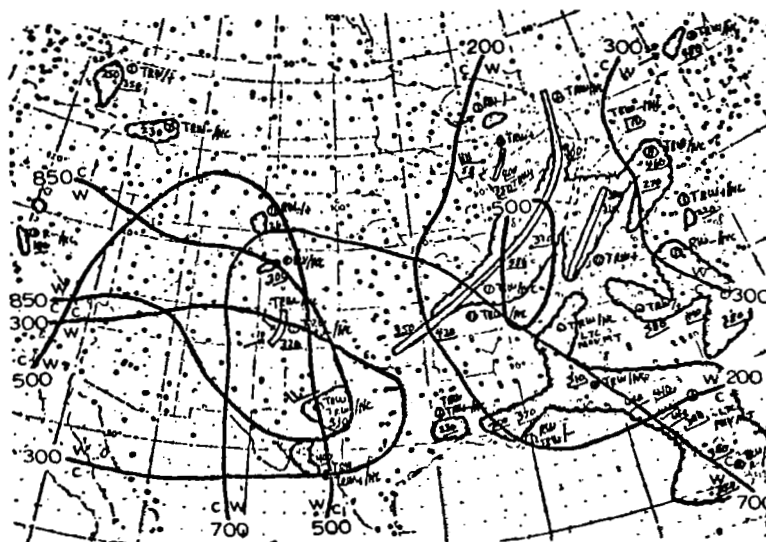
119

(c) Areas of temperature advection are outlined for
each level in solid lines superimposed on the
composite radar summary. W indicates the side
of the line where warm advection occurs. C
indicates the side of the line where cold or
neutral advection occurs.
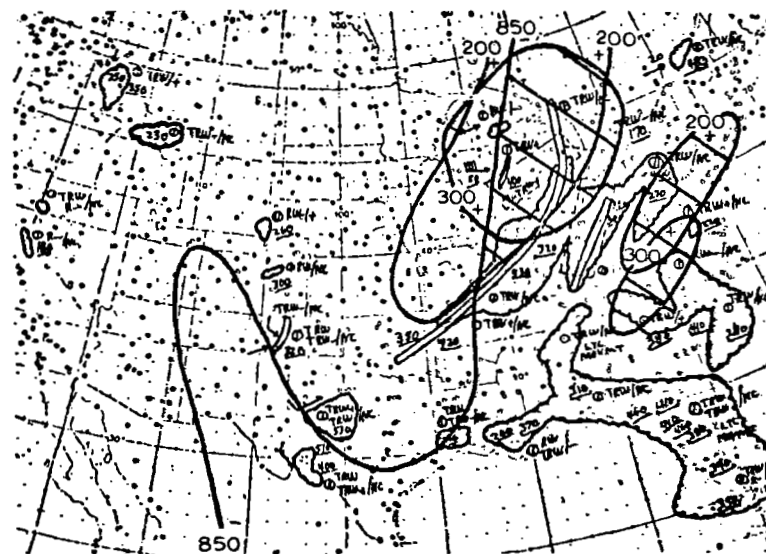
(d) Areas of divergence at each level are outlined
in solid lines superimposed on the composite
radar summary. The sign of divergence (±) is
indicated on that side of the line where diver-
gence occurs. Hatched areas are areas where
divergence occurs over convergence.

Fig. 48. (cont'd from previous page)

120

shows that most of the echoes are within the 5C limit of temperature-dew
point spread used as an indicator of sufficient low-level moisture. Radar
echoes in the area of eastern Pennsylvania are outside the 5C limit. In
the southeastern United States, Fig. 48b indicates sufficient low-level
moisture in all areas of radar echoes except southern Mississippi. In
most of the area of radar echoes from west Texas to southeastern Wyoming
and also in southern Montana, Fig. 48b indicates insufficient low-level
moisture. It may be that the difference between the ambient and dew-point
temperatures at 850 mb is not a good measure of low-level moisture in the
western United States since the 850-mb level may be near or even below
the ground level. For the small areas of radar echoes in California and
northern Idaho, Fig. 48b indicates sufficient low-level moisture. In
the area of radar echoes in the central United States, Fig. 48c shows
warm advection at 200 mb affecting all but the southern tip of the area.
Warm advection at 700, 500, and 300 mb is shown in Fig. 48c affecting
parts of the echo area in the central United States; however, thermal
advection does not appear to be sufficient to account for these echoes.

In the southeastern United States, Fig. 48c shows warm advection at
700 and 200 mb that affects part of the areas of radar echoes. Warm
advection is not sufficient to initiate convection in this area. For the
area of scattered radar echoes from west Texas to southeastern Wyoming,
Fig. 48c shows warm advection affecting all or part of the area at 850,
700, 500, and 300 mb. By the adiabatic method, positive vertical motion
in the area of warm advection may be sufficient to initiate convection.
In California, Fig. 48c shows warm advection at 850 mb in the area of
the radar echoes. In the central United States, Fig. 48d shows conver-
gence at 850 mb over much of the echo area and divergence aloft (300 and
200 mb) over at least part of the area. However, an examination of maps
(not shown) of space-mean contours and Z' fields reveals that at 850 mb
the winds are light and Z' fields at 300 and 200 mb are poorly defined.
Therefore, the magnitude of convergence at 850 mb and divergence at 300
and 200 mb is small. Similarly, in the southern and southeastern United
States convergence at 850 mb, shown in Fig. 48d, is small in magnitude.
It is unlikely that positive vertical motion in the mid-troposphere,
indicated by the hatched areas in Fig. 48d, is of sufficient magnitude

121

to initiate the large areas of radar echoes. In the southeastern United States, surface heating may be sufficient to initiate convection. In the central United States, it is unlikely that surface heating alone would initiate convection in organized lines which, in this case, are several hundred miles long. The triggering mechanism for convection in the central United States comes from neither thermal advection nor the advection of vorticity at 300 and 200 mb. An examination of the surface map (not shown) reveals a cold front moving to the east parallel to and just to the west of the longer line of showers in the central United States. The cold front triggers this line of radar echoes by providing enough lift in moist, conditionally-unstable air to initiate convection.

Figure 49 shows that all radar echoes are contained within the limits set for this investigation for conditional instability. It shows also that radar echoes in the southern United States are in areas of sufficient low-level moisture as defined for this investigation. Figure 49b shows that abundant moisture is present in most echo regions. In the southern United States, Fig. 49c shows warm advection at 850 and 700 mb throughout all areas of radar echoes and warm advection at 500, 300, and 200 mb affecting part of the area. By the adiabatic method, there should be positive vertical motion in the mid-troposphere throughout much of the southern United States. In the northern half of the area of radar echoes centered over the Ohio River Valley, Fig. 49c shows warm advection only at 200 mb affecting part of the echo area. Vertical motion by the adiabatic method would not be sufficient to create radar echoes in this area. Figure 49d shows convergence at 850 and 700 mb in almost all areas where radar echoes are reported. The hatched area encompasses radar echoes from north Texas through Arkansas and Missouri. Figure 49d shows convergence at 850 and 700 mb in the area of radar echoes centered over the Ohio River Valley. Divergence at 300 or 200 mb in Fig. 49d affects only a part of the echo area. The large area of radar echoes centered over the Ohio River Valley is associated with the cold front mentioned in the discussion of Fig. 48.
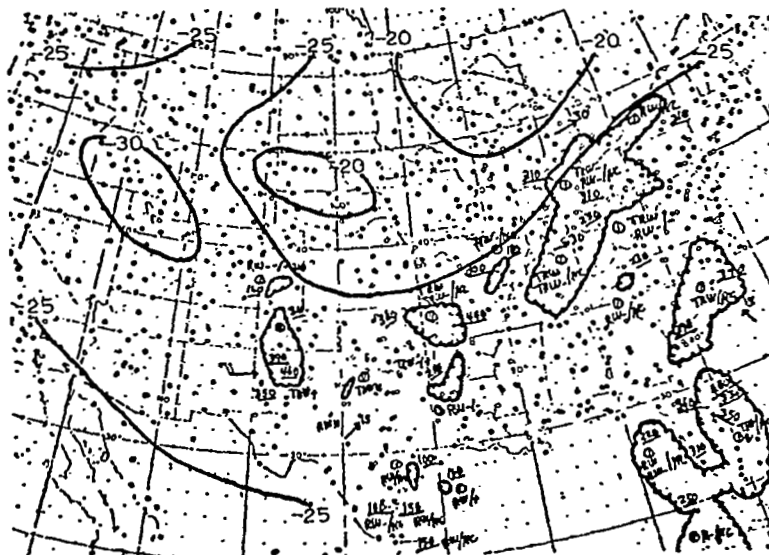
(a) The difference between the 500- and 850-mb temperatures is shown in solid lines superimposed on the composite radar summary.
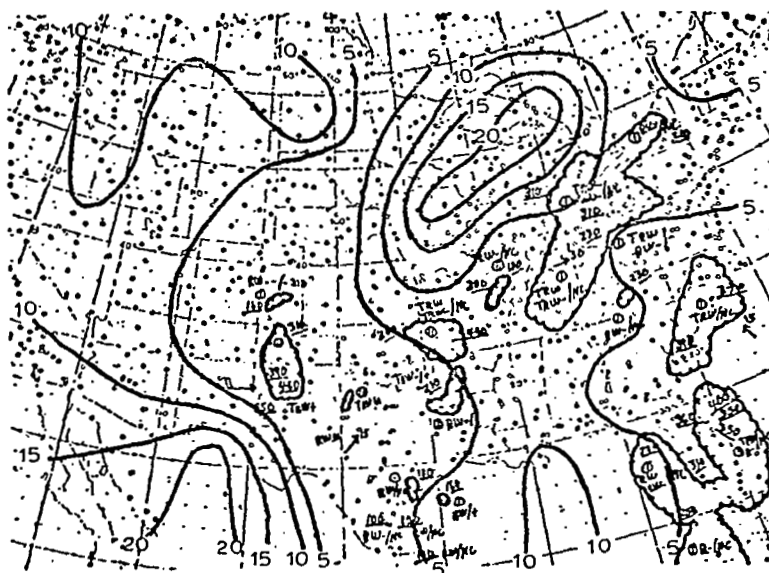

(b) The spread of the ambient and dew-point temperatures at 850 mb is shown in solid lines superimposed on the composite radar summary.

Fig. 49.   Charts of the difference between the 500- and 850-mb temperatures, the spread of the ambient and dew-point temperatures at 850 mb, and areas of thermal advection and divergence at each level for 12Z, 13 June 1969.
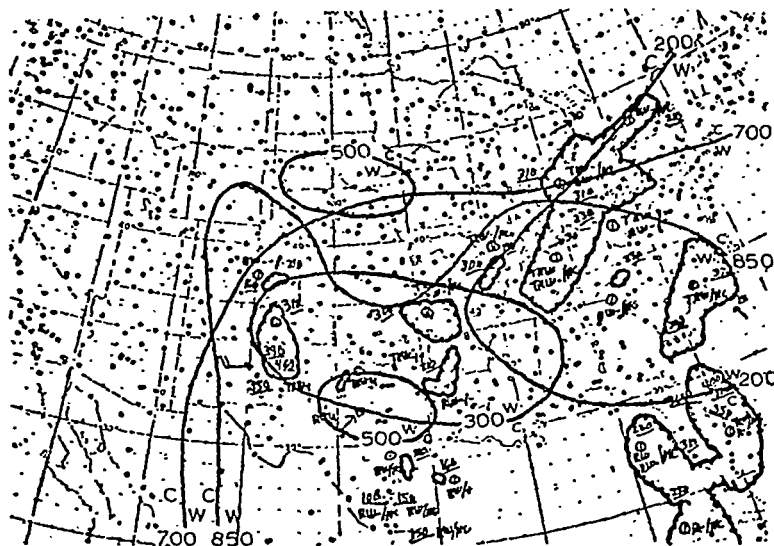
(c) Areas of temperature advection are outlined for
each level in solid lines superimposed on the
composite radar summary. W indicates the side
of the line where warm advection occurs. C
indicates the side of the line where cold or
neutral advection occurs.
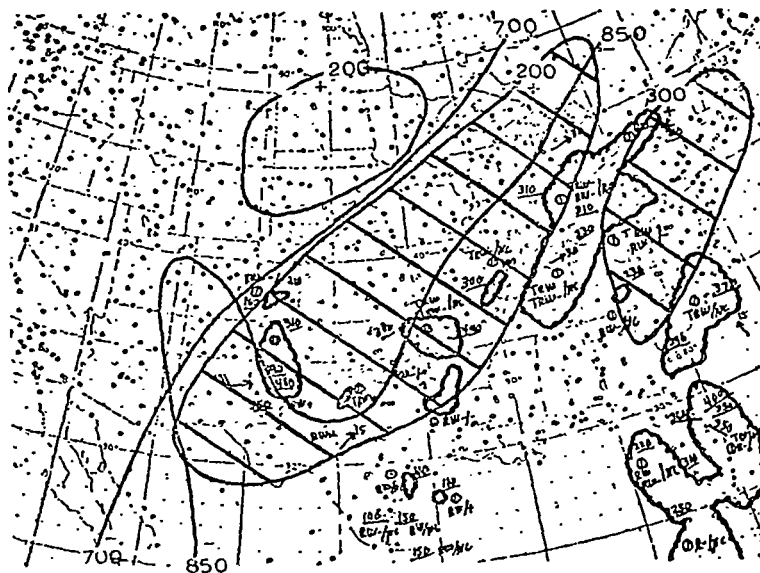
(d) Areas of divergence at each level are outlined
in solid lines superimposed on the composite
radar summary. The sign of divergence (+) is
indicated on that side of the line where diver-
gence occurs. Hatched areas are areas where
divergence occurs over convergence.

Fig. 49. (cont'd from previous page)

124

Within the previously established limits, Fig. 50a shows a conditionally unstable lapse rate between 850 and 500 mb in all areas of radar echoes except the areas over Iowa, Minnesota, and North Dakota. Also, Fig. 50b shows sufficient low-level moisture in all areas of radar echoes except an area in western Tennessee. Warm advection at 700 mb is shown in Fig. 50c to affect most of the areas of radar echoes with smaller areas of warm advection at other levels. The figure does not show warm advection at any level coincident with the radar echoes of the western or north central United States. Convergence at 850 and 700 mb, shown in Fig. 50d, affects most of the radar echoes in the eastern half of the United States. Radar echoes in North Dakota and Nevada are not explained by the methods of this report.

b) Curvature of the Vertical Wind Profile

Figure 51 shows the results of the analysis of curvature for 12Z, 11 June 1969. The corresponding composite radar chart is shown in Fig. 45. The expected echo region through the Central Plains and Upper Midwest coincided closely with that observed through to Illinois. The expected area through Ohio, Pennsylvania, Northern Maryland, and Delaware failed to show any observed echoes except in Northern Maryland. The expected area in South Carolina was confirmed by the observed reports but the expected area was considerably smaller than the observed area. The isolated areas observed in Florida and Texas did not coincide with any expected area of echoes. The scattered showers in central Texas were in an area of low-level convergence with upper-level divergence, but the soundings in this area failed to show sufficient moisture in the lower levels. Insufficient data for Southern Florida may explain the lack of expected echoes in that area.

Figure 52 shows the results of the analysis of curvature for 00Z, 12 June 1969. The corresponding composite radar chart is shown in Fig. 46. The expected regions in the Central Plains and Upper Midwest coincide very well with the observed areas of echoes. The large area of echoes in the southeastern United States did not coincide with any expected area of echoes, but this is a region of upper-level divergence and the eastern half of this area had sufficient moisture reported. The radar reports indicated there were scattered showers and thundershowers throughout this area. The time
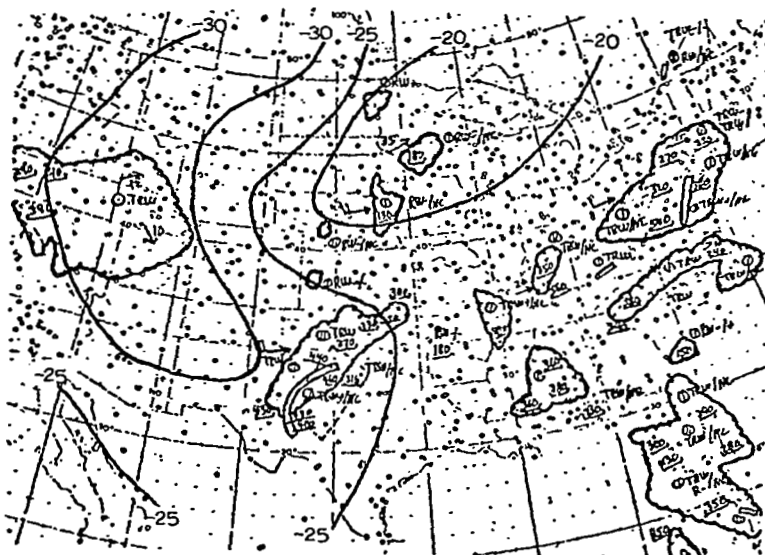
125

(a) The difference between the 500- and 850-mb temperatures is shown in solid lines superimposed on the composite radar summary.
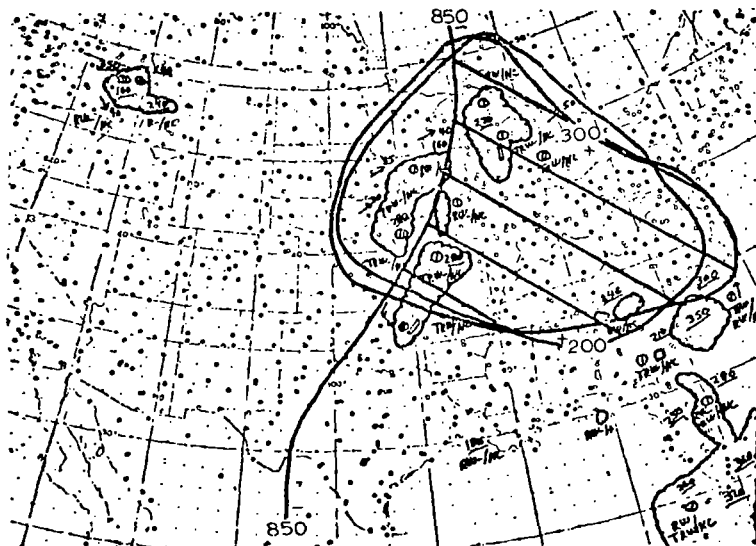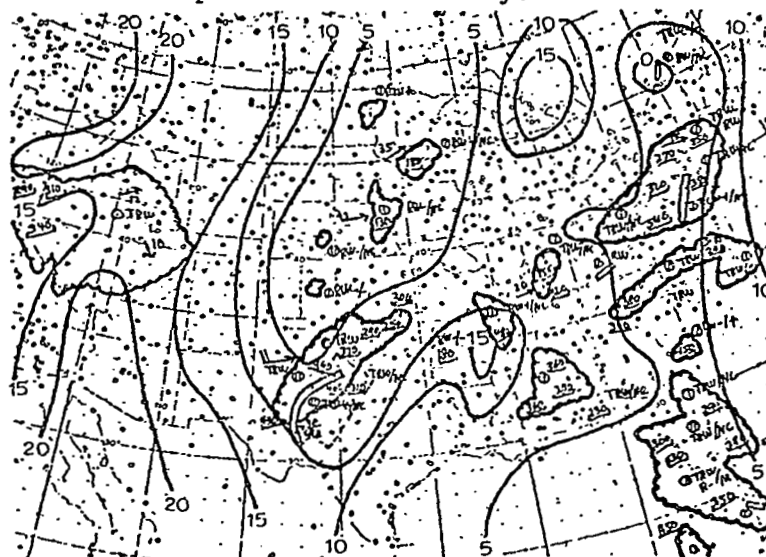

(b) The spread of the ambient and dew-point temperatures at 850 mb is shown in solid lines superimposed on the composite radar summary.

Fig. 50. Charts of the difference between the 500- and 850-mb temperatures, the spread of the ambient and dew-point temperatures at 850 mb, and areas of thermal advection and divergence at each level for 00Z, 14 June 1969.
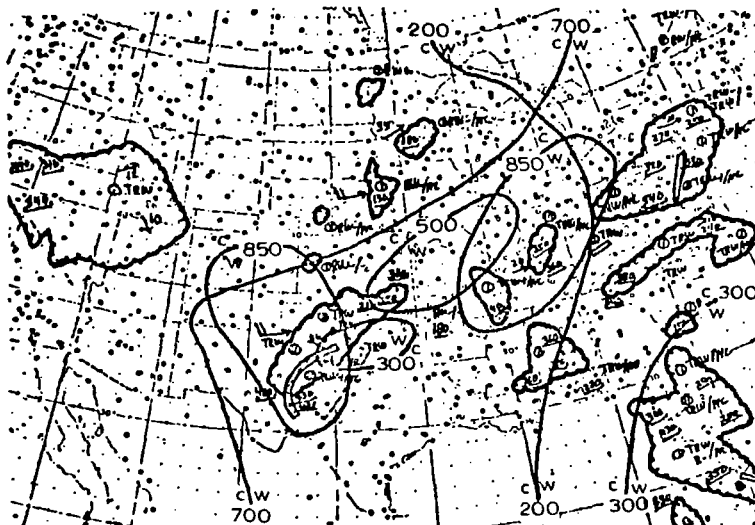
126

(c) Areas of temperature advection are outlined for
each level in solid lines superimposed on the
composite radar summary. W indicates the side
of the line where warm advection occurs. C
indicates the side of the line where cold or
neutral advection occurs.
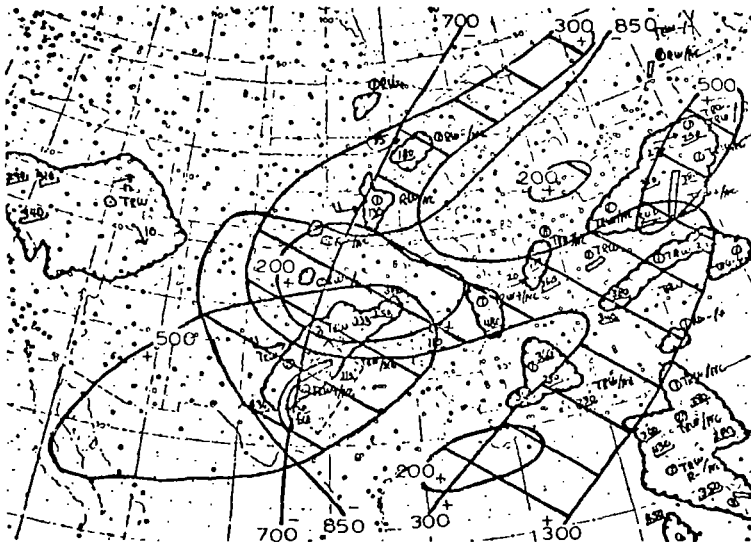
(d) Areas of divergence at each level are outlined
in solid lines superimposed on the composite
radar summary. The sign of divergence (+) is
indicated on that side of the line where diver-
gence occurs. Hatched areas are areas where
divergence occurs over convergence.

Fig. 50. (cont'd from previous page)

127
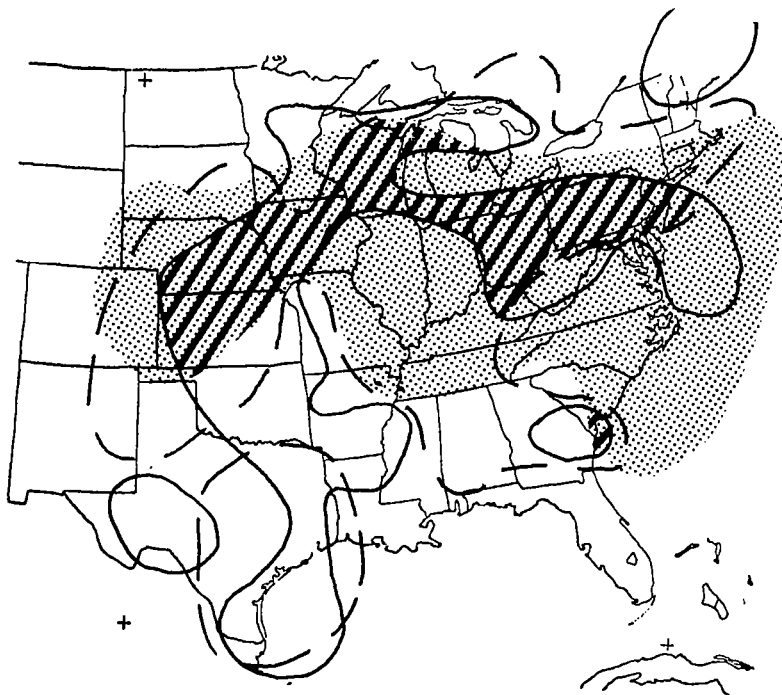
Fig. 51. Results of curvature analysis for
12Z, 11 June 1969.
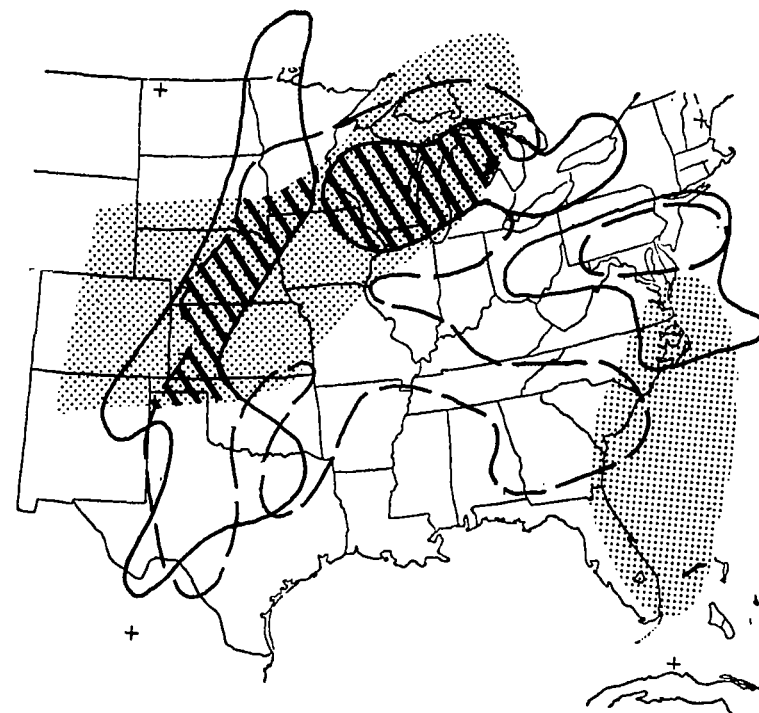
Fig. 52. Results of curvature analysis for
00Z, 12 June 1969.

NOTE: In each figure the area of low-level convergence is enclosed by a solid line and the area of
upper-level divergence by a dashed line. The shaded areas represent $T - T_D \leq 5°C$, while the
hatched areas represent those of expected echoes.
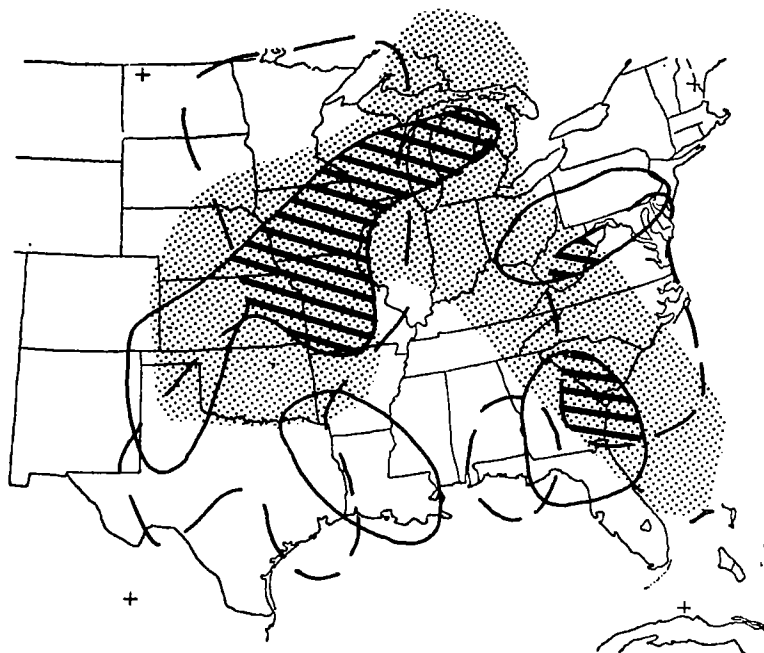
Fig. 53. Results of curvature analysis, for
12Z, 12 June 1969. (The area of low-
level convergence is enclosed by a
solid line and the area of upper-level
divergence by a dashed line. The shaded
areas represent $T - T_D \leq 5°C$, while the
hatched areas represent those of expected
echoes.)

of day was late afternoon and it can be assumed that these showers were due to isolated areas of low-level convergence due to surface heating. This convergence would not be accounted for in the calculations.

Figure 53 shows the results of the analysis of curvature for 12Z, 12 June 1969. The corresponding composite radar chart is shown in Fig. 47. The expected areas of echoes in the Central Plains and upper Great Lakes regions again coincided very well with the observed echoes. A small expected area in West Virginia failed to produce echoes. The expected area in Georgia and South Carolina coincided fairly well with that observed. This situation is 12 hours after the previous one and is in the early morning. The area of observed echoes in the southeast United States is much smaller due to the lack of surface heating. The observed echoes coincide with an expected area since there is large-scale convergence in this region, whereas 12 hours earlier there was no large region of low-level convergence and only isolated areas due to heating.

5) Summary of Results for the June Period

This case is an example of a typical summer situation and differs from the previous case in that synoptic-scale waves and vorticity centers are poorly defined. Radar echoes, indicative of mesoscale systems, fluctuate greatly between morning and evening radar summaries. In some areas positive vorticity advection aloft (500, 300, or 200 mb) is associated with observed radar echoes. Thermal advection does not appear to contribute significantly to positive vertical motion in the mid-troposphere. The "article of faith" is not generally valid in this case. Large areas of radar echoes are present in the southeastern United States and apparently are a result of daytime surface heating rather than synoptic control.

c. December Period

1) Synoptic Conditions

An examination of the map series (not shown) for December 1969 reveals a well-developed trough which slopes westward with height in the central United States. Vorticity fields are best defined at upper levels (500, 300, and 200 mb). Scattered radar echoes are present between the trough and downstream ridge. The trough moves to the eastern United States and

130

becomes very broad with well-defined fields of vorticity at all levels.
Radar echoes, indicative of mesoscale systems, move eastward with the trough.

2) Moisture

Figures showing the spread of the ambient and dew-point temperatures at
850 mb are included with other figures for each time period for this case.
Most radar echoes are present where the spread of the ambient and dew-point
temperatures at 850 mb is less than 10C.

3) Vertical Motion

a) Kinematic and Adiabatic Methods

A well developed synoptic trough and associated vorticity fields make
areas of convergence or divergence (based on the vorticity equation) easily
recognizable at each level. By Dines' Compensation Principle, areas of
positive vertical motion in the mid-troposphere can be inferred. Addition-
ally, thermal gradients are large and areas of positive thermal advection
by the space-mean wind can be determined. By use of these tools, it is
possible to determine areas where mesoscale systems should be present.

If Fig. 54a, the spread of the ambient and dew-point temperatures at
850 mb is shown in solid lines superimposed on the composite radar summary.
The figure shows that many of the echoes are present in air that by previ-
ously established criteria is not moist at 850 mb. However, it should be
remembered that even with only a relatively small moisture content, if the
air is lifted sufficiently, condensation and precipitation eventually occur.
In Fig. 54b, areas of positive temperature advection are outlined for each
level in solid lines superimposed on the composite radar summary. The fig-
ure shows warm advection at 850 mb through the main area of radar echoes
in the central United States. Also, warm advection at 700 and 200 mb af-
fects part of the echo area. By the adiabatic method, there will be
vertical motion in the mid-troposphere in the main echo area. In Fig. 54c,
areas of convergence are outlined at the lower levels (850 and 700 mb) and
divergence at the upper levels (500, 300, and 200 mb). Figure 54c shows
convergence at 850 mb throughout the principal area of radar echoes in the
central United States. Convergence at 850 mb may contribute to positive
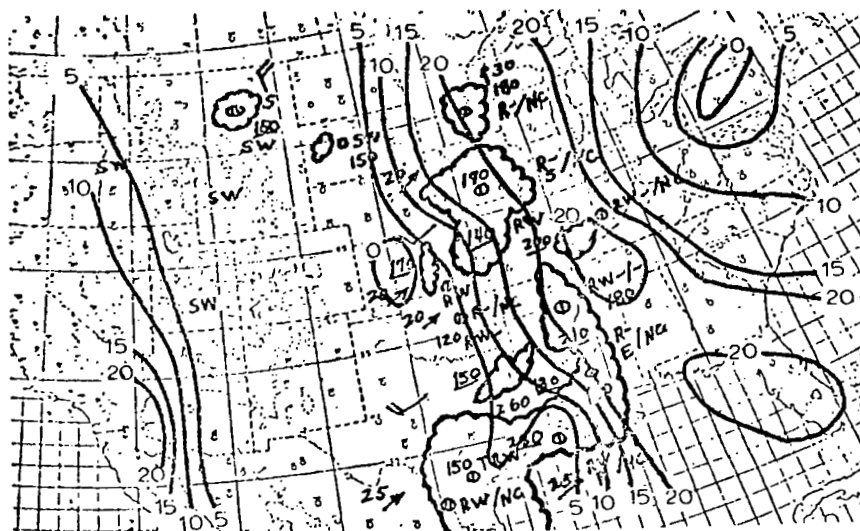
131

(a) The spread of the ambient and dew-point tem-
    peratures at 850 mb is shown in solid lines
    superimposed on the composite radar summary.
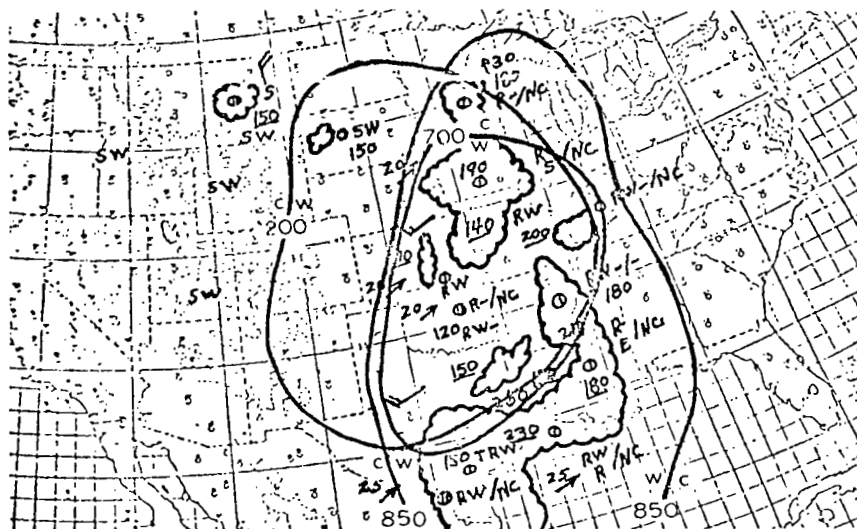
(b) Areas of positive temperature advection are
    outlined for each level in solid lines super-
    imposed on the composite radar summary. W
    indicates the side of the line where warm
    advection occurs. C indicates the side of the
    line where cold or neutral advection occurs.

Fig. 54.   Charts of the spread of the ambient and
            dew-point temperatures at 850 mb, and
            areas of thermal advection and divergence
            at each level for 12Z, 5 December 1969.
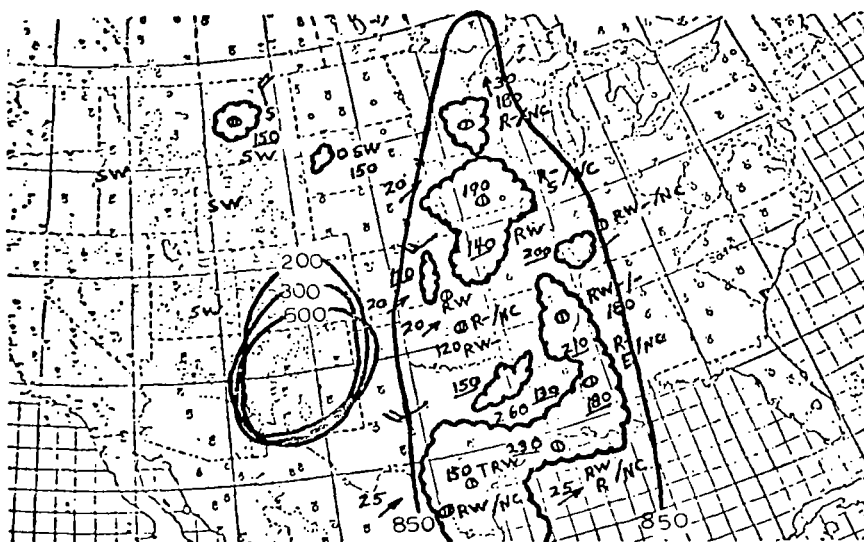
132

(c) Areas of convergence are outlined (or enclosed
     between lines) at the lower levels (850 and
     700 mb) and divergence at the upper levels
     (500, 300, and 200 mb) in solid lines super-
     imposed on the composite radar summary.

Fig. 54.   (cont'd from previous page)

vertical motion in the mid-troposphere. Areas of divergence shown in Fig. 54c at 500, 300, and 200 mb are a result of PVA (figures not shown) at those levels. Radar echoes are not present in these areas, possibly because of negative temperature advection (figures not shown) in the same areas.

In Fig. 55a it is shown that most of the radar echoes are present where the spread of the ambient and dew-point temperatures is less than 10C. A comparison of Figs. 54a and 55a shows an increase of moisture coincident with a larger and more consolidated pattern of radar echoes. Warm advection, shown in Fig. 55b, at 850, 700, 500, 300, and 200 mb, affects most of the principal area of radar echoes in the central United States. By the adiabatic method, Fig. 55b indicates positive vertical motion in the mid-troposphere in the main area of radar echoes. Figure 55c shows convergence at 850 and 700 mb affecting the principal area of radar echoes in the central United States. Divergence shown in Fig. 55c at 500, 300, and 200 mb and centered over the panhandle of Texas is associated with positive vorticity advection at these levels. Divergence aloft and convergence at 850 and 700 mb, affecting at least the eastern half of the radar echoes in the panhandle of Texas, creates positive vertical motion in the mid-troposphere, hence radar echoes have developed. The main area of radar echoes in the central United States is in the area where both the adiabatic method and the method based on the vorticity equation indicate positive vertical motion in the mid-troposphere. Scattered radar echoes in New Mexico, Wyoming, and South Dakota are not explained by the methods considered here.

Figure 56a shows that the spread of the ambient and dew-point temperatures is less than 10C in most areas where radar echoes are present. A comparison of radar echoes in Figs. 55 and 56 shows that the main area of precipitation in Fig. 55 has spread eastward through the Gulf Coast and southeastern United States. Radar echoes in the northern part of the main area of precipitation in Fig. 55 have increased in size while remaining stationary and becoming separated from radar echoes in the southern part. Radar echoes in the panhandle of Texas in Fig. 55 moved southward to central Texas as indicated in Fig. 56. The figure shows warm advection at 850, 700, 300, and 200 mb affecting most of the area of radar echoes. By the
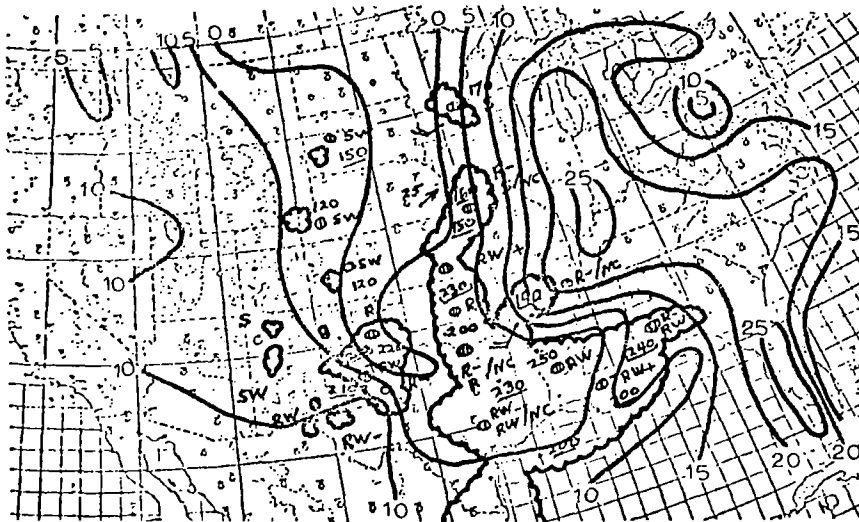
(a) The spread of the ambient and dew-point tem-
peratures at 850 mb is shown in solid lines
superimposed on the composite radar summary.
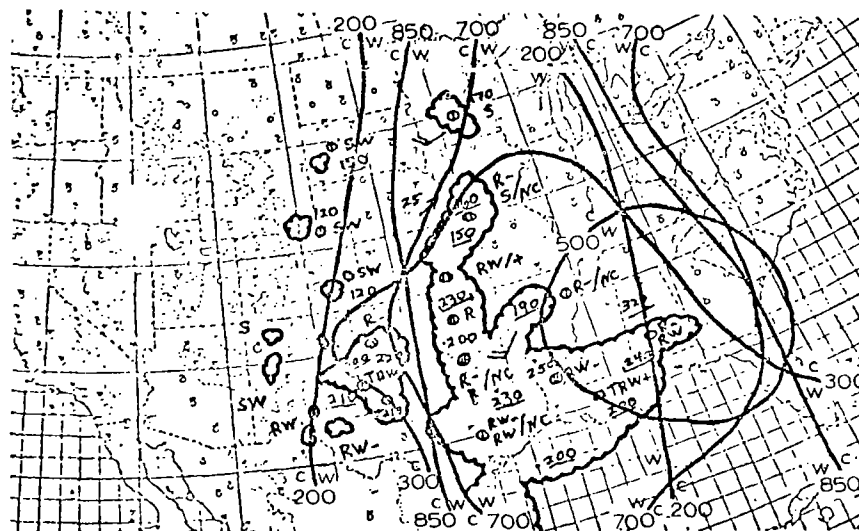
(b) Areas of positive temperature advection are
outlined for each level in solid lines super-
imposed on the composite radar summary. W
indicates the side of the line where warm
advection occurs. C indicates the side of the
line where cold or neutral advection occurs.

Fig. 55. Charts of the spread of the ambient and
dew-point temperatures at 850 mb, and
areas of thermal advection and divergence
at each level for 00Z, 6 December 1969.
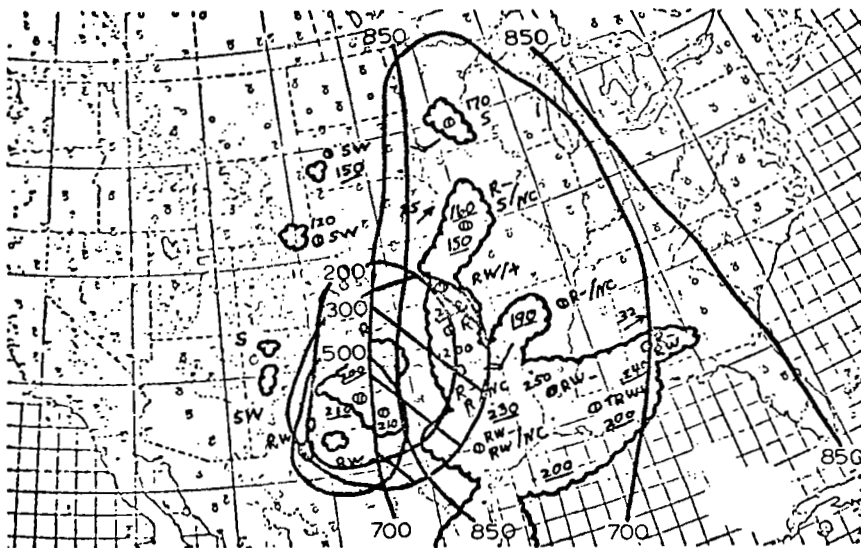
135

(c)   Areas of convergence are outlined (or enclosed
between lines) at the lower levels (850 and
700 mb) and divergence at the upper levels
(500, 300, and 200 mb) in solid lines super-
imposed on the composite radar summary.

Fig. 55. (cont'd from previous page)
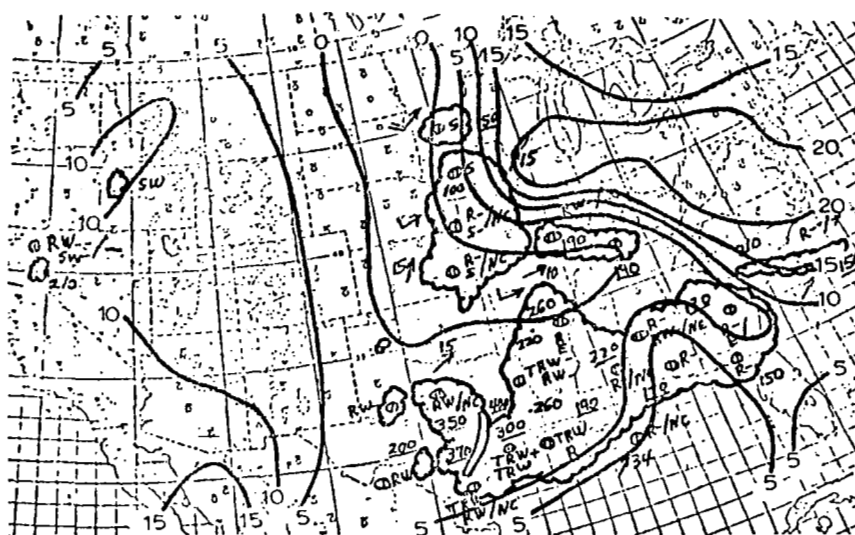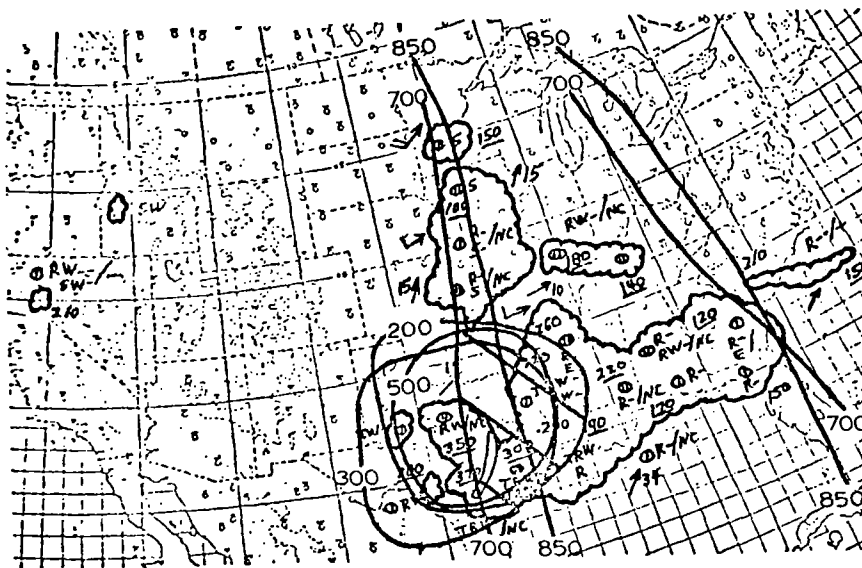
136

(a) The spread of the ambient and dew-point tem-
peratures at 850 mb is shown in solid lines
superimposed on the composite radar summary.

(b) Areas of positive temperature advection are
outlined for each level in solid lines super-
imposed on the composite radar summary. W
indicates the side of the line where warm
advection occurs. C indicates the side of the
line where cold or neutral advection occurs.

Fig. 56. Charts of the spread of the ambient and
dew-point temperatures at 850 mb, and
areas of thermal advection and divergence
at each level for 12Z, 6 December 1969.

(c) Areas of convergence are outlined (or enclosed
     between lines) at the lower levels (850 and
     700 mb) and divergence at the upper levels
     (500, 300, and 200 mb) in solid lines super-
     imposed on the composite radar summary.

Fig. 56. (cont'd from previous page)

138

adiabatic method, from Fig. 56b, areas of positive vertical motion in the mid-troposphere are indicated that coincide well with observed radar echoes.

Figure 56c shows convergence at 850 and 700 mb throughout most of the principal areas of radar echoes. A comparison of Figs. 55c and 56c shows that areas of divergence at 500, 300, and 200 mb centered over the panhandle of Texas in Fig. 55c have moved southeastward, and in Fig. 56c are centered over central Texas. Movement of the areas of divergence, associated with the movement of vorticity fields, is coincident with movement of radar echoes from the Texas panhandle in Fig. 55c to central Texas in Fig. 56c. The line of echoes, as well as echoes with the greatest vertical development, shown in Fig. 56c in central Texas, are in the hatched area where convergence at 700 mb and divergence at 500, 300, and 200 mb create positive vertical motion in the mid-troposphere. In addition, an examination of charts of space-mean contours and vorticity fields (not shown) reveals that the Z' field at 500 mb over Texas has increased in intensity in the 12-hour period prior to Fig. 56. Increased PVA at 500 mb over central Texas increases the magnitude of divergence at that level and is responsible for the increased cloud heights (radar echoes) which moved from the panhandle of Texas in Fig. 55c to central Texas in Fig. 56c. Radar echoes in California and Idaho are not explained by the methods considered here.

In Fig. 57a most radar echoes are in the area where the spread of the ambient and dew-point temperatures is less than 10C. Warm advection at 850, 700, 300, or 200 mb throughout the principal areas of radar echoes is shown in Fig. 57b. By the adiabatic method, areas of positive vertical motion in the mid-troposphere are indicated that coincide well with the existing pattern of radar echoes (Fig. 57b). Figure 57c shows areas of convergence at 850 and 700 mb that create positive vertical motion in the mid-troposphere and that coincide well with the main body of radar echoes. The figure does not indicate convergence at low levels along the western fringes of the large area of radar echoes scattered over the eastern half of the United States. A comparison of Figs. 56c and 57c shows that the areas of divergence at 500 and 300 mb centered over central Texas in Fig. 56c have moved eastward, and in Fig. 57c are centered over Louisiana. Concurrent with the movement of areas of divergence at 500 and 300 mb is
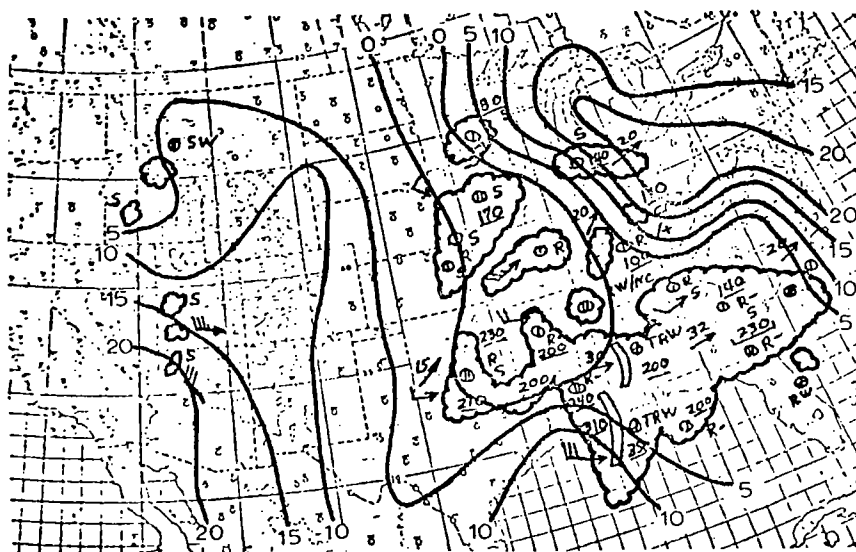
139

(a) The spread of the ambient and dew-point temperatures at 850 mb is shown in solid lines superimposed on the composite radar summary.
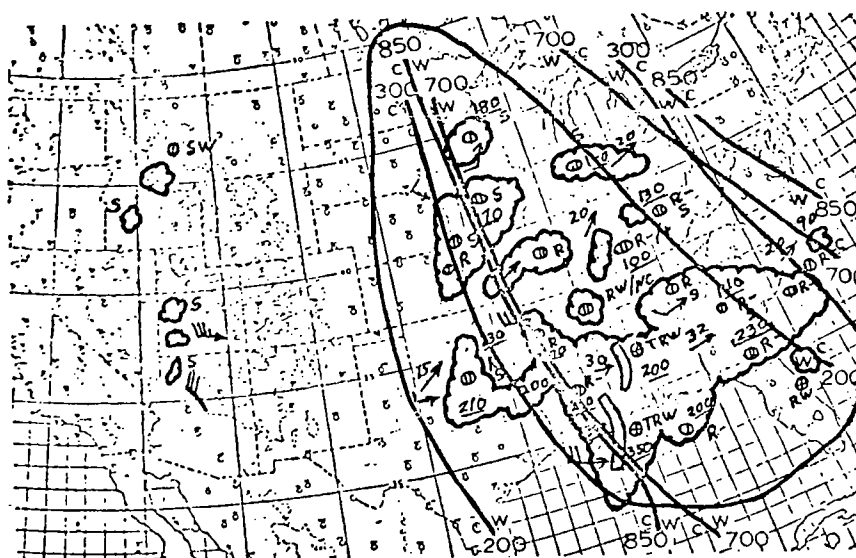
(b) Areas of positive temperature advection are outlined for each level in solid lines superimposed on the composite radar summary. W indicates the side of the line where warm advection occurs. C indicates the side of the line where cold or neutral advection occurs.

Fig. 57. Charts of the spread of the ambient and dew-point temperatures at 850 mb, and areas of thermal advection and divergence at each level for 00Z, 7 December 1969.
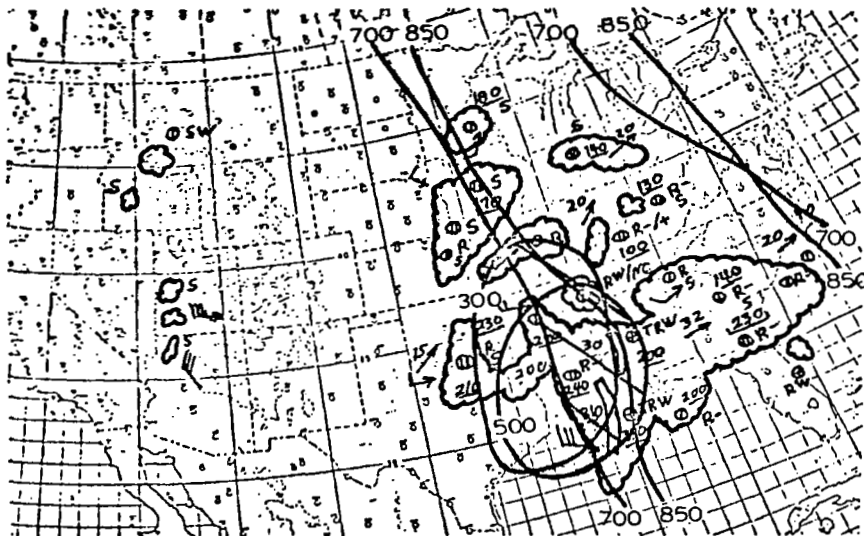
(c) Areas of convergence are outlined (or enclosed
     between lines) at the lower levels (850 and
     700 mb) and divergence at the upper levels
     (500, 300, and 200 mb) in solid lines super-
     imposed on the composite radar summary.

Fig. 57. (cont'd from previous page)

141

the movement of the line of radar echoes, in central Texas in Fig. 56c, to southeastern Louisiana in Fig. 57c. An examination of charts of space-mean contours and vorticity fields (not included) shows that the vorticity center has disappeared at 200 mb in the 12 hours prior to Fig. 57, and has decreased in intensity at 500 and 300 mb. The decrease in the vorticity center decreases the magnitude of vertical motion in the mid-troposphere. The decreased magnitude of vertical motion explains the decrease of cloud heights in the hatched area from Fig. 56c to Fig. 57c. Radar echoes in north central Texas, southern Oklahoma, and northeastern Kansas, as well as scattered radar echoes in the western United States, are not explained by the methods considered and may not be directly related to synoptic-scale weather systems.

Most radar echoes are present in the areas of Fig. 58a where the spread of the ambient and dew-point temperatures is less than 10C. A comparison of radar echoes in Figs. 57 and 58 shows that all radar echoes have moved eastward. Radar echoes in the southern United States have increased in areal coverage. Warm advection is shown in Fig. 58b at all levels through-out the large region of the eastern United States where radar echoes are reported. By the adiabatic method, Fig. 58b indicates positive vertical motion in the mid-troposphere in most areas of radar echoes. In Fig. 58c, areas of convergence are outlined at the lower levels (850 and 700 mb) and divergence at upper levels (500, 300, and 200 mb) in solid lines super-imposed on the composite radar summary. Figure 58c shows convergence at 850 and 700 mb, hence positive vertical motion at least as high as 700 mb in the troposphere occurs in a part of the area of radar echoes. An exam-ination of charts of space-mean contours and Z' fields (figures not shown) reveals that the trough centered in the central United States, though well-defined at each level, is very broad, and vorticity fields exist on the eastern side of the trough. Thus, PVA leading to divergence is offset on the east side of the trough by the south wind which leads to convergence, and the resulting sign of divergence often cannot be determined without computation. Therefore, in Fig. 58c large areas of divergence at 300 and 200 mb are not indicated in the principal area of echoes.

Advection of a small vorticity center in Arizona at 300 and 200 mb (figures not shown) creates areas of divergence at these levels, as shown
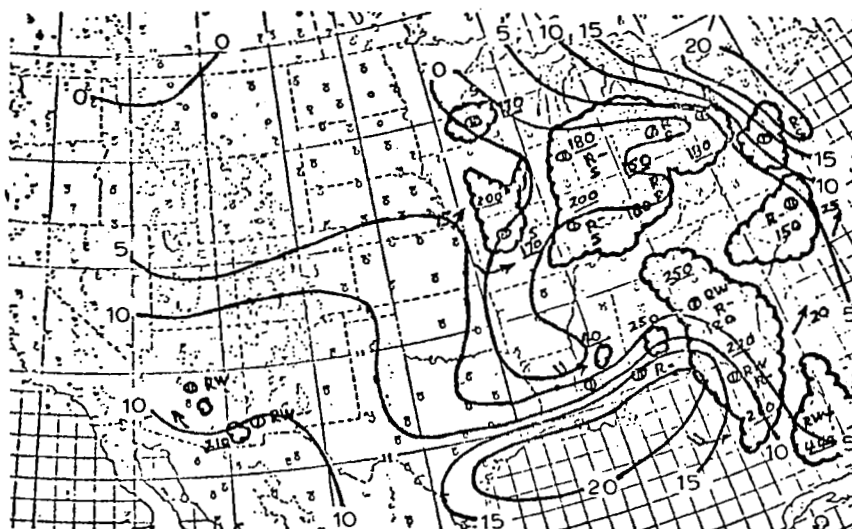
(a) The spread of the ambient and dew-point temperatures at 850 mb is shown in solid lines superimposed on the composite radar summary.

(b) Areas of positive temperature advection are outlined for each level in solid lines superimposed on the composite radar summary. W indicates the side of the line where warm advection occurs. C indicates the side of the line where cold or neutral advection occurs.

Fig. 58. Charts of the spread of the ambient and dew-point temperatures at 850 mb, and areas of thermal advection and divergence at each level for 12Z, 7 December 1969.
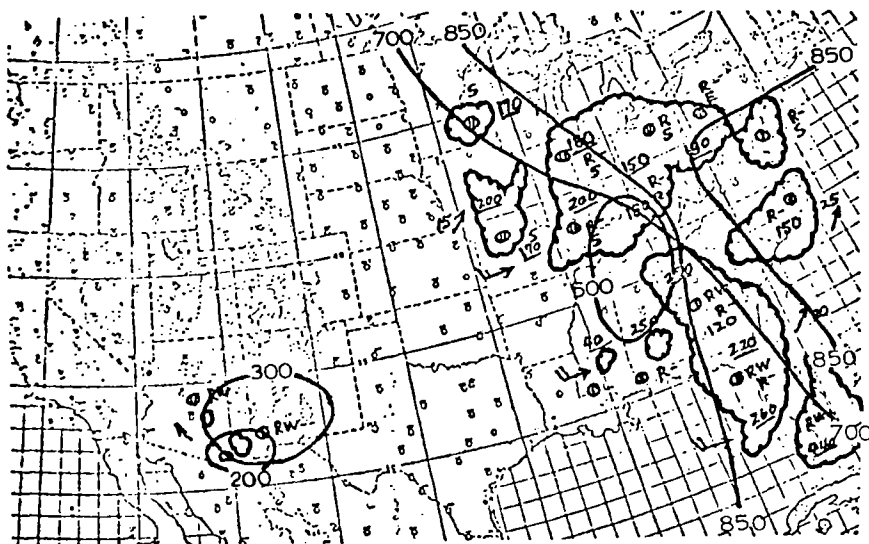
143

(c) Areas of convergence are outlined (or enclosed between lines) at the lower levels (850 and 700 mb) and divergence at the upper levels (500, 300, and 200 mb) in solid lines superimposed on the composite radar summary.

Fig. 58. (cont'd from previous page)

in Fig. 58c over Arizona and New Mexico, hence positive vertical motion occurs in the mid-troposphere by (3) and the radar echoes show up in southeastern Arizona. To summarize, the principal area of radar echoes in Fig. 58c is a result of positive vertical motion in the mid-troposphere created by warm advection at all levels. Convergence at 850 and 700 mb also contributes to positive vertical motion in the principal area of radar echoes, but to a lesser extent than thermal advection.

That most radar echoes are present in areas where the spread of the ambient and dew-point temperatures at 850 mb is less than 10C is shown in Fig. 59a. A comparison of radar echoes in Figs. 58 and 59 shows that the echoes have moved eastward to the east coast of the United States. Figure 59b shows that warm advection is present at at least one level in the areas of radar echoes in the eastern United States. By the adiabatic method, warm advection in Fig. 59b indicates positive vertical motion in the mid-troposphere in the principal area of radar echoes. Convergence at 850 and 700 mb is shown in Fig. 59c in the area of radar echoes in the eastern United States. If there is convergence in the layer from the surface to 700 mb, then there should be positive vertical motion in the troposphere at least to a height of 700 mb. Radar echoes along the east coast of the United States and in the area centered over Pennsylvania are a result of positive vertical motion in the mid-troposphere caused by warm advection and low-level (850 and 700 mb) convergence. The radar echo in Minnesota may be a result of positive vertical motion caused by divergence at 200 mb as well as warm advection at other levels. Radar echoes over the panhandle of Texas, Utah, and Wyoming may be a result of orographic effects.

b) Curvature of the Vertical Wind Profile

Figure 60 shows the results of the analysis of curvature for 12Z, 5 December 1969. The corresponding composite radar chart is shown in Fig. 54. A comparison of actual and expected areas of echoes shows that the expected areas along the Gulf and through the Plains States corresponds fairly well to the actual areas. Radar reports indicated no echoes in

(a) The spread of the ambient and dew-point tem-
peratures at 850 mb is shown in solid lines
superimposed on the composite radar summary.
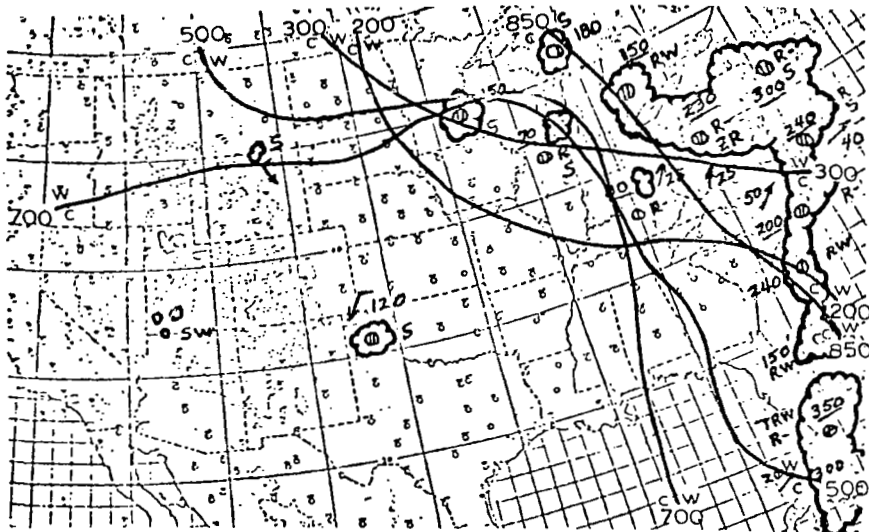
(b) Areas of positive temperature advection are
outlined for each level in solid lines super-
imposed on the composite radar summary. W
imdicates the side of the line where warm
advection occurs. C indicates the side of the
line where cold or neutral advection occurs.

Fig. 59. Charts of the spread of the ambient and
dew-point temperatures at 850 mb, and
areas of·thermal advection and divergence
at each level for 00Z, 8 December 1969.

146

(c) Areas of convergence are outlined (or enclosed
      between lines) at the lower levels (850 and
      700 mb) and divergence at the upper levels
      (500, 300, and 200 mb) in solid lines super-
      imposed on the composite radar summary.

Fig. 59.   (cont'd from previous page)

147
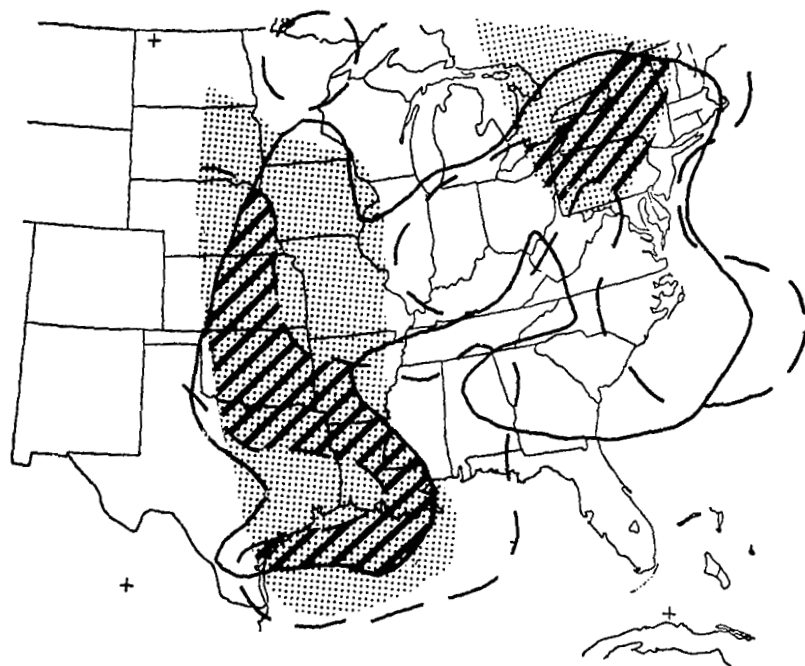
Fig. 60.   Results of curvature analysis for
12Z, 5 December 1969.
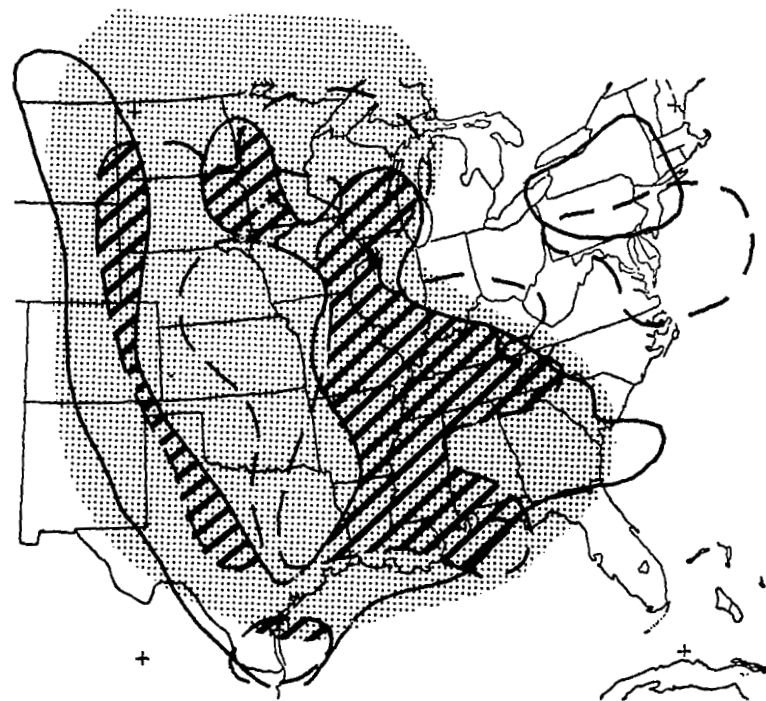
Fig. 61.   Results of curvature analysis for
12Z, 6 December 1969.

NOTE: In each figure the area of low-level convergence is enclosed by a solid line and the
area of upper-level divergence by a dashed line. The shaded areas represent
$T - T_D \leq 5°C$ at 850 mb, while the hatched areas represent those of expected echoes.

New York or Pennsylvania, but the surface synoptic chart indicated scattered snow showers corresponding to the expected area of echoes in that region.

Figure 61 shows the results of the analysis of curvature for 12Z, 6 December 1969. The corresponding composite radar chart is shown in Fig. 56. The widespread area of echoes through the Gulf States compares favorably to the expected areas. The several smaller areas of echoes located in the Midwest fit reasonably well with the expected pattern. Scattered showers fell in South Carolina which, according to the expected areas, should have been free of echoes. The expected band of echoes through the Central Gulf States and Northern Texas coincides fairly well with the expected area in that region. Smaller areas of echoes occurred in sections of Iowa, Illinois, and Indiana where sufficient moisture and upper-level divergence were present. Although the gradients for low-level convergence were weak, they were sufficient to produce echoes in this region. There was an area of echoes in Central Georgia where vertical motion was not indicated. However, from consideration of weaker gradients, this region could be included in the expected areas.

Figure 62 shows the results of the analysis of curvature for 00Z, 7 December 1969. The corresponding composite radar chart is shown in Fig. 57. The expected area of echoes over much of the Southeast coincided with the observed area except over parts of Georgia and Alabama. Low-level convergence was not indicated in this region although high-level divergence and sufficient moisture were present. Small areas of convective activity were observed in the Midwest which were not included in the expected area. The entire area bounding all radar echoes could be included in the expected area if a combination of low-level convergence or high-level divergence and moisture were considered.

4) Summary of Results for the December Period

This case is an example of a well-developed trough with associated mesoscale systems. Radar echoes are present east of the trough and move to the east with the trough. The "article of faith" appears to have some validity for this case. By use of the method based on the vorticity equation as well as the adiabatic method, broad areas were delineated in which mesoscale systems were present. Thermal advection in this case is equally
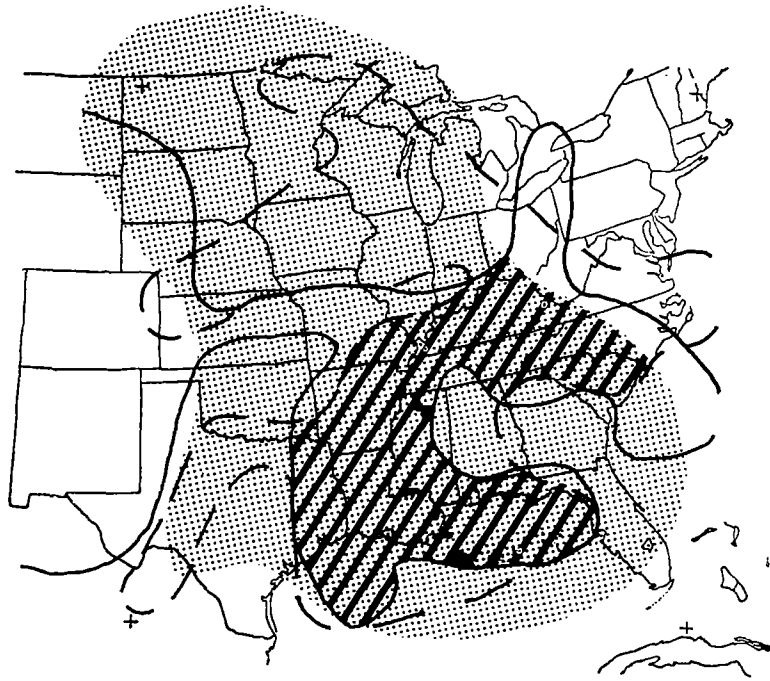
Fig. 62. Results of curvature analysis for 00Z,
7 December 1969. (The area of low-level
convergence is enclosed by a solid line
and the area of upper-level divergence
by a dashed line. The shaded areas
represent $T - T_D \leq 5°C$ at 850 mb, while
the hatched areas represent those of
expected echoes.)

as important as vorticity advection in determining the sign of vertical
motion in the mid-troposphere. This case differs from the June case in
that the trough and vorticity centers are well developed. However, this
case is very similar to the March case in that mesoscale systems are
present where synoptic-scale conditions are favorable.

d. September Period

1) Synoptic Conditions

Initially a synoptic-scale wave is centered along a line at 850 mb
from Arizona northward through Montana; this wave slopes westward with
height. Vorticity fields are best defined at upper levels (300 and 200
mb). The trough drifted slowly to the east during the period, increased
in amplitude during the first three time intervals, and finally became
diffuse and hard to locate at 850 mb. Radar echoes are scattered along
and east of the 850-mb trough. The echoes move to the east with the
trough and intensify over the Great Plains. A smaller wave is located
at upper levels (300 and 200 mb) over the Ohio River Valley. The trough
moves eastward and by the third time period was off the east coast. As-
sociated radar echoes moved eastward with the trough and also were off the
East Coast by the third time period.

In the eastern Gulf of Mexico, near the Florida panhandle, a distur-
bance is present that appears to be of tropical origin. The disturbance
moves slowly inland during the period. Associated radar echoes are wide-
spread over the eastern Gulf of Mexico and Florida. Other radar echoes
are present in the Western Gulf and may be a result of another tropical
disturbance.

2) Moisture

Figures showing the spread of the ambient and dew-point temperatures
at 850 mb, superimposed on the composite radar summary, are shown together
with other figures for each time period. In almost all cases the spread
of the ambient and dew-point temperatures at 850 mb is less than 10C in
areas of radar echoes.

3) Vertical Motion

    a) Kinematic and Adiabatic Methods

In Fig. 63a, the spread of the ambient and dew-point temperatures at 850 mb is shown in solid lines superimposed on the composite radar summary. The figure shows that most of the radar echoes are present where the spread of the ambient and dew-point temperatures is less than 10C. Areas of positive temperature advection are outlined in solid lines superimposed on the composite radar summary in Fig. 63b. With the exception of the precipitation area over Nevada, Idaho, and Montana, Fig. 63b shows warm advection at two or more levels in all areas of radar echoes, and by the adiabatic method, there may be positive vertical motion in the mid-troposphere associated with the mesoscale systems. However, by the adiabatic method, large areas in which positive vertical motion in the mid-troposphere is indicated contain no radar echoes (Fig. 63b).

An examination of charts of space-mean contours and isotherms (not shown) reveals very weak thermal gradients. Hence, the magnitude of positive vertical motion in the mid-troposphere indicated by the adiabatic method is small and may not be sufficient to produce mesoscale systems. In Fig. 63c, areas of convergence are outlined at the lower levels (850 and 700 mb) and divergence at the upper levels (500, 300, and 200 mb). Areas where convergence is present at low levels and divergence at upper levels are hatched; these are areas where vertical motion in the mid-troposphere is strongly indicated.

In the western United States, Fig. 63c shows divergence at 500, 300, and 200 mb over the scattered radar echoes. If there is divergence aloft (500, 300, and 200 mb), then positive vertical motion in the mid-troposphere is probable. An examination of charts of space-mean contours and vorticity fields (not shown) reveals poorly defined vorticity fields over the western United States. Therefore, divergence, shown in Fig. 63c at 500, 300, and 200 mb over the western United States is small in magnitude. Vertical motion, inferred from divergence, also is small in magnitude. This explains why radar echoes are scattered and the maximum reported height of cloud tops is only 20×10^3 ft. The hatched area shown in Fig. 63c in the western United States does not coincide with any radar echoes.
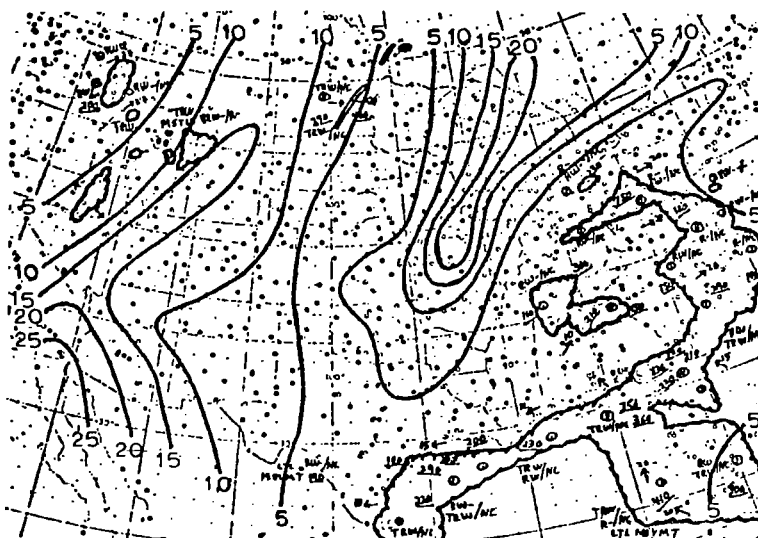
(a) The spread of the ambient and dew-point temperatures at 850 mb is shown in solid lines superimposed on the composite radar summary.

(b) Areas of positive temperature advection are outlined (or enclosed between lines) for each level in solid lines superimposed on the composite radar summary. W indicates the side of the line where warm advection occurs. C indicates the side of the line where cold or neutral advection occurs.

Fig. 63.   Charts of the spread of the ambient and dew-point temperatures at 850 mb, and areas of thermal advection and divergence at each level for 12Z, 20 September 1969.
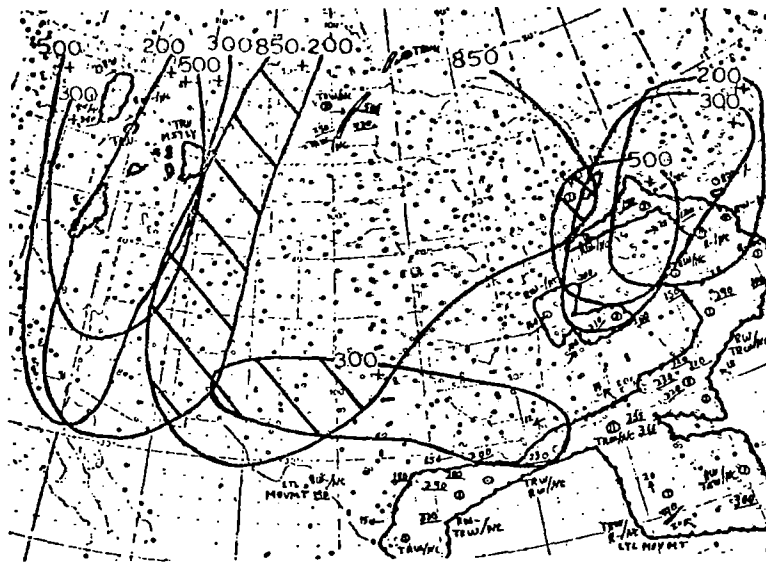
153

(c) Areas of convergence are outlined (or enclosed
     between lines) at the lower levels (850 and
     700 mb) and divergence at the upper levels
     (500, 300, and 200 mb) in solid lines
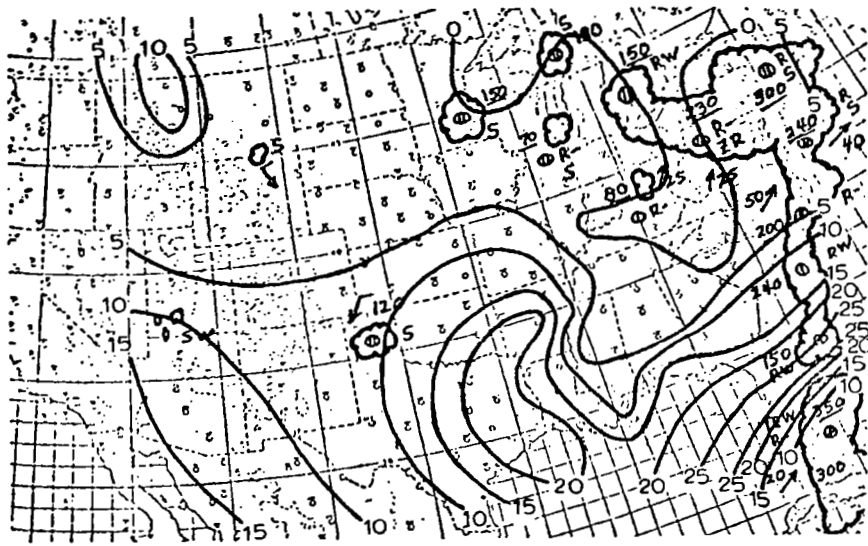   superimposed on the composite radar summary.
     Areas where convergence occurred at the lower
   levels and divergence at the upper levels are
     hatched and represent probable areas of positive
     vertical motion in the mid-troposphere.

Fig. 63.   (cont'd from previous page)

In the central United States, the squall line shown in Fig. 63c in North Dakota is isolated and does not appear to be related to other radar echoes. Although Fig. 63c shows convergence at 850 mb in the area of the squall line, this probably is not the "triggering mechanism" for the squall line since convergence at 850 mb is evident over a large area in which no radar echoes are reported. The squall line in North Dakota may be a result of surface fronts or may not be directly related to synoptic-scale weather systems.

In the area of radar echoes over the Ohio River Valley, Tennessee, and North Carolina, Fig. 63c shows divergence at 500, 300, and 200 mb; positive vertical motion in the mid-troposphere is probable. An examination of charts of space mean contours and vorticity fields (not shown) reveals a trough and associated vorticity field over the Ohio River Valley at 500, 300, and 200 mb. The magnitude of vorticity is largest at 300 mb. Although Fig. 63c does not show divergence throughout the area of radar echoes, it is probable that all the radar echoes in the area of the Ohio River Valley, Tennessee, and North Carolina are a result of positive vertical motion in the mid-troposphere created by positive vorticity advection aloft (500, 300, and 200 mb).

In the southern United States, a large area of radar echoes is present along the Gulf Coast from Texas through Florida. No explanation for these radar echoes is available from Fig. 63c except for the area south of Louisiana where divergence at 300 mb may contribute to positive vertical motion in the mid-troposphere. To retrogress, Fig. 63b shows warm advection at several levels over much of the area of echoes, but thermal advection alone does not appear to be sufficient to explain the large area of radar echoes in the southeastern United States. An examination of surface and standard-level charts (not included) reveals an ill-defined disturbance in the eastern Gulf of Mexico that may be of tropical origin. This disturbance is responsible for the widespread precipitation present in the Gulf of Mexico.

Figure 64a shows that most of the radar echoes are present where the spread of the ambient and dew-point temperatures is less than 10C. Exceptions to this occur in the western United States where numerous scattered showers are present in an area where the spread of the ambient and
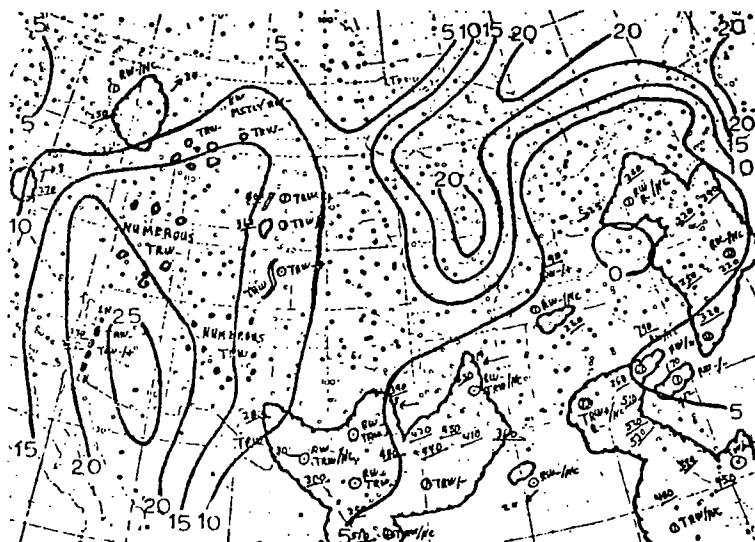
(a) The spread of the ambient and dew-point temperatures at 850 mb is shown in solid lines superimposed on the composite radar summary.
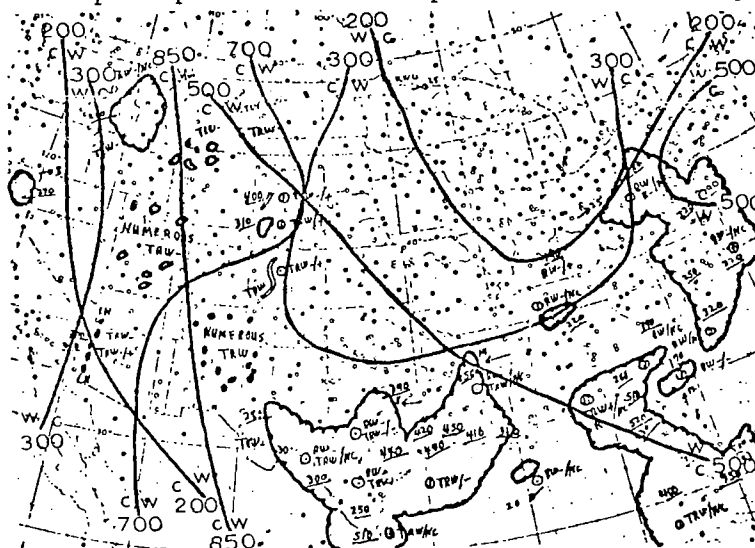
(b) Areas of positive temperature advection are outlined (or enclosed between lines) for each level in solid lines superimposed on the composite radar summary. W indicates the side of the line where warm advection occurs. C indicates the side of the line where cold or neutral advection occurs.

Fig. 64. Charts of the spread of the ambient and dew-point temperatures at 850 mb, and areas of thermal advection and divergence at each level for 00Z, 21 September 1969.

(c)   Areas of convergence are outlined (or enclosed
between lines) at the lower levels (850 and
700 mb) and divergence at the upper levels
(500, 300, and 200 mb) in solid lines
superimposed on the composite radar summary.
Areas where convergence occurred at the lower
levels and divergence at the upper levels are
hatched and represent probable areas of positive
vertical motion in the mid-troposphere.

Fig. 64.   (cont'd from previous page)

157

dew-point temperatures is greater than 10C. As stated previously, the spread of the ambient and dew-point temperatures at 850 mb may be a poor measure of the availability of moisture in the western United States, since the 850-mb level is near or below the ground level. By the adiabatic method, Fig. 64b indicates positive vertical motion in the mid-troposphere in most areas in which radar echoes are reported. However, an examination of charts of space-mean contours and isotherms (figures not shown) reveals weak thermal gradients; therefore, the magnitude of thermal advection is small, and positive vertical motion, which may be indicated by the adiabatic method over much of the United States in Fig. 64b, is small in magnitude. Positive temperature advection, shown in Fig. 64b, is not the principal cause of positive vertical motion in the mid-troposphere.

In the area of scattered radar echoes covering much of the western United States, Fig. 64c shows that divergence at 500, 300, and 200 mb and convergence at 850 mb affects all or part of the area, and by Dines Compensation Principle positive vertical motion in the mid-troposphere is probable. An examination of charts of space-mean contours and vorticity fields (not shown) reveals that vorticity fields are well-defined at 300 mb over Idaho, and at 200 mb over Idaho and Southern California. Hence, divergence is strongest in the area of maximum PVA at 300 and 200 mb. The large radar echo in western Montana is evidence of positive vertical motion in the mid-troposphere created by divergence at 300 and 200 mb.

The line of radar echoes in western Arizona is probably associated with PVA east of a vorticity center (not shown) at the 200-mb level over southern California. Radar echoes are not continuous over western Arizona; this may be because of the lack of low-level (850 mb) moisture in the area. The moisture shortage is indicated in Fig. 64a. The hatched area in Fig. 64c is coincident with numerous scattered radar echoes. In the eastern United States, radar echoes in the vicinity of the Ohio River Valley in Fig. 63 have moved eastward and in Fig. 64 are located near Pennsylvania. An examination of charts of space-mean contours and vorticity fields (not shown) for the dates corresponding to Figs. 63 and 64 shows that the trough located over the Ohio River Valley at the time of Fig. 63 has moved eastward, and at the time of Fig. 64 is over Pennsylvania with a well-defined vorticity center at 200 mb.

Although Fig. 64c does not show the large radar echo centered near Virginia to be completely within lines of positive divergence at 500, 300, and 200 mb, from a careful examination of charts of space-mean contours and vorticity fields (not shown), it is believed that the large echo is a result of positive vertical motion in the mid-troposphere created by divergernce at 500, 300, and/or 200 mb.

The radar echo in Tennessee may be a remnant from radar echoes present in the same area at the previous time period. In the southeastern United States, radar echoes from Georgia through Florida are not explained by the methods of this report. An examination of the surface and standard pressure maps (not shown) reveals that the disturbance in the Gulf of Mexico, which was mentioned in the discussion of Fig. 63, is still present and is responsible for the radar echoes from Georgia southward through Florida. Also, a "break" in the radar echoes east of Georgia is present in Fig. 64 which is not present in Fig. 63. This "break" separates radar echoes associated with the trough over Pennsylvania from echoes associated with the disturbance in the Gulf.

In the area of radar echoes in Texas and Louisiana, Fig. 64c shows convergence at 850 mb affecting much of the area. If there is convergence from the surface up to 850 mb, then there will be positive vertical motion at least to a height of 850 mb, and this may cause mesoscale systems. In west Texas, Fig. 64c shows convergence at 850 mb and divergence at 300 and/or 200 mb, and by Dines' Compensation Principle, there will be positive vertical motion in the mid-troposphere. A comparison of radar echoes over Texas and Louisiana in Figs. 63 and 64 shows that radar echoes in the Gulf (Fig. 63) have spread inland over Texas and Louisiana (Fig. 64). Probably many of the echoes over the Gulf are a result of a tropical disturbance over that area. The extension of these echoes inland is primarily a result of positive vertical motion caused by convergence at 850 mb. Radar echoes in northern California may be a result of orographic effects and may not be directly related to synoptic-scale weather systems.

Figure 65a shows that most radar echoes are present where the spread of the ambient and dew-point temperatures is less than 10C. Figure 65b, as with previous figures of thermal advection, shows a confused and unsystemmatic pattern. Although in some areas positive thermal advection
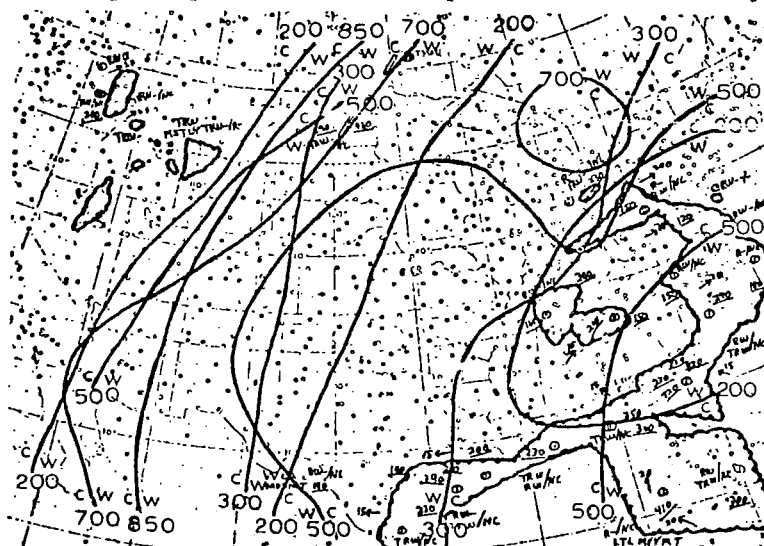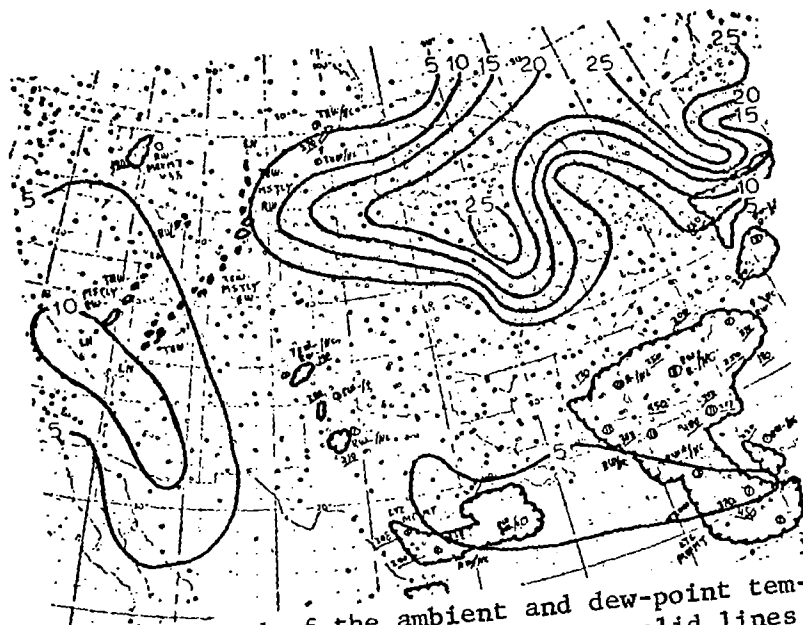
(a) The spread of the ambient and dew-point temperatures at 850 mb is shown in solid lines superimposed on the composite radar summary.
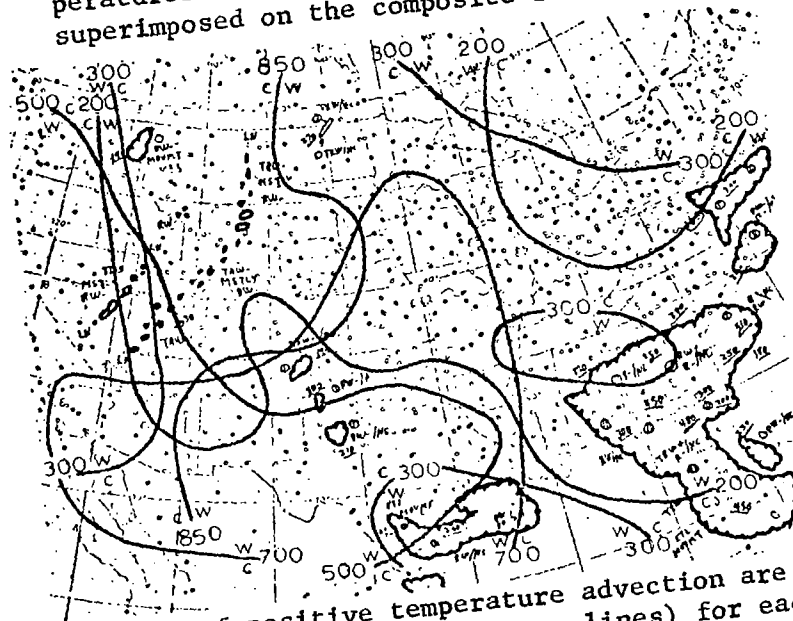
(b) Areas of positive temperature advection are outlined (or enclosed between lines) for each level in solid lines superimposed on the composite radar summary. W indicates the side of the line where warm advection occurs. C indicates the side of the line where cold or neutral advection occurs.

Fig. 65.   Charts of the spread of the ambient and dew-point temperatures at 850 mb, and areas of thermal advection and divergence at each level for 12Z, 21 September 1969.
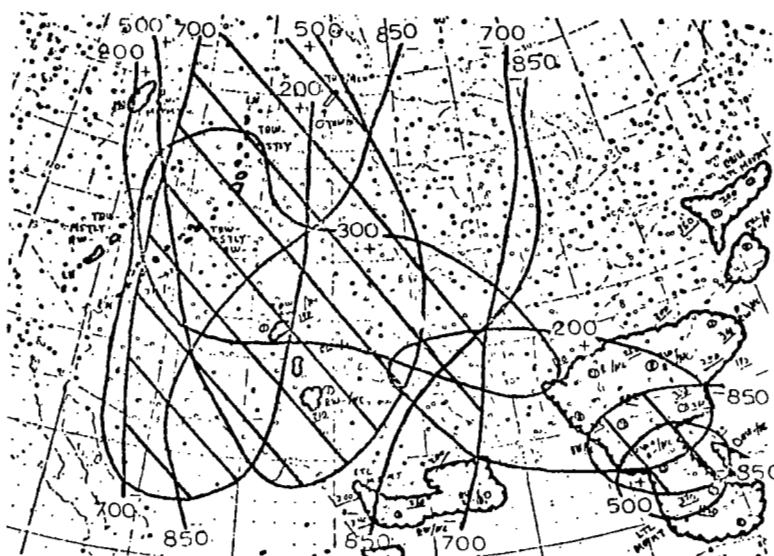
(c) Areas of convergence are outlined (or enclosed between lines) at the lower levels (850 and 700 mb) and divergence at the upper levels (500, 300, and 200 mb) in solid lines superimposed on the composite radar summary. Areas where convergence occurred at the lower levels and divergence at the upper levels are hatched and represent probable areas of positive vertical motion in the mid-troposphere.

Fig. 65. (cont'd from previous page)

probably contributes to positive vertical motion in the mid-troposphere, it is not possible from Fig. 65b to determine accurately where, by the adiabatic method, there will be positive vertical motion in the mid-troposphere.

In the western United States, scattered radar echoes are present in North Dakota and along a line from Montana to Utah. In this area convergence is present at 700 mb (Fig. 65c), and divergence at 500 and 200 mb (Fig. 65c). A comparison of charts of space-mean contours and vorticity fields (not shown) for this and the previous 12-hour time period shows that the vorticity center at 300 mb previously over Idaho, is now over the Great Salt Lake. At 200 mb, the comparison shows that the vorticity field present over southern California 12 hours previously has dissipated; the vorticity field previously over Idaho now is over northwestern Montana and is not as well defined.

Radar echoes shown in Fig. 64 in western Arizona that were associated with the vorticity field at 200 mb are not present in Fig. 65. Radar echoes over Idaho in Fig. 64 moved into western Montana and decreased in areal coverage coincident with the movement and decrease of the vorticity field at 200 mb. Radar echoes in the panhandle of Texas are in an area where convergence at 850 and 700 mb (Fig. 65c) and divergence at 500, 300, or 200 mb (Fig. 65c) are present, and by Dines' Compensation Principle, there will be positive vertical motion in the mid-troposphere.

In the eastern United States, Fig. 65c does not show any indication of positive vertical motion in the area of radar echoes over the Atlantic Ocean east of Virginia and North Carolina. However, an examination of upper-level charts (not shown) shows that the trough aloft (500, 300, and 200 mb), which at the time of Fig. 64 was over Pennsylvania, is now over the Atlantic coast and is moving out of the analysis area.

Radar echoes east of Virginia and North Carolina are associated with the trough aloft. In the large area of radar echoes in the southeastern United States, Fig. 65c shows convergence at 850 mb, and divergence at 500 and 200 mb affecting much of the area. By Dines' Compensation Principle, Fig. 65c shows positive vertical motion in the mid-troposphere, hence clouds and precipitation occur over much of the area of radar echoes in the southeastern United States. An examination of surface and standard-

level charts (not shown) reveals the continuing presence of a disturbance which appears to be of tropical origin.

Figure 66a shows that most radar echoes are present where the spread of the ambient and dew-point temperatures at 850 mb is less than 10C. In the area of scattered radar echoes extending from North Dakota south to Texas, Fig. 66b shows warm advection at 850, 700, and 200 mb, and co,d or neutral advection at 500 and 300 mb. By the adiabatic method, Fig. 66b indicates positive vertical motion in this area of scattered radar echoes. Figure 66c shows convergence at low levels (850 and 700 mb) and divergence aloft (500, 300, and 200 mb) affecting much of the large area of scattered radar echoes from Texas through North Dakota. In the area of radar echoes in the southeastern United States, Fig. 66b shows warm advection at 850, 700, and 500 mb, thus indicating positive vertical motion in this area. The hatched area, strongly indicating the possibility of positive vertical motion in the mid-troposphere, encompasses most of the radar echoes in the Great Plains including the thunderstorms with greatest vertical development that are present over the Texas Panhandle.

The radar echo in western Montana may be a result of orographic effects and may not be directly related to synoptic scale weather systems. In south Texas, radar echoes may be explained partially on the basis of convergence shown in Fig. 66c at 850 and 700 mb. However, Fig. 66c shows that many of the radar echoes are present south of the indicated area of convergence at 850 and 700 mb. From an examination of surface and standard-level maps (not shown) it is believed the area of radar echoes in south Texas is at least partially the result of a disturbance in the Gulf. In the area of radar echoes in the southeastern United States, Fig. 66c shows divergence at 200 mb over a part of the area of echoes. Divergence at 200 mb may indicate positive vertical motion in the mid-troposphere. An examination of surface and standard-level charts (not shown) reveals the presence of a disturbance which may be of tropical origin in the eastern Gulf near the Florida panhandle. The disturbance in the Gulf, which is not clearly defined by the data available, creates the large area of precipitation in the southeastern United States.

Figure 67a shows that most radar echoes are present where the spread of the ambient and dew-point temperatures at 850 mb is less than 5C. As
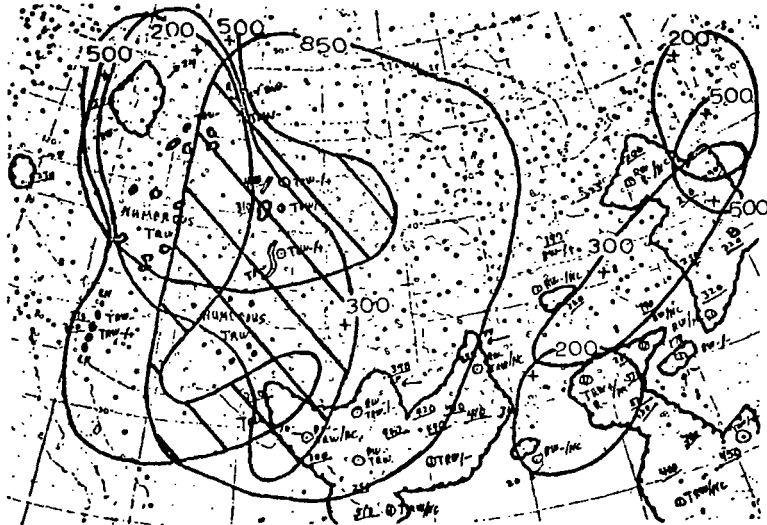
(a) The spread of the ambient and dew-point temperatures at 850 mb is shown in solid lines superimposed on the composite radar summary.
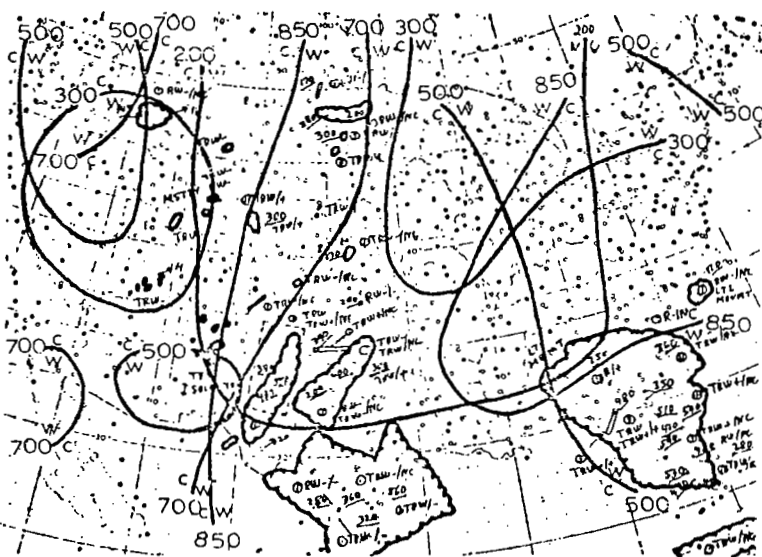
(b) Areas of positive temperature advection are outlined (or enclosed between lines) for each level in solid lines superimposed on the composite radar summary. W indicates the side of the line where warm advection occurs. C indicates the side of the line where cold or neutral advection occurs.

Fig. 66. Charts of the spread of the ambient and dew-point temperatures at 850 mb, and areas of thermal advection and divergence at each level for 00Z, 22 September 1969.
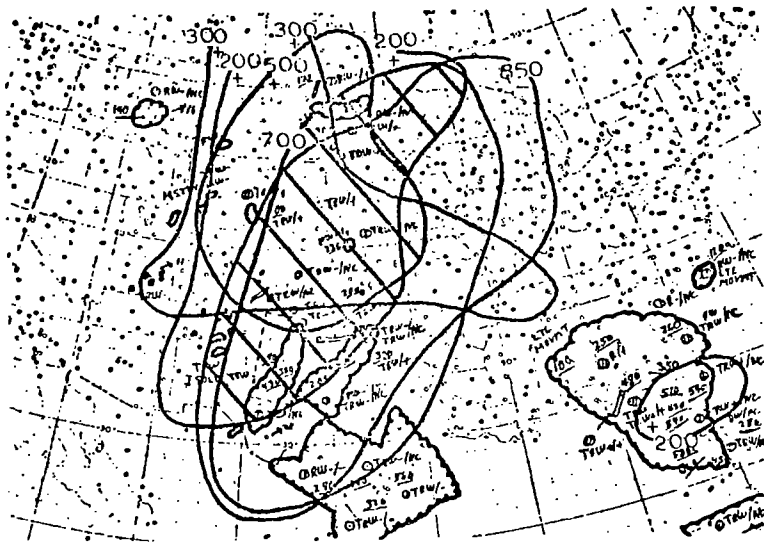
(c)   Areas of convergence are outlined (or enclosed
      between lines) at the lower levels (850 and
      700 mb) and divergence at the upper levels
      (500, 300, and 200 mb) in solid lines
      superimposed on the composite radar summary.
      Areas where convergence occurred at the lower
      levels and divergence at the upper levels are
      hatched and represent probalbe areas of positive
      vertical motion in the mid-troposphere.

         Fig. 66.   (cont'd from previous page)
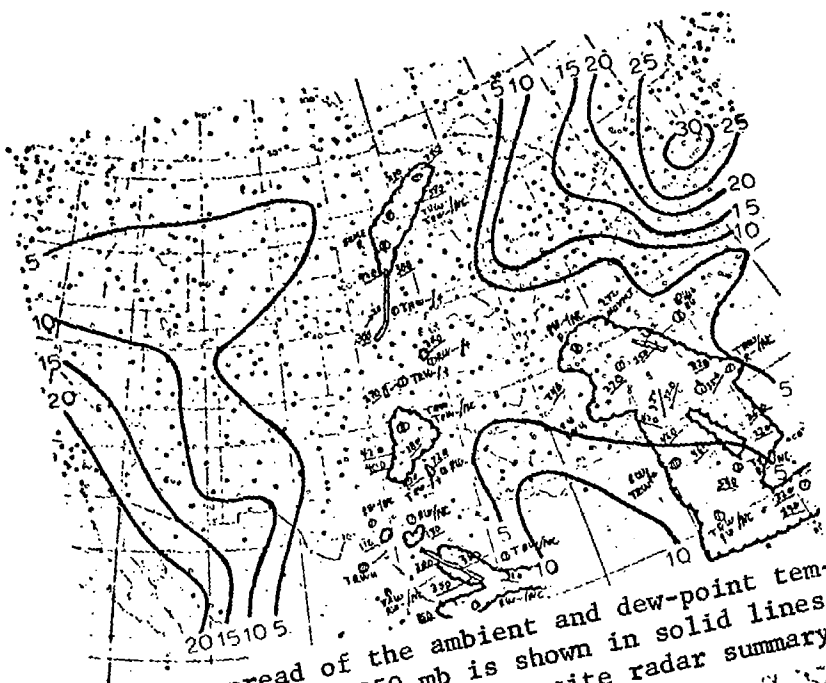
(a) The spread of the ambient and dew-point temperatures at 850 mb is shown in solid lines superimposed on the composite radar summary.
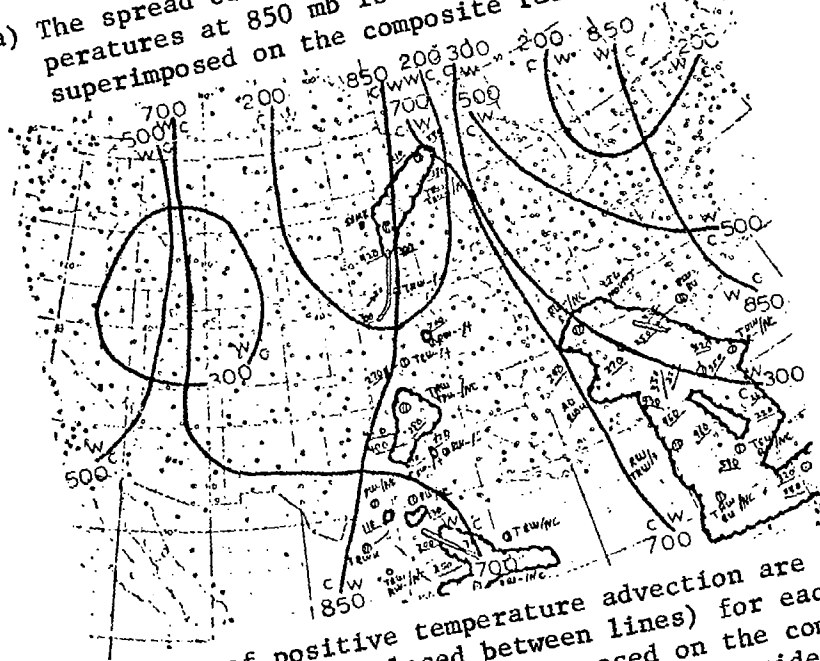
(b) Areas of positive temperature advection are outlined (or enclosed between lines) for each level in solid lines superimposed on the composite radar summary. W indicates the side of the line where warm advection occurs. C indicates the side of the line where cold or neutral advection occurs.

Fig. 67. Charts of the spread of the ambient and dew-point temperatures at 850 mb, and areas of thermal advection and divergence at each level for 12Z, 22 September 1969.
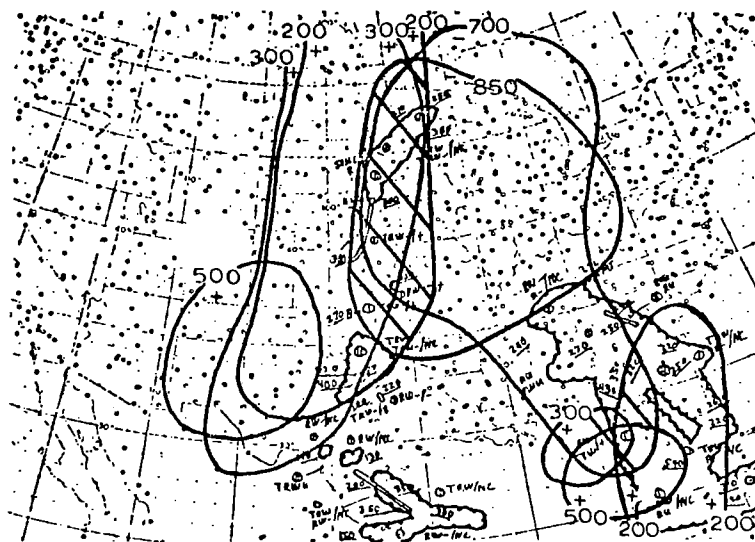
(c) Areas of convergence are outlined (or enclosed
     between lines) at the lower levels (850 and
     700 mb) and divergence at the upper levels
     (500, 300, and 200 mb) in solid lines super-
     imposed on the composite radar summary. Areas
     where convergence occurred at the lower levels
     and divergence at the upper levels are hatched
     and represent probable areas of positive verti-
     cal motion in the mid-troposphere.

Fig. 67. (cont'd from previous page)

167

with some of the previous figures of thermal advection for this period, Fig. 67b shows an unsystemmatic distribution of thermal advection. It is not possible to assess the contribution to positive vertical motion in the mid-troposphere from the figure. However, Fig. 67b shows that warm advection at 850 and 700 mb in the area of radar echoes in south Texas and positive vertical motion, indicated in this case by the adiabatic method, may be sufficient to create radar echoes. The hatched area in Fig. 67c outlines many of the radar echoes in the Great Plains. Radar echoes in north central Texas, which are not in the hatched area, are in an area where Fig. 67c shows divergence at 300 and 200 mb.

In the area of radar echoes in the southeastern United States, Fig. 67c shows convergence at low levels (850 and 700 mb) and/or divergence at upper levels affecting much of the echo area. The hatched area in the eastern Gulf is coincident with many of the tallest cloud tops. An examination of surface and standard-level maps (not shown) reveals that the disturbance which may be of tropical origin is still centered over the Florida panhandle and is responsible for the widespread precipitation in the southeastern United States.

Most radar echoes are present where the spread of the ambient and dew-point temperatures at 850 mb is less than 5C as shown in Fig. 68a. Fig. 68b shows an almost random arrangement of thermal advection at each level as has frequently been the case for September. The figure shows that, for this particular date and time, thermal advection does not contribute significantly to positive vertical motion in the mid-troposphere. Divergence at 500, 300 and 200 mb is shown over much of the large area of radar echoes which are present in Fig. 68c from western Texas northeastward to Minnesota. Radar echoes in south Texas, as well as echoes in northern Idaho, are not explained by the methods considered in this study.

Radar echoes in the southeastern United States are associated with the disturbance in the Gulf that is now centered over southern Alabama. An examination of charts of surface and standard levels (not shown) shows that the disturbance has drifted northward and decreased in intensity. Figure 68c shows divergence aloft (500, 300, and 200) over part of the radar echoes in the southeastern United States.
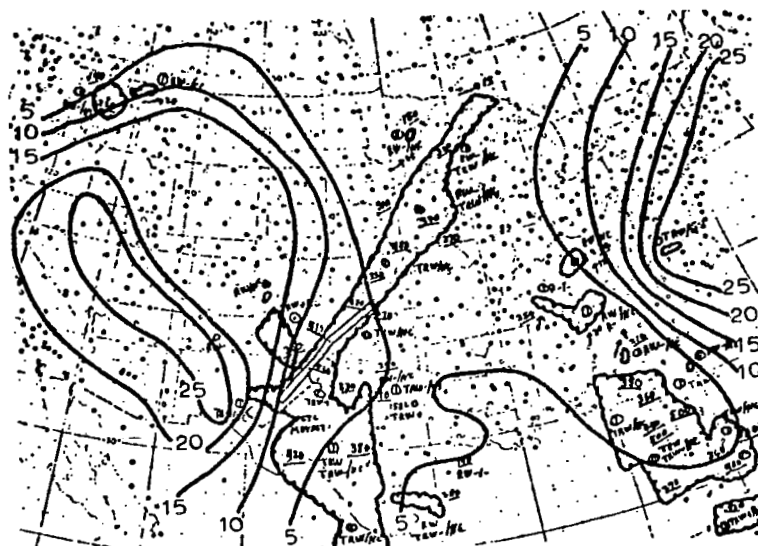
(a) The spread of the ambient and dew-point tem-
peratures at 850 mb is shown in solid lines
superimposed on the composite radar summary.
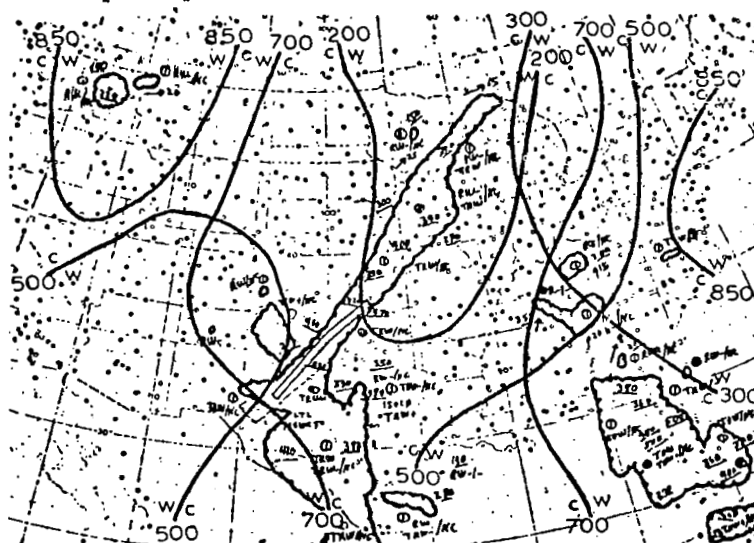
(b) Areas of positive temperature advection are
outlined (or enclosed between lines) for each
level in solid lines superimposed on the com-
posite radar summary. W indicates the side
of the line where warm advection occurs. C
indicates the side of. the line where cold or
neutral advection occurs.

Fig. 68.   Charts of the spread of the ambient and
dew-point temperatures at 850 mb, and
areas of thermal advection and divergence
at each level for 00Z, 23 September 1969.

(c) Areas of convergence are outlined (or enclosed
      between lines) at the lower levels (850 and
      700 mb) and divergence at the upper levels
      (500, 300, and 200 mb) in solid lines super-
      imposed on the composite radar summary. Areas
      where convergence occurred at the lower levels
      and divergence at the upper levels are hatched
      and represent probable areas of positive verti-
      cal motion in the mid-troposphere.

Fig. 68. (cont'd from previous page)

b)   Curvature of the Vertical Wind Profile

Figure 69 shows the results of the analysis of curvature for 12Z, 20 September 1969. The corresponding composite radar chart is shown in Fig. 63. The expected area of echoes from the middle Atlantic region through Kentucky failed to be supported by observed echoes. The large area of observed echoes along the Gulf Coast, through Florida and up the Atlantic Coast was not accounted for by an expected area probably due to a lack of data in these areas.

Figure 70 shows the results of the analysis of curvature for 00Z, 21 September 1969. The corresponding composite radar chart is shown in Fig. 64. The expected area in Pennsylvania, Maryland, and Delaware coincided closely with echoes observed in that area. As in the previous time, there were large areas of observed echoes off the Gulf Coast and through Florida with the only expected areas being in Louisiana, and in Georgia and Alabama. This lack of expected echoes could have been due to the lack of data off the coast.

Figure 71 shows the results of the analysis of curvature for 12Z, 21 September 1969. The corresponding composite radar chart is shown in Fig. 65. The expected areas along the Texas and Louisiana Gulf Coast, and in Maryland and Delaware, coincided closely with the observed areas or echoes. The expected area in Kentucky and Tennessee failed to be confirmed. The large area of observed echoes in Alabama, Florida, Georgia, and South Carolina was not covered by an expected area. However, this was a region of sufficient moisture and of upper-level divergence. Weak convergence was probably present in this area giving the necessary upward motion for the formation of clouds.

4)   Summary of Results for the September Period

This case is an example of an autumn situation in which Z' fields are not well defined. Initially, the principal trough is centered over the western United States and no large areas of associated radar echoes are present. A secondary wave is present at upper levels (500, 300, and 200 mb) over the Ohio River Valley. The secondary wave has a well-defined vorticity center and associated radar echoes. By the time of
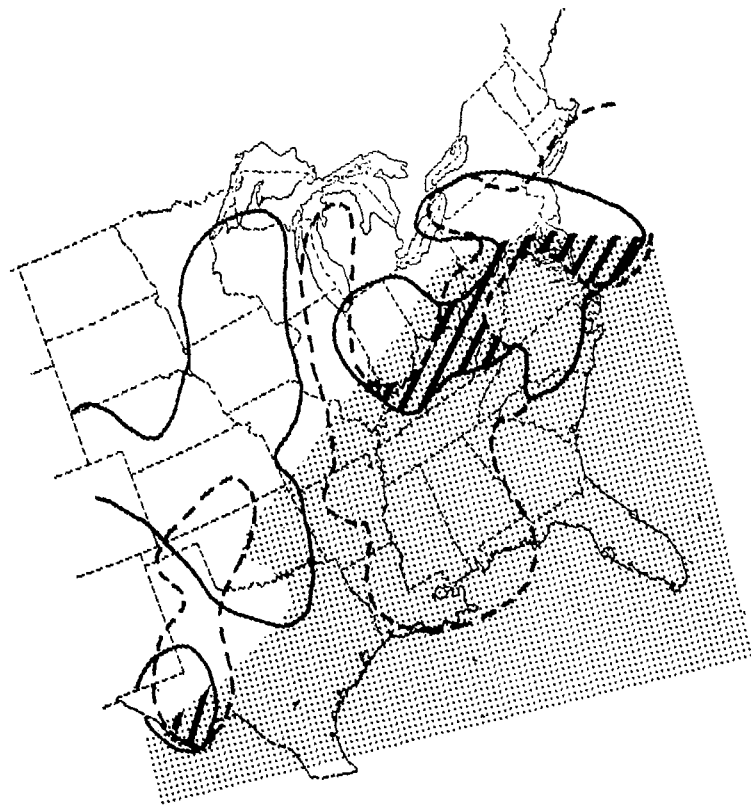
Fig. 69. Results of curvature analysis for 12Z, 20 September 1969.
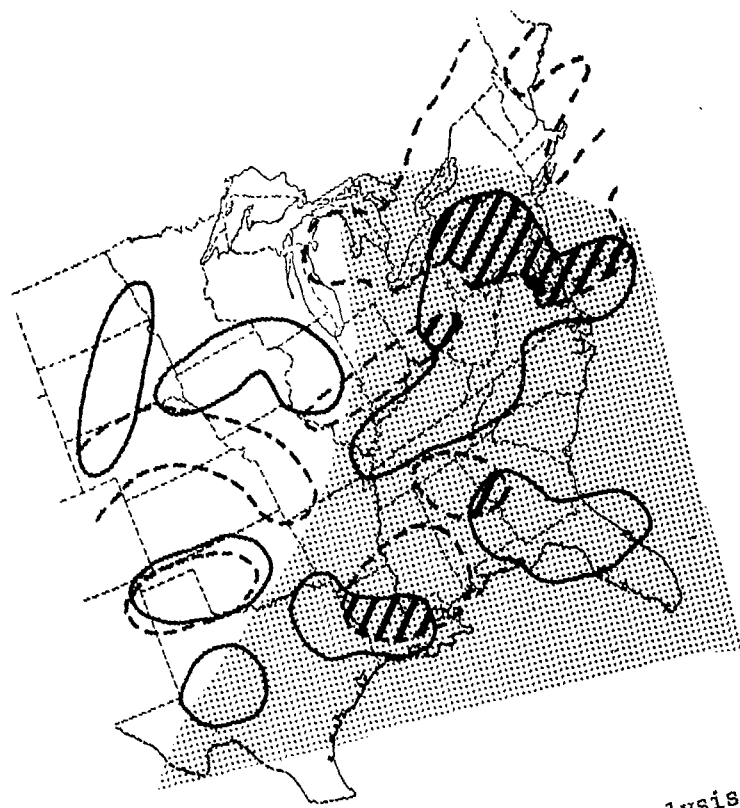
Fig. 70. Results of curvature analysis for 00Z, 21 September 1969.

...vel convergence is enclosed by a solid line and ...ashed line. The shaded areas represent ...represent those of expected echoes.
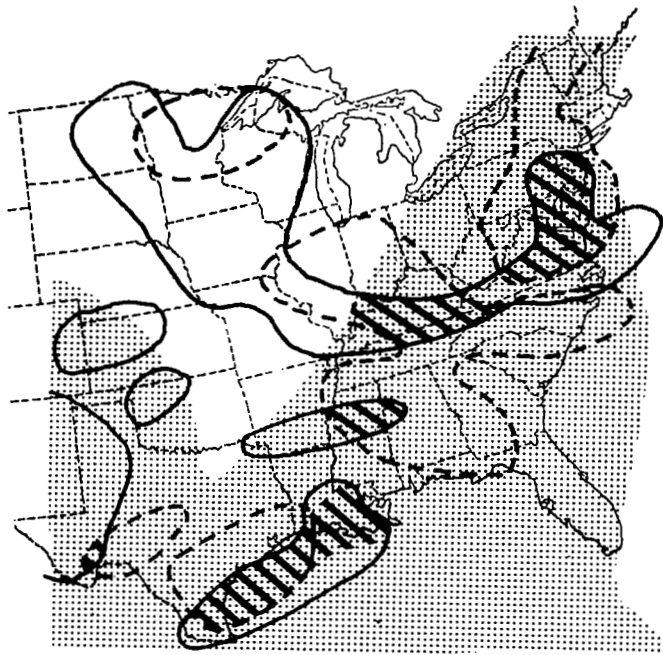
Fig. 71. Results of curvature analysis for
12Z, 21 September 1969. (The area
of low-level convergence is enclosed
by a solid line and the area of
upper-level divergence by a dashed
line. The shaded areas represent
$T - T_D \leq 5°C$ at 850 mb, while the
hatched areas represent those of
expected echoes.)

Fig. 64, this secondary wave is located off the East Coast and out of the analysis area. During the period studied, the principal trough in the western United States drifted eastward. The trough has the greatest amplitude, and vorticity centers are best defined, at upper levels (500, 300 and 200 mb). The space-mean trough is very poorly defined at 850 mb during the last two time periods. Hence, divergence based on PVA at the upper levels (500, 300, and 200 mb) shows the best correlation with observed radar echoes.

Throughout most of this case, thermal advection did not appear to contribute significantly to positive vertical motion in the mid-troposphere. Radar echoes which appear to be associated with the disturbance in the Gulf of Mexico are not explained by the methods of this report until the disturbance begins to move inland over a close network of reporting stations. The "article of faith" has some validity in the central United States but does not adequately explain many mesoscale systems, especially those in the southeastern United States. This case differs from the June case in that for this case there appears to be a relationship between meso- and synoptic-scale phenomena, at least in some cases. However, the relationship is not as clear-cut as in the March and December cases.

7. SUMMARY AND CONCLUSIONS

The principal objective of this research was to determine in a semi-quantitative manner to what degree the occurrence and extent of meso- or small-scale systems could be related from synoptic-scale systems. In long-range forecasts it is necessary to assume that small-scale systems are determinable from synoptic-scale systems. The premise that such a relationship exists has been referred to as the "article of faith."

Four periods (during March, June, September, and December) of three days each with significant weather and mesoscale systems as revealed by radar echoes were chosen for study. Synoptic charts for all standard pressure levels from the surface to 200 mb were prepared and analyzed in the usual manner. These charts, combined with nephanalyses and radar summary charts, were used in the analysis.

The first approach was to determine statistical relationships between the gradients of temperature and height, and clouds and radar echoes. The gradients of height and temperature were extracted from the 850-, 500-, and 300-mb levels from analyzed charts at 11 stations scattered over the eastern United States for four time intervals. Radar summary charts were used to determine if echoes appeared within 100 nautical miles of each station, and a nephanalysis was performed for each chart and for each time period to determine if a ceiling (0.6 or more cloud coverage) was present below 5000 and 10,00 ft within 100 n mi of each station. Various combinations of these data were plotted in the form of scatter diagrams and linear correlation coefficients and linear regression lines computed. In addition, the relationshp between three variables and echoes/no echoes was investigated for the June and December periods.

A number of statistically significant correlation coefficients were found for each period, but a systematic trend between the periods was not found. During three of the four periods, a significant correlation coefficient was observed between the gradient of height at 850 and 500 mb when radar echoes were observed within 100 n mi of the station, and during three of the four periods a significant correlation was found between the gradient of temperature at 850 and 500 mb when no radar echoes were observed within 100 n mi of the station. When no ceiling was observed below 5000 ft, the

175

linear correlation coefficient between the gradient of height at 850 and
300 mb was found to be significant in three of the four periods, while
those between the gradient of temperature at 850 and 500 mb were found to
be significant in three of the four periods when ceilings were observed.
When there was no ceiling observed at heights less than 10,000 ft, a
significant correlation was found between the gradient of temperature at
850 and 500 mb during three of the four periods; however, when a ceiling
was observed below 10,000 ft, no significant correlations were found in
any category for three of the four periods. There was no trend indicated
in the correlations between gradients taken from different charts and
radar echoes and ceilings, and the addition of height and temperature
gradients to form a three-way distribution did not appear to improve the
relationships found when only two of the variables were used.

In the second approach, areas of positive vertical motion in the mid-
troposphere were determined from the synoptic charts by use of the
simplified vorticity equation combined with Dines' Compensation Principle,
the adiabatic method, the curvature of the vertical wind profile, and the
structure of the synoptic waves (March period only). Space-mean and devia-
tion charts were prepared for each pressure level, and the sign of divergence
estimated from the simplified vorticity equation. Dines' Compensation
Principle was then used to estimate the sign of vertical motion in the
mid-troposphere. An equation was derived which gave an estimate of the
relative vorticity in the vicinity of troughs and ridges based on the
amplitude and wavelength of the synoptic waves. The sign of vertical motion
was estimated in a manner similar to that using the simplified vorticity
equation. In the adiabatic method, only the advection of temperature was
considered. This method was used only as a supplement to the other methods.
The sign of divergence was estimated from the gradients of curvature com-
puted at several levels, and areas of divergence superimposed to infer
regions of positive vertical motion in the mid-troposphere by use of Dines'
Compensation Principle. This method gave results similar to those obtained
from the simplified vorticity equation.

Areas of positive vertical motion, sufficient low-level moisture, and
conditional instability (June case only) are areas in which mesoscale
systems (radar echoes) were expected. The expected areas were compared

APPENDIX A

A REVIEW OF FORECASTING CAPABILITY

by

Henry E. Fuelberg
Department of Meteorology
Texas A&M University

1. Introduction

A "weather forecast" means different things to different people. For most earth-bound people it is related to cloudiness, precipitation, temperature, and surface wind at a given location as a function of time. This class of people is not interested in wind at high altitudes, how high the clouds extend, whether or not it rains 50 miles from them, or the mechanisms which produced the weather in the first place. On the other hand, an aviator is interested in forecasts of the heights of the bases and tops of the clouds, visibility, and precipitation at his take-off and landing points as well as wind speed and direction, clouds, visibility, turbulence, and temperature at flight level along his flight path. Along his flight track he is usually not interested in weather which occurs at the ground. A meteorologist may consider a forecast to be the height of a constant-pressure surface, the position of the jet stream, or the likelihood of vertical motion over an area. All of these are examples of "weather forecasts." Just what is meant by a weather forecast may depend on the specific interests of those who wish to use it as well as the degree of knowledge one possesses of atmospheric processes.

Weather (clouds, precipitation, thunderstorms, fog, etc.) results usually from many complicated processes superimposed. Some of the systems may be only a few hundred meters across, others may be a few to several tens of kilometers across, and still others may have dimensions of a few thousand kilometers. These systems move relative to each other, and form and dissipate at irregular intervals. In general, the large systems are more predictable than the small systems over long time periods. Forecasts over periods of 1 or 2 days may be based primarily on relatively small-scale systems whereas forecasts for periods of 3 days to a week and longer are based on systems with dimensions of perhaps a few thousand kilometers or more. Since meso- and sub-synoptic-scale systems (less than 1500 km across) are responsible for most of the clouds and precipitation observed at any given location, it is easy to understand why forecasts over a long period of time are not as good as those over a shorter period of time.

The degree of forecast verification is indicated in several ways. The percent of forecasts which were correct, frequently called forecast accuracy, is the simplest method. The number of correct forecasts is divided by the total number of forecasts.

The skill score is used to indicate forecast performance referenced to chance. The skill score is defined as the number of correct forecasts

minus the number of correct forecasts due to chance divided by the total number of forecasts minus t`~~ number of correct chance forecasts (Teweles and Horst, 1953). A positive score indicates that the method of forecasting is better than chance; a skill score of +1.0 indicates perfect forecasts, while a negative score indicates that the forecasts were worse than those of chance. Forecasts based upon chance would have a skill score of zero. Skill scores and accuracy scores cannot be obtained conveniently from each other.

Although a forecast scheme may yield a high accuracy, the skill score may be very low or even negative. For example, if a desert region expects only a few rain days per year and these are forecast incorrectly, the skill score would be low. The accuracy would be high however, since most of the forecasts were correct. High skill scores are associated with high accuracies, but high accuracies are not always associated with high skill scores.

A summary of what can be forecast and with what accuracy is given in the following sections. No attempt has been made to present a complete and through review inasmuch as literally hundreds of papers have been published on the subject of forecasting weather. This is a summary primarily of the more recent methods employed and some of the results obtained.

2. Types of Forecasting

Three major methods of forecasting are in use today--subjective, objective, and numerical. Statistical and deterministic methods are included in the objective method, and the deterministic method is included also in the numerical method. While each method can be used independently, they are frequently used together. These methods are described briefly in this section while applications to specific forecasting problems are discussed in later sections.

2.1 The Subjective Method

Many practicing meteorologists use the subjective method of forecasting. Each meteorologist using this method goes through his own individual forecasting technique by personally analyzing the data available on various charts, checking areas that look suspicious to him, and then drawing upon his meteorological training and a certain amount of intuition to arrive at a forecast. The accuracy of the subjective method depends on the forecaster's ability to apply meteorological principles and his previous experience to the current situation. The details of the methods used by this type of forecaster are varied, and for this reason the forecasts issued for the same area by several meteorologists with identical data may be quite different.

2.2 The Objective Method

An objective method consists of a predetermined set of techniques which is applied to a specific forecasting problem. Once the method has been devised, there is little recourse to personal judgments of the forecaster, but objective methods are frequently used as aids by the subjective forecaster. The techniques may involve the substitution of several current meteorological parameters into previously prepared empirical forecast equations or diagrams which then give the forecast. The diagrams and equations are statistically derived and based on previous occurrences of the particular event. They utilize current data based on parameters which historically have been shown to be important in the forecast problem to obtain the forecast.

The derivation of an objective method is usually quite complicated. It involves finding variables which are statistically important to the forecasting problem, and then organizing them so that the highest probability of an accurate forecast is obtained. A particular objective procedure is usually helpful only in a small geographic area and in a particular season of the year.

2.3 The Numerical Method

Accurate and long-range forecasts using the numerical method is the ultimate aim of the theoretical meteorologist. The Glossary of Meteorology defines this method as "the forecasting of the behavior of atmospheric disturbances by the numerical solution of the governing fundamental equations of hydrodynamics, subject to observed initial conditions." Beginning with observed conditions, the equations of motion, continuity, first law of thermodynamics, and equation of state are solved for a given instant by use of computers. Computed values of the variables are then used to solve for values at a later time. The results for the specified time are used to draw prognostic maps.

The accuracy and resolution of the initial data determine the accuracy of the numerical product. No numerical model will be able to produce accurate results if inaccurate or insufficient initial data are supplied, and the area from which data are needed increases with the length of the forecast period. For accurate forecasts of one week to two months in length, it is estimated that data will be needed over the entire earth from a depth of 100 m in the oceans to an altitude of about 60 km in the atmosphere (see Fig. 1). Leith (1971) suggests that atmospheric predictability could be lengthened by about one day for each factor of two increase in the resolution of observations.
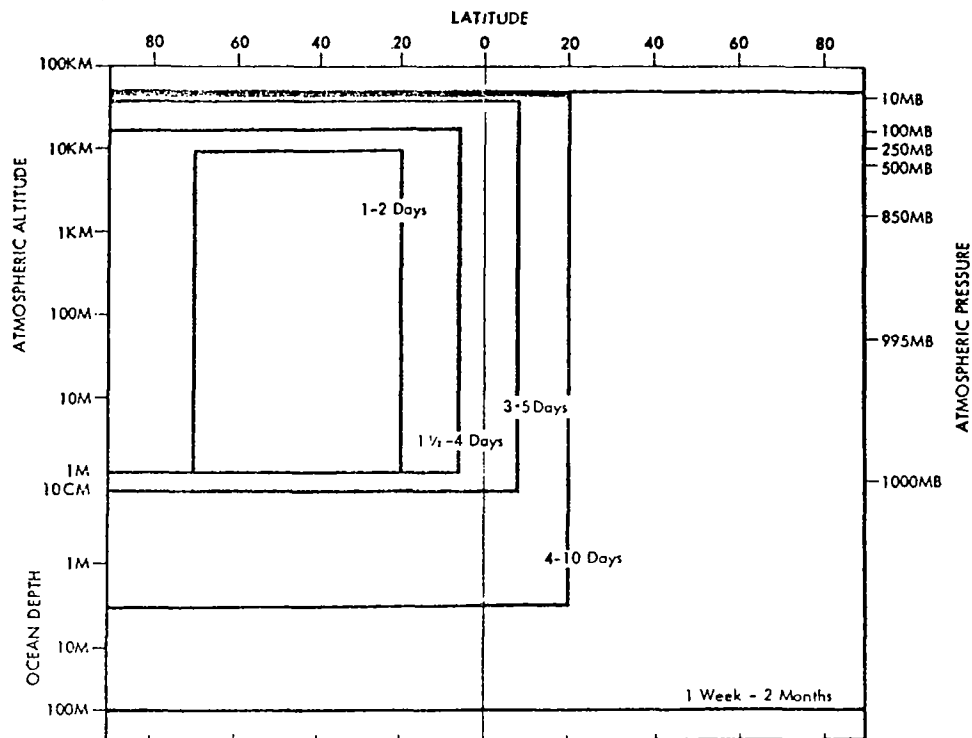
LATITUDE

Fig. 1. Schematic of the data required for forecasts in the
mid-latitudes for different forecast periods. (Anon. BAMS
50(9), p666.)

The World Weather Watch (WWW) and the Global Atmospheric Research Program (GARP)
are attempting to improve the observational network.

Several numerical models have been developed. They differ in the number
of simplifying assumptions made to reduce the number of calculations and,
therefore, in the degree of accuracy and resolution of the final product.
While numerical methods do not predict "weather," they are used often as aids
for the subjective forecaster. One serious limitation of numerical methods,
particularly for periods exceeding two or three days, is that only features
of large-scale systems (a few thousand kilometers) can be predicted. Interme-
diate- and small-scale systems which produce and/or enhance a large part of
the significant weather, cannot be predicted with sufficient accuracy. If
these systems are included in the models, they are expressed in terms of the
predictable large-scale systems. The methods employed to relate small-scale
systems to large-scale systems are inadequate and not well understood.

3. Forecasts of the Pressure Field

Forecasts of the pressure field are important since they serve as the basis
for other forecasts such as those of precipitation and temperature.   The

various methods of long- and short-range forecasts of the pressure field will be discussed along with their respective accuracies.

3.1 Subjective Forecasts of the Pressure Field

There are many subjective methods used to forecast the pressure field. As the meteorologist scans his current data prior to making a forecast, he may use any number of techniques such as Dines' Compensation Principle, temperature advection, or climatology which he has learned through formal training or practical experience. Subjective methods will not be discussed separately but rather with the results of other forecasting procedures.

3.2 Objective Forecasts of the Pressure Field

Although forecasts of sea level pressure up to 12 hours are frequently made by extrapolation and other subjective methods, Lund (1963) showed that improvements could be made at one station by use of linear regression equations with sea level pressure, pressure changes, and pressure differences as variables. His 6-hour method reduced errors by 81% when compared to subjective methods then in use, and the 11-hour method reduced errors by 80%. By deriving similar equations for many other stations, Lund believes that accurate 6- and 12-hr surface pressure charts can be made for large areas.

Objective methods for forecasting the movement and degree of intensification, if any, of pressure centers have been developed. This is especially valuable since weather phenomena are frequently associated with cyclonic centers. Veigas and Ostby (1963) used multiple regression prediction equations to compute 24-hr movements and intensity changes for cyclones along the East Coast. Operational results yielded a vector position root-mean-square (rms) error of 2.25 degrees of latitude and an rms error of 8.14 mb for central pressure changes. The National Weather Analysis Center had rms errors of 3.87 degrees of latitude and 7.25 mb for the same period. George and Wolff (George, 1960) developed a type of graphical correlation technique for forecasting which was based on relations between selected meteorological variables. Borsting and Sheehan (1964) compared this method with the method of Veigas and Ostby and found that there was no significant difference in accuracy between the two procedures in the regions for which they were derived. Palmer (1948) made 30-hr forecasts of the direction of movement of winter cyclones by use of scatter diagrams with variables such as previous movement and isallobaric gradients. Average directional errors using his technique were 10.7 degrees compared to 15.8 degrees for the National Weather Analysis Center.

Objective methods also have been derived for forecasting the movement
and intensity change of anticyclones. Martin et al. (1963) used stepwise
regression analysis techniques to make 24-hr forecasts in much the same
manner as Veigas and Ostby. Tests on independent data gave a 24-hr vector
rms error of 290 n. mi. (4.8 degrees of latitude) and a central pressure
rms error of 4.2 mb.

Objective methods for forecasting the pressure field reduce errors,
and subjective forecasters undoubtedly use these techniques, or the principles
on which they were based, to some extent in making forecasts of short-range.
Objective methods are of little value, however, in determining detailed
pressure fields in long-range forecasting. White and Galligan (1956)
made 24-, 72-, and 120-hr forecasts of pressure for the 1000-, 500-, and
200-mb levels by deriving regression equations with initial conditions as
variables. They found that their statistical methods applied at 1000 mb
were more accurate than official forecasts for periods greater than 36 hours.
Their method was superior also to official forecasts at the 500- and 200-mb
levels up to 36 hours. Official upper-air maps past 36 hours were not
available for comparison.

3.3 Numerical Methods of Forecasting the Pressure Field

Numerical methods show great promise in forecasting both medium- and large-
scale features of the pressure field. Improvements in numerical accuracy
will occur as theoretical meteorologists make further progress in under-
standing the atmosphere and as better data are obtained. Numerical methods
now in use by the National Meteorological Center and methods under develop-
ment are discussed in this section.

3.31 Models Used by the National Meteorological Center

The US Weather Bureau has used numerical forecasting methods on an opera-
tional basis for 14 years. At the present time, a six-layer primitive
equation model is used for periods up to 48 hours, and a barotropic model
is then used from 48 to 144 hours (Andrews, 1970). The six-layer model
(Shuman and Hovermale, 1968) became operational in June 1966. Input data
is geopotential height and temperature from the 10 mandatory levels from
1000 to 100 mb (1000, 850, 700, 500, 400, 300, 250, 200, 150, and 100 mb).
The model is theoretically capable of forecasting the pressure field in
detail; both short and long waves are indicated. Examples of 24- and 120-
hour forecasts from the six-level model are shown in Figs. 2 and 3 together
with their verifications.
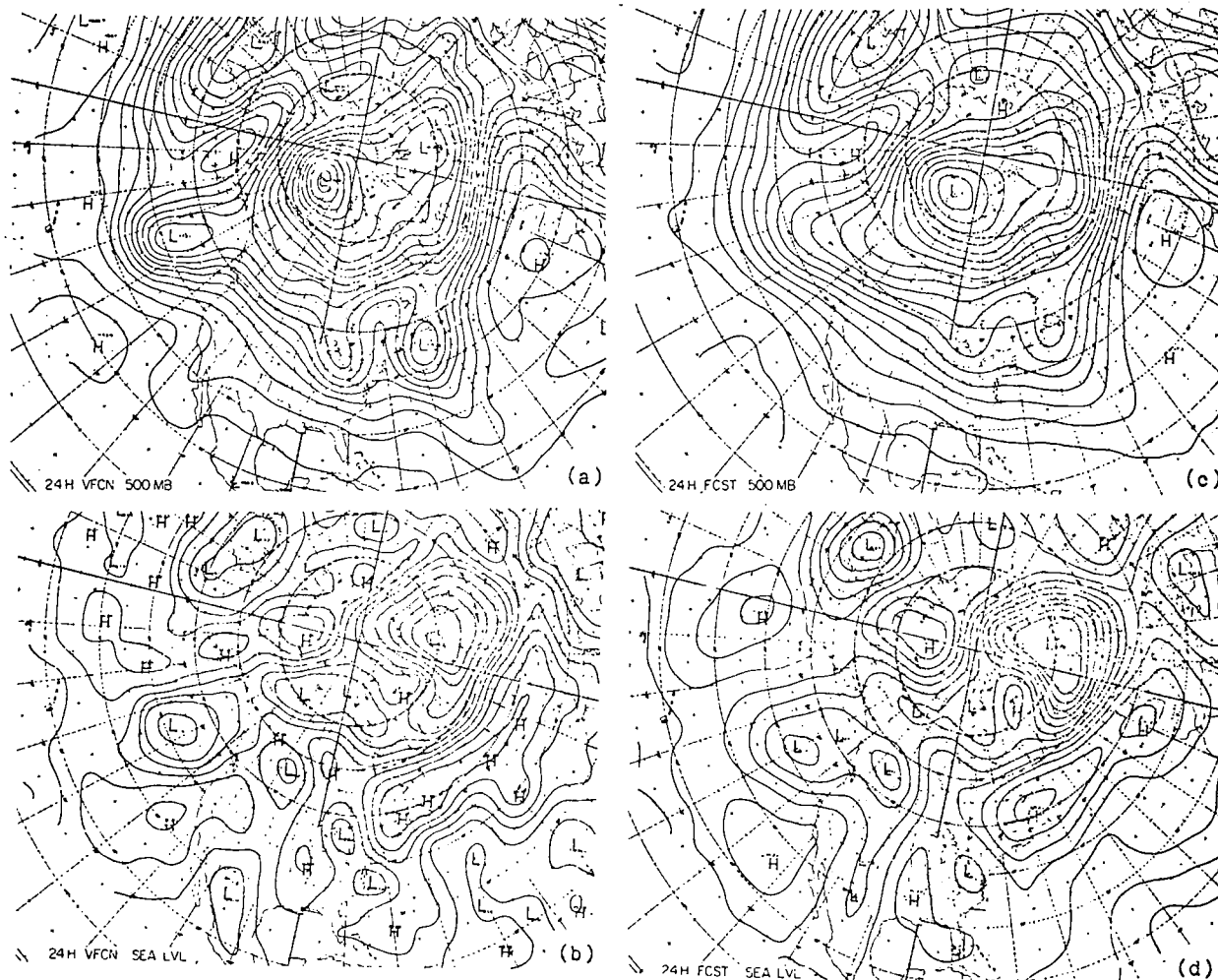
Fig. 2. Twenty-four hours after initial time: a. 500 mb observed, b. sea level observed, c. 500 mb predicted, d. sea level predicted. The predicted charts are "raw" primitive equation product, unmodified by human analysts. (after Shuman and Hovermale, 1968)

(a) 120H VFCN 500 MB

(b) 120H VFCN SEA LVL

(c) 120H FCST 500 MB

(d) 120H FCST SEA LVL
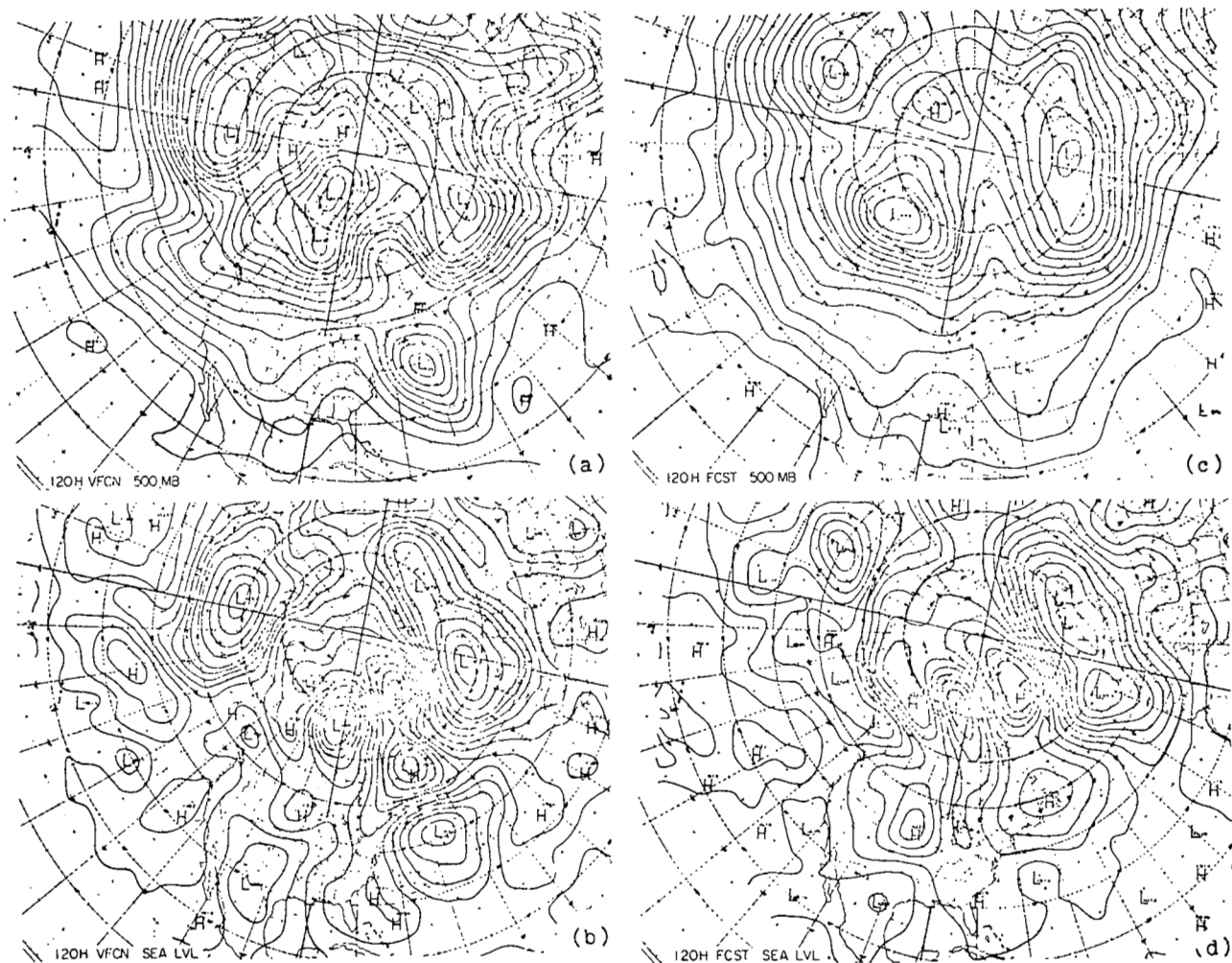
Fig. 3. One hundred and twenty hours (five days) after initial time.
a. 500 mb observed, b. sea level observed, c. 500 mb predicted,
d. sea level predicted. The predicted charts are "raw" primitive
equation product, unmodified by human analysts. (after Shuman and
Hovermale, 1968)

The forecast and verification charts are similar for the 24-hour forecast although results at 500 mb are superior to those obtained at sea level. The locations and intensities of the various systems are accurately forecast. The forecast accuracies decrease rapidly with time so that results of the 120-hour forecast are poor. There is still a good resemblance, however, between the numerical product and the verification chart, especially at 500 mb.

Table 1 gives S-1 scores[1] (Teweles and Wobus, 1954) for the six-layer

Table 1. S-1 Scores for six-layer primitive
equation model introduced 6 June 1966.

Month	A&FD sea level 30-hr	NWP 500-mb 36-hr	Barotropic 36-hr
June 1966	58.6	44.5	50.2
July 1966	56.9-Tied July	44.5	48.5
August 1966	55.7-Record month	49.0	52.5
September 1966	55.6-Record month	44.0	46.1
October 1966	56.0-Tied October	43.5	52.0
November 1966	55.3-Record month	39.8-Record month	47.8
December 1966	53.8-Record month	43.2	56.5
January 1967	56.5-Tied January	40.2-Tied January	48.4
February 1967	53.0-Record February	38.8-Record month	43.5
March 1967	55.6-Record March	36.0-Record month	43.8
April 1967	52.6-Record month	42.1	48.5
May 1967	55.0-Record May	41.2-Record May	45.7
June 1967	54.6-Record June	39.1-Record June	45.5
July 1967	54.9-Record July	40.8-Record July	44.0
August 1967	51.7-Record month	41.1-Record August	43.7

(after Shuman and Hovermale, 1968)

model compared to the older barotropic model. As shown by the table, the Analysis and Forecast Division's (A&FD) 30-hr surface prognosis (the raw computer output was modified manually) consistently broke or tied previous 20-year forecast records. A good record was also established by 36-hr 500-mb prognosis when compared to the older barotropic model. The superiority of the six-layer model is also demonstrated in Figs. 4 and 5 where it is compared to older numerical models and to pre-numerical methods. Figure 6 compares the six-layer model to other forecasting models. The numerical method was superior to the subjective method until about the fifty day, but subjective modifications to the output increased the skill at each forecast time.

---

[1]S-1 scores are a type of skill score where 0 is a perfect forecast and 200 is the worst possible forecast. A score of 20, however, is usually considered to be virtually perfect and 70 is considered to be worthless (Shuman and Hovermale, 1968).

AVERAGE   36 HR.   500 MB S_1 (NORTH AMERICA)
A OCT.-MAY.   PRE-NWP.   1955-1958
B OCT.-MAY.   BAROTROPIC   1965-1966
C OCT.-MAY.   3 LEVEL   1965-1966
D OCT.-MAY.   BAROTROPIC   1966-1967
E OCT.-MAY.   6 LAYER   1966-1967
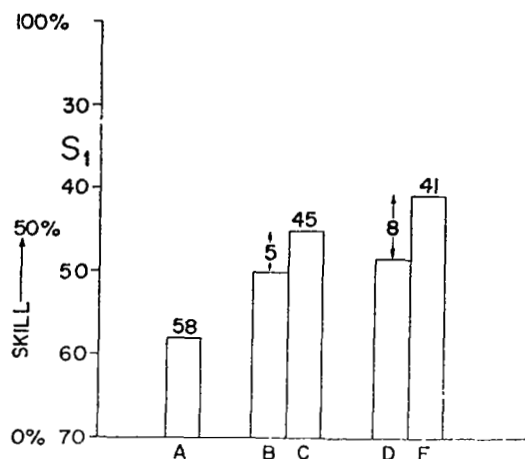
Fig. 4. S-1 scores for 500-mb 36-hr predictions. Bars B, C, D, and E show that the new six-layer model gains eight S-1 points over the barotropic, whereas the previous operational model gains only five. Also shown (bar A) for the same eight months is the S-1 average for the three years immediately prior to the introduction of operational numerical weather prediction. (after Shuman and Hovermale, 1968)

AVERAGE S_1 30HR SURFACE PROG
A 1947-1958   PRE-NWP.
B 1959-MAY 1966   3 LVL. AND
                       BAROTROPIC GUIDANCE
C JUNE 1966-AUG. 1967 6 LYR. GUIDANCE

AVERAGE S_1 48HR SURFACE PROG
D JULY 1964-MAY 1966   3 LVL. GUIDANCE
E JUNE 1966-AUG. 1967 6 LYR. GUIDANCE

Fig. 5. S-1 scores show a long term trend in increase of prediction accuracy at sea level. Comparison of bars B and C show the impact of the new six-layer operational model on quality. The scores shown are for manual charts, but in the case of bar C, they are usually mere modifications of the six-layer guidance, which by itself scores 61 S-1 points by coincidence the same as bar B. (after Shuman and Hovermale, 1968)

A-10

DAILY PRESSURE
MAP CORRELATIONS
(Standardized Departures)
NORTH AMERICA

14 cases to 96 hours
12 cases to 120 hours
6 cases to 144 hours

Fig. 6. Comparative correlations R between forecast and observed sea level pressure over North America. "Subjective I" were forecasts made by experienced forecaster in the Extended Forecast Division with essentially the same materials which are now available to them under operational conditions. After they made these forecasts, the automatic predictions from six-layer primitive equation model were made available to them, and they then modified their forecasts to produce those whose scores are shown as "Subjective II." (after Shuman and Hovermale, 1968)

Although this model is an improvement over older models, there are still certain systematic geographical and seasonal errors in the forecast. Leary (1971) has observed systematic errors in 36-hour sea level prognosis. He noted that the model does not forecast storms deep enough over the oceans but that storms forming on the lee slopes of the Rocky Mountains were forecast too deep and too soon. Most observed storms were found to fill more slowly and deepen more rapidly than the model predicted. Rapidly intensifying cyclones had a tendency to move to the left of the forecast track. Andrews (1970) studied 500-mb errors in the operational model of the National Meteorological Center. The model (barotropic after 48 hours) consistently underforecast the amplitude of most troughs and ridges. The error patterns were established by 48 hours and increased in magnitude with time until the end of the forecast run (144 hours). The errors varied according to the normal seasonal circulation. These errors will no doubt decrease in the future.

3.32 The Nine-Level Model

A "high resolution, nine-level, hemispheric, moist general circulation model" was under development at the Geophysical Fluid Dynamics Laboratory of ESSA in

1969 (Miyokoda et al., 1969). This model requires 10 hours of computing time on a UNIVAC 1108 computer, plus an extra hour for checking, for each day of prediction. The model has been used for two winter cases with rather good results. The correlation coefficient between the observed and computed heights for the 1000-, 500-, and 50-mb levels above 20°N are shown in Fig. 7.
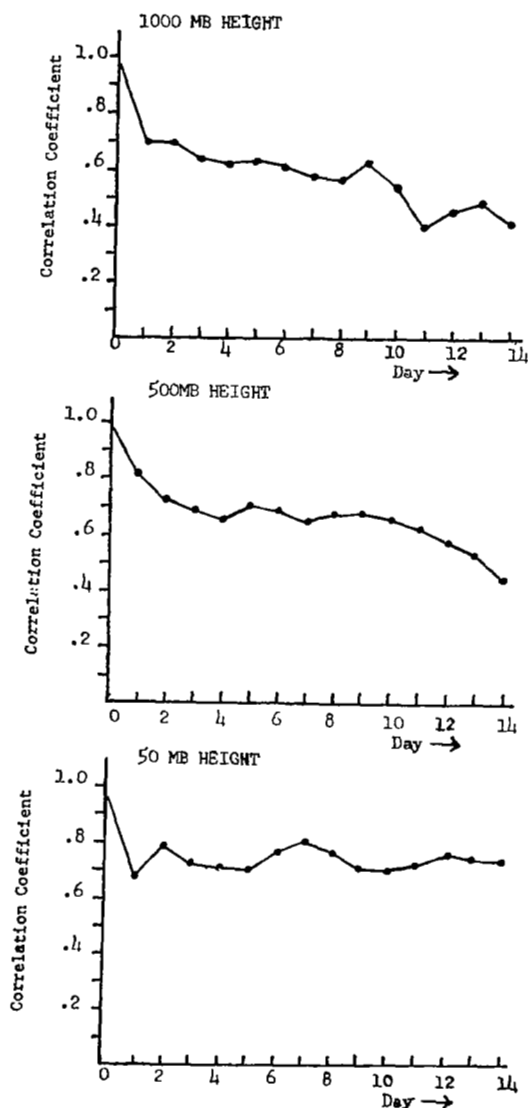
Fig. 7. Correlation coefficient between the observed and the forecast pattern of the change in geopotential height from the initial time for the domain north of 20°N. (after Miyakoda et al., 1969)

The correlation coefficient varied from 0.7 at day 1 to 0.45 at day 14 at the 1000-mb level. The coefficient varied from 0.8 at day 1 to 0.5 at day 14 at the 500-mb level; at 50 mb, it remained at about 0.75 from day 1 through day 14. Smagorinsky (1969) states that "the 1000-mb flow already began to verify rather poorly by 7 days and was virtually randomly related to reality at 10. At 500 mb, the situation is somewhat better. The forecast could be classed as poor at 9 or 10 days, and is more or less random by 13 days." It was still possible to find a one-to-one correspondence between observed and predicted cyclones out to 14 days, and the model was able to forecast the birth of second- and even third-generation cyclones and their subsequent behavior. Speed of the moving troughs was well forecast; by day 14, the error was only 10-15 degrees longitude. Faster computers, better input data, and better techniques will improve results in the future.

4. Forecasts of Wind

Forecasts of wind speed and direction are related directly to forecasts of the pressure field since winds and pressures are related through the geostrophic and gradient wind equations. If one is able to forecast pressures accurately, the wind also may be forecast with reasonable accuracy. Some work has been done toward developing multiple regression equations for short range forecasts of wind. For example, Russo et al. (1964) used a screening method of multiple regression to forecast the u and v wind components for 2, 3, 5, and 7 hours. They found that errors could be reduced by about one third over subjective methods for 3-, 5-, and 7-hour predictions. At 7 hours their method gave a skill score[2] of 0.399 compared to 0.249 for subjective methods.

An example of errors in 36-hour forecasts of wind from a numerical model is given in Table 2 (Fawcett, 1969) for the six-layer model of Shuman and Hovermale (1968). The forecast root-mean-square vector (rmsv) geostrophic wind at 300 mb is compared with the observed rmsv 300 mb geostrophic wind for two months. Table 2 indicates that the six-layer model underforecasts the mean west wind component. An example of 24-hr vector wind errors in

---

[2]Skill scores are designed to give a measure of forecast accuracy with the effects of chance removed. They are positive for forecasts better than chance and negative for forecasts worse than chance. A skill of 1.00 is the best possible. See the introduction for a further explanation of skill scores.

Table 2. Observed and forecast geostrophic winds for September and October 1968.

	RMSV geos.fcst.	RMSV geos.obsvd.	Percent difference (fcst.-obsvd.)
Sept. 1968------------	30.3 kt	31.8 kt	-5
Oct. 1968------------	34.8 kt	37.0 kt	-11

(after Fawcett, 1969)

Table 3. RMS vector wind error over the North Atlantic and Western Europe.

	In meters per second Type of Forecast		
Surface, mb	JNWP	Subjective	Persistence
700	7.69	8.44	10.80
300	14.4	16.6	22.4

(after Thompson, 1961)

Table 4. RMS vector wind error over Northwest Europe.

	In meters per second Type of Forecast		
Surface, mb	JNWP	Subjective	Persistence
700	6.9	7.7	11.3
300	11.8	15.6	23.7

(after Thompson, 1961)

October and November, 1958, is given in Tables 3 and 4 for several different types of forecasts. The superiority of the numerical forecasts is quite noticeable, and these forecasts were made with an older 2-level model (Thompson, 1961). The forecast errors increase rapidly with height.

Wind errors for official forecasts during the winter of 1966-67 averaged 10.8 knots at 20,000 ft (500 mb), and 9.8 knots at 5000 ft (850 mb) (Roberts and Proter, 1967).

A-14

5. Forecasts of Moisture-Related Parameters

Forecasts of moisture (rain, snow, etc.) is of great interest to the public because of restrictions to outdoor activities. It is of even greater interest to the aviation industry since such phenomena as fog, clouds, and precipitation can seriously hamper aircraft operations. This section will examine the methods and accuracies of forecasts of clouds and precipitation.

5.1 Forecasts of Fog

Fog forecasts are usually of short range; they are rarely more accurate than climatology forecasts for periods greater than 24 hours. Many subjective methods such as advection and temperature changes can be used to forecast fog, but these will not be discussed. Local objective methods also have been derived, and some of these have shown improvements over subjective and persistence methods. Gringorten (1949) developed an objective method to forecast fog for Randolph Field, Texas, that produced a forecast 13½ hours ahead of the beginning of a 6-hr period of interest. Skill scores based on whether conditions would be serious enough to close the airport showed improvement over the local subjective and persistence forecasts during the winter of 1947-48. The skill scores were:

Objective method:	0.44
Local station subjective methods:	0.14
8-year persistence:	0.18

Hoover (1950) forecast radiation fog at Elkins, West Virginia, on the following night from data of the preceding evening using an objective technique. His method was accurate 89% of the time for a fog or no-fog forecast compared to 69% accuracy of official airways forecasts.

5.2 Forecasts of Ceiling

Forecasts of ceilings, especially for low ceilings, are quite important to the aviation industry, but like fog and visibility forecasts, good results have been obtained only for short time periods. Brown and Tillotson (1957) devised an objective technique for forecasting ceilings below 5000 ft for Denver; they produced forecasts for two 6-hr time periods. The forecast was made 6 hours before the beginning of each 6-hr period. For one time period, they obtained a skill score of 0.84 while a persistence forecast would have scored 0.71. The technique produced a skill score of

0.73 for the second time period while a persistence forecast would have scored 0.58. The Techniques Development Laboratory has developed an automated statistical approach which forecasts ceiling heights in five categories from less than 100 ft to more than 3000 ft (Klein, 1970). Verifications of forecasts given in percent improvement over climatology, is given in Table 5. An improvement of about 45% over climatology was obtained for 2-hour forecasts, but little improvement over climatology was obtained for 7-hour forecasts.

Table 5. Comparative verification of *probability forecasts of ceiling and* visibility made by equations based on a network of stations and equations derived from local data alone (single-station equations).

Ceiling		% Improvement over climatology	
		Network	Single-station
ALB	2-hour	41%	41%
	3-hour	35	33
JFK	2-hour	48	45
	3-hour	42	36
	5-hour	33	29
	7-hour	29	23
ORD	2-hour	52	47
	3-hour	43	38
	5-hour	36	30
	7-hour	33	24
Visibility			
ALB	2-hour	34	37
	3-hour	27	28
JFK	2-hour	38	35
	3-hour	30	27
	5-hour	22	19
	7-hour	16	14
ORD	2-hour	37	31
	3-hour	29	24
	5-hour	21	19
	7-hour	17	14

(after Klein, 1970)

5.3 Forecasts of Visibility

Forecasts of visibility are closely related to fog forecasts since fog is a major cause of serious reductions invisibility. Heavy rain is

another cause of visibility reduction that will be treated in more detail later. The Techniques Development Laboratory of NOAA is presently conducting research into short-range statistical forecasting of visibility (Klein, 1970). Multiple regression equations are used on an automated basis to compute probabilities of having visibilities in 5 categories from less than three eighths of a mile to greater than five miles. One technique uses only local data (single station method), and a second method uses data from surrounding stations as well (network method). The bottom half of Table 5 shows the improvement over climatology by use of single station and network methods at Albany (ALB), New York City (JFK), and Chicago (ORD). Accuracy improvement over climatology were about 35% for a 2-hour forecast, but values at 7 hours were reduced to about 17% at two of the three stations. The visibility forecast, like the fog forecast, is of a very short-range nature.

5.4 Forecasts of Clouds

Most interest in forecasts of clouds centers around the formation of low clouds which will hamper aviation activity. Handy (1950) used graphical correlation methods to predict winter-time stratus at Kansas City 4 hours ahead of an 8 hour morning period. His method gave a skill score of 0.35 and accuracy of 78.4%[3]. Jenrette (1959), using a somewhat similar technique, forecasted summer stratus at Bryan, Texas, 12 hours ahead of time and obtained 80% accuracy. Gerrity (1967) used a physical-numerical model to produce 12-hr forecasts of low clouds in the Eastern U.S. He found that he could improve the accuracy of low-cloud predictions in regions of dense data.

Work has been done on the forecasting of higher clouds and for periods greater than 12 hours. Chisholm et al. (1965) used Regression-Estimation-of-Event-Probabilities (REEP) equations to forecast the amounts of total, low, middle, and high clouds for 12, 24, 36, and 48 hours in advance. They obtained better results from their method than from persistence for each cloud height and for each forecast interval.

---

[3]See the introduction for an explanation of these scores.

Each of the numerical and some of the objective methods for forecasts of precipitation attempt to forecast clouds. These methods usually derive quantities which indicate the presence of precipitation-causing processes. Certain values of these quantities are required for the occurrence of precipitation. Lower values are set which should indicate clouds without precipitation. Information concerning the skill of the cloud forecast aspect of numerical forecasting could not be located, but the skills of the precipitation techniques will be examined in the appropriate sections of this report.

5.5 Forecasts of Precipitation

5.51 Rainfall

5.511 Objective Methods

Besides subjective methods of making forecasts of rain, there are numerous objective methods. Most of these methods are for individual stations and for particular seasons. While poor results have been obtained on some studies when compared to official forecasts, other studies have yielded good results. Several examples are given here.

Beebe (1950) devised a method for forecasting winter precipitation at Atlanta through the use of scatter diagrams. He combined such variables as moisture and temperature advection, and flow patterns from the 850- and 700-mb charts to make a forecast 6 hours ahead of a 24-hour period. The objective method gave better results than official forecast during two winter cases as shown in Table 6.

Table 6. A comparison of official and objective methods of precipitation forecasting at Alanta. (after Beebe, 1950)

Winter 1947-1948		
Official Forecast	76% correct	0.49 skill
Objective Forecast	94% correct	0.89 skill
Winter 1948-1949		
Official Forecast	78% correct	0.50 skill
Objective Forecast	84% correct	0.68 skill

Williams (1950) used an objective method at Salt Lake City to fore-
cast summer precipitation 6 hours ahead of an 18-hour forecast period.
He obtained 85% accuracy with a skill score of 0.45; the official fore-
casts had 89% accuracy with a skill of 0.55. Schmidt (1952) used flow
patterns, and moisture and temperature variables at several levels to
forecast precipitation during May at Washington, D.C. His objective
method produced 89.7% accuracy while official forecasts yielded an ac-
curacy of 83.3%. Schmidt also derived objective methods for Washington,
D.C. for other seasons (Schmidt, 1951a, and b).

Objective techniques also have been devised for estimating rainfall
totals in specific localities. Thompson (1950) developed a method of
graphical integration of selected variables for estimating winter rain-
fall at Los Angeles. The forecast was prepared 6 hours ahead of a 30-
hour forecast period and predicted rainfall in five categories from no
rain to over 1.50 inches. A slight improvement was obtained over of-
ficial forecasts, but it was not considered significant. One test case
gave an objective skill score of 0.47 compared to the official forecast
skill score of 0.35. Rapp (1949) forecast precipitation amounts 6½ hours
ahead of a 14-hour period in Washington, D.C. He used 4 categories ranging
from no rain to over 0.30 inches and obtained 75% accuracy and a skill
score of 0.49 during the winter of 1945-46.

5.512 Current Accuracies

Older forecasting techniques were primarily subjective or objective,
however, newer methods tend to be more numerical in nature. Before dis-
cussing numerical methods, it would be well to see the current accuracy
of precipitation forecasts. Figure 8 shows that short-range forecast
accuracies have been steadily improving (Roberts and Porter, 1967). The
12- to 24-hour precipitation forecasts are about 85% correct, and the
24- to 36-hour precipitation forecasts are about 82% correct.

5.513 Numerical Methods

The Techniques Development Laboratory is investigating numerical preci-
pitation forecasts which are not direct products of the hemispherical
numerical models. Klein, Crockett, and Andrews (1965) found a relation
between 700-mb heights and clouds, and precipitation at 40 stations in
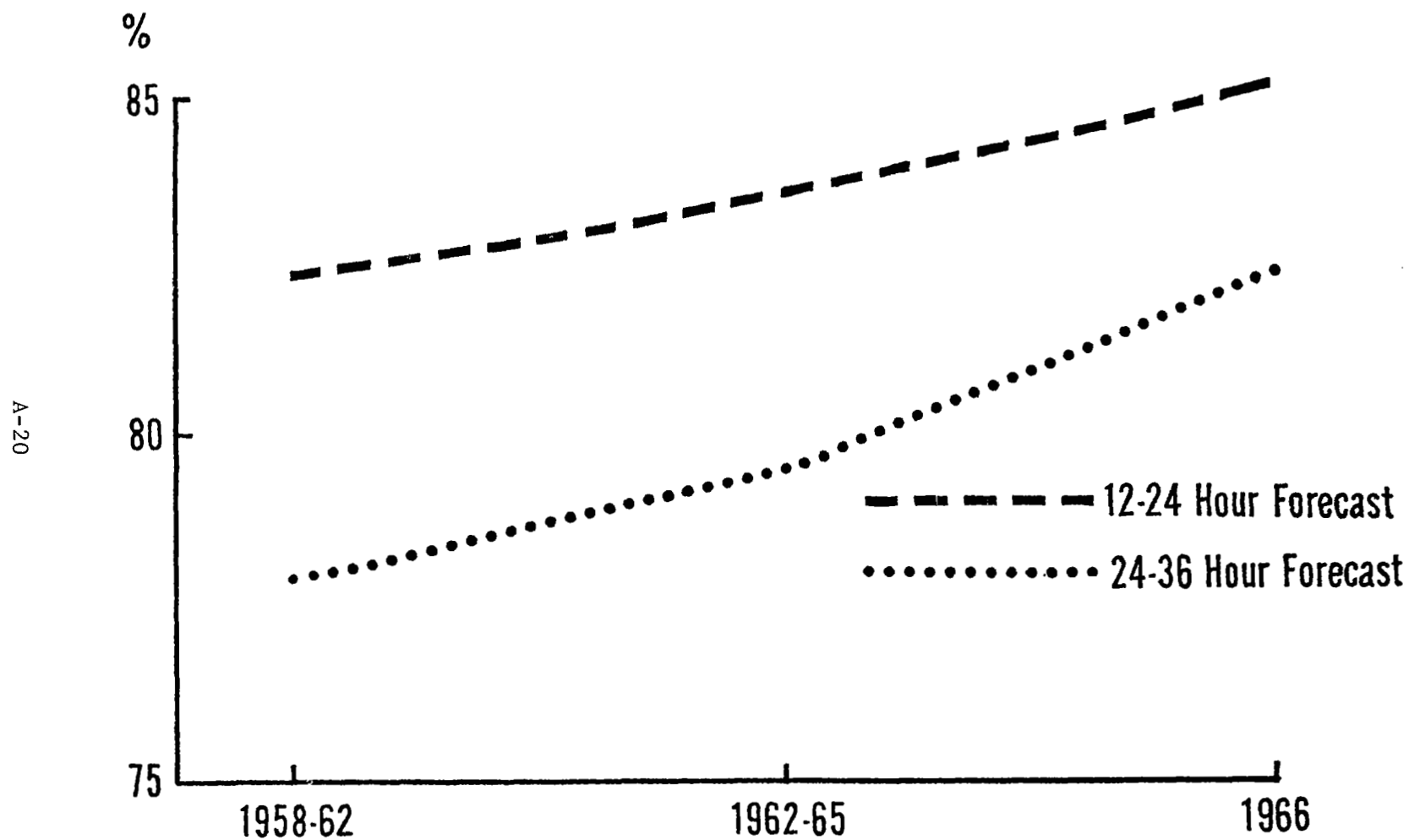the United States. By using the screening method of multiple regression,

Fig. 8. Percentage correct of local precipitation and no precipitation forecasts 1958-1966 (250 Stations). (after Roberts and Porter, 1967).

they could explain an average of 36% of the variance of clouds and precipitation at a single station through the use of five 700-mb heights. The 36-hour baroclinic prognoses made by the National Meteorological Center were then used in conjunction with their multiple regression equations to make rainfall forecasts. These objective forecasts were consistently better than persistence, but they were not as good as subjective forecasts made by experienced forecasters. Further work is being done in expanding the technique. Other promising work includes 12-hour probability of precipitation forecasts along the East Coast through the use of a subsynoptic advection model (Klein, 1970).

The six-layer primitive equation model used by the National Weather Service has been programmed to predict rainfall amounts (Shuman and Hovermale, 1968); examples of 1-, 2-, and 5-day precipitation forecasts and verifications are given in Figure 9. Results at 24 hours were good but both precipitation areas and amounts were forecast less accurately as the time period increased. There was little relation between the observed and forecast precipitation areas at 120 hours. Changes have been introduced into the model since 1968 so that while it used to overpredict the frequency of occurrences of precipitation (1967-1968), it now underpredicts precipitation occurrences (Spar, 1969). Spar interpolated between the hourly grid-point predictions to give precipitation forecasts at specific stations in the eastern United States. He noted that the onset time of the "first measureable precipitation" during the winter of 1968-69 was too late by an average of one hour within a 30-hour period which began 6 hours after data time. The mean of the absolute error was 6.3 hours in the same time period. Results for the winter of 1969-70 indicated that the method predicted precipitation too infrequently and too late (Spar, 1971).

The nine-level model of the Geophysical Fluid Dynamics Laboratory of NOAA has been used to make precipitation forecasts. Figure 10 shows that the humidity error in the model is below that of persistence for periods up to eight or nine days, but vertical motion and stability must be considered also in precipitation forecasting. The average skill of the precipitation forecast (rain or no rain), Fig. 11, shows that the model scored better than persistence until about the ninth day. Any

12-24 hr after initial time

36-48 hr after initial time

108-120 hr after initial time
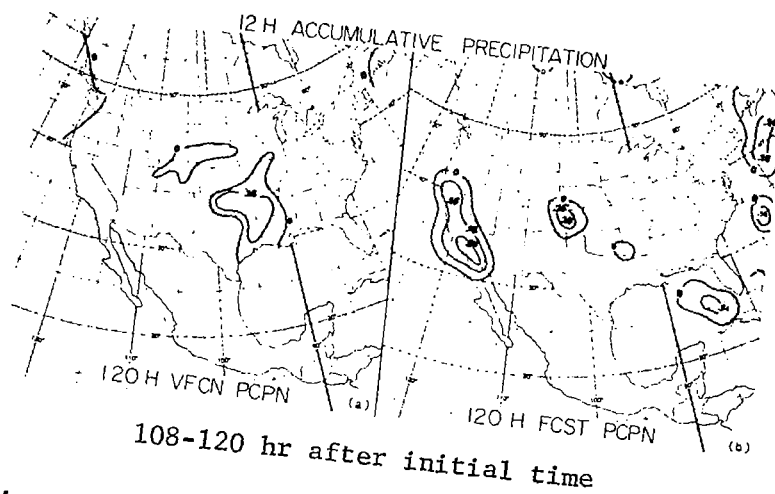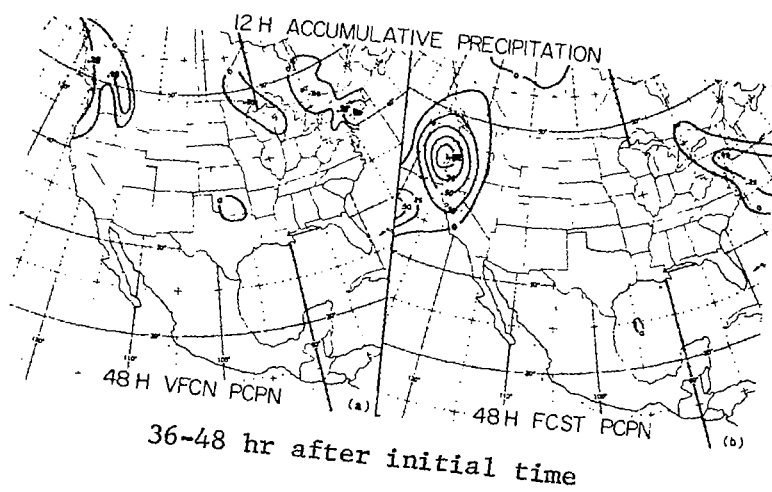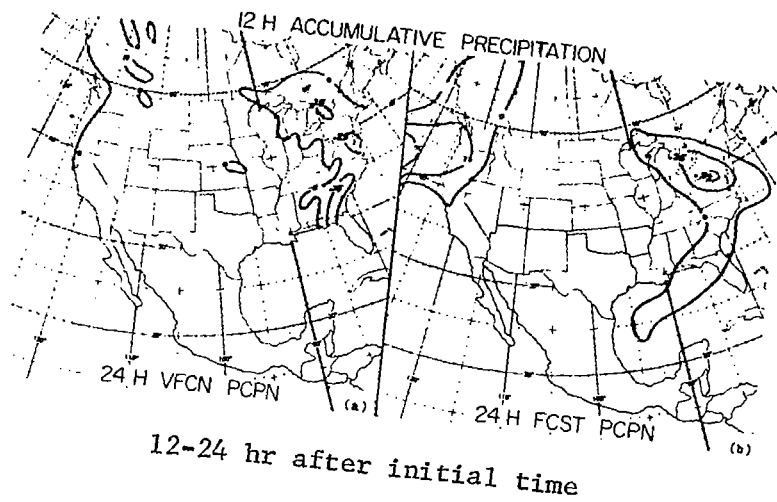
Fig. 9. Accumulation of precipitation for various time periods after initial time. (a. observed, b. predicted) (after Shuman and Hovermale, 1968)
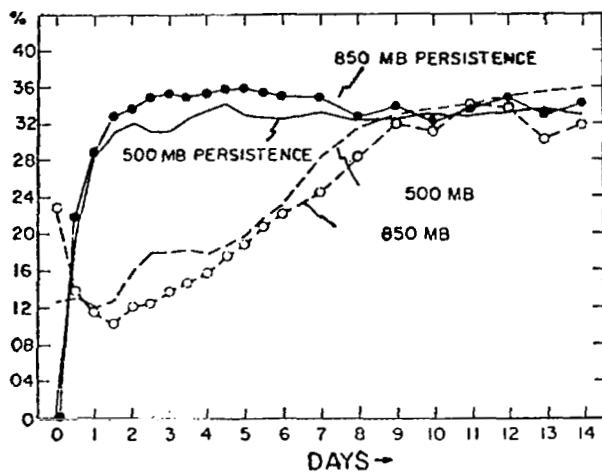
Fig. 10. Standard deviation of the humidity "error" at 850 mb and 500 mb (dashed curves). The corresponding persistence forecast errors (solid lines) are shown as a reference for the natural variability.
(after Smagorinsky, 1969)

AVERAGE SKILL OF PRECIPITATION FORECAST
53J AND 61J
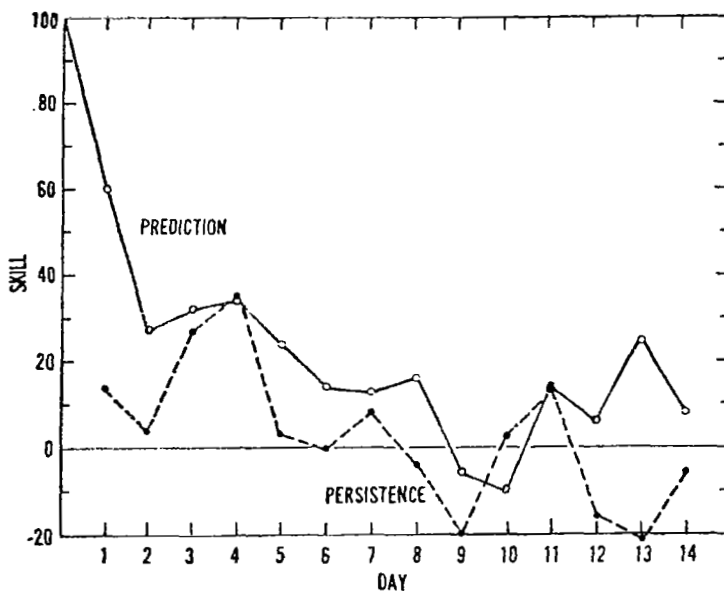
Fig. 11. Skill score for each day for the precipitation forecast for the United States and part of Canada. The average is shown for the 1964 and 1966 cases. (Solid line) forecast and (dashed line) persistence.
(after D. L. Gilman, 1968)

rainfall amount less than 0.10 inch was considered as a no-rain case; the graph is the average of two forecast runs of 14 days each. Some examples of precipitation areas forecast by the nine-level model are shown in Figs. 12 and 13. Good results are indicated on the first and second days, but heavy rain, which did not occur, was forecast along the west coast on the third and fourth days. Some improvement along the west coast is shown on the fifth and sixth days, but subsequent agreement of the forecast areas with the observed areas is slight.

5.52 Snow

Even if the forecaster knows that precipitation will occur, he must decide if it will be in liquid or solid form. Objective aids for selected cities have been derived to help answer this question. Pandolfo (1957) obtained 95% accuracy (0.80 skill) in deciding between rain or snow or sleet for New York City. He made his forecast 6 hours before the beginning of a 14-hour period, and used such parameters as surface temperature, freezing level, and temperature advection at 850 mb. Laird and Dickey (1953) used 700-mb parameters to decide if there would be rain or snow at Denver.

The areas where snowfall should be expected when covered by a cyclone have been determined. Younkin (1968) found that snowfall in the western United States usually occurred ahead of maximum vorticity values at 500 mb. Heavy snowfall in the central and eastern United States was found to lie ahead and slightly to the left of the position of the storm at 850 mb (Browne and Younkin, 1970). Spar (1969) found a relation between rain and snow and the predicted boundary layer potential temperatures. He indicated that this relation would be useful in numerical snow forecasting, but recent results indicate that the quality of the snow forecasts was not good enough for accurate local prediction (Spar, 1971).

5.53 Severe Weather

Convective activity including showers, thunderstorms, and tornadoes is difficult to forecast. Meteorologists can locate relatively large areas where such activity is likely to occur, but they cannot pinpoint the exact locations of the storms. Many types of subjective methods and objective aids are used in this work. Various types of stability indices are especially important. Work is presently being done in using data

OBSERVED, DAYS. 1st and 2d

1st and 2d, DAY FORECAST. EXP. 3

OBSERVED, DAYS. 3d and 4th

3d and 4th, DAY FORECAST. EXP. 3

OBSERVED, DAYS. 5th and 6th

5th and 6th, DAY FORECAST. EXP. 3

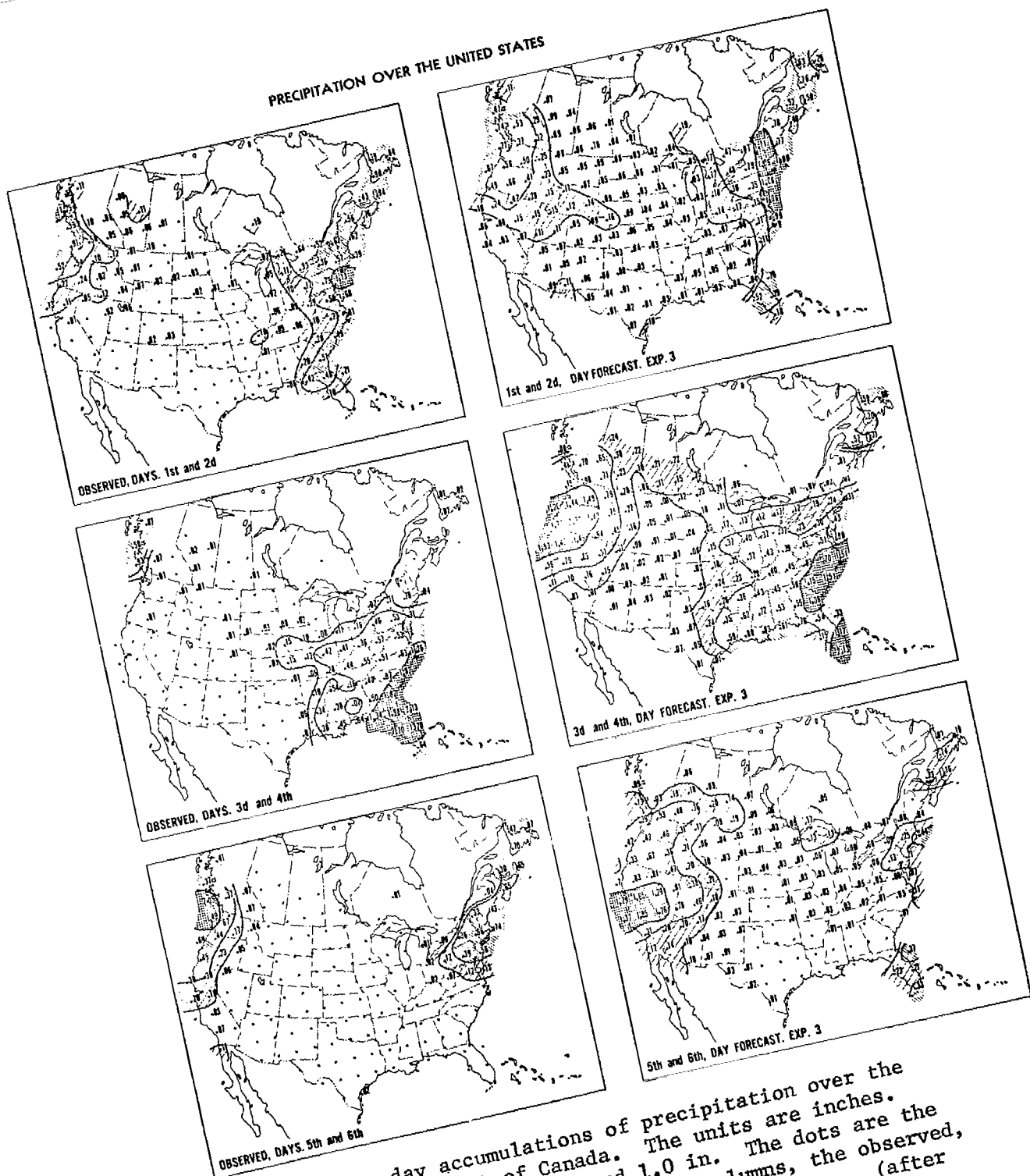Fig. 12. Two-day accumulations of precipitation over the
United States and part of Canada. The units are inches.
The contours are at 0.1, 0.3, and 1.0 in. The dots are the
points used for computation. Left columns, the observed,
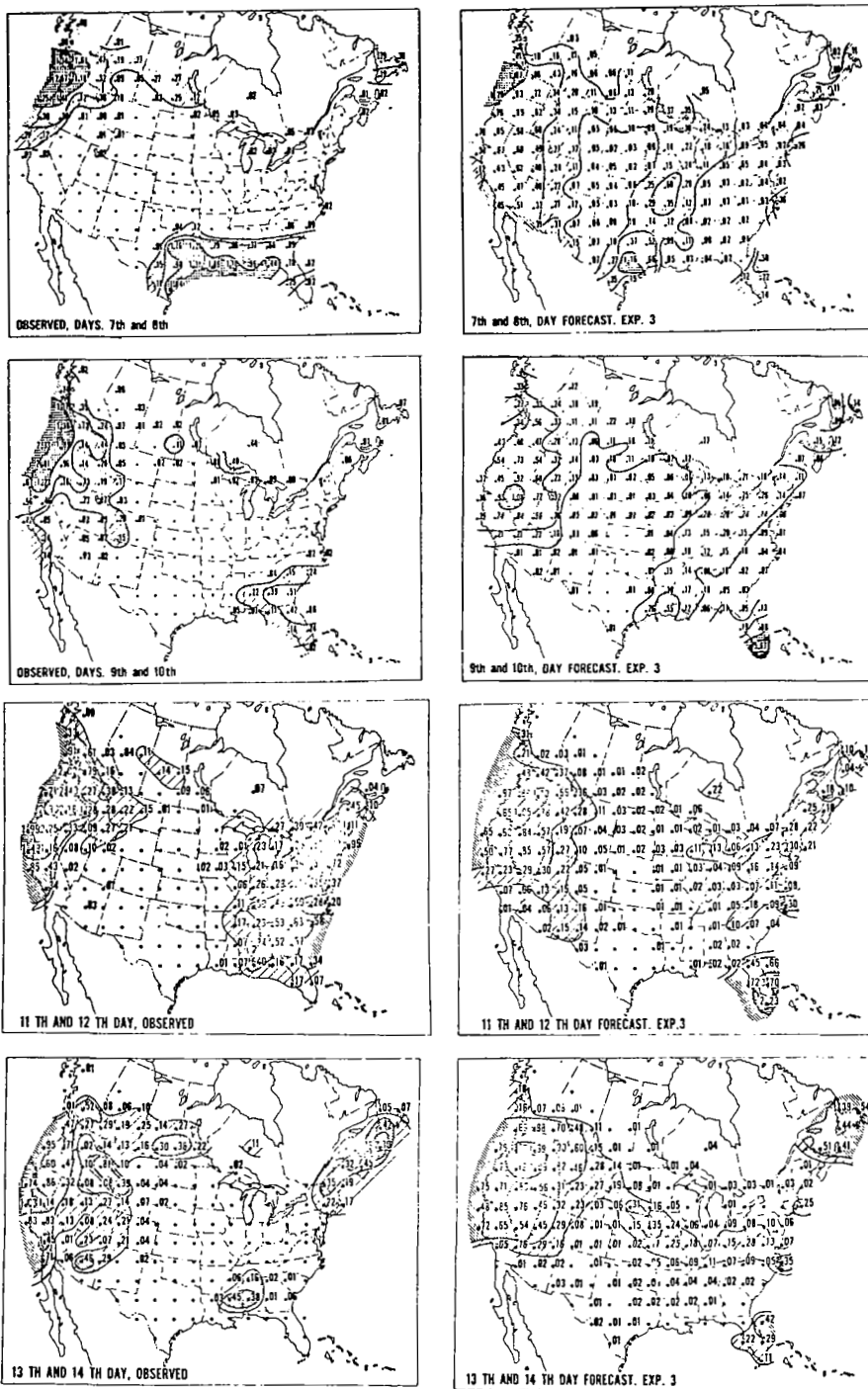Experiment 3, for the 1964 case. (after

Fig. 13. Two-day accumulations of precipitation over the United States and part of Canada. The units are inches. (after Miyakoda et al., 1969)

A-26

from numerical models to locate potential severe weather areas. Temperature and moisture output from these models can be used to compute stability indices and to locate suspicious regions, but the output is usually not of sufficient quality after only a short period. The Techniques Development Laboratory is computing backward air trajectories from prognostic wind components generated by the primitive equation model to aid in severe weather forecasting (Klein, 1970). Forecasts of temperatures and dew points obtained through the use of air trajectories have been better than or equal to corresponding forecasts by the primitive equation model. Further research in this area is presently being conducted.

6. Forecasts of Temperature

Temperatures are frequently forecast by such methods as advection and air mass movement. Objective aids for forecasting surface temperature also have been developed. Gilbert (1953) developed a method for forecasting minimum temperatures for the following 12-24 hours by using variables such as sea-level pressures and pressure changes, and temperatures at 700 mb and at the surface. Both the objective method and the official forecast had an average error of about 5°F.

Another method of temperature forecasting involves the screening method of multiple regression analysis. This method was first used to predict 5-day mean surface temperature from prior anomalies of 700-mb height and surface temperature (Klein et al., 1960). Prediction equations were derived for 39 cities for three seasons. For each city and season, the computer would scan the temperature and height fields and then select as many as seven predictors for use in the equation. The 5-day averages of observed and predicted heights and temperatures were used with these equations to make the 5-day mean temperature forecasts. Modifications were then made to give mean, maximum, and minimum temperature forecasts from one to three days in advance using basically the same method as before except for the use of daily instead of mean input (Klein, 1966). Further changes gave maximum and minimum temperature readings from 12-60 hours in advance using equations derived for 2-month periods (Klein et al., 1967). Possible variables were expanded to include extreme surface temperature values, 700-mb heights, 700-1000-mb thickness, and the day of the month. For forecasts past 12 hours, numerical prognostic heights were used as input. Further program changes also were made in

1968 (Klein and Lewis, 1970). Mean absolute temperature errors are given
in Table 7 for the objective method, the persistence method, and for a

Table 7. Mean absolute error of maximum and minimum temperature forecasts
(°F) during 18 months at 60 cities in the United States for objective (Obj),
subjective (A&FD), and persistence (Pers) predictions. The ratio of sub-
jective to objective errors is also given. (after Klein and Lewis, 1970)

	Spring Mar.-May 1968	Summer June-Aug. 1968	Fall Sept.-Nov. 1968	Winter Dec.1968- Feb.1969	Spring Mar.-May 1969	Summer June-Aug. 1969	Mean
			24-hr projection				
Obj	4.5	3.3	4.0	5.3	5.0	3.2	4.2
A&FD	4.1	3.0	3.6	4.5	3.8	2.9	3.7
Pers	6.3	4.3	5.6	7.2	5.9	4.0	5.5
A&FD/Obj	0.93	0.90	0.92	0.86	0.90	0.90	0.90
			36-hr projection				
Obj	5.2	3.8	4.6	6.1	4.9	3.6	4.7
A&FD	4.8	3.6	4.2	5.3	4.6	3.5	4.3
Pers	8.7	5.7	7.5	9.7	8.0	5.3	7.5
A&FD/Obj	0.94	0.95	0.93	0.87	0.94	0.95	0.93
			48-hr projection				
Obj	5.7	4.2	4.9	6.7	5.4	4.0	5.2
A&FD	5.3	3.9	4.6	5.9	4.9	3.8	4.7
Pers	8.7	3.7	7.5	9.7	8.0	5.3	7.5
A&FD/Obj	0.93	0.93	0.94	0.89	0.92	0.95	0.93
			60-hr projection				
Obj	6.3	4.4	5.3	7.5	5.9	4.2	5.6
A&FD	6.0	4.3	5.0	6.7	5.5	4.1	5.3
Pers	9.8	6.1	8.3	10.5	8.6	5.9	8.2
A&FD	0.95	0.95	0.91	0.89	0.93	0.97	0.94

subjective method with objective guidance. The latter method is used by
the National Meteorological Center and has mean absolute errors of 3.7°F
for 24-hour forecasts, and 5.3°F for 60-hour forecasts. The objective
method was better than persistence but not as good as the subjective method
which used the objective material as an aid. The objective method produced
mean absolute errors of 42°F at 24 hours, and 5.6°F at 60 hours. Forecasts
of this nature are now prepared operationally for 131 stations in the
United States, and a computer program is being written to use data from

the six-layer model instead of the barotropic model in order to improve the results (Klein, 1970).

Temperature data is also a direct by-product of the numerical models. An example of average errors in temperature as a function of altitude for the 9-level model is given in Fig. 14. Temperatures were consistently
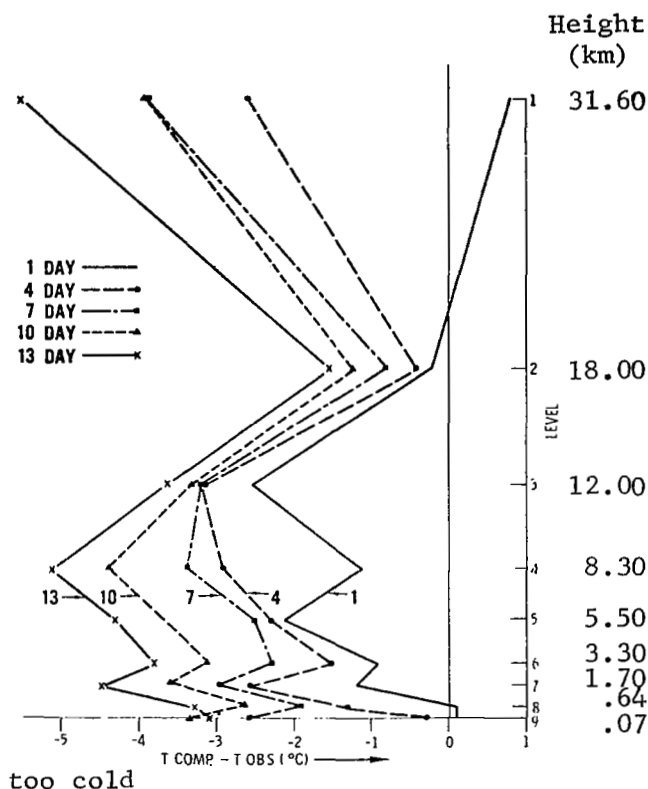
Fig. 14. Hemispherically averaged temperature error for Experiment 3 at 1, 4, 7, 10, and 13 days. The ordinate is the vertical level. (after Miyakoda et al., 1969)

forecast too low at all levels. An example of present surface temperature errors of the National Weather Service are given in Fig. 15 for Salt Lake City. The number of days with a temperature forecast error greater than 10°F has dropped from 53 in 1950 to 25 in 1966.

7. Summary of Forecasting Skills

A summary of forecasting skills for selected parameters is shown in Table 8. Data in this table were assembled and pieced together from the many reports and papers discussed in the previous sections. Very little skill in forecasting any of the variables is shown beyond a period of three days. It
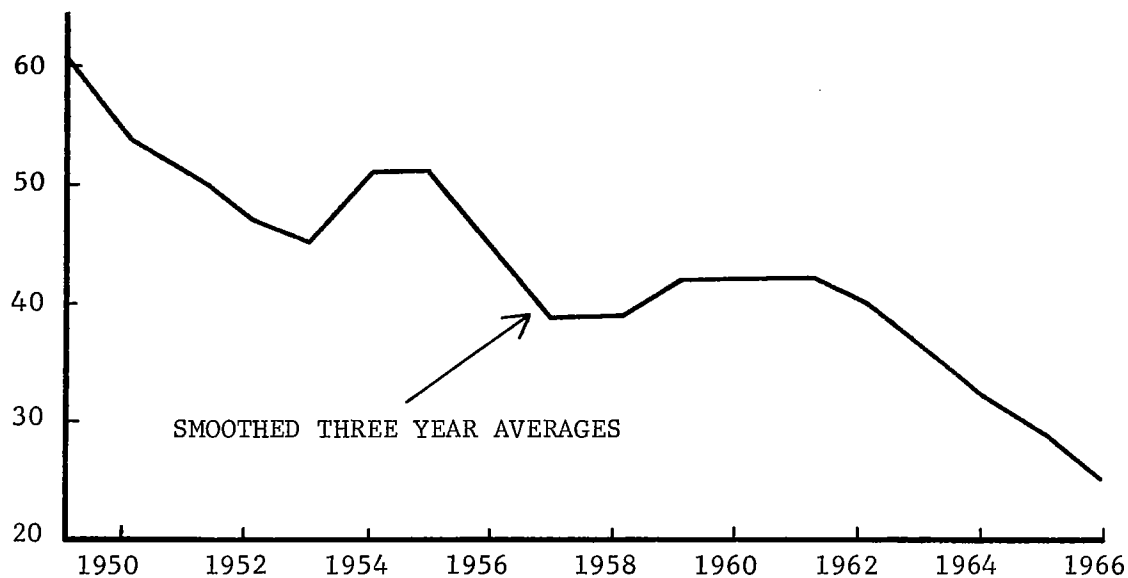
Fig. 15. Number of temperature forecast errors equal to or greater than 10°F for Salt Lake City, Utah. (after Roberts and Porter, 1967)

Table 8. Summary of present forecast skills.

	PRESSURE	CEILING	VISIBILITY	PRECIPITATION	TEMPERATURE
12 Hrs. —	R=.90	SS=.5	SS=.5		
1 Day —	R=.70	Forecast	Forecast	85% Correct	3.7 Error
36 Hrs. —	R=.68	Climatology	Climatology	82% Correct	4.3 Error
2 Days —	R=.65			SS=.50	4.7 Error
60 Hrs. —	R=.61			SS=.45	5.3 Error
3 Days —	R=.58			SS=.38	
4 Days —	R=.45			SS=.29	
5 Days —	R=.34			SS=.22	
6 Days —	R=.15			SS=.15	
7 Days —	R=0			SS=.10	
8 Days —				SS=.05	
9 Days —				SS= 0	
10 Days —				Forecast Climatology	
11 Days —					
12 Days —					
13 Days —					
14 Days —					

R is the correlation coefficient between observed and forecast parameters

SS is the Skill Score

Error is the mean absolute error of maximum and minimum temperatures

A-30

is interesting to note that forecasts of ceiling and visibility are quite poor for a period as short as 12 hours, and at 24 hours the skill is no better than climatology. This points out that much remains to be done before the accuracy of forecasts become satisfactory. Also, emphasis should be placed on the development of short range as well as long range forecast methods.

CITED REFERENCES

Andrews, James F., 1970: Evaluation of 500-Millibar Daily and 5-Day
    Mean Numerical Predictions. MWR 98 (5), 385-398.

Beebe, Robert G., 1950: Forecasting Winter Precipitation for Atlanta,
    Georgia. MWR 78(4), 59-68.

Borsting, J. R., and F. F. Sheehan, 1964: The Evaluation of Several
    Cyclone Prediction Techniques. JAM 3(2), 132-135.

Brown, Merle J., and Kenneth C. Tillotson, 1957: Forecasting Ceilings
    at Denver, Colorado. BAMS 38(4), 193-205.

Browne, Richard F., and Russel J. Younkin, 1970: Some Relationships
    Between 850-mb Low and Heavy Snow Occurrence Over the Central and
    Eastern United States. MWR 98(5), 399-401.

Chisholm, D. A., and Gordon B. Lassow, 1965: Circulation-Cloud Prognostic
    Relationships; Summer and Fall. U.S.A.F. Systems Command: Bedford,
    Massachusetts, TR 65-14, 77 pp.

Fawcett, E. B., 1969: Systematic Errors in Operational Baroclinic
    Prognosis at the National Meteorological Center. MWR 97(9), 670-682.

George, J. J., 1960: Weather Forecasting for Aeronautics. Academic
    Press, New York, 673 pp.

Gerrity, Joseph P., Jr., 1967: A Physical-Numerical Model for the
    Prediction of Low Cloudiness. MWR 95(5), 261-282.

Gilbert, C. G., 1953: An Aid for Forecasting the Minimum Temperature
    at Denver, Colorado. MWR 81(8), 233-245.

Gilman, D. L., 1968: The rimitive Equations in Extended Forecasting.
    (abstract), Transactions, American Geophysical Union, 99(1), 183.

Gringorten, Irving I., 1949: A Study in Objective Forecasting.
    BAMS 30(1), 10-15.

Handy, Burton, Jr., 1950: Forecasting Winter-Time Stratus at Kansas City,
    Missouri. BAMS 31(2), 38-43.

Hocver, Robert A., 1950: Forecasting Radiation Fog at Elkins, West
    Virginia. MWR 78(5), 75-80.

Jenrette, James P., 1959: Development of an Objective Method for
    Forecasting Gulf Stratus Clouds at Bryan Air Base, Texas in the
    Summer Season. BAMS 40(12), 613-619.

Klein, W. H., B. M. Lewis, C. W. Crockett, and Isadore Enger, 1960: Application for Numerical Heights to Surface Temperature Forecasts. Tellus, 12(4), 378-392.

_____, C. W. Crockett, and J. F. Andrews, 1965: The Objective Prediction of Daily Precipitation and Cloudiness. Journal of Geophysical Research, 70(4), 801-813.

_____, 1966: Objective Forecasts of Surface Temperature from One to Three Days in Advance. JAM 5(2), 138-147.

_____, Frank Lewis, and George P. Casely, 1967: Automated Nationwide Forecasts of Maximum and Minimum Temperature. JAM 6(2), 216-228.

_____, 1970: The Forecasts Research Programs of the Techniques Development Laboratory. BAMS 51(2), 133-142.

_____, and Frank Lewis, 1970: Computer Forecasts of Maximum and Minimum Temperatures. JAM 9(3), 350-359.

Laird, Harly B., and Woodrow W. Dickey, 1953: Forecasting Rain or Snow at Denver, Colorado, September-November. BAMS 34(7), 287-292.

Leary, Collen, 1971: Systematic Errors in the Operational National Meteorological Center Primitive-Equation Surface Prognosis. MWR 99(5), 409-413.

Leith, C. E., 1971: Atmospheric Predictability and Two-Dimensional Turbulence. JAS 28(2), 145-161.

Lund, Iver A., 1963: Experiments in Predicting Sea-Level Pressure Changes for Periods of Less Than Twelve Hours. JAM 2(4), 517-525.

Martin, F. L., J. R. Borsting, F. J. Streckbeck, and A. H. Manhard, Jr., 1963: Statistical Prediction Methods for North American Anticyclones. JAM 2(4) 508-516.

Miyakoda, K., J. Smagorinsky, R. F. Stricker, G. D. Hembree, 1969: Experimental Extended Predictions With a Nine-Level Hemispheric Model. MWR 97(1), 1-76.

Palmer, Wayne C., 1948: On Forecasting the Direction and Movement of Winter Cyclones. MWR 76(9), 181-201.

Pandolfo, Joseph P., 1957: An Objective Method for Forecasting Precipitation Type During the Winter Months at New York City. BAMS 38(12), 571-574.

Rapp, R. R., 1949: On Forecasting Winter Precipitation Amounts at Washington, D. C. MWR 77(9), 251-256.

Roberts, Charles F., and John M. Proter, 1967: Recent Trends in the Accuracy and Quality of Weather Bureau Forecasting Service. USWB Technical Memorandum WBTM FSCT-8, 14 pp.

Russo, J. A., Jr., Isadore Enger, and Edna L. Sorenson, 1964: A Statistical Approach to the Short-Period Prediction of Surface Winds. JAM $\underline{3}$(2), 126-131.

Schmidt, Reinhart C., 1951: A Method of Forecasting the Occurrences of Winter Precipitation Two Days in Advance. MWR $\underline{79}$(5), 81-95.

_____, 1951: A Method of Forecasting Precipitation 28-40 Hours in Advance During October. MWR $\underline{79}$(5), 116-124.

_____, 1952: An Objective Aid in Forecasting Precipitation at Washington, D. C. during May. BAMS $\underline{33}$(6), 227-232.

Shuman, Frederick G., and John B. Hovermale, 1968: An Operational Six-Layer Primitive Equation Model. JAM $\underline{7}$(4), 525-547.

Smagorinsky, Joseph, 1969: Problems and Promises of Deterministic Extended Range Forecasting. BAMS $\underline{50}$(5), 286-311.

Spar, Jerome, 1969: An Experiment in Localized Numerical Weather Prediction. JAM $\underline{8}$(6), 854-862.

_____, 1971: Further Experiments in Localized Numerical Weather Prediction. JAM $\underline{10}$(2), 180-185.

Teweles, S., and H. Wobus, 1954: Verification of Prognostic Charts. BAMS $\underline{35}$, 455-463.

Teweles, Sidney, Jr., and Albert L. Forst, 1953: Forecasting Winter Precipitation 36 to 48 Hours in Advance at Des Moines, Iowa. MWR $\underline{8}$(11), 357-367.

Thompson, J. C., 1950: A Numerical Method for Forecasting Rainfall in the Los Angeles Area. MWR $\underline{78}$(7), 113-124.

Thompson, Philip D., 1961: Numerical Weather Analysis and Prediction. The MacMillan Company, New York, 137-150.

Veigas, K. W., and F. P. Ostby, Jr., 1963: Application of a Moving Coordinate Prediction Model to East Coast Cyclones. JAM $\underline{2}$(1), 24-38.

White, Robert M., and Agnes M. Galligan, 1956: The Comparative Accuracy of Statistical and Synoptic Forecasting Techniques. BAMS $\underline{37}$(1), 1-7.

Williams, Philip, Jr., 1950: An Objective Method of Forecasting Summer Precipitation at Salt Lake City, Utah. MWR $\underline{78}$(8), 148-152.

Younkin, Russel J., 1968: Circulation Patterns Associated With Snowfall Over the Western United States. MWR $\underline{96}$(12), 851-853.

APPENDIX B

Symbols Used in This Study

ζ = relative vorticity

f = coriolis parameter

d/dt = total derivative with respect to time (individual derivative)

$\vec{\nabla}$ = three-dimensional del operator

$\vec{\nabla}_2$ = two-dimensional (horizontal) del operator

β = change of coriolis parameter with respect to change in latitude

u = zonal velocity component (positive is from west to east)

v = meridional velocity component (positive is from south to north)

w = vertical velocity component

Z = contour height

$\bar{Z}$ = space-mean height

Z' = the difference between the contour height and space-mean height; directly proportional to geostrophic relative vorticity

u_g = zonal geostrophic velocity component (positive is from west to east)

v_g = meridional geostrophic velocity component (positive is from south to north)

ζ_g = geostrophic relative vorticity

d = distance between grid points used to construct space mean charts

T = temperature

t = time

γ_d = dry adiabatic lapse rate of temperature

γ = the existing lapse rate of temperature

APPENDIX C

Symbols Used on Radar Summaries

⟋⟋	line of radar echoes (squall line)
⟨⟩	area of radar echoes
<u>hhh</u>	height of tops of clouds in hundreds of feet
⟊	0.1 - 0.5 of area covered by radar echoes
⟊⟊	0.6 - 0.9 of area covered by radar echoes
⊕	greater than 0.9 of area covered by radar echoes
R	rain
RW	rain shower
TRW	thundershower
L	drizzle
S	snow
SW	snow showers
E	sleet
↗ᵛ ᵛ	speed and direction of radar echo movement (knots)
⟍	area or line movement
—	light precipitation/or decreasing intensity of echo
——	very light precipitation
+	heavy precipitation/or increasing intensity of echo
++	very heavy precipitation
u	unknown
NC	no change